JOURNAL OF THE AERONAUTICAL SCIENCES

VOLUME 23 OCTOBER, 1956 NUMBER 10

ST. LOUIS OCT 18 1956 PUBLIC

CONTENTS

Rapid Laminar Boundary-Layer Calculations by Piecewise Application of Similar Solutions ..... A. M. O. SMITH 901

The Effect of Heating and Cooling on the Stability of the Boundary-Layer Flow of a Liquid over a Curved Surface ..... R. C. DI PRIMA AND D. W. DUNN 913

The Dynamic Response of a Large Airplane to Continuous Random Atmospheric Disturbances ..... FRANKLIN W. DIEDERICH 917

Experiments on Circular Cones at Yaw in Supersonic Flow ..... MAURICE HOLT AND JOHN BLACKIE 931

On Heat Transfer in Laminar Boundary Layers at High Prandtl Number ..... GEORGE W. MORGAN AND W. H. WARNER 937

The Behavior of Transverse Cylindrical and Forward Facing Total Pressure Probes in Transverse Total Pressure Gradients ..... J. L. LIVESEY 949

Nonlinear Minimum-Weight Design of Planar Structures ..... LOUIS G. VARGO 956

On Transonic Airfoil Theory ..... GOTTFRIED GUDERLEY 961

Readers' Forum 970–980

Published by

INSTITUTE OF THE AERONAUTICAL SCIENCES, INC.

JOURNAL OF THE AERONAUTICAL SCIENCES

Editor: W. R. SEARS

Director, Graduate School of Aeronautical Engineering, Cornell University

Associate Editor: ROBERT R. DEXTER

Managing Editor: RITA J. TURINO

Editorial Assistant: CAROLINE TAYLOR

Editorial Committee

Aerodynamics and Fluid Mechanics

Holt Ashley
H. Julian Allen
Dean R. Chapman
Francis H. Clauser
Hugh L. Dryden
John C. Evvard
Antonio Ferri
Alexander Flax
Wallace D. Hayes
R. T. Jones
Carl Kaplan
H. W. Liepmann
C. C. Lin
H. F. Ludloff
Harold Luskin
Clark B. Millikan
C. D. Perkins
H. J. E. Reid
George S. Schairer
G. B. Schubauer
John Stack
Theodore Theodorsen
Arthur N. Tifford
Th. von Kármán

Flight Testing

R. R. Gilruth
Melvin N. Gough
W. L. Howland
W. F. Milliken, Jr.

Rotating Wing Aircraft

F. B. Gustafson
K. H. Hohenemser
Bartram Kelley
R. B. Maloy
Ralph McClarren
R. H. Miller
R. H. Prewitt
Igor I. Sikorsky

Structures

John E. Duberg
N. J. Hoff
Samuel Levy
J. F. McBrearty
W. Ramberg
E. E. Sechler
F. R. Shanley
C. R. Strang
S. Timoshenko

Meteorology

C. F. Brooks
D. M. Little
F. W. Reichelderfer
K. C. Spengler

Vibration and Flutter

Lee Arnold
M. A. Biot
R. L. Bisplinghoff
Harold A. Cheilek
I. E. Garrick
Martin Goland

Aircraft Design

W. E. Beall
E. H. Heinemann
Hall L. Hibbard
Richard Hutton
C. L. Johnson
A. A. Kartveli
E. G. Stout
F. K. Teichmann
Robert J. Woods

Electronics

Welcome W. Bender
K. C. Black
M. V. Kiebert, Jr.
David S. Little
S. B. Rogers
Paul Rosenberg
L. M. Sherer

Physiologic Problems

H. G. Armstrong
Louis H. Bauer
Robert J. Benford
W. Randolph Lovelace, II
Ross A. MacFarland

Flight Propulsion

William Bollay
George W. Brady
R. P. Kroon
Frank E. Marble
Abe Silverstein
Martin Summerfield
E. S. Taylor

Instruments

Alan G. Binnie
Charles H. Colvin
Frank R. Cook
C. S. Draper
S. G. Eskin
C. F. Savage
R. C. Sylvander

SUBSCRIPTION RATES

JOURNAL OF THE AERONAUTICAL SCIENCES, Published Monthly.—United States and Possessions: 1 Year, $15.00; Single Copies, $1.50. Foreign Countries Including Canada (American Currency Rates): 1 Year, $16.00; Single Copies, $1.50.

AERONAUTICAL ENGINEERING REVIEW, Published Monthly.—United States and Possessions: 1 Year, $3.00; Single Copies, $0.50. Foreign Countries Including Canada (American Currency Rates): 1 Year, $3.50; Single Copies, $0.50.

Notices of change of address should be sent to the Institute at least 30 days prior to actual change of address.

Manuscripts for publication, proofs, and all correspondence should be addressed to the Editorial Office of the JOURNAL.

Correspondence regarding subscriptions may be addressed to the Editorial Office of the JOURNAL OF THE AERONAUTICAL SCIENCES, 2 East 64th Street, New York 21, N.Y., or to the Publication Office, 20th and Northampton Sts., Easton, Pa.

© *Copyright, 1956, by the Institute of the Aeronautical Sciences, Inc.*

Entered as Second Class Matter at the Post Office, Easton, Pa., May 1, 1937. Acceptance for mailing at a special rate of Postage provided for in the Act of August 24, 1912. Authorized April 29, 1937.

JOURNAL OF THE AERONAUTICAL SCIENCES

VOLUME 23 OCTOBER, 1956 NUMBER 10

Rapid Laminar Boundary-Layer Calculations by Piecewise Application of Similar Solutions

A. M. O. SMITH*

Douglas Aircraft Company, Inc.

SUMMARY

A method is presented for the rapid calculation of the incompressible laminar boundary layer in an arbitrary flow around either a two-dimensional or a rotationally-symmetrical body. The solution is obtained without recourse to von Kármán's momentum equation by means of a coarse step-by-step procedure in which each segment of the velocity distribution is approximated by one of the Falkner-Skan family of similar flows.

Solutions have at least as much accuracy as those of any other one-parameter approximate method, and in certain cases the solutions become exact. In regions of accelerating velocity, the accuracy appears to be very high. In decelerating flows, separation is predicted somewhat early compared with exact solutions —that is, the method is conservative in contrast to the von Kármán-Pohlhausen procedure which sometimes fails to predict separation that actually exists.

The method is the most rapid hand procedure known to the author, provided the full history of the boundary layer is required. If only a thickness such as θ is needed at one point on a surface, then it is about equal in speed to the quadrature method. But, if several values of θ or other properties along a surface are required, it is appreciably faster than the quadrature method. Characteristically, only four steps are needed between the forward stagnation point and the pressure peak. Once the velocity-distribution data are available, each step in a two-dimensional calculation requires about 5 minutes, using a slide rule.

SYMBOLS

a = cross-sectional area of a body of revolution
A = maximum cross-sectional area of a body of revolution
c = the wing chord or other characteristic reference length
H = the boundary-layer shape factor, δ^*/θ
k = an arbitrary constant in Eq. (1)
l = dimensionless skin friction, $(\theta/U)\ (\partial u/\partial y)_{y=0}$; see Eq. (16).
m = exponent in Eq. (1), defining free-stream velocity variation; also $m = \beta/(2 - \beta)$
r = radius of a body of revolution
R = maximum radius of a body of revolution
R_c = reference Reynolds Number, $U_\infty c/\nu$
R_θ = boundary-layer Reynolds Number, $U\theta/\nu$
u = velocity in the boundary layer in the x-direction
U = velocity at edge of the boundary layer
U_∞ = reference velocity, usually the free-stream velocity
x = distance along the surface of the body measured from the upstream stagnation point
X = distance along the chord or axis of a body
y = distance perpendicular to the surface of the body
Z = a measure of the length of a step in the step-by-step solution; see Eq. (12).
β = Hartree's beta, $2m/(m + 1)$
θ = momentum thickness of the boundary layer
Θ = dimensionless momentum thickness; see Eq. 3.
λ = Pohlhausen's lambda, $(\delta^2/\nu)\, dU/dx$
Λ = a measure of the velocity gradient in the step-by-step method; see Eq. (9).
ν = kinematic viscosity
ρ = mass density of the fluid
τ_0 = local wall shear stress

Note: Barred symbols represent equivalent two-dimensional flows derived from rotationally symmetrical types by the Mangler transformation.

Received September 22, 1955.

* Supervisor, Aerodynamic Research, El Segundo Division.

INTRODUCTION

FROM A STUDY OF such references as 1, 2, and 3, it becomes obvious that a large variety of methods exist for calculating the incompressible laminar boundary layer. So many methods and modifications exist that even a cursory review of them becomes impossible in the present short article. Therefore, we shall be content to divide the available methods roughly into two classes: (a) low accuracy but usually fast methods—e.g., the von Kármán-Pohlhausen and quadrature methods, and (b) high accuracy but generally slower methods—viz., the two-parameter, finite-difference, and series methods.

Highly accurate methods are seldom needed except where the boundary-layer profile must be determined quite accurately, as for stability calculations. But, in general, when such accuracy is demanded, only the finite-difference and series methods can supply it, for the accuracy requirement becomes so severe that even the two-parameter methods that invoke both the

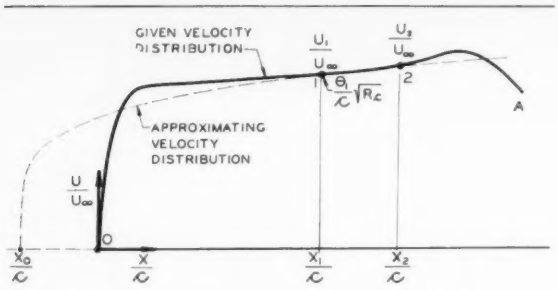

FIG. 1. The approximation scheme.

momentum and energy equations still fall short.

Other types of problems usually require only a knowledge of simpler properties, such as some characteristic thickness of the boundary layer, the local or total skin friction, or the separation point. In this field, high accuracy is unnecessary, and a number of methods already exist that are capable of supplying results having acceptable engineering accuracy. Hence, a major justification for further development in the field of category (a) lies in the reduction of computing labor.

Since about 1948, a very quick approximate method devised by the writer and falling into category (a) has been in casual use for rough calculations. Until 1954, it was thought to be appreciably deficient in accuracy as compared with Pohlhausen's and other established procedures, chiefly because the method was too easy. During this year, its accuracy was checked and found to be as high, in general, as that of any other method of category (a). Sometimes it was better than other methods, sometimes worse, but it was never enough in error to be of any concern. It predicts separation somewhat early, but this feature is not necessarily a serious drawback—first, because, in many technical applications, turbulence sets in prior to laminar separation; and, second, unlike some methods, the procedure supplies conservative results since it will always predict separation if separation exists.

The boundary-layer profiles are members of the Falkner-Skan family instead of being expressed by some sort of polynomial or other explicit mathematical expression. This in itself is an advantage, for it makes possible the approximate application of a great deal of stability information and other data developed for the family of similar flows. The success of the present procedure appears to warrant like efforts with the more complicated flows involving compressibility or mass transfer.

THE METHOD

Consider an arbitrary velocity distribution represented by the curve 0–A in Fig. 1. In this Figure, as throughout, we let

U = local stream velocity at the edge of the boundary layer
U_∞ = reference stream velocity
x = distance along surface from the front stagnation point
c = the chord or any other reference length
R_c = reference Reynolds Number, $U_\infty c/\nu$

At some segment 1–2 of the flow, the flow at point 1 will have a definite set of properties such as U_1/U_∞, $(\theta_1/c)\sqrt{R_c}$, H_1, etc. Now, of course, it is possible to match U_1/U_∞ and $(\theta_1/c)\sqrt{R_c}$ at this same point by many different types of flow, one of which could be a similar flow of the type $U/U_\infty = k(x/c)^m$, where k and m are constants. This equivalent flow, in general, will not have the same boundary-layer profile, but, nevertheless, its momentum thickness and velocity will match at point 1.

Our equivalent flow may not necessarily begin at $x/c = 0$. Once this fact is realized, it becomes obvious that the Falkner-Skan similar flow can be described by the following equation, where x_0/c represents an arbitrary origin:*

$$U/U_\infty = k[(x/c) - (x_0/c)]^m \tag{1}$$

Because Eq. (1) contains three unknown constants, k, x_0/c, and m, it usually becomes possible to provide a similar flow that produces the proper value of $(\theta_1/c)\sqrt{R_c}$ and matches the given velocity at points 1 and 2. Only in rare cases will it match the entire velocity curve between these points, but, in most cases, the difference will be small. If $(\theta_1/c)\sqrt{R_c}$ and U_1/U_∞ are properly matched at point 1, $(\theta/c)\sqrt{R_c}$ at point 2 should be predicted rather accurately by formulas from the "similar solutions," for the main source of error comes only from the slight difference in the paths taken by the given and the approximating velocities between the points 1 and 2.

If the approximation is possible, then at points 1 and 2, respectively, the velocity ratios can be written

$$U_1/U_\infty = k[(x_1/c) - (x_0/c)]^{\beta/(2-\beta)} \tag{2a}$$

$$U_2/U_\infty = k[(x_2/c) - (x_0/c)]^{\beta/(2-\beta)} \tag{2b}$$

where now we introduce the Hartree β to replace the exponent m. Various properties of the boundary layer can be matched at the ends of any interval 1–2, but the most logical is θ, the momentum thickness. Since the momentum deficiency in a boundary layer is $\rho U^2\theta$, failure to match θ at the junction of two segments implies a discontinuity in momentum, which, of course is impossible in ordinary low-speed boundary-layer flow. When the origin is variable, a convenient formula for the momentum thickness is[5]

$$\frac{\theta}{c}\sqrt{R_c} = \sqrt{\frac{(x/c) - (x_0/c)}{U/U_\infty}\,(2-\beta)\Theta^2} \tag{3}$$

The dimensionless momentum thickness Θ, a function of β, is given in Table I.

* This form of the equation is not new, but the method of using it is. Eckert,[2, 4] for example, used it as a basis for heat-transfer calculations. Mangler[7] derived it and discussed it in his treatise on the possibilities of similar solutions.

TABLE I
Boundary-Layer Parameters
(Compiled from Reference 5)

β	Θ	Δ^*	H	$\Theta F''(0)$	$(2-\beta)\Theta^2$
−0.19884	0.58543	2.35885	4.02923	0	0.75360
−0.195	0.58136	2.11705	3.64153	0.03207	0.74186
−0.19	0.57652	2.00676	3.48079	0.04941	0.72790
−0.18	0.56771	1.87157	3.29673	0.07303	0.70260
−0.16	0.55219	1.70665	3.09067	0.10535	0.65861
−0.14	0.53856	1.59590	2.96327	0.12911	0.62070
−0.10	0.51504	1.44270	2.80111	0.16444	0.55706
−0.05	0.49046	1.31236	2.67575	0.19634	0.49313
0	0.46960	1.21678	2.59110	0.22052	0.44105
0.05	0.45174	1.14174	2.52894	0.23993	0.39793
0.10	0.43546	1.08032	2.48089	0.25563	0.36029
0.20	0.40823	0.98416	2.41079	0.28033	0.29997
0.30	0.38574	0.91099	2.36171	0.29885	0.25295
0.40	0.36669	0.85263	2.32521	0.31331	0.21514
0.50	0.35027	0.80455	2.29694	0.32494	0.18403
0.60	0.33591	0.76397	2.27435	0.33451	0.15797
0.80	0.31185	0.69868	2.24047	0.34936	0.11670
1.00	0.29234	0.64790	2.21623	0.36033	0.08546
1.20	0.27611	0.60690	2.19803	0.36881	0.06099
1.60	0.25041	0.54402	2.17248	0.38100	0.02508
2.00	0.23078	0.49743	2.15541	0.38938	0

At points 1 and 2 there are three values that must be matched—namely, U_1/U_∞, U_2/U_∞, and $(\theta_1/c)\sqrt{R_c}$. Since Eqs. (2) and (3) together provide three equations, it is possible to compute x_0/c, k, and β. We shall solve for β. When Eq. (2b) is divided by Eq. (2a), one obtains

$$\frac{U_2}{U_1} = \left[1 + \frac{(x_2/c) - (x_1/c)}{(x_1/c) - (x_0/c)}\right]^{\beta/(2-\beta)} \tag{4}$$

Eq. (3) now can be used to eliminate x_0/c, giving

$$\frac{U_2}{U_1} = \left\{1 + \frac{(x_2/c) - (x_1/c)}{[(\theta_1/c)\sqrt{R_c}]^2} \cdot \frac{(2-\beta)\Theta^2}{U_1/U_\infty}\right\}^{\beta/(2-\beta)} \tag{5}$$

Eq. (5) provides a solution for β since, at the beginning of a step, we know U_1/U_∞, x_1/c and $(\theta_1/c)\sqrt{R_c}$, and, at the end, we know x_2/c and U_2/U_∞. However, the solution from Eq. (5) directly is awkward. The following procedure transforms Eq. (5) into a form suitable for chart solution.

Let Z represent the quantity in Eq. (5) as follows:

$$Z = \frac{(x_2/c) - (x_1/c)}{(U_1/U_\infty)\,[(\theta_1/c)\sqrt{R_c}]^2} \tag{6}$$

Then Eq. (5) can be written

$$U_2/U_1 = [1 + (2-\beta)\Theta^2 Z]^{\beta/(2-\beta)} \tag{7}$$

Now after subtracting 1 from both sides of Eq. (7), we divide through by Z but keep Z in its original form on the left side. We get, after some rearranging,

$$\frac{(U_2/U_\infty) - (U_1/U_\infty)}{(x_2/c) - (x_1/c)}\left(\frac{\theta_1}{c}\sqrt{R_c}\right)^2 = \frac{1}{Z}\left\{[1 + (2-\beta)\Theta^2 Z]^{\beta/(\beta-2)} - 1\right\} \tag{8}$$

Let the expression on the left be designated as Λ—that is,

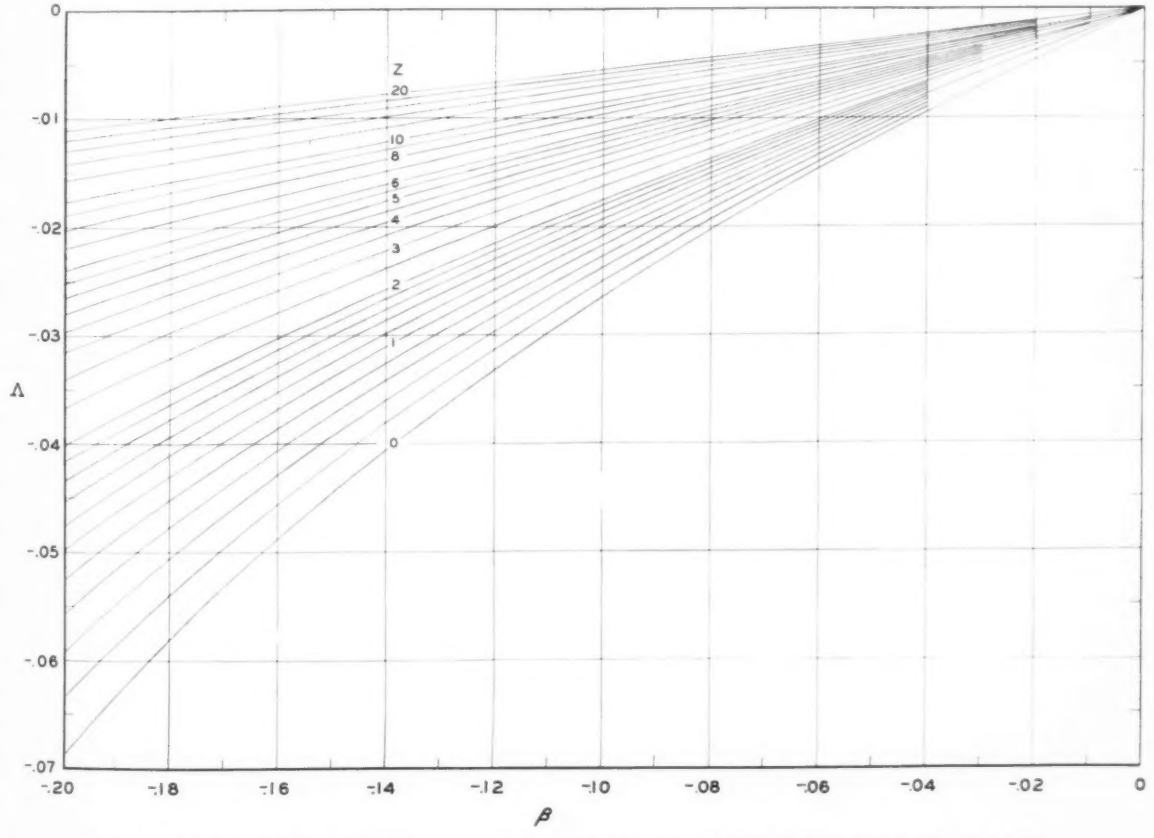

FIG. 2a. Solution of the equation $\Lambda Z = [1 + (2-\beta)\Theta^2 Z]^{\beta/(2-\beta)} - 1$, Falkner-Skan boundary-layer family.

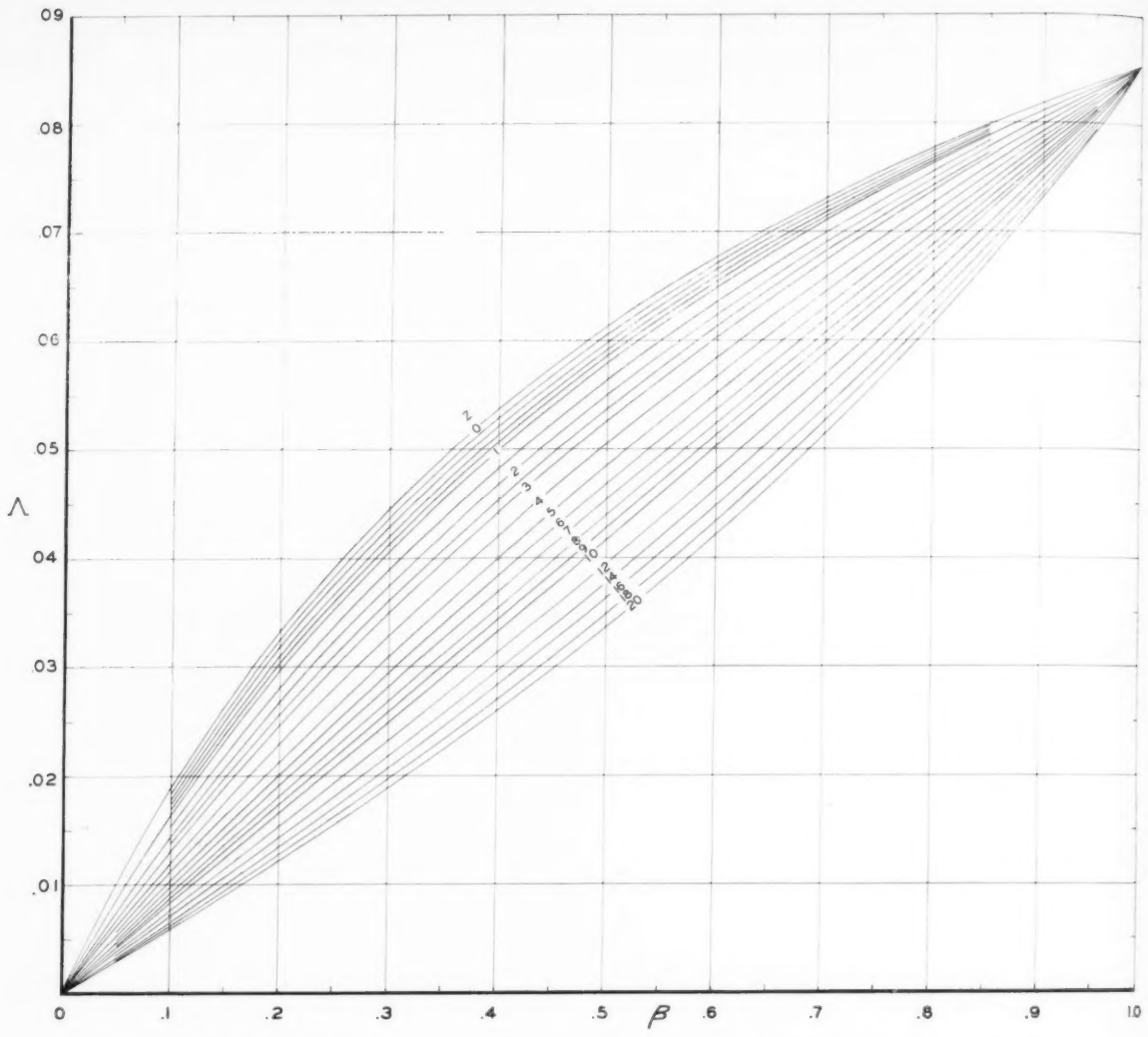

FIG. 2b. Solution of the equation $\Lambda Z = [1 + (2 - \beta)\Theta^2 Z]^{\beta/(2-\beta)} - 1$, Falkner-Skan boundary-layer family.

$$\Lambda = \frac{(U_2/U_\infty) - (U_1/U_\infty)}{(x_2/c) - (x_1/c)} \left(\frac{\theta_1}{c}\sqrt{R_c}\right)^2 \qquad (9)$$

so that Eq. (8) becomes

$$\Lambda Z = [1 + (2 - \beta)\Theta^2 Z]^{\beta/(2-\beta)} - 1 \qquad (10)$$

As Λ and Z involve only θ_1, both can be evaluated readily at the start of a step. β can be found conveniently by means of a plot of Eq. (10). Fig. 2 is such a chart from which β can be read immediately once Λ and Z are known.

What are the meanings of the quantities Λ and Z? First of all, from Eqs. (7) and (10) we see that the product ΛZ equals $(U_2 - U_1)/U_1$—that is, ΛZ represents the per cent of change in velocity in a particular step. Now we write out the expression for Λ in full:

$$\Lambda = \frac{(U_2/U_\infty) - (U_1/U_\infty)}{(x_2/c) - (x_1/c)} \cdot \frac{\theta_1^2}{c^2} \cdot \frac{U_\infty c}{\nu} = \frac{\theta_1^2}{\nu} \frac{\Delta U}{\Delta x} \qquad (11)$$

As Pohlhausen's λ is $(\delta^2/\nu)\, dU/dx$, Λ has a similar meaning except that it is based on θ. Therefore, Λ can be thought of as a finite-difference variation of Pohlhausen's λ, hence the designation Λ.

Now we write out Z in full:

$$Z = \frac{(x_2/c) - (x_1/c)}{U_1/U_\infty} \cdot \frac{c^2}{\theta_1^2} \cdot \frac{\nu}{U_\infty c} = \frac{1}{R_{\theta_1}} \frac{\Delta x}{\theta_1} \qquad (12)$$

Therefore, Z represents the length of a step referred to the momentum thickness, making due allowance for the boundary-layer Reynolds Number.

Once β is determined, x_0/c and k are easily evaluated by the use of Eqs. (2) and (3). For example, from Eq. (3)

$$\frac{x_0}{c} = \frac{x_1}{c} - \frac{[(\theta_1/c)\sqrt{R_c}]^2\,(U_1/U_\infty)}{(2 - \beta)\Theta^2} \qquad (13)$$

In the usual problem, x_0/c is of no direct interest, for the goal is the evaluation of θ at the end of the step—that is, the computation of $(\theta_2/c)\sqrt{R_c}$. Since β is constant across an interval, we have by Eq. (3)

$$\left(\frac{\theta_2}{c}\sqrt{R_c}\right)^2 = \frac{[(x_2/c) - (x_0/c)]\,(2-\beta)\Theta^2}{U_2/U_\infty} \quad (14)$$

Furthermore, by the use of Eq. (13) to eliminate x_0/c and the subsequent use of Z to eliminate $[(x_2/c) - (x_1/c)]$, Eq. (14) can be reduced to

$$[(\theta_2/c)\sqrt{R_c}]^2 = (U_1/U_2)\,[(\theta_1/c)\sqrt{R_c}]^2 \times [1 + Z\,(2-\beta)\Theta^2] \quad (15)$$

Values of $(\theta/c)\sqrt{R_c}$ between points 1 and 2 must, of course, be computed by Eqs. (3) and (13) because Eq. (15) applies only to the end of the interval.

In summary, the computations proceed as follows, assuming U/U_∞ is already known as a function of x/c. Notice the derivative $d(U/U_\infty)/d(x/c)$ never needs to be evaluated. (a) Compute Z and Λ by Eqs. (6) and (9) and $[(\theta_1/c)\sqrt{R_c}]^2$. (b) Read β from Fig. 2. (c) Read $(2-\beta)\Theta^2$ from a chart constructed from Table 1. (d) Compute $[(\theta_2/c)\sqrt{R_c}]^2$ by Eq. (15). (e) Repeat for the next step, now treating $[(\theta_2/c)\sqrt{R_c}]^2$ as $[(\theta_1/c)\sqrt{R_c}]^2$.

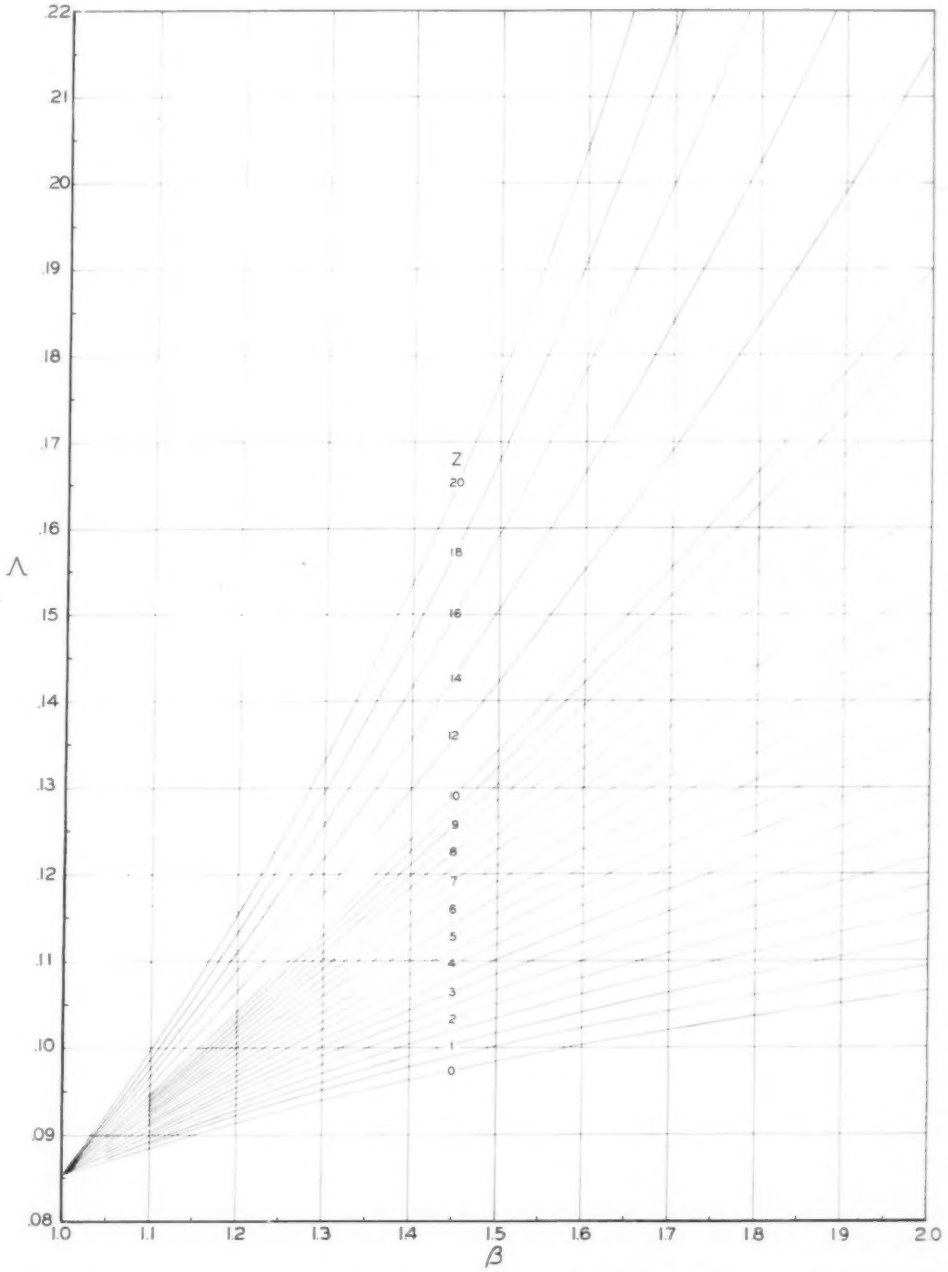

FIG. 2c. Solution of the equation $\Lambda Z = [1 + (2-\beta)\Theta^2 Z]^{\beta/(2-\beta)} - 1$, Falkner-Skan boundary-layer family.

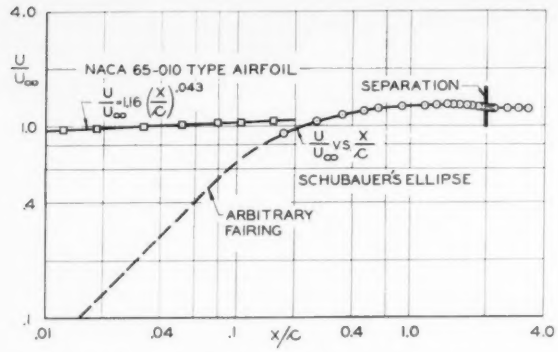

FIG. 3. Typical velocity distributions, logarithmic plot, experimental data.

The first parameters supplied by the process are θ and β. The latter is the key to the remainder of the boundary-layer properties. For example, separation is assumed to occur when $(\partial u/\partial y)(0) = 0$, which corresponds to $\beta = -0.1988$. The dimensionless shear stress l can be found as follows:[5]

$$l \equiv (\theta/U)\,(\partial u/\partial y)_0 = (\tau_0/\rho U^2)\cdot(U\theta/\nu) = \Theta F''(0) \quad (16)$$

The product $\Theta F''(0)$ is included in Table I. For the boundary-layer profiles themselves, the reader must refer either to reference 5 or 6. The profiles in both references are presented in the form of u/U vs. Y, a dimensionless height. Hence, the scaling constants become obvious by comparison of the actual θ and the dimensionless Θ of reference 5—that is,

$$\left.\begin{aligned} y/Y &= \theta/\Theta \\ u/U &= F'(Y) \end{aligned}\right\} \quad (17)$$

THE STARTING PROCEDURE

First Method

Up to here, the analysis has assumed that initial values were available for each step. We now consider how to start the computations. Two approaches have been found equally satisfactory; in fact, getting started is simple.

Mangler,[7] among others, has pointed out that the potential flow past a two-dimensional semi-infinite wedge of total interior angle $\beta\pi$ ($\beta \geqslant 0$) is $U = kx^{\beta/(2-\beta)}$. For example, if the included angle is 0° (flat plate), $\beta = 0$ and $U = k$. If the included angle is 180°, $\beta = 1$ and $U = kx$. This knowledge enables one to observe the geometry of a surface and know immediately the initial value of β, which then can be used with the Falkner-Skan solutions in the ordinary manner. If the flow is past an ordinary blunt-nosed airfoil, we know $\beta = 1$, initially. If the airfoil is a symmetrical supersonic diamond type with nose angle $\beta\pi$ operating at low speed and zero angle of attack, then the initial value of β is again known, but it is considerably lower since the wedge angle is quite small. Similar information is known from the work of Mangler for bodies of revolution.[8] A blunt body of revolution begins with a flow whose initial value of β is 1/2. Therefore, in the first method, the initial value of β is determined by the geometry of the body. Then a short step of the order of $0.01c$ to $0.05c$ is taken.

Second Method

The equation $U = kx^m$ plots as a straight line with slope m on logarithmic graph paper. The second method uses a plot on log paper of the initial part of the velocity distribution as in Fig. 3. In many cases, particularly with low-drag airfoils, it will be found that a considerable portion of the velocity distribution forms a straight line. The NACA 65-010 type airfoil has such a velocity distribution for $0.01 \leqslant x/c \leqslant 0.16$. Since the geometric slope on square log paper equals the exponent, we know that, somewhere forward of $x/c = 0.01$, the curve must bend down toward a 45° slope. However, this portion is so small that it can safely be neglected, and one formula and one β will describe the flow at least to $x/c = 0.16$. When such fortunate conditions occur, a substantially exact solution may be available over the entire region of laminar flow.

Schubauer's ellipse presents a slightly different problem. The points shown represent all the measured data, but they do not approach as close to the beginning of the flow as desired. Additional data, of course, could be computed, but studies show the work is unnecessary. A convenient method of obtaining the initial portion of the distribution is to fair the curve into an arbitrary straight line whose slope on the logarithmic scale is 1, as shown by the dashed line. One can see that even cruder methods are acceptable, in view of the basic formula,

$$(\theta/c)\sqrt{R_c} = \sqrt{(x/c)\,(2-\beta)\Theta^2\,(U/U_\infty)}$$

At a particular value of x/c terminating the first step, since U/U_∞ is established, the only factor influencing the value of $(\theta/c)\sqrt{R_c}$ is the quantity $(2-\beta)\Theta^2$. Examination of Table I in the interval $0 \leqslant \beta \leqslant 1$ shows

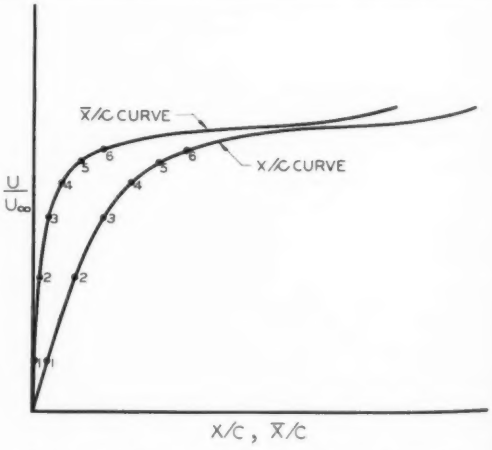

FIG. 4. Illustration of the Mangler transformation.

that it is a slowly varying function, and, therefore, provided the initial step is reasonably short, any value of β between about 0 and 1 will produce acceptable accuracy farther downstream. The first value of $(\theta/c)\sqrt{R_c}$ may have a large error percentagewise, but, if the step is short, the actual error remains trivial.

Modification for Bodies of Revolution

With only a small additional amount of labor, Mangler's transformation[2, 8] extends the method to all bodies of revolution except ones that are excessively slender. Following Mangler, let unbarred symbols represent the original flow about the body of revolution and let barred symbols represent the transformed two-dimensional equivalent flow. The major properties of the transformation can be written as follows:

$$\bar{U} = U$$

i.e., velocities at the edge of the boundary layer are transformed unchanged.

$$\frac{\bar{x}}{c} = \int_0^{x/c} \frac{r^2}{R^2}\, d\left(\frac{x}{c}\right) \tag{18}$$

$$\bar{y}/c = (r/R)\,(y/c) \tag{19}$$

$$\bar{u}[(\bar{x}/c), (\bar{y}/c)] = u[(x/c), (y/c)] \tag{20}$$

$$\bar{\beta} = \beta$$

In the above equations, r is the radius of the body at any point, and R is the maximum radius. For convenience, the ratio r^2/R^2 will usually be replaced by its equivalent, the area ratio a/A. Fig. 4 illustrates the transformation of a velocity distribution.

Examination of this curve makes the modification obvious. Assume we wish to calculate between points 1 and 2 in Fig. 1. In computing Λ and Z, it is seen that $[(x_2/c) - (x_1/c)]$ must be modified by Eq. (18). The modification is

$$\frac{\bar{x}_2}{c} - \frac{\bar{x}_1}{c} = \int_{x_1/c}^{x_2/c} \frac{a}{A}\, d\left(\frac{x}{c}\right) = \frac{\bar{a}}{A}\left(\frac{x_2}{c} - \frac{x_1}{c}\right) \tag{21}$$

where $\bar{a}/A$ represents a mean value for the interval. Intervals can be selected in such fashion that mean values of a/A can be read easily from the given data for the body. The calculations proceed step by step as with the two-dimensional case, using values of Λ and Z modified per Eq. (21). Eq. (15) is used unchanged. The values of momentum thickness are now, of course, in the transformed plane—that is, they are values of $(\bar{\theta}/c)\sqrt{R_c}$. But Eq. (19) shows that the values for the actual body of revolution are

$$(\theta/c)\sqrt{R_c} = (\bar{\theta}/c)\sqrt{R_c}\cdot(R/r), \text{ etc.} \tag{22}$$

Because the only modification to the boundary-layer profiles is multiplication by a constant, β remains the same in either plane. An example for a body of revolution will be given in the next section to clarify the procedure; the simplifications for a two-dimensional case should be obvious.

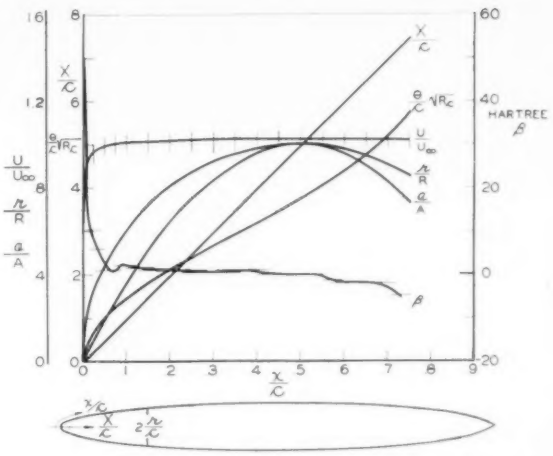

Fig. 5. Sample calculations for a body of revolution whose fineness ratio is 9.14. Chart shows both given data and results of calculations.

An Example

Fig. 5 and Table II represent the calculations as applied to the body of revolution shown. The forward part is an ellipsoid of revolution whose fineness ratio is 9:1. The tail fairing illustrated in Fig. 5 increases the fineness ratio to 9.14. As with any method of boundary-layer calculation, the first problem is to determine the relationship between axial and peripheral distance; for all methods of boundary-layer calculation, use the $(x/c,\ U/U_\infty)$ plane. The relation is plotted in Fig. 5. For slender bodies similar to the one of this example, the difference between x/c and X/c could safely be neglected, and only for the sake of correctness and illustration is it retained in the example.

The data required for setting up the calculations are U/U_∞, r/R, and a/A vs. x/c. The next problem is the selection of the intervals. About the only requirement is that both U/U_∞ and a/A be reasonably smooth curves within any interval and that they do not deviate greatly from a chord drawn between the termini of the step. Calculations for a body of revolution require mean values of a/A, Eq. (21). Therefore steps should be so chosen that mean values of a/A can be read with reasonable accuracy. In brief, two-dimensional flows require observation of the U/U_∞ vs. x/c curve for selection of the intervals; rotationally symmetrical flows require simultaneous consideration of both U/U_∞ vs. x/c and a/A vs. x/c.

The present example happens to represent an unusually careful calculation, for it contains two or three times as many steps as should normally be necessary. Calculations began by using the first method of starting—namely, by assuming $\beta = 1/2$ for $0 \leqslant x/c \leqslant 0.01$. Then, purely by observing the a/A and U/U_∞ curves, steps were chosen as indicated by the marks on the U/U_∞ curve of Fig. 5. With these chosen, columns 1–11 of Table II can be filled out completely prior to commencement of the actual boundary-layer computations.

TABLE II

SAMPLE CALCULATIONS—BODY OF REVOLUTION

① x/c	② x/c	③ U/U_∞	④ a AVE. A	⑤ r/R	⑥ $\Delta x/c$	⑦ $\Delta\bar{x}/c$	⑧ $\Delta U/U_\infty$	⑨ $\frac{\Delta\bar{x}}{c} \div \frac{\Delta U}{U_\infty}$	⑩ U_1/U_2	⑪ $\frac{\Delta\bar{x}}{c} \div \frac{U_1}{U_\infty}$	⑫ $\left(\frac{\bar{\theta}}{c}\sqrt{R_c}\right)^2$	⑬ Λ	⑭ Z	⑮ β	⑯ $(2-\beta)\Theta^2$	⑰ $(2-\beta)\Theta^2 Z+1$	⑱ $\frac{\bar{\theta}}{c}\sqrt{R_c}$	⑲ $\frac{\theta}{c}\sqrt{R_c}$	⑳ $\ell = \Theta F''(0)$
	FIG. 5	FIG. 5	FIG. 5	FIG. 5	$= X_2/C - X_1/C$ FROM ①	④ × ⑥	FROM ③	⑧ ÷ ⑦	FROM ③	⑦ ÷ ③	⑩ × ⑫ × ⑰	⑨ × ⑫	⑪ ÷ ⑫	FIG. 2	CHART OR TABLE I	⑯ × ⑭ + 1	$\sqrt{⑫}$	⑱ ÷ ⑤	CHART OR TABLE I
0	0	0		0							0			.50	.182		0	0	.324
			.027		.01	.00027			0										
.01	.008	.845		.210							.000058						.0076	.0362	
			.070		.015	.00105	.109	103.8	.886	.00124		.00604	21.32	.103	.357	8.611			.257
.025	.023	.954		.316							.000444						.0211	.0668	
			.140		.025	.0035	.043	12.28	.957	.00367		.00545	8.273	.06	.388	4.210			.243
.05	.048	.997		.432							.001787						.0423	.0979	
			.223		.025	.00558	.005	.896	.995	.00560		.00160	3.134	.01	.430	2.348			.225
.075	.072	1.002		.515							.004175						.0646	.1254	
			.310		.025	.00775	.006	.774	.994	.00773		.00323	1.851	.022	.418	1.774			.230
.10	.097	1.008		.596							.007362						.0858	.1440	
			.433		.05	.0216	.007	.324	.993	.02143		.00239	2.911	.017	.424	2.234			.227
.15	.146	1.015		.721							.01633						.1278	.1772	
			.576		.05	.0288	.004	.139	.996	.02857		.00227	1.737	.012	.427	1.742			.226
.20	.195	1.019		.803							.02833						.1683	.2096	
			.694		.05	.0347	.002	.0576	.998	.0340		.00163	1.200	.008	.432	1.519			.224
.25	.245	1.021		.868							.04293						.2071	.2386	
			.792		.05	.0396	.001	.0252	.999	.0388		.00108	.9038	.006	.434	1.392			.223
.30	.295	1.022		.918							.05971						.2443	.2661	

STARTING: $\left(\frac{\bar{\theta}}{c}\sqrt{R_c}\right)^2 = \frac{(\bar{x}/c)(2-\beta)\,\Theta^2}{U/U_\infty} = \frac{.00027 \times .182}{.845} = .000058 \qquad \left(\beta = \tfrac{1}{2}\right)$

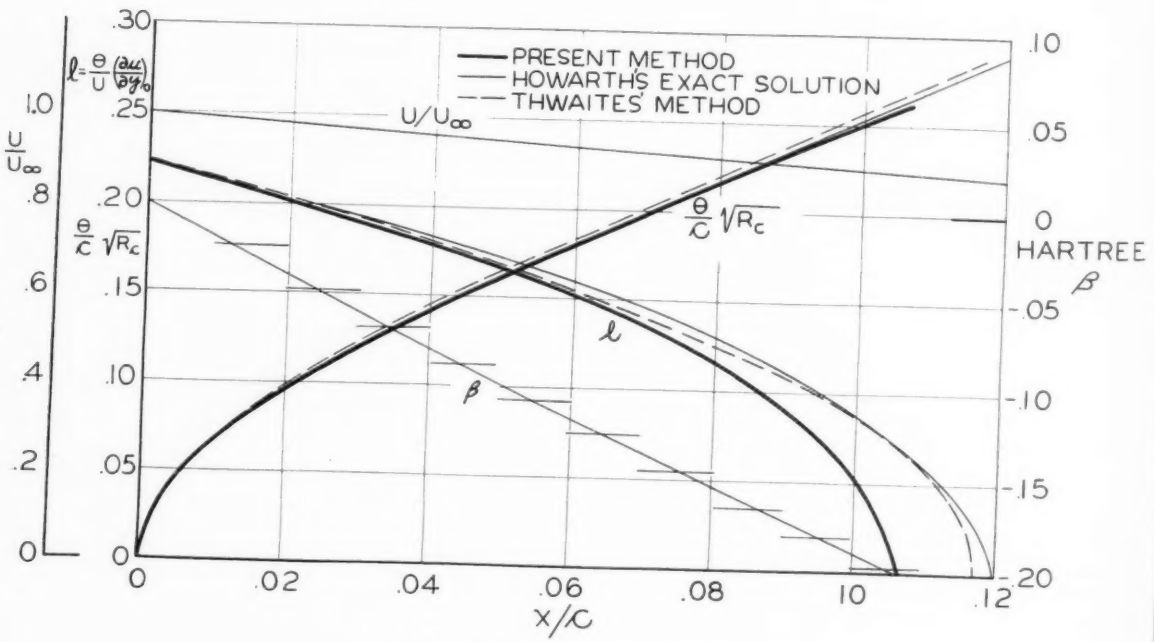

FIG. 6. The flow $U/U_\infty = 1 - (x/c)$.

The table should be self-explanatory, being a straightforward evaluation of Eqs. (11), (12), (15), and (21). A curve of $(2 - \beta)\Theta^2$ versus β should be constructed in order to facilitate evaluation of column 16.

If the flow is two-dimensional, columns 4 and 5 are equal to unity, column 7 becomes equal to column 6, and column 19 to column 18. In order to conserve space, only about half the calculations are shown, but the fundamental results are presented in Fig. 5.

Accuracy

Introductory Comments

The purpose of this section is two-fold: to supply the user additional guidance concerning the length and number of steps to use in a particular problem, and to indicate the general level of accuracy that can be expected of the method, together with its strong and weak features. The assessment of accuracy and comparison of this method with the impressively large number of methods already available could well form a long paper by itself. Fortunately, because considerable evaluation of many of the methods already exists (e.g., references 1, 2, and 3), a significant evaluation is to compare results with the quadrature method, particularly as presented by Thwaites.[9] More precise methods exist, of course, but all are slow and laborious. The present method is rapid but less accurate and, therefore, should be compared with others in this category of which the quadrature method is generally accepted as the best developed to date. Therefore, the method will be evaluated by a sort of contest with Thwaites' method for three different problems, which are believed to form a representative sample. They are the flow[10] $U/U_\infty = 1 - (x/c)$, the flow past an NACA 0012 airfoil,[11] and the flow past Schubauer's ellipse.[12] The first case has 100 per cent decelerating flow, prior to separation; the second has about 30 per cent accelerating and 70 per cent decelerating; and the third has 60 per cent accelerating and 40 per cent decelerating. At this time, it is well to point out that the number of steps used in these three examples is about twice as many as necessary. The three cases are examples meant to represent the highest accuracy producible by either method.

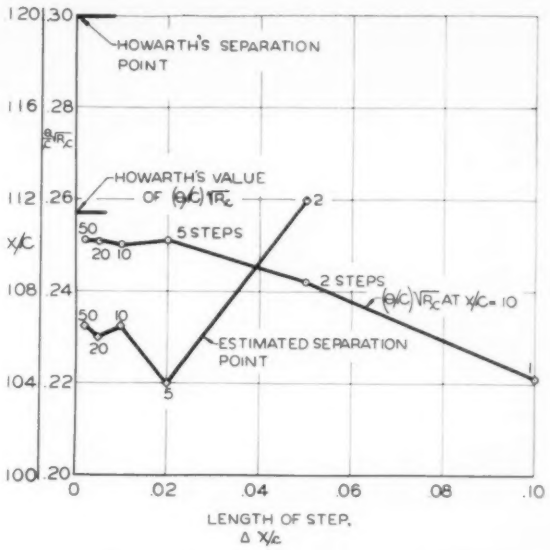

FIG. 7. The flow $U/U_\infty = 1 - (x/c)$: Effect of length of step on the computed values of the separation point and of $(\theta/c)\sqrt{R_c}$ at $x/c = .10$.

The Flow $U/U_\infty = 1 - (x/c)$

The general results are presented in Fig. 6. Three solutions are presented: Howarth's exact solution, Thwaites' quadrature solution taken from reference 9, and the piecewise solution. The major observations about the solutions are: (a) Thwaites' method pre-

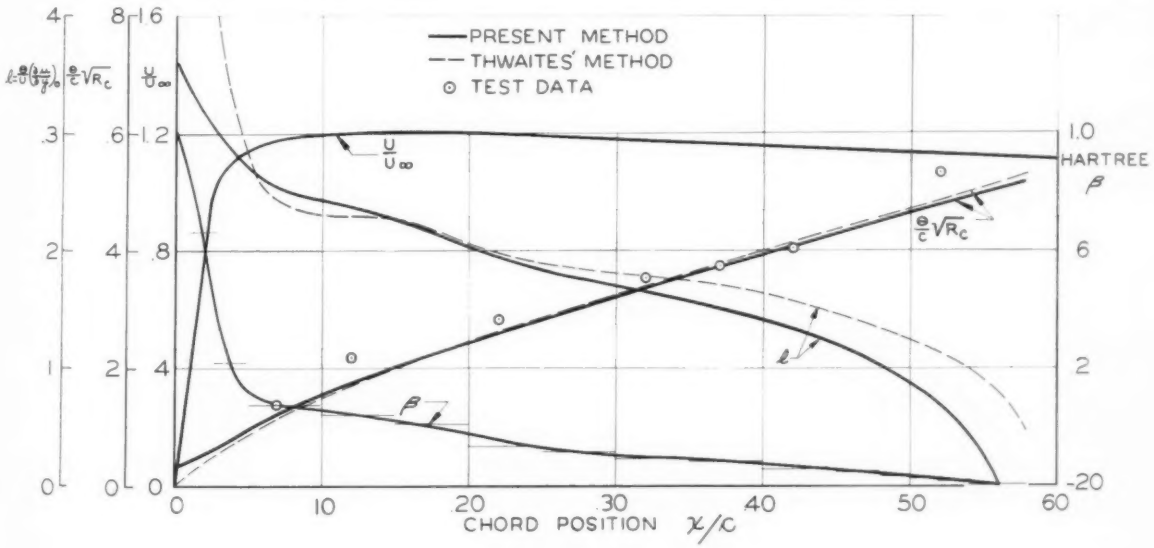

FIG. 8. NACA 0012 airfoil ($\alpha = 0°$).

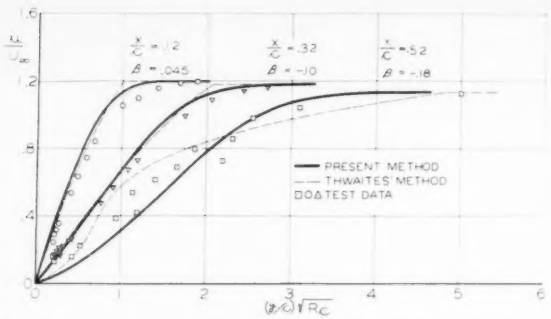

FIG. 9. NACA 0012 airfoil ($\alpha = 0°$). Calculated and experimental boundary-layer profiles.

dicts separation slightly early, the piecewise method appreciably early. (b) The piecewise method is inferior to Thwaites' in the prediction of l, the local skin friction. However, the accuracy of either method is acceptable in the first half of the flow. (c) The piecewise method is slightly superior to Thwaites' in the prediction of $(\theta/c)\sqrt{R_c}$ and, in fact, is very precise as far aft as $x/c = 0.05$.

As shown by the β curve, Fig. 6 represents an eleven-step solution, a number more than sufficient to develop the full accuracy of the method. Fig. 7 provides clues about convergence for this same case using the quantities indicated as measures of accuracy. Since separation occurs at $x/c \approx 0.1065$, the intervals shown, 0.10, 0.05, 0.02, 0.01, 0.005, 0.002, represent solutions of approximately 1, 2, 5, 10, 20, and 50 steps, respectively. For this flow, even the one-step solution predicts $(\theta/c)\sqrt{R_c}$ within 10 per cent of the correct value. The convergence is so rapid that five steps should usually be sufficient unless the very best estimate of separation is to be made, in which case a ten-step solution appears desirable. Yet, even a two-step prediction of separation disagrees with the ten-step prediction by only 5 per cent.

The Flow over an NACA 0012 Airfoil

Results are presented in Figs. 8 and 9. Since no exact solution is available, the present method must be compared with Thwaites' method and the test data. Fig. 8 indicates the following: (a) The two methods are in such good agreement that they appear more accurate than the measurements, as evidenced by the scatter in the experimental values of $(\theta/c)\sqrt{R_c}$. (b) Again the present method predicts separation earlier than Thwaites' method. The experimental location has never been measured, but it apparently lies in the range $0.55 \leq x/c \leq 0.60$.

Fig. 9 compares experimental and calculated boundary-layer profiles. Observe again the large disagreement between several of the measured and calculated values of $(\theta/c)\sqrt{R_c}$, especially at $x/c = 0.12$. Experimental measurement of such profiles becomes very difficult because of the thinness of the boundary layer. Hence, since the test points indicate considerable experimental scatter, a close check with the measured boundary-layer profiles can hardly be expected.

In the forward portion of this airfoil, the fine agreement between Thwaites' method and the piecewise

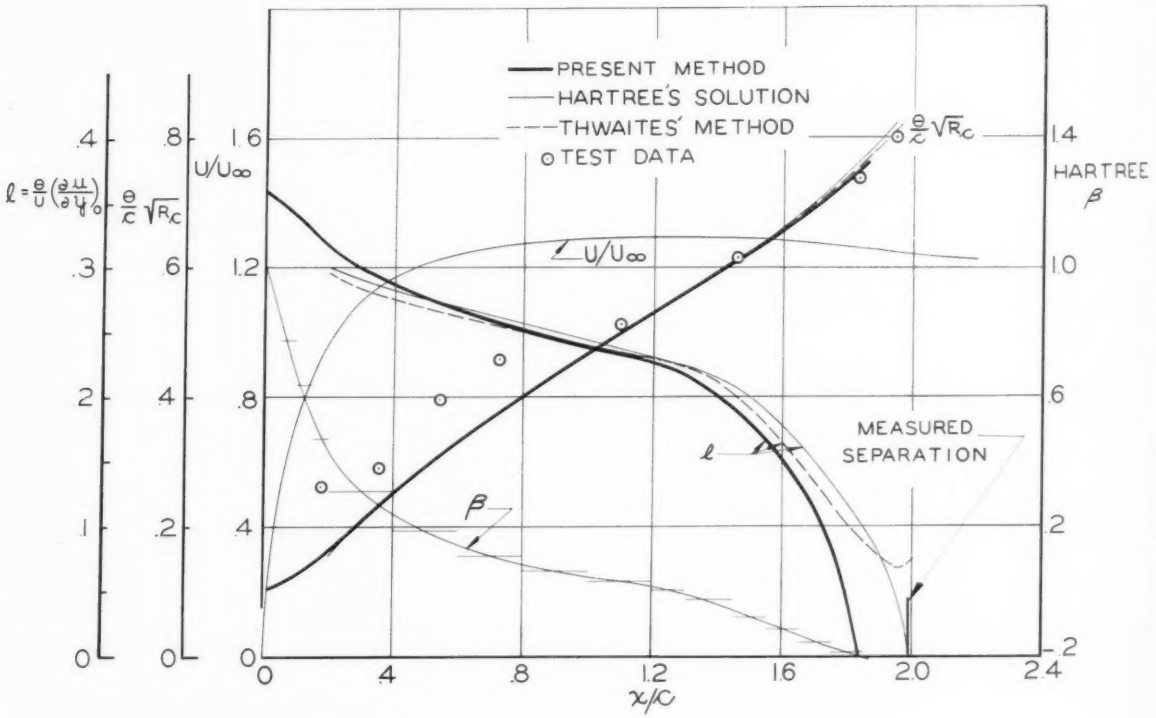

FIG. 10. Schubauer's ellipse.

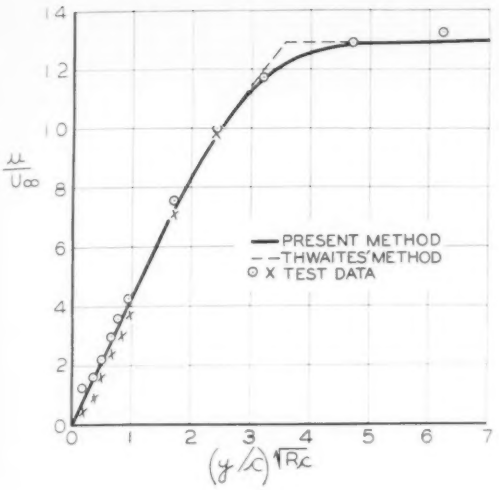

FIG. 11 Schubauer's ellipse. Calculated and experimental boundary-layer profiles at $x/c = 1.457$.

method indicates that calculations should be more accurate than measurement. Von Doenhoff's report shows excellent agreement between experiment and the method of von Kármán and Millikan.[13] It is probable that this agreement was obtained by adjusting the thickness of the calculated profile to match experiment, for the interest was centered around the shape of the profile. Furthermore, the method of reference 13 approximates a particular velocity distribution only in a very general way.

Therefore Fig. 9 brings out the following additional features: (c) Except for thickness discrepancies, the piecewise method approximates the measured profiles rather well. (d) For the first two locations the Thwaites approximation is acceptable but not so good. At $x/c = 0.52$, it is not acceptable.

The Flow Past Schubauer's Ellipse

Results are presented in Figs. 10, 11, 12, and in Table III. Fortunately, this example has an exact solution computed by Hartree on a differential analyzer.[15] Experimental data again are available, but, as with von Doenhoff's test, there is considerable uncertainty about their accuracy. The measured values of $(\theta/c) \times \sqrt{R_c}$ (our c corresponds to Schubauer's L, etc.) shown in Fig. 10 strongly emphasize the difficult experimental problem. From Fig. 10 the following conclusions are evident: (a) Again the piecewise method predicts separation somewhat early. (b) Thwaites' method, however, fails to predict separation. (c) Both methods produce values of $(\theta/c)\sqrt{R_c}$ with substantially three-place accuracy until well back in the region of decelerating flow. Ahead of the pressure peak, the accuracy is too high to show differences graphically, and, for this reason, several selected values are listed in Table III.

Further aft, where the accuracy is deteriorating, we present the profile at $x/c = 1.457$ (Fig. 11). Fig. 11 shows: (d) Both methods produce accurate boundary-layer profiles as far aft as $x/c = 1.457$. (e) The profile produced by the piecewise method is a slightly better approximation. Still further aft, the accuracy of the boundary-layer profiles computed by both methods deteriorates rapidly.

TABLE III
Accuracy Comparison, Schubauer's Ellipse

	Hartree		Thwaites*		Piecewise	
x/c	l	$(\theta/c)\sqrt{R_c}$	l	$(\theta/c)\sqrt{R_c}$	l	$(\theta/c)\sqrt{R_c}$
0.6	0.270	0.331	0.233	0.329	0.269	0.332
1.0	0.242	0.468	0.238	0.465	0.242	0.470
1.4	0.216	0.592	0.211	0.593	0.204	0.592

* Taken from reference 9.

Fig. 12 presents results of a convergence study for this third case. Two indicators of the accuracy are used—the separation point and the value of $(\theta/c)\sqrt{R_c}$ at $x/c = 1.8$. Even two steps indicate the separation point rather well. The results show that, unless the ultimate in accuracy is sought, nine steps are ample. In fact, four steps supply a better prediction of separation than eighteen.

FINAL REMARKS

One of the noticeable characteristics of the piecewise method is that separation is always predicted a trifle prematurely. This quality sometimes may be a drawback, but sometimes it may be an advantage, for it ensures that one will never encounter the difficulty brought out by Schubauer's experiment where separation existed but Pohlhausen's method said it did not. This quality of predicting separation early was shown in striking fashion by Pretsch.[14] He derived the relation between β and Pohlhausen's λ when the entire flow is of the type $U = kx^m$. The relation is

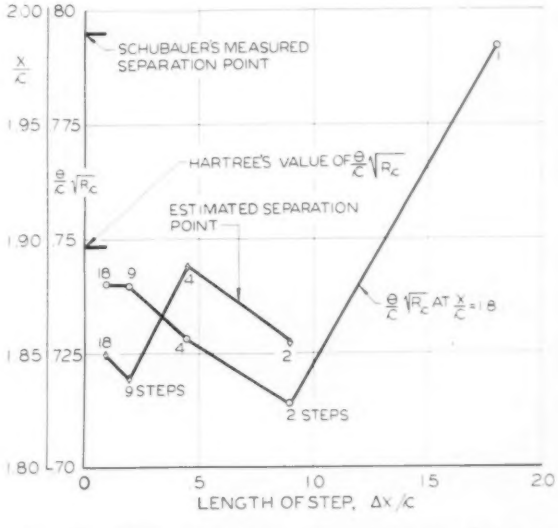

FIG. 12. Schubauer's ellipse. Effect of length of step on the computed values of the separation point and of $\theta/c\sqrt{R_c}$ at $x/c = 1.8$.

$$m = \frac{\beta}{2 - \beta} = -\frac{1}{3} + \frac{10.08\,\lambda^2 - 161.28\,\lambda + 2419.2}{0.6\,\lambda^3 + 36\,\lambda^2 - 1123.2\,\lambda + 7257.6} \quad (23)$$

When $\beta = -0.1988$, corresponding to incipient separation, λ is approximately equal to -8—that is, according to the Pohlhausen method, separation is not ready to occur since λ must reach -12 for such occurrence. At the other extreme, however, the correspondence is good, for Eq. (23) indicates that when $\lambda = +12$, $\beta = +2$.

This latter relation brings up another feature: sometimes the Pohlhausen method breaks down because it is entirely possible for $\lambda = (\delta^2/\nu)\, dU/dx$ to exceed $+12$. Under the same circumstances, the piecewise method would also break down. The difficulty has been encountered several times with erratic pressure distributions where some local irregularity caused dU/dx to be excessively great. In practice, such a "bump" in the plot of velocity distribution will not extend far. Then, one means of avoiding the difficulty is to take a longer step in order to reduce dU/dx. Another is to continue the step as if $\beta = 2$, for no great error in $(\theta/c)\sqrt{R_c}$ will be introduced. Of course, if the interest is in this particular region, the present method is inadequate, and some finite-difference method probably must be used. Thwaites' method shows no obvious breakdown, but it also is likely to prove inadequate, for such special flows are outside the range of approximation in which the quadrature formula has been found to be valid.

References

[1] Goldstein, S., *Modern Developments in Fluid Dynamics*, 1st Ed., Vol. I, Chapter IV; Oxford, 1938.

[2] Mangler, W., *Steady Laminar Boundary Layers; Approximate Methods*, A.V.A. Monographs, Betz, A. (Ed.) Available as British Reports and Translations No. 1002, March 15, 1948.

[3] Wieghardt, K. E. G., *On a Simple Method for Calculating Laminar Boundary Layers*, The Aeronautical Quarterly, Vol. V, Part 1, pp. 25–38, May, 1954.

[4] Eckert, E. R. G., and Livingood, J. N. B., *Method for Calculation of Laminar Heat Transfer in Air Flow Around Cylinders of Arbitrary Cross Section (including large temperature differences and transpiration cooling)*, NACA TR No. 1118, 1953.

[5] Smith, A. M. O., *Improved Solutions of the Falkner and Skan Boundary-Layer Equation*, Sherman M. Fairchild Fund Paper No. FF-10, Institute of the Aeronautical Sciences, March, 1954.

[6] Hartree, D. R., *On an Equation Occurring in Falkner and Skan's Approximate Treatment of the Equations of the Boundary Layer*, Proc. Camb. Philo. Soc., Vol. 33, pp. 223–239, 1937.

[7] Mangler, W., *Die "ähnlichen" Lösungen der Prandtlschen Grenzschichtgleichgungen*, Zeitschr. f. angew. Math. u. Mech., Bd. 23, Heft 5, pp. 241–251, October, 1943.

[8] Mangler, W., *Boundary Layers on Bodies of Revolution in a Symmetrical Flow*, Göttingen A.V.A. Report 45/A/17, 1945.

[9] Thwaites, B., *Approximate Calculation of the Laminar Boundary Layer*, The Aeronautical Quarterly, Vol. I, Part 3, pp. 245–280, November, 1949.

[10] Hartree, D. R., *A Solution of the Laminar Boundary-Layer Equation for Retarded Flow*, British R&M No. 2426, 1949.

[11] von Doenhoff, A. E., *Investigation of the Boundary Layer about a Symmetrical Airfoil in a Wind Tunnel of Low Turbulence*, NACA Wartime Report No. L-507, August, 1940.

[12] Schubauer, G. B., *Air Flow in a Separating Boundary Layer*, NACA TR No. 527, 1935.

[13] von Kármán, Th., and Millikan, C. B., *On the Theory of Laminar Boundary Layers Involving Separation*, NACA TR No. 504, 1934.

[14] Pretsch, J., *The Stability of Two-dimensional Laminar Flow with Pressure Drop and Pressure Rise*, Jahrbuch 1941 d. deutschen Luftfahrtforschung, pp. I/158–175. Also available as British Reports and Translations No. 22, File No. B.I.G.S.-37.

[15] Hartree, D. R., *The Solution of the Equations of the Laminar Boundary Layer for Schubauer's Observed Pressure Distribution for an Elliptic Cylinder*, British R&M No. 2427, 1949.

The Journal of Fluid Mechanics

The *Journal of Fluid Mechanics*, the first issue of which appeared in May, 1956, exists for the publication of theoretical and experimental investigations of all aspects of the mechanics of fluids and is issued in six parts per volume.

Authors wishing to have papers published should communicate them to any one of the persons below, choosing one in their own country where possible.

Editor: Dr. G. K. Batchelor, Cavendish Laboratory, University of Cambridge, Cambridge, England. Assistant Editors: Dr. T. B. Benjamin and Dr. I. Proudman. Associate Editors: Prof. G. F. Carrier, Pierce Hall, Harvard University, Cambridge 38, Mass. Prof. W. C. Griffith, Palmer Physical Laboratory, Princeton University, Princeton, N.J. Prof. M. J. Lighthill, Department of Mathematics, The University, Manchester, England.

Price, £1 ($3.00) per part. *Subscription price*, £5 10*s*. per volume of six parts, post free ($16.50 in U.S.A. and Canada). *Agents for U.S.A. and Canada:* Academic Press Inc., 125 East 23rd St., New York 10, N.Y.

The Effect of Heating and Cooling on the Stability of the Boundary-Layer Flow of a Liquid over a Curved Surface*

R. C. DI PRIMA† AND D. W. DUNN‡
Massachusetts Institute of Technology

SUMMARY

The theory of the three-dimensional instability of laminar boundary layers over curved concave surfaces is extended to include the effects of heat transfer. Results of numerical calculations for the boundary-layer flow of water indicate that heating and cooling of the wall have only a small influence on this type of instability compared to their effect on the usual two-dimensional instability.

(1) INTRODUCTION

THE STABILITY of the isothermal laminar boundary layer over curved surfaces was first considered by Görtler.[1] He found that, for concave curvature, instability occurs with respect to a class of three-dimensional disturbances corresponding to vortices with axes parallel to the principal flow direction. He also obtained the important result that this type of instability, in contrast to that for the two-dimensional Tollmien-Schlichting waves, is relatively insensitive to the shape of the basic velocity profile—i.e., to free-stream pressure gradient—when the relevant parameters are expressed in terms of boundary-layer momentum thickness. Later work on the same problem by other authors[2–5] has been concerned mainly with the procedure for solving the eigenvalue problem.

In the present investigation the theory is extended to the case of a heated or cooled wall. For simplicity, the results are restricted to liquids, so that viscous dissipation and variations in density can be neglected. Detailed numerical calculations for the boundary-layer flow of water over a curved wall show that, just as for pressure gradient, the influence of heating and cooling is also small, at least for liquids, in spite of the effects of temperature disturbances and large variations in basic flow temperature and viscosity.

Received September 26, 1955.

* This investigation was carried out with the support of the Office of Naval Research under Contract N5 ori-07872. The authors would like to thank Prof. C. C. Lin for suggesting this problem and for many helpful discussions. Thanks are also due to the Aeroelastic Computing Laboratory and P. L. Phipps for assistance with the numerical calculations and to R. F. McIntosh for permission to use his unpublished tables of boundary-layer functions.

† Formerly, with the Department of Mathematics, M.I.T. Now, at the Division of Applied Science, Harvard University.

‡ Formerly, with the Department of Mathematics, M.I.T. Now, at the Department of Aeronautics, The Johns Hopkins University.

(2) FORMULATION OF BASIC EQUATIONS FOR THE DISTURBED FLOW

Consider the boundary-layer flow over a curved cylindrical surface with radius of curvature $r(x)$, taken as positive for the concave side of the surface. Let x, y, z be orthogonal curvilinear coordinates, where x is the distance along the arc length of the surface, y the normal distance from the surface, and z the distance in a direction normal to these.

Now consider the complete Navier-Stokes equations in these coordinates for the quantities u, v, w, p, ρ, T (the three velocity components, pressure, density, and temperature, respectively). In the usual manner of the theory of hydrodynamic stability, divide each such quantity $q(x, y, z, t)$ into a steady part $\bar{q}$ and a time-dependent disturbance q' as follows:

$$q(x, y, z, t) = \bar{q}(x, y) + q'(x, y, z, t) \qquad (2.1)$$

Both the quantities $\bar{q}$ and q are to satisfy the complete equations. Linearized equations for the disturbances q' are found in the usual way by neglecting all terms quadratic in the disturbances.

The equations for the basic steady flow, corresponding to the quanties $\bar{q}$, may be reduced to the standard boundary-layer equations after applying the approximations appropriate to the boundary-layer flow of a liquid—e.g., see reference 6. In the present problem, the neglect of density variations is found to be justified, but variations of viscosity and thermal conductivity are appreciable and so must be considered.

The complete linearized disturbance equations are very lengthy in the coordinates used here. A careful examination of them, however, shows that, with the use of approximations analogous to those used in previous investigations,[1, 2, 4, 5] they can be reduced to the following simplified equations:**

$$\bar{\rho}[(\partial u'/\partial t) + (\bar{u}\partial u'/\partial x) + v'(\partial \bar{u}/\partial y)] = -(\partial p'/\partial x) + \bar{\mu}\Delta u' + (\partial \bar{\mu}/\partial y)(\partial u'/\partial y) + \mu'(\partial^2 \bar{u}/\partial y^2) + (\partial \mu'/\partial y)(\partial \bar{u}/\partial y) \qquad (2.2)$$

** Smith[3] retains additional terms in the corresponding equations for the isothermal case.

$$\bar{\rho}[(\partial v'/\partial t) + \bar{u}(\partial v'/\partial x) + 2(\bar{u}u'/r)] = -(\partial p'/\partial y) + \bar{\mu}\Delta v' + 2(\partial\bar{\mu}/\partial y)(\partial v'/\partial y) + (\partial\mu'/\partial x)(\partial\bar{u}/\partial y) \quad (2.3)$$

$$\bar{\rho}[(\partial w'/\partial t) + \bar{u}(\partial w'/\partial x)] = -(\partial p'/\partial z) + \bar{\mu}\Delta w' + (\partial\bar{\mu}/\partial y)[(\partial v'/\partial z) + (\partial w'/\partial y)] \quad (2.4)$$

$$(\partial u'/\partial x) + (\partial v'/\partial y) + (\partial w'/\partial z) = 0 \quad (2.5)$$

$$c_p\bar{\rho}[(\partial T'/\partial t) + \bar{u}(\partial T'/\partial x) + v'(\partial\bar{T}/\partial y)] = \bar{k}\Delta T' + (\partial\bar{k}/\partial y)(\partial T'/\partial y) + k'(\partial^2\bar{T}/\partial y^2) + (\partial k'/\partial y)(\partial\bar{T}/\partial y) \quad (2.6)$$

Here $\Delta = (\partial^2/\partial x^2) + (\partial^2/\partial y^2) + (\partial^2/\partial z^2,)$ and c_p, μ, and k are the specific heat at constant pressure, the viscosity, and the thermal conductivity, respectively. The quantities c_p, μ, and k are in general functions of T for a given liquid at a given pressure p. The variation of c_p is neglected here, since it is very small in the cases considered.

The neglect of terms involving the curvature in these equations causes relative errors of which the largest are of order δ/r, where δ is the boundary-layer thickness. There are similar errors in the boundary-layer equations for the basic flow. Normally these are very small. Also, just as for the basic flow, terms are neglected that arise from variations in density or that are associated with viscous dissipation and pressure effects in the energy equation. These have been estimated and found to be very small also under normal conditions.

The most important approximation in the equations is that of a *nearly-parallel flow*, according to which the x-dependence of the basic flow quantities is neglected as well as the $\bar{v}$ component of the basic velocity. This is one of the standard approximations of the theory of boundary-layer stability, and is usually justified by noting that $\bar{v} \ll \bar{u}$ and $\partial\bar{q}/\partial x \ll \partial\bar{q}/\partial y$ for a boundary layer.

The boundary conditions on the disturbances are that $u' = v' = w' = T' = 0$ for $y = 0$ and $y \to \infty$. The vanishing of the temperature disturbance on the solid boundary (even in the steady case of neutral stability) is a consequence of the rapid spatial oscillation of the disturbances in the cases of interest in this problem. It can be demonstrated by considerations analogous to those in references 7 and 8.

(3) Equations for the Amplitude Functions for Periodic Disturbances

We now introduce nondimensional variables and the particular class of disturbances appropriate to this problem* as follows:

$$\left.\begin{aligned} \bar{u} + u' &= U_1\{U + u(\eta)\cos\alpha z\exp(\beta t)\} \\ v' &= (U_1/R)\{v(\eta)\cos\alpha z\exp(\beta t)\} \\ w' &= U_1\{w(\eta)\sin\alpha z\exp(\beta t)\} \\ \bar{p} + p' &= \rho_1 U_1^2\{P + p(\eta)\cos\alpha z\exp(\beta t)\} \\ \bar{T} + T' &= (T_1 - T_0)\{\Theta + \theta(\eta)\cos\alpha z\exp(\beta t)\} \\ \bar{\mu} + \mu' &= \mu_1\{\mu + (d\mu/d\Theta)T'/(T_1 - T_0)\} \\ \bar{k} + k' &= k_1\{k + (dk/d\Theta)T'/(T_1 - T_0)\} \\ \eta = y/\delta, \quad R &= U_1\delta/\nu_1, \quad a = \alpha\delta, \quad b = \beta\delta^2/\nu_1, \quad \bar{\rho} = \rho_1 \end{aligned}\right\} \quad (3.1)$$

The subscripts 0 and 1 refer to wall and free-stream values, respectively. All the reference quantities are evaluated at the local value of x.

It is to be noted that in order to have disturbances of this special form the neglect of the x-dependence of the coefficients in Eqs. (2.2) to (2.6) is again required.

The final equations for the disturbance amplitude functions u, v, w, p, θ may be reduced to the following, after elimination of p and w:

$$\frac{d}{d\eta}\left(\mu\frac{du}{d\eta}\right) - a^2\mu u + \frac{d}{d\eta}\left(\frac{\partial U}{\partial\eta}\frac{d\mu}{d\Theta}\theta\right) - bu - \frac{\partial U}{\partial\eta}v = 0 \quad (3.2)$$

$$\frac{d^2}{d\eta^2}\left(\mu\frac{d^2v}{d\eta^2}\right) - 2a^2\frac{d}{d\eta}\left(\mu\frac{dv}{d\eta}\right) + \left(a^4\mu + a^2\frac{\partial^2\mu}{\partial\eta^2}\right)v + Sa^2Uu - b\left(\frac{d^2v}{d\eta^2} - a^2v\right) = 0 \quad (3.3)$$

$$\frac{d}{d\eta}\left(k\frac{d\theta}{d\eta}\right) - a^2k\theta + \frac{d}{d\eta}\left(\frac{dk}{d\Theta}\frac{\partial\Theta}{\partial\eta}\theta\right) - \sigma_1\left(\frac{\partial\Theta}{\partial\eta}v + b\theta\right) = 0 \quad (3.4)$$

where $\sigma_1 = c_p\mu_1/k_1$ is the Prandtl Number at temperature T_1 and $S = 2R^2\delta/r$. The boundary conditions are

$$u = v = dv/d\eta = \theta = 0 \quad (3.5)$$

for $\eta = 0$ and $\eta \to \infty$.

As pointed out previously, the most important approximation in all this work is the assumption of a nearly-parallel basic flow. There are indications that, although this approximation is probably accurate for large values of a or b, it may not be as satisfactory for small values. Hence, there is expected to be some inaccuracy in the determination of the curve of neutral stability, for example, for small values of a.† How-

* Disturbances which amplify in x rather than t may be more significant physically. In this case $\exp(\beta t)$ should be replaced by $\exp(\beta x)$ in Eqs. (3.1) (a further refinement being suggested by Smith[3]). The results for neutral stability are the same in either formulation.

† For the isothermal boundary layer, the discrepancy between the neutral curves of Görtler[1] and Hämmerlin[5] for small a is due to the failure of Görtler's numerical procedure in this case, and not to the difficulty mentioned above. Both authors use the equations corresponding to the approximation of a nearly parallel flow.

ever, since we are interested in only a rough estimate of the effect of heating and cooling, the simplified equations for a nearly-parallel flow are adequate for present purposes.

A more complete derivation of the basic equations of this theory and a detailed analysis of the various approximations involved will be presented in a future paper.

(4) Solution of the Eigenvalue Problem

Henceforth we consider just the case of neutral stability—i.e., $b = 0$—for which the eigenvalue S is a function of a only. In the solution of the eigenvalue problem, it is convenient to use the Galerkin method. A general discussion of this is given in reference 9, and applications to problems in hydrodynamic stability are described in references 3 and 4. The method may be expected to give good results in stability problems of the present type where there is no inner critical layer through which the eigenfunction varies rapidly.

The three differential equations of this problem are of the form $L_\alpha(u) + M_\alpha(v) + N_\alpha(\theta) = 0$, $\alpha = 1, 2, 3$, where L_α, M_α, N_α are linear differential operators. If u, v, θ are each expanded in terms of a complete set of functions as follows:

$$u = \sum_1^\infty a_i u_i \qquad v = \sum_1^\infty b_i v_i \qquad \theta = \sum_1^\infty c_i \theta_i \tag{4.1}$$

where each of the functions u_i, v_i, θ_i satisfies the boundary conditions (3.5), then formal application of the Galerkin method leads to the following equations for the determination of the constants a_i, b_i, c_i:

$$\sum_{i=1}^\infty \left\{ a_i \int_0^\infty u_j L_1(u_i)\,d\eta + b_i \int_0^\infty u_j M_1(v_i)\,d\eta + c_i \int_0^\infty u_j N_1(\theta_i)\,d\eta \right\} = 0 \tag{4.2}$$

with $j = 1, 2, 3, \ldots$, plus two similar sets of equations obtained from the second and third differential equations with v_j and θ_j, respectively, in place of u_j. Thus, if each of u, v, and θ is approximated by n terms in its series expansion, we obtain an eigenvalue determinant of order $3n$, which, when set equal to zero, determines $S(a)$.

For the functions u_i, v_i, θ_i it is convenient to take*

$$\left.\begin{aligned} u_i &= \zeta^{(i+1)/2}(1-\zeta), && i = 1, 3, 5, \ldots; \\ u_i &= \zeta(1-\zeta)^{(i+2)/2}, && i = 2, 4, 6, \ldots; \\ v_i &= \zeta(1-\zeta)u_i, && \theta_i = (1-\zeta)u_i \end{aligned}\right\} \tag{4.3}$$

where $\zeta = 1 - \exp(-\eta)$. In an eigenvalue problem of the present type, great care is required in making a *finite* selection from the functions u_i, v_i, θ_i to give a good approximation to the eigenfunction with a finite number of terms, since the characteristic length scale of the eigenfunction depends on the parameter a. In fact, a study of the analytical behavior of the solutions of Eqs. (3.2) to (3.4) shows that in general u, v, and θ fall away to zero for $\eta = 0(1/a)$ when $b = 0$.

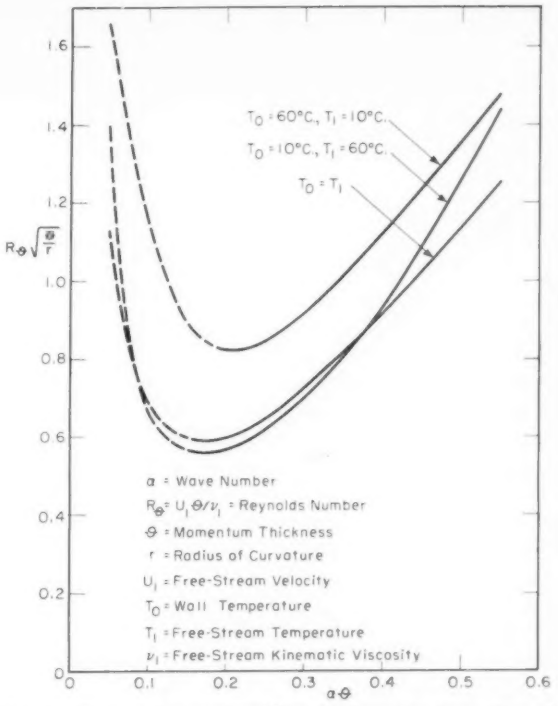
$T_0 = 60°C.$, $T_1 = 10°C.$
$T_0 = 10°C.$, $T_1 = 60°C.$
$T_0 = T_1$
$R_\vartheta\sqrt{\frac{\vartheta}{r}}$
$a\vartheta$
a = Wave Number
$R_\vartheta = U_1\vartheta/\nu_1$ = Reynolds Number
ϑ = Momentum Thickness
r = Radius of Curvature
U_1 = Free-Stream Velocity
T_0 = Wall Temperature
T_1 = Free-Stream Temperature
ν_1 = Free-Stream Kinematic Viscosity

Fig. 1. Curves of neutral stability for boundary-layer flow of water over heated and cooled curved surfaces.

In the present work, we use two-term approximations involving u_i, v_i, θ_i for $i = 1$ and 7,† and take $\delta = 6\vartheta$ (ϑ being the momentum thickness) as a convenient reference length of the order of the boundary-layer thickness. Consideration of the behavior of the eigenfunction (u, v, θ) mentioned above shows that this combination of the functions u_i, v_i, θ_i should give satisfactory results in the range of values of a of order unity. Such values, which correspond to wave lengths of the order of the boundary-layer thickness, are expected to be of most interest physically.

It should be pointed out, of course, that this approximate calculation procedure is likely to fail for small wave numbers just as Görtler's did for the isothermal case.[1, 5] However, in the region of interest the results should be sufficiently accurate to give the magnitude of the effects of heating and cooling. Moreover, Hämmerlin's accurate neutral curve[5] for such values of a in the isothermal case is still not too different from that obtained by Görtler or the present authors.

Numerical calculations of the stability characteristics have been carried out for the boundary-layer flow of water with zero free-stream pressure gradient in three cases—(a) heated wall with $T_0 = 60°C.$, $T_1 = 10°C.$, (b) cooled wall with $T_0 = 10°C.$, $T_1 = 60°C.$, and (c) insulated wall. For a liquid, the last case is essentially the isothermal boundary layer with Blasius velocity

* Although the functions u_i (and thus v_i and θ_i) are not linearly independent, it is useful to list them all in order to have a wider selection for an approximation involving a finite number of terms.

† Any other combination not too different from this should give equally satisfactory results.

distribution[10] considered by Görtler. For the heated and cooled walls, the distributions of velocity, temperature, viscosity, and thermal conductivity in the boundary layer were obtained from exact numerical computations carried out by McIntosh.[11] For convenience, the exact distributions were approximated in all cases by means of polynomials in the variable ζ. The results of the calculations are shown in Fig. 1.

(5) Discussion of Results and Concluding Remarks

The neutral curve for the isothermal case in Fig. 1 agrees closely with that obtained by Görtler using a different method of calculation. The curves for the other two cases indicate that heating stabilizes the boundary layer while cooling destabilizes it. However, the effects are relatively small, considering the strong temperature dependence of the viscosity and the corresponding large variations in the viscosity across the boundary layer. That is, even though the temperature change of 50° is a small amount on the absolute scale the viscosity is changed by a factor of 3 (in our case, $\mu_0/\mu_1 = 0.358$ for heating and $\mu_0/\mu_1 = 2.79$ for cooling). Even with the use of more accurate equations and a more accurate calculation procedure for small wave numbers (see reference 5), these conclusions are expected to remain the same.

The present results are in marked contrast to those for the two-dimensional Tollmien-Schlichting type of instability, which is extremely sensitive to heating and cooling. In fact, McIntosh[11] calculated the minimum critical Reynolds Number for this type of instability in the two cases considered here, and found that heating increased it and cooling decreased it* from the isothermal value[12] by factors of the order of ten.

The strong dependence of this two-dimensional type of instability on the wall temperature is ultimately due to the presence of an inner critical layer through which the eigenfunction varies rapidly. The results thus depend critically on the *local* properties of the basic-flow velocity, temperature, and viscosity distributions (especially on $\partial^2\bar{u}/\partial y^2$, for example), which are very sensitive to the wall temperature. For the three-dimensional type of instability considered here, however, there is no inner critical layer and the centrifugal force is the controlling factor. Hence, the results depend only on the overall properties of these basic-flow distributions, such as the average velocity gradient U_1/δ, which are much less influenced by the wall temperature. The relative importance of the wall temperature in the two types of instability is therefore similar to that of the free-stream pressure gradient, as discussed by Görtler.[1]

The present conclusion, that heating and cooling have only a slight influence on the three-dimensional instability of boundary layers over curved surfaces for a liquid, is likely also true for a gas at low Mach Numbers and rates of heat transfer, when density variations are negligible. It may not be true, however, in other circumstances, since the disturbance equations for a gas, with density variations included, are considerably more complicated than the present ones, even after all possible simplifications are made.

* The effects for a liquid are opposite to those for a gas because of the opposite variation of viscosity with temperature.

References

[1] Görtler, H., *Über eine dreidimensionale Instabilität laminarer Grenzschichten an konkaven Wänden*, Gess. d. Wiss. Göttingen, Nachr. a.d. Math., Bd. 2, Nr. 1, 1940 (translated as NACA TM 1375).

[2] Meksyn, D., *Stability of Viscous Flow over Concave Cylindrical Surfaces*, Proc. Roy. Soc. London A, Vol. 203, pp. 253–265, 1950.

[3] Smith, A. M. O., *On the Growth of Taylor-Görtler Vortices along Highly Concave Walls*, Quart. Appl. Math., Vol. 13, pp. 233–262, 1955.

[4] Di Prima, R. C., *Application of the Galerkin Method to Problems in Hydrodynamic Stability*, Quart. App. Math., Vol. 13, pp. 55–62, 1955.

[5] Hämmerlin, G., *Über die Lösung des Eigenwertproblems der Görtlerschen Instabilitäten laminarer Grnezschichten längs konkaven Wänden*, J. Rat. Mech. and Anal., Vol. 4, pp. 279–328, 1955.

[6] Howarth, L., *Modern Developments in Fluid Dynamics—High Speed Flow*, Vol. II, pp. 760–761, pp. 766–769, Oxford University Press, 1953.

[7] Dunn, D. W., and Lin, C. C., *On the Stability of the Laminar Boundary Layer in a Compressible Fluid*, Journal of the Aeronautical Sciences, Vol. 22, No. 7, pp. 455–477, July, 1955.

[8] Dunn, D. W., *On the Theory of the Stability of the Boundary Layer in a Compressible Fluid*, (to be published).

[9] Frazer, R. A., Duncan, W. J., and Collar, A. R., *Elementary Matrices*, pp. 224–231, Cambridge University Press, 1950.

[10] Goldstein, S., *Modern Developments in Fluid Dynamics*, Vol. I, pp. 135–139, Oxford University Press, 1938.

[11] McIntosh, R. F., Unpublished Investigation, M.I.T. Mathematics Department, 1954.

[12] Lin, C. C., *On the Stability of Two-Dimensional Parallel Flows*, Part III, Quart. App. Math., Vol. 3, No. 4, pp. 277–301, 1946.

The Dynamic Response of a Large Airplane to Continuous Random Atmospheric Disturbances

FRANKLIN W. DIEDERICH*

Langley Aeronautical Laboratory, NACA

SUMMARY

The statistical approach to the gust-loads problem, which consists in considering flight through turbulent air to be a stationary random process, is extended by including the effect of lateral variations of the instantaneous gust intensity on the aerodynamic forces and on the resultant motions and stresses of rigid and flexible airplanes. By means of some calculations of normal and rolling accelerations, as well as of the root bending moment, it is shown that these effects may be significant for large airplanes.

SYMBOLS

A	= aspect ratio
b	= span
BM	= root bending moment
$\bar{c}$	= average chord, S/b
$C(k)$	= Theodorsen's unsteady lift function
$\tilde{C}(k)$	= generalized Theodorsen function
C_{L_α}	= wing lift-curve slope
C_{l_p}	= coefficient of damping in roll
cc_l	= section loading coefficient
EI	= bending stiffness
g	= acceleration due to gravity
$h(t)$	= response to unit impulsive gust or other input
$h(t, y)$	= response influence function
$H(\omega)$	= complex amplitude of response to sinusoidal gust or other input of unit amplitude, Fourier transform of $h(t)$
$H(\omega, y)$	= complex amplitude of response influence function, Fourier transform of $h(t, y)$ with respect to t
$\tilde{H}(\omega, \eta)$	= autoconvolution function for $H(\omega, y)$
$\hat{H}(\omega, \omega')$	= Fourier transform of $H(\omega, y)$ with respect to y
I_x	= mass moment of inertia about the roll axis
J_1	= Bessel function of the first kind, order 1
k	= reduced frequency, $\omega\bar{c}/2U$
k'	= dimensionless frequency, $\omega L^*/U$
K_0, K_1	= modified Bessel functions of the second kind
l	= lift per unit span
L	= lift
L'	= rolling moment
L''	= generalized lift associated with first free-free bending mode
L^*	= scale of turbulence
m	= mass per unit span
M	= airplane mass
M_w	= wing mass
M'	= generalized mass associated with the first free-free bending mode
N	= number of peaks per unit time above a given level
Δn	= load-factor increment
p	= rate of roll
q	= dynamic pressure
S	= wing area
t	= time
U	= flying speed
w	= vertical component of gust velocity
x	= longitudinal displacement
y	= lateral displacement
y^*	= dimensionless lateral displacement, $y/(b/2)$
$\bar{y}$	= lateral ordinate of center of pressure
$\bar{y}$	= lateral ordinate of center of wing mass
z	= normal displacement
z^0	= normal displacement of nodal point
z_1	= generalized normal displacement for the first free-free bending mode
z^*	= dimensionless normal displacement, $z/(\bar{c}/2)$
α	= local angle of attack
$\gamma(y)$	= spanwise distribution of the influence function $h(t, y)$
$\gamma_L(y)$	= lift influence function, $[cc_l/\bar{c}C_{L_\alpha}]_{\alpha=1}$
$r_L'(y)$	= rolling moment influence function, $[cc_l/\bar{c}(-C_{l_p})]_{\alpha=y^*}$
$\Gamma(\eta)$	= autoconvolution of $\gamma(y)$
η	= lateral space displacement, Δy
η^*	= dimensionless lateral space displacement, $\eta/(b/2)$
ζ	= mode shape of first free-free bending mode
κ	= airplane mass parameter, $8M/C_{L_\alpha}\rho S\bar{c}$
κ_r	= airplane rolling-inertia parameter, $8I_x/(-C_{l_p})\rho S^2 b$
ρ	= air density
σ	= stress
τ	= time displacement, Δt
ψ	= one-dimensional correlation function
Ψ	= two-dimensional correlation function
φ	= one-dimensional power spectrum
$\bar{\varphi}$	= two-dimensional power spectrum
$\bar{\Phi}$	= double Fourier transform of Ψ
$\hat{\varphi}$	= double Fourier transform of Ψ for axisymmetric case
ϕ	= Sears' unsteady lift function for gust penetration
ω	= frequency

Presented at the Aeroelasticity Session, Twenty-Third Annual Meeting, IAS, New York, January 24–27, 1955.

* Head, Dynamic Loads Analysis Section.

The author wishes to acknowledge the assistance furnished by Messrs. Kermit G. Pratt, Robert T. Yntema, Floyd V. Bennett, and John M. Eggleston of Langley Aeronautical Laboratory, NACA, in performing the calculations described herein.

INTRODUCTION

THE LOCAL AIR velocity fluctuations sensed by an airplane flying through atmospheric turbulence are functions of time defined in only a statistical sense—that is, they constitute a stochastic or random process. Consequently, the responses of the airplane, such as the motions or stresses, can also be known as functions of time in only a statistical sense.

The problem of relating the statistical characteristics of the input of a dynamic system to those of the

output gives rise to the relatively new field of statistical dynamics. (Some of the fundamental papers in this field are compiled in reference 1.) The techniques of this field, in particular those related to the generalized harmonic analysis of stationary random processes, have been applied to the gust-loads problem and related problems in aeronautics in recent years to an ever increasing extent.[2–6]

In these analyses the assumption has been made that the variation of the instantaneous gust intensity along the span can be disregarded. The type of gust structure envisioned in this approach is thus, in effect, the one shown in the *upper* part of Fig. 1, which will be referred to hereafter as the one-dimensional gust. The purpose of this paper is to take into account the variation along the span and to treat the more realistic gust structure represented in the *lower* part of Fig. 1, which will be referred to as the two-dimensional gust.

Thus, the problem is essentially one of determining the response of a linear system—namely, the airplane—to a multidimensional stationary random process—namely, atmospheric turbulence. (The assumptions of linearity and stationarity have been made in references 2 to 6 and are valid for many practical purposes connected with the gust-loads problem.) The somewhat similar problem of a finite-length correction for a hot-wire anemometer has been treated in references 7 and 8; some phases of the present problem have been considered in reference 9; and a fairly extensive analysis of the problem is given in reference 10, which forms the basis of the present paper.

The solution to the problem will be outlined briefly in the following, and the results of some calculations of the accelerations and bending moments in continuous random turbulence will then be presented in an effort to indicate the possible magnitude of the effects under consideration. The derivation of the solution presented here and some of the details of the calculations are given in the Appendixes.

The Basic Relations Between the Input and Output of a System Subjected to a Random Input

Summary of the Relations Appropriate to a One-Dimensional Gust Structure

Before discussing the analysis of the loads and motions corresponding to a two-dimensional random gust structure, a brief outline of the analysis for a one-dimensional random gust structure may be in order.

The bridges which link the statistical characteristics of the input and the output of a dynamic system subjected to a stationary random input are certain relations between the correlation functions or the power spectra of the input and output, respectively. For the present case the input is the gust intensity w, and its correlation function is defined by

$$\psi_w(\Delta x) = \overline{w(x)w(x + \Delta x)} \tag{1}$$

where the bar designates a time average. The correlation function is a statistical characteristic which is a measure of the extent to which the value of one random variable, in this case $w(x + \Delta x)$, can be predicted from a knowledge of that of another random variable, in this case $w(x)$; it contains the mean square value of the quantity of interest, inasmuch as

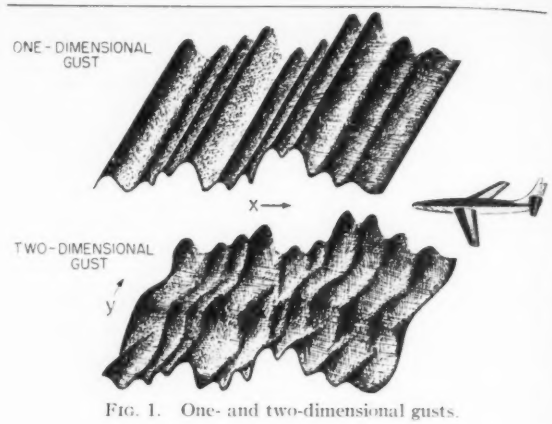

Fig. 1. One- and two-dimensional gusts.

$$\overline{w^2} = \psi_w(0) \tag{2}$$

and contains certain additional information. For instance, the mean square value of the derivative of w is given by

$$\overline{(dw/dx)^2} = -\left\{ [d^2/d(\Delta x)^2]\, \psi_w(\Delta x) \right\}_{\Delta x = 0} \tag{3}$$

A possibly even more useful statistical characteristic is the Fourier transform of the correlation function—namely,

$$\varphi_w(\omega) = \frac{1}{\pi} \int_{-\infty}^{\infty} e^{-i\omega(\Delta x/U)}\, \psi_w(\Delta x)\, d\left(\frac{\Delta x}{U}\right) \tag{4}$$

(The flying speed U is introduced here because the airplane senses the turbulent excitation fundamentally as a function of time, whereas the statistical characteristics of turbulence of interest here are functions primarily of space displacements. These space displacements have to be identified with equivalent time displacements in calculating the response of the airplane.) The function $\varphi_w(\omega)$ is referred to as the power spectrum of w. It represents the part of the mean square value associated with various frequencies. In other words, if the random process w were passed through a filter which permitted only frequencies within a band of unit width about the frequency ω to pass, the mean square value of the filtered process would be $\varphi_w(\omega)$. Thus, the information it contains includes the mean square value of the process,

$$\overline{w^2} = \int_0^{\infty} \varphi_w(\omega)\, d\omega \tag{5}$$

as well as the mean square value of the time derivative of the process,

$$\overline{\dot{w}^2} = \int_0^{\infty} \varphi_w(\omega)\, \omega^2\, d\omega \tag{6}$$

The correlation function and power spectrum of the

output—say the load factor increment Δn—are defined in a similar manner. The input-output relation for stationary random processes then becomes in this case

$$\varphi_{\Delta n}(\omega) = \left| H_{\Delta n}{}^{w}(\omega) \right|^2 \varphi_w(\omega) \tag{7}$$

where $H_{\Delta n}{}^{w}(\omega)$ is the transfer function of the system, which represents the complex amplitude of the load factor response of the airplane to sinusoidal gusts of unit amplitude and of wave length $2\pi U/\omega$.

From the power spectrum of the output such statistical quantities as the mean square value and the mean square derivative can then be obtained directly by the equivalent of Eqs. (5) and (6). From these quantities, in turn, other statistical characteristics of interest can be obtained on the basis of certain assumptions. For instance, if the probability distribution of the process is Gaussian, the expected number N of peaks in the load factor exceeding a given level Δn per unit time can be obtained from Rice's asymptotic expression given in reference 1—namely,

$$N = (1/2\pi) \sqrt{\overline{\Delta \dot{n}^2}/\overline{\Delta n^2}}\, e^{-(1/2)[(\Delta n)^2/\overline{\Delta n^2}]} \tag{8}$$

valid for $\Delta n > 2\sqrt{\overline{\Delta n^2}}$. This expression, which also furnishes an estimate of the expected time $1/N$ required to encounter a peak load factor increment equal to or greater than Δn, is shown plotted in Fig. 2. The ratio $\sqrt{\overline{\Delta \dot{n}^2}}/\sqrt{\overline{\Delta n^2}}$ has the dimensions of a frequency and can be considered to be a representative or predominant frequency of the time history of Δn. If the transfer function has the characteristics of a narrow band-pass filter, which may be the case if the airplane is on the verge of an instability condition (due to loss of aerodynamic damping or aeroelastic action), this representative frequency is the frequency ω_0 at which the airplane or wing tends to oscillate.

The Input-Output Relation for a Two-Dimensional Gust Structure

For the two-dimensional gust, the progression from input to output is fundamentally the same. However, some of the concepts referred to in the preceding paragraphs have to be generalized. A two-dimensional correlation function for the input can be defined as

$$\bar{\varphi}_w(\Delta x, \Delta y) = \overline{w(x, y)\, w(x + \Delta x, y + \Delta y)} \tag{9}$$

This correlation function relates the gust velocities at points x, y and $x + \Delta x$, $y + \Delta y$. In most cases its value should be independent of the orientation of the two points relative to each other and depend only on the distance between them, so that an airplane flying from east to west senses the same gust variation, in a statistical sense, as an airplane flying north to south, or in any other direction. In this case, the two-dimensional correlation function can readily be expressed in terms of the one-dimensional function,

$$\bar{\varphi}_w(\Delta x, \Delta y) = \psi_w(\sqrt{\Delta x^2 + \Delta y^2}) \tag{10}$$

This property of the turbulence is referred to as axisymmetry (with respect to a vertical axis) and represents a less restrictive assumption than that of isotropy, which is usually assumed in studies of turbulence. In the following, the turbulence under consideration will be assumed to have this property.

A two-dimensional power spectrum may then be defined as the Fourier transform with respect to Δx of the two-dimensional correlation function,

$$\bar{\varphi}_w(\omega, \Delta y) = \frac{1}{\pi} \int_{-\infty}^{\infty} e^{-i\omega(\Delta x/U)}\, \psi_w(\Delta x, \Delta y)\, d\left(\frac{\Delta x}{U}\right) \tag{11}$$

In deriving an input-output expression which relates the power spectrum of some output, say, the stress σ at some point in the wing, to this two-dimensional input spectrum, a convenient starting point is the superposition integral which relates the instantaneous value of the output to the past history of the input at various stations on the wing,

$$\sigma(t) = \int_{-\infty}^{\infty} \int_{-(b/2)}^{b/2} h(t_1, y)\, w(t - t_1, y)\, dy\, dt_1 \tag{12}$$

The required response function $h(t, y)$ is actually an influence function, which defines the influence of the gust intensity at a station y and a time t on the output. This function represents the response, say the stress σ, to a very narrow impulsive gust which at time $t = 0$ impinges on the wing at station y. In principle, such a response function could be calculated if the indicial pressure or lift distribution on the wing were known for impulsive gusts impinging on the wing over a very narrow front. For a given location y of gust impingement and a given time t, such a lift-distribution function would tend to look similar to the one indicated by cross hatching in the upper part of Fig. 3. The desired influence function $h(t, y)$ could then be obtained by calculating the integrals and moments and, hence, the stresses associated with this lift distribution for each value of t and y. For a stress which is propor-

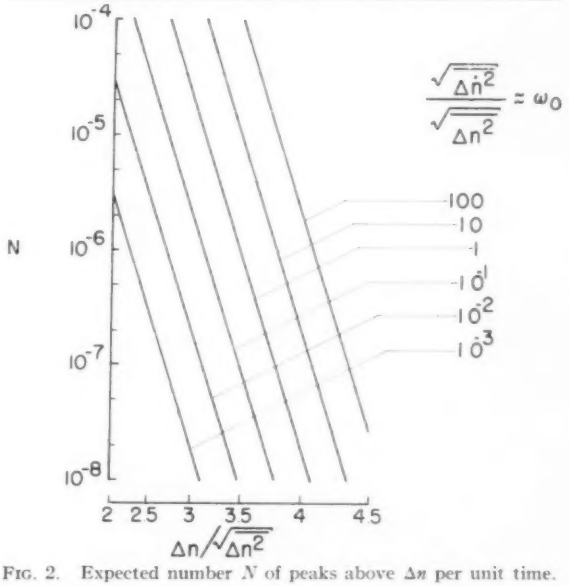

FIG. 2. Expected number N of peaks above Δn per unit time.

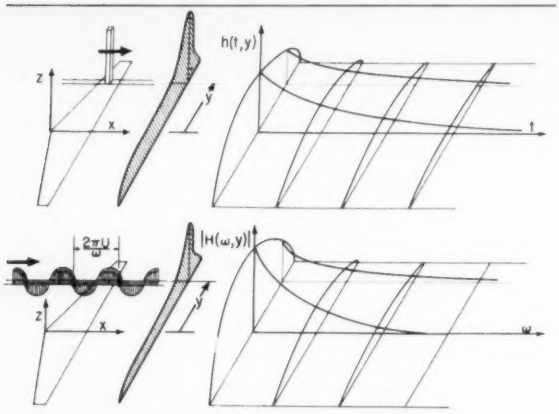

FIG. 3. Influence functions for two-dimensional gust.

tional to the total lift or vertical shear, such a function is shown at the right in the upper part of Fig. 3.

For practical purposes, this direct approach suffers from the fact that the required indicial pressure- and lift-distribution functions are very difficult to calculate. However, the integrals and moments of these functions and, hence, the desired function $h(t, y)$ can be identified with relatively easily calculated lift distributions on the same wing in reverse flow by means of the reciprocity theorem of linearized lifting-surface theory.[11]

The Fourier transform $H(\omega, y)$ of $h(t, y)$ represents the complex amplitude of the response to sinusoidal gusts of unit amplitude and with wave length $2\pi U/\omega$ impinging on the wing at station y, as indicated in the lower part of Fig. 3. The direct calculation of this function again requires a knowledge of pressure or lift distributions due to very narrow sinusoidal gusts, which are very difficult to calculate, and, for a given y and ω, would look like the one indicated by cross-hatching. But again, the required integrals and moments can be identified with certain lift distributions on the wing in reverse flow. The specific nature of these lift distributions for the various cases considered here is indicated in Appendix B.

In terms of the two-dimensional input spectrum $\tilde{\varphi}_w(\omega, \Delta y)$ and the influence function $H_\sigma{}^w(\omega, y)$, the output spectrum can then be expressed as follows:

$$\varphi_\sigma(\omega) = \int_{-(b/2)}^{b/2} \int_{-(b/2)}^{b/2} H_\sigma{}^w(\omega, y_2)\, [H_\sigma{}^w(\omega, y_1)]^* \times \tilde{\varphi}_w(\omega, y_2 - y_1)\, dy_1 dy_2 \quad (13)$$

where the asterisk designates that the complex conjugate of $H_\sigma{}^w(\omega, y_1)$ is to be taken. This expression then represents the input-output relation for the two-dimensional gust, analogous to Eq. (7) for the one-dimensional gust.

Once the power spectrum of σ has been obtained in this manner, the mean square value and the value of the mean square derivative are obtained by integration [see Eqs. (5) and (6)], and other statistical characteristics, such as the expected number of peaks, can then be calculated from these values, as before.

RESULTS OF CALCULATIONS

Spectrum of the Lift Due Directly to Turbulence

One of the basic quantities in any calculation of the dynamic response of an airplane to turbulence is the lift produced directly by the turbulence. In order to indicate how this lift is affected by the averaging effect of the span, the spectrum $\varphi_{w_e}(\omega)$—in dimensionless form—of the gust velocity averaged over the span (with a weighting factor which depends on the lift-producing capabilities of the various stations along the span, and which is here taken as unity) is shown in Fig. 4. The abscissa is a reduced frequency and the parameter a dimensionless span, both of which contain a length L^* which will be referred to as the scale of turbulence. The scale of turbulence is here defined as twice the integral of the function $\psi_w(\Delta x)$ divided by $\overline{w^2}$—that is,

$$L^* = 2 \int_0^\infty \frac{\psi_w(\Delta x)}{\overline{w^2}}\, d(\Delta x) \quad (14)$$

or

$$L^* = \pi U [\varphi_w(0)/\overline{w^2}] \quad (15)$$

Intuitively, it may be thought of as a distance such that the instantaneous gust velocities at points separated by less than that amount tend to be similar, whereas those at points separated by a greater amount tend to be substantially independent of each other in a statistical sense.

The correlation function $\psi_w(\Delta x)$ to which these calculations pertain is indicated at the right of Fig. 4; this correlation function is a simple analytical expression suggested by measurements of turbulence in wind tunnels; it agrees fairly well with the available knowledge of the correlation function of atmospheric turbulence[2, 5] and has been used previously for gust-loads calculations in reference 4. On the basis of the available knowledge the scale of atmospheric turbulence appears to be in the order of at least several hundred feet, although near the ground it may be somewhat smaller.

When the span is very small, there is no averaging effect, and $\varphi_{w_e}(\omega)$, the spectrum of the averaged gust intensity, becomes $\varphi_w(\omega)$, the spectrum of the unaveraged gust intensity. This function is the one

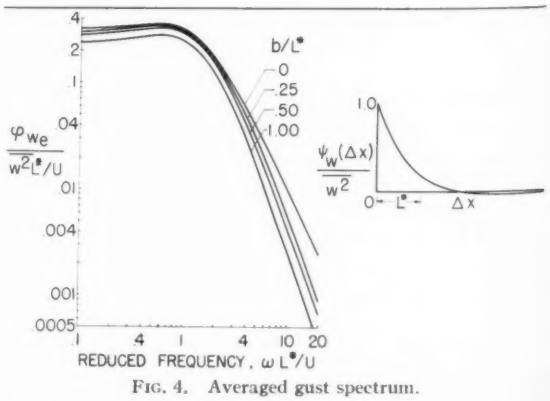

FIG. 4. Averaged gust spectrum.

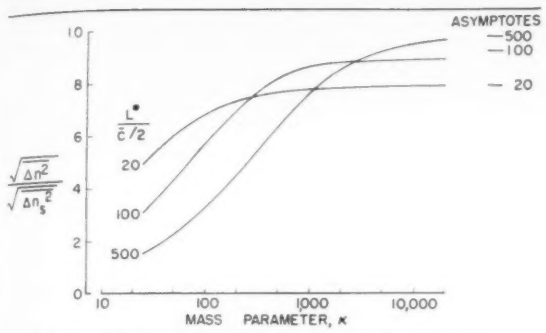

FIG. 5. Effect of airplane mass on normal acceleration.

shown for $b/L^* = 0$. As the span increases, the averaging effect becomes more and more pronounced and serves to attenuate the spectrum at all frequencies, but particularly at high frequencies, as may be expected since the tendency for gusts of very short wave lengths (or high frequencies) to cancel each other is much greater than that of gusts of larger wave lengths.

The spectrum of the lift is obtained essentially by multiplying the spectrum for the averaged gust velocity by the absolute square of the unsteady lift function for gust penetration (the so-called Sears function in the case of two-dimensional incompressible flow), and the mean square of the lift is then obtained by integrating the lift spectrum. Inasmuch as this unsteady lift function is unaffected by the averaging process, the effects of averaging on $\varphi_w(\omega)$ are reflected in similar effects on the lift spectrum and, hence, on the mean square lift.

Mean Square Normal Load Factor Increment

In calculating the loads produced by the lift discussed in the preceding section, the motions of the airplane must be taken into account. Before considering the averaging effects of the span on these loads, however, a brief discussion of some results obtained for the one-dimensional gust case may be in order.

If the airplane is considered to be subjected to continuous random turbulence with the spectrum $\varphi_w(\omega)$ given by the curve for $b/L^* = 0$ in Fig. 4, and if the airplane is permitted to move vertically only, the mean square load factor can be calculated readily.[4] Some typical results are presented in Fig. 5. The ordinate is the ratio of the root mean square load factor calculated in this manner to the root mean square load factor given by the sharp-edged gust formula and, thus, represents an alleviation factor for the value obtained from this formula; the abscissa is an airplane mass parameter

$$\kappa \equiv 8M/C_{L_\alpha}\rho S\bar{c}$$

The results indicate, as may be expected, that the sharp-edged gust formula which, in effect, disregards the motions of the airplane and unsteady-lift effects, is most accurate for large values of the mass parameter, which imply small motions on the part of the airplane. Also, the alleviation factor and, hence, the mean square load factor are seen to depend on the ratio of the scale of turbulence to the mean chord.

Now if a two-dimensional gust input is to be used, the result will depend on the ratio of the span to the scale of turbulence, as was the case in Fig. 4, as well as on the ratio of the mean chord to the scale of turbulence, as in the case in Fig. 5. However, for a given airplane these two ratios are not independent, since the ratio of the span to the average chord is fixed. Therefore, it was felt that, for a realistic appraisal of the averaging effect of the span, the two ratios should be varied simultaneously in such a way as to maintain a fixed airplane geometry.

The results of such an analysis are indicated in Fig. 6, where the ordinate is the ratio of the mean square load factor obtained from an analysis using a two-dimensional gust structure to the value obtained for a one-dimensional gust for a given value of κ—namely, 100. The abscissa is the span ratio b/L^*. Curves are shown for three aspect ratios. The value of the ratio of the scale of turbulence to one-half of the average chord can be determined for each point on the curves from the relation

$$L^*/(\bar{c}/2) = 2A/(b/L^*)$$

The results presented in Fig. 6 indicate that, if the variation of gust intensity along the span is taken into account, the mean square normal load factor is reduced by an amount which depends on the aspect ratio of the wing and the ratio of the span to the scale of turbulence. For wings of high aspect ratio and spans of the order of one-quarter or more of the scale of turbulence, this reduction appears to be quite substantial. However, as will be indicated presently, the results presented in this Figure do not imply that the stresses are necessarily lower.

Mean Square Rolling Acceleration

Fig. 7 pertains to a problem which can be analyzed only by taking into account the spanwise variation of gust intensity—namely, the problem of rolling response to vertical gusts—because if the gust intensity is the same along the span there is no tendency to roll. The mean square rolling acceleration has been calculated

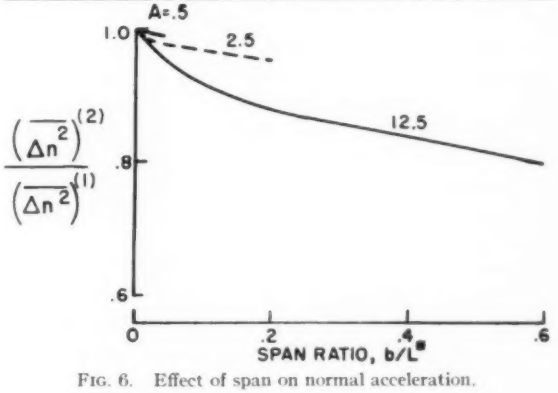

FIG. 6. Effect of span on normal acceleration.

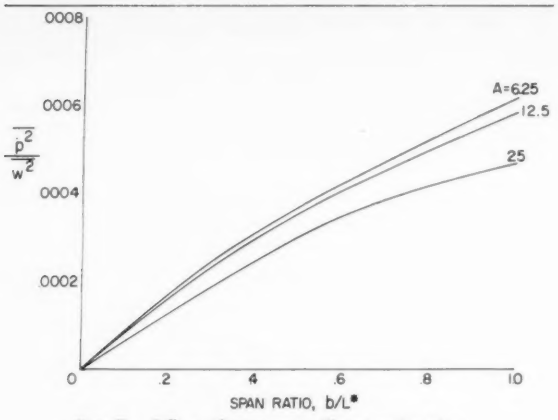

FIG. 7. Effect of span on rolling acceleration.

for one value of a rolling moment of inertia parameter analogous to the mass parameter—i.e.,

$$\kappa_r \equiv 8I_x/(-C_{lp})\rho S^2 b$$

which has a value of 25.75 for the calculations represented in Fig. 7 and for several values of the chord and span ratios.

As may be expected, as the span goes to zero, so does the effect of variations in gust intensity along the span and, hence, the tendency to roll. (If the span were much larger than the scale of turbulence, and, therefore, beyond the range of practical interest in connection with the gust-loads problem, the local values of the gust intensity along the span would tend to cancel each other and again produce no tendency to roll, although the curves are not shown here for sufficiently large values of the span ratio to demonstrate this point.)

In considering these results the fact that the airplane also rolls due to side gusts acting on the vertical tail should be kept in mind. Some estimates indicate that for large airplanes the effect considered here is likely to predominate. In any event, the two contributions to the rolling motion are statistically independent if the turbulence is isotropic, so that the spectra can be added directly to obtain the spectrum of the total rolling acceleration.

Mean Square Root Bending Moment of a Rigid Wing

In order to obtain a more direct measure of the effect of spanwise variation in gust intensity on the stresses in an airplane the mean square root bending moment has been calculated for a rigid and a flexible wing. Fig. 8 pertains to an airplane with a rigid wing, which is permitted to move vertically only. The mass parameter is 100. The ratio of the mean square bending moment to a mean square bending moment calculated from a sharp-edge gust formula, which includes no inertia or unsteady-lift effects, is shown as a function of the ratio of the wing mass to the total mass of the airplane. The curve labeled $b/L^* = 0.25$ represents the results calculated by taking spanwise variations of the gust intensity into account, whereas the curve labeled $b/L^* = 0$ represents the results of calculations in which these variations are ignored. The aspect ratio of the wing considered here is 12.5, and the scale ratio $L^*/(\bar{c}/2)$ is 100 in both cases.

The effect of taking spanwise variations into account is to decrease the mean square bending moment slightly if most of the mass of the airplane is contained in the fuselage, but to increase it if much or most of the weight is in the wing. For the airplane with most of the weight in the fuselage the decreased moment reflects to a large extent the decreased normal load factor. On the other hand, for the extreme case of a flying wing, which contains its entire mass in the wing, the net root bending moment is zero if the gust is uniform along the span, provided the mass distribution and lift distribution have the same lateral centroid location, because the bending moments due to the turbulence directly, due to the motion of the airplane, and due to the inertia effects then cancel each other. If, for the same case, the variation of the gust intensity along the span is considered, however, a net bending moment does exist. Thus, the mean square bending moment shown in the Figure for a mass ratio of unity is due entirely to the spanwise variation of gust intensity, and, at mass ratios between one-half and one, this effect results in large increases in the mean square bending moment.

Mean Square Root Bending Moment of a Flexible Wing

The mean square root bending moment of an airplane with a flexible wing and a higher value of the mass parameter κ—namely, 175—is shown in Fig. 9. The airplane is now considered to be free to move vertically, and the wing is assumed to distort in the first symmetrical free-free bending mode. The fact that the fundamental bending frequency and the mode shape change as the mass is redistributed from the fuselage to the wing is taken into account.

For this case a one-dimensional gust produces a bending moment even when all the mass is in the wing. The effect of taking the spanwise variation of gust intensity into account is again to reduce the mean square bending moment when most of the mass is in the fuselage and to increase it if most of the mass is in

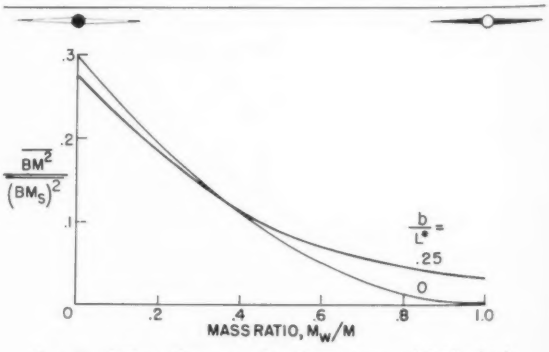

FIG. 8. Effect of span on bending moment (rigid wing).

the wing; however, the magnitude of the effect appears to be considerably greater than it was for the rigid wing. (In view of the different mass parameters the results presented in Figs. 8 and 9 should not be compared with each other in an attempt to deduce the effects of wing flexibility.)

Discussion

Some Limitations of Analyses of Airplane Response to Continuous Random Excitation

The purpose of the analysis presented here has been to determine how the results of an analysis based on a one-dimensional random gust are modified if a two-dimensional random gust is considered. Before discussing the results presented, a short discussion of some of the limitations and implications of this type of analysis may be in order.

The assumptions of linearity and stationarity commonly made in analyses based on a one-dimensional gust structure have been carried over. Linearity primarily implies small motions superimposed on a steady mean motion. Stationarity, in a statistical sense, implies that the statistical characteristics of the turbulence along the flight path remain substantially invariant for a sufficiently long period of time—that is, a period of time several times longer than either the time required for any transient aerodynamic and dynamic effects to subside or the time required to travel a distance equal to the scale of turbulence, whichever is greater. This condition is likely to be satisfied in turbulence of low or medium intensity; however, whether or not the turbulence encountered in thunderstorms satisfies this condition is not known at present.

The present study of the response to two-dimensional turbulence, as well as the previous studies of the response to one-dimensional turbulence, are thus concerned with only a part of the gust-loads picture. They furnish an estimate of the expected number of peak loads per unit time above a given level for any *specified* mean square intensity of the turbulent input, but this information must be combined with the *probability of encountering a given input intensity* in a given period of time, which represents a meteorological and operational problem, in order to arrive at an estimate of the time required to exceed a given peak load in a *given type of operation*. This problem is discussed in reference 12.

The additional assumption of axisymmetry made in this paper is valid whenever the turbulence has no preferred direction in the horizontal plane. This condition is likely to be satisfied in general, except near the ground (where the turbulence may be the result of obstacles on the ground which have a definite orientation, such as a mountain range) and possibly at the edges of the jet stream. If the turbulence does not have this property, the analysis of this paper can readily be extended to cover this situation; however, more knowledge, in the form of two-dimensional correlation

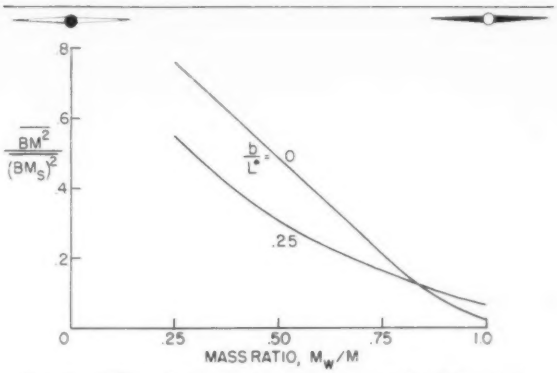

FIG. 9. Effect of span on bending moment (flexible wing).

functions or the corresponding power spectra, would then be required than is now available.

A characteristic of atmospheric turbulence which appears to play a prominent part in the calculation discussed here is the scale of turbulence, although if an experimentally obtained input spectrum had been used instead of the analytical expressions used here this quantity would not have appeared explicitly. It is very difficult to obtain experimentally, because its measurement requires long periods of time, during which the assumption of stationarity is likely to be violated. Therefore, if this quantity is to be obtained from experimental results, the best procedure may be to fit an experimentally obtained correlation function or spectrum by an analytic expression and then to deduce the scale of turbulence from this expression, using Eq. (14) or (15).

Appraisal of the Calculated Results

As pointed out in this paper, the lateral variation of gust intensity may affect the response to turbulence to various extents. In some problems this effect constitutes a refinement of an analysis based on a one-dimensional gust structure, as in the case for the normal load factor, for instance; in others this effect is the primary cause of the response, as in the case for the rolling accleration or the root bending moment on a rigid flying wing.

On the basis of the results of the calculations, the effects considered here may be significant if the span of the airplane is one-tenth or more of the scale of turbulence, that is, for airplanes with a span as low as 50 ft. in some cases. However, in other problems these effects may be significant only for the very largest airplanes. As was demonstrated, they may serve to increase or decrease the loads and motions, although some of the problems where the increase is very large, such as the root bending moment on a flying wing, may be those for which gust loads are not likely to be critical. The effects considered here appear to be more significant for relatively flexible than for relatively rigid airplanes, and on the basis of calculations performed elsewhere[13] they appear to affect the response in the higher modes to an even larger

extent than the response in the lower modes considered in the calculations of the present paper.

Although only calculations of mean square values have been presented, the values of the mean square derivatives could have been presented as well, inasmuch as they can be obtained directly from the spectra which were used to obtain the mean square values. Hence, the expected number of peaks could have been calculated. It is not expected that such calculations would alter the conclusions reached here.

Application to Other Problems

The effects discussed here may find application to other problems. For instance, some phases of the buffeting problem may be amenable to analysis on the basis of assumptions of linearity and stationarity. If so, the effects of spanwise variation of input intensity are likely to be very much larger than in the gust-loads problem, because the scale of turbulence is small compared to the wing span in this problem. Whether the assumption of axisymmetry will yield useful results or whether two-dimensional input correlation functions and spectra will have to be obtained remains to be seen.

Concluding Remarks

An approach has been outlined for taking into account the spanwise variations in instantaneous intensity of a continuous random gust structure. The results of some calculations have been presented which indicate that this effect, which may serve to decrease or increase the loads and motions, depending on the individual case, may be significant even on medium-sized airplanes for certain gust responses. One such response is the root bending moment, particularly if the wing is flexible, and another is the rolling acceleration. However, for other responses, such as the normal acceleration, this effect is likely to be small even for the larger airplanes. Thus, in quantitative studies of some, but not all, responses to continuous random turbulence, the effects of spanwise variation of gust intensity will have to be taken into account for large airplanes.

Appendix A—Derivation of the Input-Output Relation and Various Transfer Functions for a One-Dimensional Gust Structure

In this Appendix the relation between the power spectra of the input and output of a linear dynamic system subjected to a stationary random input will be derived in a form which can readily be generalized to the analysis of a two-dimensional gust structure. (See references 3, 4, and 6 for greater detail.) The transfer functions required in the calculations discussed in this paper will then be derived for the case of a one-dimensional gust structure.

The Input-Output Relation

The correlation function of a stationary random process $f(t)$ will be defined as

$$\psi_f(\tau) = \overline{f(t)f(t+\tau)} \tag{A-1}$$

where the bar designates a time average,

$$\overline{(\ )} = \lim_{T\to\infty} \frac{1}{2T}\int_{-T}^{T} (\ )\, dt$$

For many purposes the Fourier transform of this function is very useful. This transform will be referred to as the power spectrum of $f(t)$ and defined by

$$\begin{aligned}\varphi_f(\omega) &= \frac{1}{\pi}\int_{-\infty}^{\infty} \psi_f(\tau)\, e^{-i\omega\tau}\, d\tau \\ &= \frac{2}{\pi}\int_{0}^{\infty} \psi_f(\tau)\cos\omega\tau\, d\tau\end{aligned} \tag{A-2}$$

If now this process represents the input to a linear dynamic system, the output of which is $g(t)$, the functions $f(t)$ and $g(t)$ can be related by the superposition integral

$$g(t) = \int_{-\infty}^{\infty} h(t_1)\, f(t - t_1)\, dt_1 \tag{A-3}$$

where $h(t)$ is the response of the given system to a unit impulse.

The correlation function for $g(t)$ can be defined in the same way as the one for $f(t)$; upon substituting Eq. (A-3) into this defining equation and making use of Eq. (A-1), this correlation function can be written as

$$\psi_g(\tau) = \int_{-\infty}^{\infty}\int_{-\infty}^{\infty} h(t_1)\, h(t_2)\, \psi_f(\tau + t_1 - t_2)\, dt_1 dt_2 \tag{A-4}$$

and upon defining a power spectrum for $g(t)$ in the same way as the one for $f(t)$, substituting Eq. (A-4) into this defining relation and using Eq. (A-2), this spectrum can be written as

$$\varphi_g(\omega) = |H(\omega)|^2\, \varphi_f(\omega) \tag{A-5}$$

where $H(\omega)$ is the Fourier transform of $h(t)$,

$$H(\omega) = \int_{-\infty}^{\infty} h(t)e^{-i\omega t}\, dt \tag{A-6}$$

and represents the complex amplitude of the output of the system when subjected to a sinusoidal input of frequency ω and unit amplitude.

When the system is an airplane flying at a mean speed U and the input to the system is the gust intensity w, cognizance should be taken of the fact that along the flight path w is a function of only one variable, either the distance traveled along the flight path, x, or the time required to travel that distance, namely $t = x/U$. In the body of this paper w has been considered as a function of distance, with the result that the definitions of ψ_w and φ_w given in the body take special forms of those given in this Appendix.

The reason for this convention is that if an airplane flies sufficiently rapidly the gust velocity at any point of its flight path does not vary significantly during the time the airplane is in the vicinity of the point, so that the statistical characteristics, in particular the

correlation function, are functions of space displacements only. (The term "vicinity" is used here to designate the space surrounding the point and of such extent that there is a strong correlation between the gust velocities at all points of that space with those at the given point.) The assumption has been made in previous analyses of the response of an airplane to continuous random atmospheric turbulence, and will be made here, that this condition, which is equivalent to Taylor's hypothesis made in studies of turbulence in wind tunnels, is satisfied. From available information concerning the properties of the atmosphere the required speed appears to be in the order of about 100 or 200 ft. per sec., so that for all higher flying speeds time displacements τ can be identified with space displacements $\Delta x = U\tau$, and vice versa.

In the calculations of this paper the following expression for the correlation function of atmospheric turbulence has been used.[4,6]

$$\psi_w(\Delta x) = \overline{w^2}[1 - (|\Delta x|/2L^*)]e^{-(|\Delta x|/L^*)} \quad \text{(A-7)}$$

The power spectrum corresponding to this correlation function is

$$\varphi_w(\omega) = (\overline{w^2}L^*/\pi U)\,[(1 + 3k'^2)/(1 + k'^2)^2] \quad \text{(A-8)}$$

where $$k' \equiv \omega L^*/U$$

The Transfer Functions for the Normal-Load-Factor Increment and the Root Bending Moment of a Rigid Airplane

The equation of motion of an airplane subjected to sinusoidal gusts and free to move vertically only can be written as

$$M\ddot{z} = -(C_{L_\alpha}qS/U)\,\bar{C}(k)\dot{z} + L_g \quad \text{(A-9)}$$

where $L_g = C_{L_\alpha}qS(w/U)\phi(k)$; and $\bar{C}(k)$ is an unsteady-lift function for changes in angle of attack, which for incompressible two-dimensional flow is the Theodorsen function $C(k)$ (see reference 14) plus an apparent-mass term $ik/2$; the function $\phi(k)$ is an unsteady-lift function for gust penetration, and is for two-dimensional incompressible flow the function first given in reference 15 and usually referred to as the Sears function. Hence, if a normal load factor increment and a mass parameter are defined by

$$\Delta n = \ddot{z}/g$$

and $$\kappa = 8M/C_{L_\alpha}\rho S\bar{c}$$

this equation can be written as

$$\Delta n = \{1/(\kappa/2) + [\bar{C}(k)/ik]\}\,(2U^2/g\bar{c})\phi(k)\,(w/U) \quad \text{(A-10)}$$

The factor multiplying w on the right side of Eq. (A-10) constitutes the required transfer function. Using a refrence value of the load factor increment defined by the sharp-edge gust formula

$$\Delta n_s = (C_{L_\alpha}qS/Mg)\,(w/U) = (2/\kappa)\,(2U^2/g\bar{c})\,(w/U) \quad \text{(A-11)}$$

and Eqs. (5) and (A-8), the mean square value of Δn can be written as

$$\frac{\overline{(\Delta n)^2}}{\overline{(\Delta n_s)^2}} = \int_0^\infty \frac{|\phi(k)|^2}{|1 + [2\bar{C}(k)/ik\kappa]|^2}\,\frac{1}{\pi}\,\frac{1 + 3k'^2}{(1 + k'^2)^2}\,dk'$$

where $\overline{(\Delta n_s)^2}$ represents the mean square value of Δn as calculated by the sharp-edge gust formula. In the calculation of $\overline{(\Delta n)^2}$ discussed in this paper the quasi-steady value of $\bar{C}(k) \backsimeq 1$ and the approximation used in references 4 and 6 for $|\phi(k)|^2$—namely,

$$|\phi(k)|^2 \backsimeq 1/(1 + 2\pi k)$$

have been used.

If the gust is uniform along the span, the aerodynamic loads due directly to the gust and due to the motion of the airplane have the same lateral center of pressure. Hence, the bending moment due to sinusoidal gusts can be written as

$$BM = (C_{L_\alpha}qS/U)\,(\bar{y}/2)\,[\phi(k)w - \bar{C}(k)\dot{z}] - (M_w/2)\bar{y}\ddot{z} \quad \text{(A-12)}$$

However, using Eq. (A-9) this equation can be simplified to

$$BM = [(\bar{y}/2)M - (\bar{y}/2)M_w]\ddot{z} = (\bar{y}/2)M[1 - (\bar{y}/\bar{y})\,(M_w/M)]\ddot{z}$$

Therefore, the transfer function for BM is equal to the transfer function for Δn multiplied by the factor

$$(\bar{y}/2)M[1 - (\bar{y}/\bar{y})\,(M_w/M)]g$$

In the calculations of the bending moments discussed in this paper the values of $\bar{C}(k)$ and $\phi(k)$ for two-dimensional incompressible flow (as corrected for finite-span effects by using the appropriate value of C_{L_α} instead of 2π) were used. A reference value of the bending moment as calculated from the equivalent of the sharp-edge gust equation,

$$BM_s = (1/2)C_{L_\alpha}qS\bar{y}(w/U) \quad \text{(A-13)}$$

was used to reduce the results to dimensionless form. The values of $\bar{y}$ and $\bar{y}$ were assumed to be identical.

Transfer Function for the Root Bending Moment of a Flexible Wing

The method of calculating the transfer function for the root bending moment of a flexible wing is based on the modal approach of reference 16.

The equation for the bending distortion of a flexible wing can be written as

$$(d^2/dy^2)\,[EI(d^2z/dy^2)] = l_g + l_m + l_i \quad \text{(A-14)}$$

where l_g and l_m are, respectively, the aerodynamic loads per unit span due to the gust directly and due to the airplane motion, and where l_i is the load per unit span due to inertia effects. If the airplane is restricted to vertical motion and to distortion in the first free-free bending mode, the function $z(y)$ can be written as

$$z(y) = z_0 + z_1\,\zeta(y) \quad \text{(A-15)}$$

The mode shape $\zeta(y)$ must satisfy the equation

$$(d^2/dy^2)\,[EI(d^2\zeta/dy^2)] = m\omega_0^2\,\zeta \qquad \text{(A-16)}$$

where ω_0 is the frequency of the oscillation in the first free-free bending mode, as well as the orthogonality condition

$$\int_{-[(b/2)}^{b/2} m\,\zeta\,dy = 0 \qquad \text{(A-17)}$$

As a result of Eqs. (A-15) and (A-16), Eq. (A-14) can, for sinusoidal gusts of frequency ω, be written as

$$z_1\omega_0^2 m\zeta = l_g - (\dot{z}_0/U)l_1 - (\dot{z}_1/U)l_\zeta + \omega^2 m(z_0 + z_1\zeta) \qquad \text{(A-18)}$$

where l_1 and l_ζ are the lift distributions due to an angle of attack equal to unity and an angle of attack distribution equal to ζ, respectively. Integrating this equation and using Eq. (A-17) and then multiplying it by ζ first and then integrating yields the pair of equations

$$\left.\begin{aligned} 0 &= L_g - (\dot{z}_0/U)L_1 - (\dot{z}_1/U)L_\zeta + \omega^2 M z_0 \\ z_1\omega_0^2 M' &= L_g'' - (\dot{z}_0/U)L_1'' - (\dot{z}_1/U)L_\zeta'' + \omega^2 M' z_1 \end{aligned}\right\} \qquad \text{(A-19)}$$

where M' is the generalized mass associated with the first free-free bending mode,

$$M' = \int_{-(b/2)}^{b/2} m\,\zeta^2\,dy$$

and where the actual and generalized lifts due to motion are defined by

$$L_1 = C_{L_\alpha} qS\bar{C}(k)$$

$$L_\zeta = C_{L_\alpha} qS\bar{C}(k)K$$

$$L_1'' = C_{L_\alpha} qS\bar{C}(k)\boldsymbol{K}$$

$$L_\zeta'' = C_{L_\alpha} qS\bar{C}(k)K'$$

and

$$\left.\begin{aligned} K &= \int_0^1 \left(\frac{cc_l}{\bar{c}C_{L_\alpha}}\right)_{\alpha=\zeta} dy^* \\ \boldsymbol{K} &= \int_0^1 \left(\frac{cc_l}{\bar{c}C_{L_\alpha}}\right)_{\alpha=1} \zeta\,dy^* \\ K' &= \int_0^1 \left(\frac{cc_l}{\bar{c}C_{L_\alpha}}\right)_{\alpha=\zeta} \zeta\,dy^* \end{aligned}\right\} \qquad \text{(A-20)}$$

For an unswept wing, which is the only case considered in the following, the constants K and $\boldsymbol{K}$ are identical by virtue of the reciprocity relations of linearized lifting surface theory.[11] Hence, both will be designated by K in the following.

For subsonic flow the required lift distributions can be obtained from reference 17. In the calculations discussed in the present paper the mode shape ζ was taken as

$$\zeta = -a + (1 + a)y^{*2} \qquad \text{(A-21)}$$

and the lift distributions given in reference 17 for a wing of aspect ratio 12, taper ratio 1/2 with uniform angle of attack and with parabolic twist were used.

Similarly, for a gust which is uniform along the span,

$$\left.\begin{aligned} L_g &= C_{L_\alpha} qS\phi(k)\,(w/U) \\ L_g'' &= C_{L_\alpha} qS\phi(k)K(w/U) \end{aligned}\right\} \qquad \text{(A-22)}$$

In terms of these lifts, Eq. (A-19) can be written in dimensionless form as

$$\begin{bmatrix} -\frac{\kappa}{2}k^2 + ik\bar{C}(k) & ikK\bar{C}(k) \\ ikK\bar{C}(k) & (k_0^2 - k^2)\frac{\kappa'}{2} + ikK'\bar{C}(k) \end{bmatrix} \begin{Bmatrix} z_0^* \\ z_1^* \end{Bmatrix} = \phi(k) \begin{Bmatrix} \frac{w}{U} \\ K\frac{w}{U} \end{Bmatrix} \qquad \text{(A-23)}$$

where $k_0 = \omega_0\bar{c}/2U$

and $\kappa' = 8M'/C_{L_\alpha}\rho S\bar{c}$

Now, the root bending moment can be expressed as

$$\begin{aligned} BM &= EI_0(d^2z/dy^2)_{y=0} \\ &= EI_0[(\bar{c}/2)/(b/2)^2]z_1^*\zeta''_0 \end{aligned}$$

where $\zeta''_0 \equiv [d^2\zeta/dy^{*2}]_{y^*=0}$

so that $$BM = H_1(w/U) + H_2K(w/U) \qquad \text{(A-24)}$$

where the transfer functions H_1 and H_2 are obtained by solving Eq. (A-23) for z_1^* and are defined by

$$\left.\begin{aligned} H_1 &= EI_0\,\frac{\bar{c}/2}{(b/2)^2}\,\zeta''_0\,\frac{-ikK\bar{C}(k)}{D(k)}\,\phi(k) \\ H_2 &= EI_0\,\frac{\bar{c}/2}{(b/2)^2}\,\zeta''_0\,\frac{-(\kappa/2)k^2 + ik\bar{C}(k)}{D(k)}\,\phi(k) \end{aligned}\right\} \qquad \text{(A-25)}$$

where

$$D(k) = (k^2 - k_0^2)k^2\frac{\kappa}{2}\frac{\kappa'}{2} - ik\bar{C}(k) \times \left\{(k^2 - k_0^2)\frac{\kappa'}{2} + k^2\frac{\kappa}{2}K'\right\} + (K^2 - K')k^2\bar{C}^2(k)$$

Hence, for the one-dimensional gust structure, the desired transfer function from the gust to the root bending moment is

$$H_{BM}{}^w = (1/U)\,[H_1 + KH_2]$$

Appendix B—Derivation of Output Spectra for a Two-Dimensional Gust Structure

The General Input-Output Relations

In analogy with Eq. (A-3), a superposition integral for an output, say $\sigma(t)$, of a system subjected to a two-dimensional input can be written as

$$\sigma(t) = \int_{-\infty}^{\infty}\int_{-(b/2)}^{b/2} h(t_1, y)\,w[U(t - t_1), y]\,dy\,dt_1 \qquad \text{(B-1)}$$

where the function $h(t, y)$ has been discussed in the body of the paper. If now the correlation function for σ is written in terms of this integral, a time average of the type $\overline{w(x, y)\, w(x + \Delta x, y + \Delta y)}$ occurs on the right side of the equation. This function will be defined as the two-dimensional correlation function $\bar{\psi}_w(\Delta x, \Delta y)$ for the vertical component of the gust velocity.

As mentioned in the body of this paper, by assuming the turbulence to be axisymmetric this function can be expressed in terms of the one-dimensional correlation function as follows:

$$\bar{\psi}_w(\Delta x, \Delta y) = \psi_w(\sqrt{\Delta x^2 + \Delta y^2}) \tag{B-2}$$

This relation will be assumed to be valid in the following.

The correlation function for σ can then be written as follows:

$$\psi_\sigma(\tau) = \int_{-\infty}^{\infty}\int_{-\infty}^{\infty}\int_{-(b/2)}^{b/2}\int_{-(b/2)}^{b/2} h(t_1, y_1)\, h(t_2, y_2) \times \psi_w\left[\sqrt{U^2(\tau + t_1 - t_2)^2 + (y_2 - y_1)^2}\right] dy_1\, dy_2\, dt_1\, dt_2 \tag{B-3}$$

By taking the Fourier transform with respect to τ of both sides of this equation, the equivalent relation for the power spectrum of σ is obtained,

$$\begin{aligned}\varphi_\sigma(\omega) &= \int_{-(b/2)}^{b/2}\int_{-(b/2)}^{b/2} H(\omega, y_2)\, [H(\omega, y_1)]^* \times \bar{\varphi}_w(\omega, y_2 - y_1)\, dy_1\, dy_2 \\ &= \int_{-(b/2)}^{b/2}\int_{-(b/2)}^{b/2} \Re\{H(\omega, y_2)\, [H(\omega, y_1)]^*\} \times \bar{\varphi}_w(\omega, y_2 - y_1)\, dy_1\, dy_2\end{aligned} \tag{B-4}$$

where $\Re\{\ \}$ designates that the real part is to be taken, and where the asterisk designates that the complex conjugate of $H(\omega, y_1)$ is to be taken. The functions $\bar{\varphi}_w$ and H are the Fourier transforms of $\bar{\psi}_w$ and h,

$$\bar{\varphi}_w(\omega, \Delta y) = \frac{1}{\pi}\int_{-\infty}^{\infty} e^{-i\omega(\Delta x/U)}\, \bar{\psi}_w(\Delta x, \Delta y)\, d\left(\frac{\Delta x}{U}\right)$$

and

$$H(\omega, y) = \int_{-\infty}^{\infty} e^{-i\omega t}\, h(t, y)\, dt$$

Eq. (B-4) represents the input-output relation for a two-dimensional stationary stochastic input to a linear system.

For axisymmetric turbulence the two-dimensional spectrum $\bar{\varphi}_w(\omega, \Delta y)$ can be obtained from the one-dimensional spectrum $\varphi_w(\omega)$ by means of the relation

$$\bar{\varphi}_w(\omega, \eta) = \varphi_w(\omega) - |\eta|\int_{|\omega|}^{\infty} \varphi_w(\omega')\, \frac{\omega'}{\sqrt{\omega'^2 - \omega^2}} \times J_1(|\eta|\sqrt{\omega'^2 - \omega^2})\, d\omega' \tag{B-5}$$

where $\eta \equiv \Delta y$.

For the correlation function and spectrum of Eqs. (A-7) and (A-8) the spectrum $\bar{\varphi}_w(\omega, \eta)$ is

$$\bar{\varphi}_w(\omega, \eta) = (\overline{w^2}L^*/\pi U)\,\{(\eta/L^*)\,[(1 + 3k'^2) \div (1 + k'^2)^{3/2}]K_1\,[(\eta/L^*)\sqrt{1 + k'^2}] - (\eta/L^*)^2\,[1/(1 + k'^2)]K_0[(\eta/L^*)\sqrt{1 + k'^2}]\} \tag{B-6}$$

The double integral of Eq. (B-4) can be reduced to a single integral by introducing an autoconvolution function of $H(\omega, y)$,

$$\tilde{H}(\omega, \eta) = 2\int_{-(b/2)}^{(b/2)-\eta} \Re\{H(\omega, y)\, [H(\omega, y + \eta)]^*\, dy \tag{B-7}$$

The expression for $\varphi_\sigma(\omega)$ then becomes

$$\varphi_\sigma(\omega) = \int_0^b \tilde{H}(\omega, \eta)\, \bar{\varphi}_w(\omega, \eta)\, d\eta \tag{B-8}$$

An alternative method of evaluation consists in using the double Fourier transform of the two-dimensional correlation function,

$$\begin{aligned}\bar{\bar{\varphi}}_w(\omega_1, \omega_2) &= \frac{1}{\pi^2}\int_{-\infty}^{\infty}\int_{-\infty}^{\infty} e^{-i[\omega_1(\Delta x/U) + \omega_2(\Delta y/U)]} \times \bar{\psi}_w(\Delta x, \Delta y)\, d\left(\frac{\Delta x}{U}\right) d\left(\frac{\Delta y}{U}\right) \\ &= \frac{1}{\pi}\int_{-\infty}^{\infty} e^{-\omega_1(\Delta y/U)}\, \bar{\varphi}_w(\omega_1, \Delta y)\, d\left(\frac{\Delta y}{U}\right)\end{aligned}$$

If the turbulence is axisymmetric, this double Fourier transform is a function only of the frequency $\sqrt{\omega_1^2 + \omega_2^2}$ —that is,

$$\bar{\bar{\varphi}}_w(\omega_1, \omega_2) = \hat{\varphi}(\sqrt{\omega_1^2 + \omega_2^2})$$

where $\hat{\varphi}_w$ can be obtained from ψ_w or φ_w by means of the following relations:

$$\left.\begin{aligned}\hat{\varphi}_w(\omega) &= \frac{2}{\pi}\int_0^\infty \frac{\Delta x}{U}\, J_0\left(\omega\,\frac{\Delta x}{U}\right) \times \psi_w(\Delta x)\, d\left(\frac{\Delta x}{U}\right) \\ \text{or } \hat{\varphi}_w(\omega) &= -\frac{2}{\pi}\int_{|\omega|}^{\infty} \frac{d\varphi_w(\omega')}{d\omega'} \times \frac{d\omega'}{\sqrt{\omega'^2 - \omega^2}} \\ &= -\frac{2}{\pi}\,\text{F.P.}\left\{\int_{|\omega|}^{\infty} \varphi_w(\omega') \times \frac{\omega' d\omega'}{(\omega'^2 - \omega^2)^{3/2}}\right\}\end{aligned}\right\} \tag{B-9}$$

where F.P. designates "the finite part of."

For the correlation function and spectrum given in Eqs. (A-7) and (A-8), the function $\hat{\varphi}_w(\omega)$ is

$$\hat{\varphi}_w(\omega) = (\overline{w^2}L^{*2}/U^2)\,(3/\pi)\,[k'^2/(1 + k'^2)^{5/2}]$$

In terms of the spectrum $\hat{\varphi}_w$ and the Fourier transform with respect to y of $H(\omega, y)$—namely,

$$\hat{H}(\omega, \omega') = \int_{-(b/2)}^{b/2} e^{-i\omega'(y/U)} H(\omega, y)\, dy \tag{B-10}$$

Eq. (B-4) can be written as

$$\varphi_\sigma(\omega) = \frac{1}{2}\int_{-\infty}^{\infty} \left|\hat{H}(\omega, \omega')\right|^2 \hat{\varphi}_w(\sqrt{\omega^2 + \omega'^2})\, d\omega' \tag{B-11}$$

which thus constitutes an alternative input-output relation.

In many cases the influence function $h(t, y)$ and, consequently, also its Fourier transform $H(\omega, y)$, have the property that they can be written as a product of functions depending on time (or frequency) and space alone—that is,

$$\left.\begin{aligned} h(t, y) &= \boldsymbol{h}(t)\ \gamma(y) \\ H(\omega, y) &= \boldsymbol{H}(t)\ \gamma(y) \end{aligned}\right\} \quad \text{and} \tag{B-12}$$

where $\boldsymbol{H}(\omega)$ is the Fourier transform of $\boldsymbol{h}(t)$. For this case the evaluation of the integral of the input-output relation is simplified considerably. For instance, Eq. (B-8) now becomes

$$\varphi_\sigma(\omega) = b\left|\boldsymbol{H}(\omega)\right|^2 \int_0^b \Gamma(\eta)\ \tilde{\varphi}_w(\omega, \eta)\, d\eta \tag{B-13}$$

where the function $\Gamma(\eta)$ defined by

$$\Gamma(\eta) = \frac{2}{b}\int_{-(b/2)}^{(b/2)-\eta} \gamma(y)\ \gamma(y + \eta)\, dy \tag{B-14}$$

is independent of frequency.

In many cases when $h(t, y)$ and $H(\omega, y)$ do not have forms indicated in Eqs. (B-12), they can be expressed as a sum of functions which do have those forms, that is

$$\left.\begin{aligned} h(t, y) &= h_1(t)\ \gamma_1(y) + h_2(t)\ \gamma_2(y) + \ldots \\ H(\omega, y) &= H_1(\omega)\ \gamma_1(y) + H_2(t)\ \gamma_2(y) + \ldots \end{aligned}\right\} \tag{B-15}$$

The manner in which this property can be used to advantage will be indicated in one of the examples that follow.

Spectrum of the Lift Due Directly to Turbulence

According to the reciprocity theorem of linearized lifting surface theory,[11] the lift influence function is equal to the lift distribution for unit angle of attack in reverse flow. If the wing is unswept, as is the case for the calculations described herein, there is no distinction between the lift distributions in direct and reverse flow. Inasmuch as the distribution of the lift on an oscillating unswept wing appears to be substantially independent of frequency, as indicated by the results calculated in reference 18, the influence function for the lift due directly to turbulence will be assumed to be expressible in the form indicated in Eq. (B-12), specifically,

$$H_{L_g}{}^w(\omega, y) = [(C_{L_\alpha} qS/Ub)\ \phi(k)]\ \gamma_L(y)$$

where $\gamma_L(y)$ is the section loading coefficient for unit angle of attack, $(cc_l/\bar{c}C_{L_\alpha})_{\alpha=1}$.

Hence, the function $\Gamma(\eta)$ becomes

$$\Gamma(\eta^*) = \int_{-1}^{1-\eta^*} \gamma_L(y^*)\ \gamma_L(y^* + \eta^*)\, dy^*$$

For instance, if the lift distribution is uniform across the span, $\gamma_L = 1$, so that

$$\Gamma(\eta^*) = 2 - \eta^* \tag{B-16}$$

Eq. (B-13) then becomes

$$\varphi_{L_g}(\omega) = \frac{b^2}{2}\left[\frac{C_{L_\alpha} qS}{Ub}\right]^2 \left|\phi(k)\right|^2 \int_0^2 \Gamma(\eta^*)\ \tilde{\varphi}_w(\omega, \eta)\, d\eta^* \tag{B-17}$$

In analogy with the expression for a one-dimensional random gust—namely,

$$\varphi_{L_g}(\omega) = [C_{L_\alpha} qS/U]^2 \left|\phi(k)\right|^2 \varphi_w(\omega)$$

Eq. (B-17) can be written as

$$\varphi(\omega)_{L_g} = [C_{L_\alpha} qS/U]^2 \left|\phi(k)\right|^2 \varphi_{w_e}(\omega) \tag{B-18}$$

where $\varphi_{w_e}(\omega)$, an effective spectrum for the vertical component of the gust velocity, is defined by

$$\varphi_{w_e}(\omega) = \frac{1}{2}\int_0^2 \Gamma(\eta^*)\ \tilde{\varphi}_w(\omega, \eta)\, d\eta^*$$

Using the functions $\Gamma(\eta^*)$ and $\tilde{\varphi}_w(\omega, \eta)$, defined by Eqs. (B-16) and (B-6), respectively, the function φ_{w_e} has been calculated and is shown in Fig. 4. From this spectrum, or its equivalent obtained with the distribution γ_L appropriate to any given case, the spectrum of the lift can then be obtained from Eq. (B-18).

Spectrum of the Normal Load Factor Increment

If the spanwise variation of gust intensity is taken into account, the term L_g on the right side of Eq. (A-9) is the lift discussed in the preceding section. However, the other terms in the equation are independent of the nature of the input, so that the transfer function in Eq. (A-10) is the same as before. Consequently, the power spectrum for Δn can be written in the same way as before, with φ_w replaced by the function φ_{w_e} defined in the preceding section. The results shown in Fig. 6 have been obtained by integrating the spectrum for Δn obtained in this manner.

Spectrum of the Rolling Acceleration

The equation of motion of an airplane in roll due to sinusoidal vertical gusts can be written as

$$I_x\dot{p} = C_{l_p} qSb\bar{C}(k)\ (pb/2U) + L'_g \tag{B-19}$$

where L'_g, the rolling moment due directly to gusts, can be written as

$$L'_g = \frac{(-C_{L_p})qSb}{U}\,\phi(k)\,\frac{1}{4}\int_{-1}^{1} \gamma_{L'}(y^*)\ w(y^*)\, dy^*$$

where the rolling moment influence function $\gamma_{L'}$ is equal to the lift distribution in roll—that is, $[cc_l \div c(-C_{l_p})]_{\alpha=y^*}$. Hence, the rolling acceleration $\dot{p}$ can be expressed in terms of w as follows:

$$\frac{\dot{p}b}{2g} = \left[\frac{U}{Sg}\,\frac{1}{\kappa_r + [\bar{C}(k)/ik]}\,\phi(k)\right]\frac{b}{2}\int_{-1}^{1} \gamma_{L'}(y^*) \times w(y^*)\, dy^*$$

so that the influence function relating $\bar{p}b/2g$ to w has the form indicated in Eq. (B-12), with $\boldsymbol{H}(\omega)$ being the function in brackets in the preceding equation, and $\gamma(y)$ being the function $\gamma_{L'}(y^*)$.

The spectrum of the rolling moment can thus be obtained in the manner employed previously for the lift, by calculating an "effective" gust spectrum and multiplying it by $|\boldsymbol{H}(\omega)|^2$.

In the calculations discussed in this paper, κ_r was taken as 25.75, U = 400 ft. per sec., and S = 1,250 sq. ft.

Spectrum for the Root Bending Moment of a Rigid Wing

If variations of the gust intensity along the span are taken into account, Eq. (A-12) becomes

$$BM = -\frac{1}{2}\frac{C_{L_\alpha}qS}{U}\,\bar{y}\bar{C}(k)\dot{z} - \frac{M_w}{2}\,y\ddot{z} + \frac{C_{L_\alpha}qSb}{4U}\,\phi(k)\int_{-1}^{1}\gamma_B(y^*)\,w(y^*)\,dy^* \quad \text{(B-20)}$$

where $\gamma_B(y^*)$ is an influence function for the bending moment and is, according to the reciprocity theorem, the lift distribution $cc_l/\bar{c}C_{L_\alpha}$ for an angle of attack distribution which is 0 on the left wing and equal to y^* on the right wing. As a result of the superposition principle, this lift distribution is equal to one-half the sum of the lift distribution due to unit symmetrical linear twist and the lift distribution due to unit antisymmetrical linear twist (damping-in-roll condition). For the calculations described herein these lift distributions, as well as $\gamma_L(y^*)$, were obtained from the results given in reference 17 for a wing of aspect ratio 12, taper ratio 1/2.

Inasmuch as $\ddot{z}$ and $\dot{z}$ can be expressed in terms of L_g by means of the transfer function discussed in connection with the normal load factor increment, the bending moment can be expressed in terms of w by means of an expression of the form of Eq. (B-15), with

$$\left.\begin{aligned} H_1(\omega) &= \frac{-(1/2)\,[C_{L_\alpha}qS/U]\,\bar{y}[\bar{C}(k)/ik] - (M_w/2)\bar{y}}{(\kappa/2) + [\bar{C}(k)/ik]} \times \frac{(2U/S)\,\phi(k)}{} \\ H_2(\omega) &= \frac{C_{L_\alpha}qS}{2U}\,\phi(k) \\ \gamma_1(y) &= \gamma_L(y^*) \\ \gamma_2(y) &= \gamma_B(y^*) \end{aligned}\right\} \quad \text{(B-21)}$$

The spectrum for BM may therefore be derived as follows. The bending moment may be written as a sum of two superposition integrals involving the Fourier transforms $h_1(t)$ and $h_2(t)$ of $H_1(\omega)$ and $H_2(\omega)$,

$$BM(t) = \int_{-\infty}^{\infty} h_1(t_1)dt_1 \int_{-(b/2)}^{(b/2)} \gamma_1(y)\,w(t - t_1, y)\,dy + \int_{-\infty}^{\infty} h_2(t_2)\,dt_2 \int_{-(b/2)}^{(b/2)} \gamma_2(y)\,w(t - t_2, y)\,dy$$

Upon forming the correlation function for BM, introducing the assumption of axisymmetry, and calculating the Fourier transform of the correlation function, the power spectrum for the bending moment is obtained as

$$\varphi_{BM}(\omega) = |H_1(\omega)|^2\,\varphi_{w_\epsilon}(\omega) + 2\Re\{H_1(\omega)\,[H_2(\omega)]^*\} \times \varphi_{w_{\epsilon_1}}(\omega) + |H_2(\omega)|^2\,\varphi_{w_{\epsilon_2}}(\omega) \quad \text{(B-22)}$$

where $\Re$ and the asterisk designate "the real part of" and call for the complex conjugate, respectively, as before; the spectrum $\varphi_{w_\epsilon}(\omega)$ has been defined previously, and the other spectra are defined as

$$\left.\begin{aligned} \varphi_{w_{\epsilon_1}}(\omega) &= \frac{1}{2}\int_0^2 \Gamma_1(\eta^*)\,\bar{\varphi}_w(\omega, \eta)\,d\eta^* \\ \varphi_{w_{\epsilon_2}}(\omega) &= \frac{1}{2}\int_0^2 \Gamma_2(\eta^*)\,\bar{\varphi}_w(\omega, \eta)\,d\eta^* \end{aligned}\right\} \quad \text{(B-23)}$$

where, in turn,

$$\Gamma_1(\eta^*) = \int_{-1}^{1-\eta^*} \gamma_L(y^*)\,\gamma'_B(y^* + \eta^*)\,dy^*$$

$$\Gamma_2(\eta^*) = \int_{-1}^{1-\eta^*} [\gamma'_B(y^*)\,\gamma'_B(y^* + \eta^*) + \gamma''_B(y^*)\,\gamma_B{}''(y^* + \eta^*)]\,dy^*$$

where $\gamma'_B(y^*)$ and $\gamma''_B(y^*)$ are, respectively, the symmetrical and antisymmetrical part of $\gamma_B(y^*)$ and, as was pointed out previously, are equal to one-half of the lift distributions $cc_l/\bar{c}C_{L_\alpha}$ for a unit linear symmetric twist and unit linear antisymmetric twist, respectively.

The contribution of the antisymmetric part of γ_B to Γ_2 and, hence, to the spectrum for the bending moment stems basically from the asymmetry of the instantaneous distribution of gust intensity over the span. This asymmetry gives rise to a rolling moment and, hence, to rolling motions, which were considered in the preceding section of this Appendix, and which contribute additional bending moments due to the aerodynamic and inertia loads associated with these motions. If, for the purpose of calculating the bending moment due to symmetrical flight through turbulent air, these motions are disregarded, the contribution of γ''_B to Γ_2 should be disregarded as well, so that the second part of the expression for Γ_2 is generally spurious and should be ignored. As pointed out in reference 10, the net bending moment due to the symmetrical part of the instantaneous gust distributions and the resulting vertical motions and the net bending moment due to the antisymmetrical part and the resulting rolling motions are statistically independent, so that their power spectra can be added directly to obtain the total net bending moment due to atmospheric turbulence and the resulting airplane motions.

Inasmuch as

$$\frac{1}{2}\int_0^2 \Gamma_1(y^*)\,dy^* = \frac{\bar{y}}{b/2}$$

and

$$\frac{1}{2}\int_0^2 \Gamma_2(y^*)\,dy^* = \left(\frac{\bar{y}}{b/2}\right)^2$$

the functions $\varphi_{w_\epsilon}(\omega)$, $\varphi_{w_{\epsilon_1}}(\omega)$ and $\varphi_{w_{\epsilon_2}}(\omega)$ reduce, respectively, to $\varphi_w(\omega)$, $[\bar{y}/(b/2)]\varphi_w(\omega)$, and $[\bar{y}/(b/2)]^2\,\varphi_w(\omega)$,

as the ratio of the span to the scale of turbulence approaches 0. Consequently, by introducing these values and the definitions of $H_1(\omega)$ and $H_2(\omega)$ given in Eq. (B-21) into Eq. (B-22), the value of $\varphi_{BM}(\omega)$ given there can readily be shown to reduce the one obtainable directly from Eq. (A-12) when the span ratio approaches 0.

Spectrum for the Root Bending Moment of a Flexible Wing

The technique of the preceding section can readily be adapted to the flexible wing. The two functions $H_1(\omega)$ and $H_2(\omega)$ defined in Eq. (A-25) can now be used directly, provided that the functions $\gamma_1(y)$ and $\gamma_2(y)$ are defined as

$$\gamma_1(y) = (1/Ub)\gamma_L(y^*) \qquad \gamma_2(y) = (1/Ub)\gamma_\zeta(y^*)$$

where $\gamma_\zeta(y^*)$ is an influence function for L''_ζ, and according to the reciprocity theorem is equal to the lift distribution $cc_l/\bar{c}C_{L_\alpha}$ due to an angle of attack distribution equal to ζ—that is, the lift distribution used previously in defining K and K' in eq. (A-20).

Eqs. (B-22) and (B-23) can thus be used directly for the flexible-wing case provided Γ_1 and Γ_2 are redefined as

$$\Gamma_1(\eta^*) = \frac{1}{U^2b^2}\int_{-1}^{1-\eta^*} \gamma_L(y^*)\ \gamma_\zeta(y^* + \eta^*)\ dy^*$$

$$\Gamma_2(\eta^*) = \frac{1}{U^2b^2}\int_{-1}^{1-\eta^*} \gamma_\zeta(y^*)\ \gamma_\zeta(y^* + \eta^*)\ dy^*$$

and provided $\varphi_{w\epsilon}(\omega)$ is now divided by U^2b^2. The power spectrum for the bending moment obtained in this manner can, again, be shown to reduce to the one obtainable from Eq. (A-24) when the span ratio approaches zero.

For the flexible-wing calculations discussed in this paper the following quantities were used:

$\kappa = 175$ $\qquad b = 125$ ft.
$EI_0 = 22 \times 10^8$ lb. ft.^{2} $\qquad \bar{c} = 10$ ft.

The wing mass was assumed to be distributed along the span in the following manner, regardless of how much of the airplane mass was in the wing:

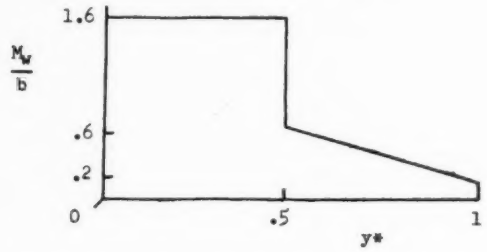

The mode shape, in particular the constant a in Eq. (A-21), was permitted to vary with the mass ratio M_w/M in such a way as to satisfy the orthogonality condition. Consequently, the frequency ω_0 and the generalized-mass parameter κ' varied with this ratio. For a value of this ratio of 0.25 the following values were used:

$$\omega_0 = 15.4 \qquad a = 0.147 \qquad \kappa' = 8.73$$

References

[1] Wax, Nelson, (Ed.), *Noise and Stochastic Processes*, Dover Publications, Inc., New York, 1954.

[2] Clementson, Gerhardt C., *An Investigation of the Power Spectral Density of Atmospheric Turbulence*, Ph.D. Thesis, Massachusetts Institute of Technology, 1950.

[3] Press, Harry, and Mazelsky, Bernard, *A Study of the Application of Power-Spectral Methods of Generalized Harmonic Analysis to Gust Loads on Airplanes*, NACA TN 2853, January, 1953.

[4] Fung, Y. C., *Statistical Aspects of Dynamic Loads*, Journal of the Aeronautical Sciences, Vol. 20, No. 5, p. 317, May, 1953.

[5] Press, Harry, and Houbolt, John C., *Some Applications of Generalized Harmonic Analysis to Gust Loads of Airplanes*, Journal of the Aeronautical Sciences, Vol. 22, No. 1, p. 17, January, 1955.

[6] Liepmann, H. W., *An Approach to the Buffeting Problem From Turbulence Considerations*, Douglas Aircraft Company Report SM-13940, March, 1951.

[7] Dryden, Hugh L., Schubauer, G. B., Mock, W. C., Jr., and Skramstad, H. K., *Measurements of Intensity and Scale of Wind-Tunnel Turbulence and Their Relation to the Critical Reynolds Number of Spheres*, NACA TR 581, 1937.

[8] Uberoi, Mahinder S., and Kovasznay, Leslie, S. G., *Influence of Resolving Power on Measurement of Correlations and Spectra of Random Fields*, Johns Hopkins University, Project Squid, Technical Report No. 30.

[9] Liepmann, H. W., *Extension of the Statistical Approach to Buffeting and Gust Response of Wings of Finite Span*, Journal of the Aeronautical Sciences, Vol. 22, No. 3, p. 197, March, 1955.

[10] Diederich, Franklin W., *The Response of An Airplane to Random Atmospheric Disturbances*, Ph.D. Thesis, California Institute of Technology, 1954.

[11] Heaslet, Max A., and Spreiter, John R., *Reciprocity Relations in Aerodynamics*, NACA TN 2700, May, 1952.

[12] Press, Harry, Meadows, May T., and Hadlock, Ivan, *Estimates of Probability Distribution of Root-Mean-Square Gust Velocity of Atmospheric Turbulence From Operational Gust-Load Data by Random Process Theory*, NACA TN 3362, March, 1955.

[13] Press, Harry, Houbolt, John C., and Diederich, Franklin W., *Some Applications of Generalized Harmonic Analysis to Problems in Airplane Dynamics*, papers read at the NACA-University Conference on Aerodynamics, Construction, and Propulsion, October 20–22, 1954, Volume I—Aircraft Structures and Materials, pp. 1-1 to 1-13.

[14] Theodorsen, Theodore, *General Theory of Aerodynamic Instability and the Mechanism of Flutter*, NACA TR 496, 1935.

[15] Garrick, I. E., *On Some Fourier Transforms in the Theory of Nonstationary Flows*, Fifth International Congress for Applied Mechanics, Cambridge, Massachusetts, 1938.

[16] Houbolt, John C., and Kordes, Eldon E., *Gust-Reponse Analysis of an Airplane Including Wing Bending Flexibility*, NACA TN 2763, August, 1952.

[17] Diederich, Franklin W., and Zlotnick, Martin, *Calculated Spanwise Lift Distributions and Aerodynamic Influence Coefficients for Unswept Wings in Subsonic Flow*, NACA TR 1228, 1955.

[18] Reissner, Eric, and Stevens, John E., *Effect of Finite Span on the Airload Distributions for Oscillating Wings. II—Methods of Calculation and Examples of Application*, NACA TN 1195, October, 1947.

Experiments on Circular Cones at Yaw in Supersonic Flow

MAURICE HOLT* AND JOHN BLACKIE†

Ministry of Supply, England

SUMMARY

Pressure measurements made in the Fort Halstead supersonic tunnel on two circular cones, of semiapex angles 15° and 20°, are given for angles of yaw up to 25° and a Mach Number of 3.53. The measured pressure distributions and lift and drag coefficients are compared with corresponding values calculated by theoretical methods, and the relative merits of these methods are then discussed.

(1) INTRODUCTION

THE PROBLEM of supersonic flow past circular cones at yaw has received considerable attention from theoretical research workers in recent years. Several methods of solution have been proposed,[1–5] and those based on Stone's paper[3] have been used as the basis for very extensive tables of data. It is, therefore, rather surprising that experimental information on this problem is comparatively scanty, and that no set of observed results comparable to the tables calculated by Kopal at Massachusetts Institute of Technology is available.

In the present paper an account is given of measurements of pressure on two circular cones of semiapex angles 15° and 20° over a range of angles of yaw between 0° and 25°. The measurements are made at one Mach Number in the Supersonic Wind Tunnel attached to the Applied Mathematics and Mechanics Division at Fort Halstead. Existing results appear to refer to cones much thinner than these and are given at somewhat arbitrary angles of yaw. The present results should, therefore, be of value in showing pressure distributions on cones producing shocks of considerable strength which, when yawed, display marked variations in entropy in the flow behind them. Further, the variation of pressure distribution with angle of yaw has been shown in a systematic manner, and the data given are probably more complete than those published previously.

The results are of value in themselves, but they are also suitable as a standard against which the more firmly established theoretical methods can be tested Accordingly, the pressure distributions at Mach Number, cone angle, and angle of yaw at which measurements are made are also calculated by three methods. The first is the original method by Stone[3] for slightly yawed cones, the second is the same method after modification to take account of an entropy correction, and the third is the second-order development of Stone's theory by Kopal,[5] for large angles of yaw. On the more slender cones, the entropy correction brings the Stone first-order theory into closer agreement with experiment, but tends to make matters worse on the 20° cone. On both cones there is no doubt that the second-order Stone theory gives the best agreement with experiment. The entropy correction, as it stands, is not sufficient to bring the first-order solution into agreement with observation. However, it is probable that this solution can be improved.

(2) EXPERIMENTAL DETAILS

The pressure distributions over the surfaces of 15° and 20° semiangled cones at Mach Number 3.5 were measured at various angles of incidence in a continuously running wind tunnel. The tunnel, of 10-in. square working section, was operated at a stagnation pressure of 38.2 in. of Hg and a working section pressure of 0.49 in. of Hg.

The cones, of 1.25-in. base diameter, were constructed of solid brass. The cone angles were within ±2 min. of arc of the nominal values and the cone surfaces true to ±0.0003 in. In the tunnel the cones were supported from the base and mounted so that angles of incidence from $-7\frac{1}{2}°$ to +25° could be obtained. Provision was also made for varying the yaw slightly for initial adjustment of the cone position. Eight pressure holes, normal to the surface of the cone and of 0.040 in. diameter were used in each model, the relative positions of the holes being shown in Fig. 1. It will be seen that in two cases there are two holes on the same generator. The pressures acting at these holes were led by hyperdermic and P.V.C. tubing through the base of the cone and the roof of the tunnel to a mercury manometer. Pressures on the manometer were read to ±0.01 in. of Hg by means of a cathetometer. Small variations in the angular positions of the pressure holes from those shown in Fig. 1 were allowed for in the final calculations.

Preliminary experiments were carried out to test for any possible disturbance of the air flow due to the size of pressure holes used. It was found that smaller holes gave the same pressure measurements but had the disadvantage that a longer time was required between readings for the mercury in the manometer to attain a

Received September 12, 1955.

* Formerly, at Armament Research & Development Establishment, Fort Halstead, Kent. Now, Assistant Professor, Division of Applied Mathematics, Brown University.

† Research Physicist, Armament Research & Development Establishment, Fort Halstead, Kent.

The authors are indebted to C. V. Hurdle and others of the ARDE wind-tunnel staff for their assistance in experimental work, to K. G. Tadman who carried out much of the numerical work, and to E. Dearden for his advice at various stages of the work.

steady level. The manometer tubes were kept as close to the tunnel working section as possible since shortening the leads also reduced the time required between readings.

The cone, with holes 1 and 2 on top, was initially set at zero yaw and incidence by adjusting its position until all the holes gave the same pressure reading to within 0.01 in. of Hg when the tunnel was running. The yaw changing mechanism was then locked and the incidence varied from $-7^1/_2°$ to 25°, pressure measurements being taken every $2^1/_2°$ over the range $-7^1/_2°$ to $+10°$ and every 5° afterwards. Calibration of the screw thread in the incidence changing mechanism enabled the angle of incidence to be measured to ±3 min. of arc. The cone was rotated through 180°, the experiment repeated, and the mean of the results taken. Close agreement was found between the two sets of results. Thus, in 83 per cent of the results, the mean value differed from an individual value by ±0.01 in. of Hg or less, and only in 3 per cent of the results did this difference exceed ±0.02 in. of Hg. Similar excessive differences also occurred occasionally between holes on the same generator. As they were quite random, they were attributed to slight irregularities in the air flow, probably tunnel shock waves.

Because of the positions of the holes and the fact that measurements were made over the range of incidences $-7^1/_2°$ to 25°, the measured pressure on any generator of the cone for angles of incidence up to $7^1/_2°$ is the mean of at least six results. Above $7^1/_2°$ it is the mean of at least three results. The standard deviation is slightly greater than 0.01 in. of Hg.

To extend the pressure measurements, a set of readings was taken with the cone rotated through $22^1/_2°$ from its original setting. Because of the close agreement obtained between the first two sets of results, it was felt unnecessary to rotate the cone through a further 180°.

(3) Details of Calculations

Values of pressure corresponding to those measured were calculated by three methods. In all of these a spherical polar coordinate system based on the vertex and axis of the solid cone is employed, as shown in Fig. 2. The same notation is also used when discussing experimental results. The position of the general point P is defined by r, the distance from the vertex O, θ, the angle between OP and the cone axis OA, and the angle between the meridian plane containing P and the meridian plane of symmetry, ϕ. The semivertex angle of the cone is α, the angle of yaw is ϵ, and the free-stream velocity is V.

The first calculations are made by Stone's method for slightly yawed cones.[3] This gives the additional pressure as the first term in a Fourier cosine series and the coefficients in these are found from the M.I.T. tables by interpolation. The same values are then obtained by the second-order theory of Kopal. The values of coefficients are found from the M.I.T. tables for large angles of yaw.[5] As has been pointed out by several writers, the M.I.T. tables are inconvenient to use as they stand since all data are given with reference to spherical polars based on the wind direction. These are particularly unsuitable when comparison is to be made with measurements, and both methods are here transformed for use with body coordinates in accordance with the procedure set out by Roberts and Riley.[6] At the same time, account has been taken of the correction to be made to the M.I.T. tables for slightly yawed cones.

The first-order results are corrected to fit in with the entropy distribution proposed by Ferri.[4] The Stone theory gives a variable entropy distribution round the cone which is in conflict with the requirement that the solid cone be a stream surface. Ferri showed that, to meet the latter requirement, all stream surfaces, after crossing the shock, curve round the cone to converge on a common generator on the leeward side of the meridian plane. Ferri then put forward a neat modification to the Stone theory to take account of this effect. This is illustrated in Fig. 3, which is a section of the field of flow on the sphere r = constant. The stream surfaces make sections which are radial lines through F, the point defining the stream direction, ahead of the shock. These are deflected through a variable angle on crossing the shock. According to the Stone theory, they then end at distributed points on the cone surface. Thus the streamline XY would end at the point adjacent to Z. This gives a variable entropy distribution round the cone. To correct this, Ferri assumes that the streamline follows the path calculated by the Stone theory after crossing the shock up to a point, Z, just outside the surface. It then turns sharply to follow the cone surface round to the point C. In other words, he introduces a vortical layer round the cone which is of infinitesimal thickness and across which the entropy changes from the value given by the Stone theory to the constant value on the cone.

The Stone theory gives a value of the entropy on the cone which is a linear function of cos ϕ. This is the value at the point on the outer edge of the vortical layer. At one point, B, in the meridian plane on the windward side, the vortical layer has zero strength, so the Stone value of the entropy here is equal to the value required on the conical surface. Hence the entropy change across the layer can be found right round the cone. The corrected value of the pressure on the cone then follows at once. The procedure for finding the correction is given in full by Ferri.[4] The details set out by Ferri are referred to shock axes, that is, spherical polars based on the cone vertex and axis of the shock cone, which is circular on the first-order theory. In the present application the correction has been worked out in terms of body axes.

(4) Results and Discussion

The measured values of pressure coefficient, defined by

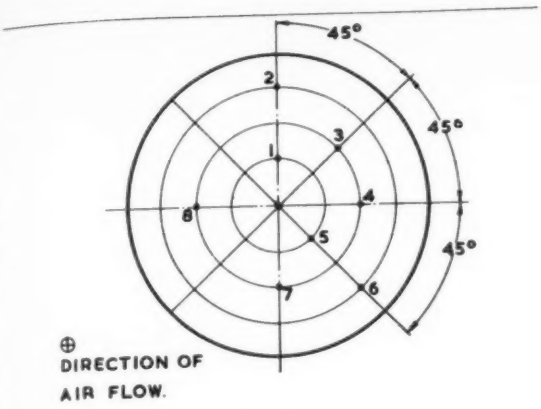

FIG. 1.

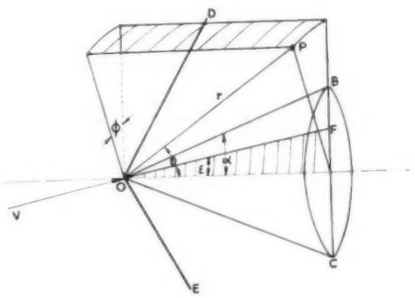

FIG. 2.

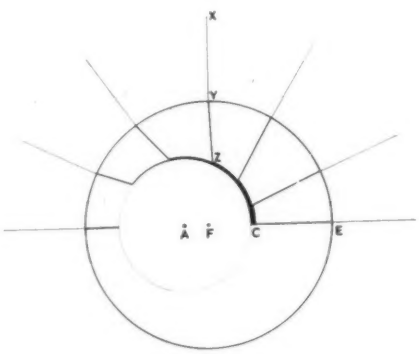

FIG. 3.

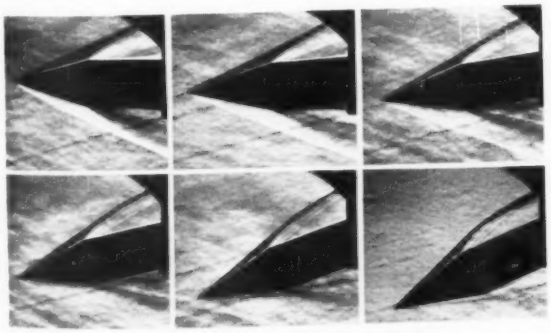

FIGS. 6–8. *Top row.* FIGS. 9–11. *Bottom row.*

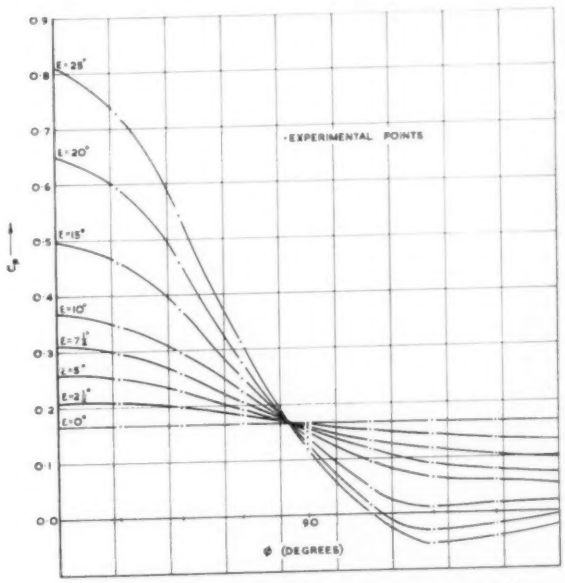

FIG. 4. Experimental values of pressure coefficient on 15° cone. $M = 3.53$.

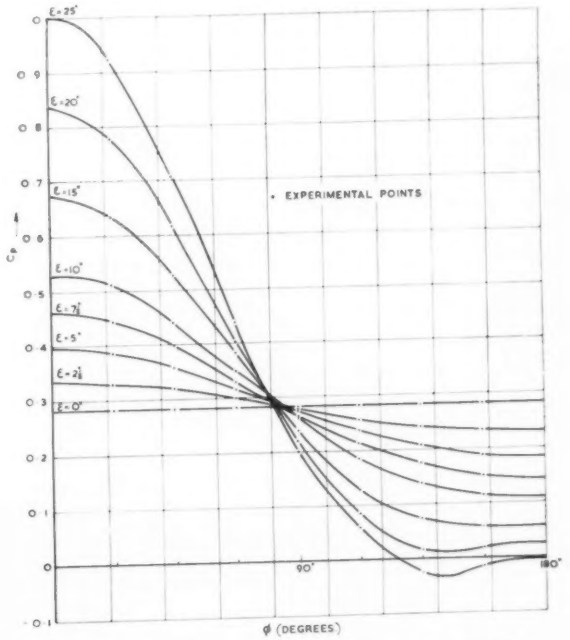

FIG. 5. Experimental values of pressure coefficient on 20° cone. $M = 3.53$.

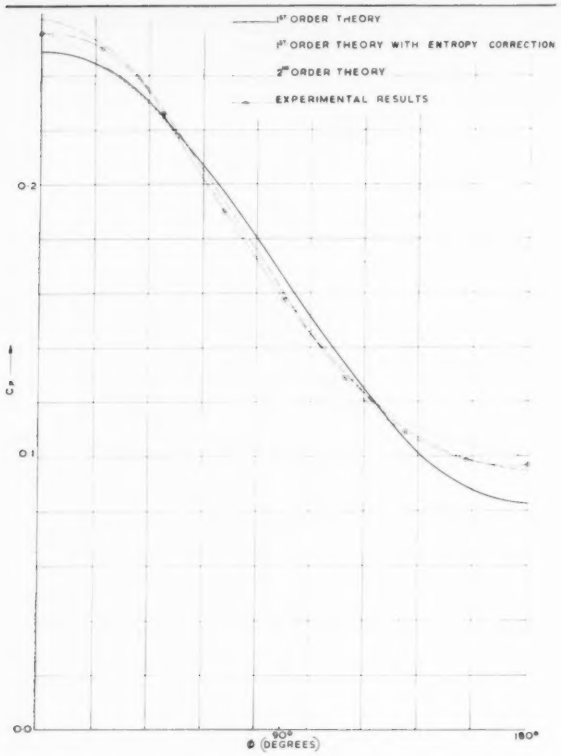

FIG. 12. Comparison of experimental and theoretical values of pressure coefficient. 15° cone, $M = 3.53$, $\epsilon = 5.°$

$$C_p = 2/(\gamma M^2)[(p/p_1) - 1]$$

where γ is the adiabatic index, p the pressure, p_1 the free-stream pressure, M the free-stream Mach Number, are shown in Fig. 4 in the case of the 15° cone and in Fig. 5 in the case of the 20° cone.

To the order of accuracy shown on the graph, all curves in Fig. 4 pass through a common point at the unyawed value. This means that one generator, just on the windward side of the middle generator, is practically unaffected by the yawing motion. The flow expands as we move from the windward to the leeward side, as we should expect, but the amount of expansion relative to that of compression is reduced as the angle of yaw is increased. When the angle of yaw exceeds the semicone angle, the pressure curve on the leeward side changes form, and a small pressure recovery takes place. At the highest angles of yaw there is a suction region on the expansion side of the cone. The characteristics of the pressure curves on the 20° cone are similar.

Schlieren photographs of the flow pattern in the meridian plane for the 15° cone are shown in Figs. 6–11. The change in shock angle on the two sides of the cone is clearly seen. When the angle of yaw exceeds the semicone angle, the trace of the shock on the leeward side disappears. We conclude that, at angles exceeding this value, a homentropic expansion region develops on the leeward side, the flow in which is independent of the flow passing through the conical shock. The conical shock changes in strength from a high value in the lower half of the plane of symmetry to a zero value above the leeward side of the cone, degenerating into the free-stream Mach cone. At the higher angles of yaw there is faint evidence of conical vortex shedding due to the cross-flow effect. Because the free-stream Mach Number in the present experiments is high, the vortices tend to be swept back very close to the cone surface.

Comparison of measured pressure coefficients with corresponding values obtained by calculation is shown in Figs. 12 and 13 in the case of the 15° cone, and in Figs. 14 and 15 on the 20° cone. On both cones two values of the angle of yaw, $\epsilon = 5°$ and $\epsilon = 15°$, are chosen.

On the 15° cone at $\epsilon = 5°$, no theory is in bad disagreement with experimental results. The Stone first-order curve deviates most from the observed values, but, when the entropy correction is applied, the first-order curve is very close to the experimental curve, particularly in the middle range of ϕ. The second-order theory gives the closest fit to the tunnel results over the whole range. On the same cone at $\epsilon = 15°$, the order of closeness of fit of the three calculated curves is unaltered, although effects are more marked. On the 20° cone at $\epsilon = 5°$, the entropy correction improves the first-order theory over most of the ϕ range but causes wide divergence from the experimental curve on the

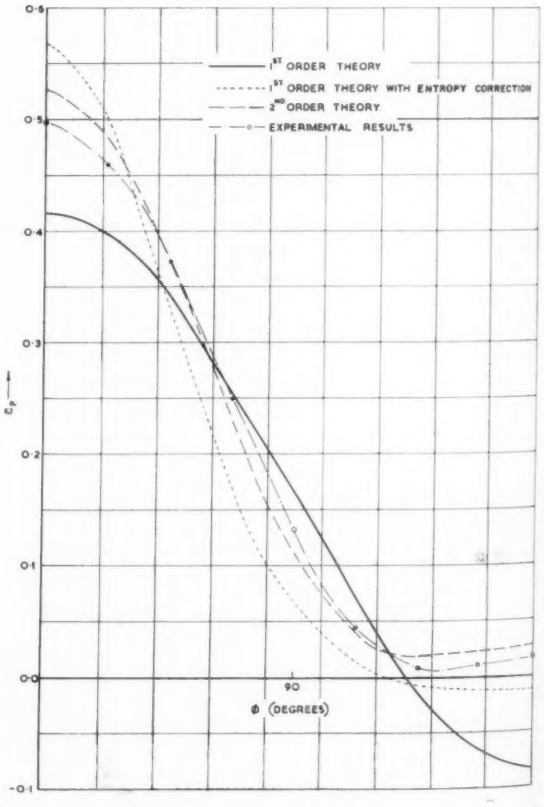

FIG. 13. Comparison of experimental and theoretical values of pressure coefficient. 15° cone, $M = 3.53$, $\epsilon = 15°$.

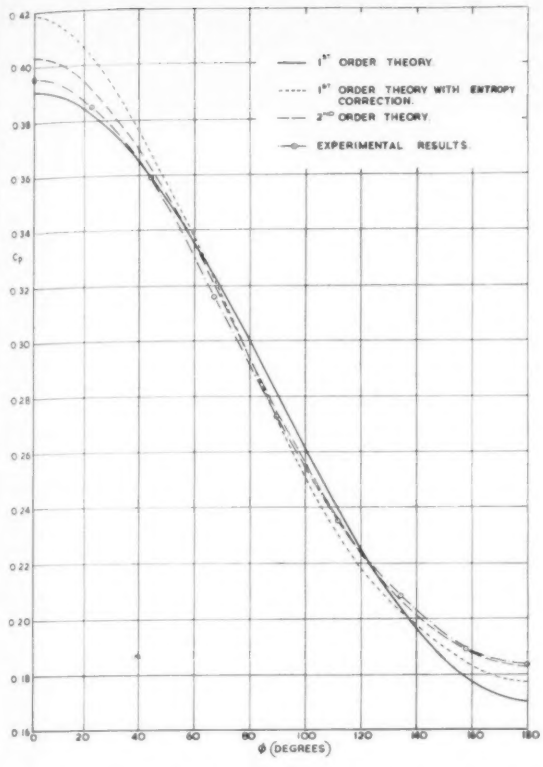

FIG. 14. Comparison of experimental and theoretical values of pressure coefficient. 20° cone, $M = 3.53$, $\epsilon = 5°$.

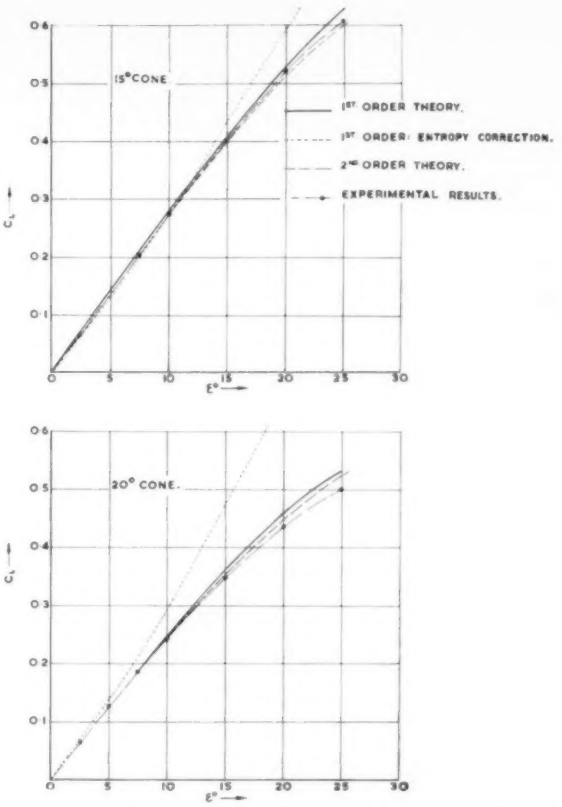

FIG. 16. Comparison of experimental and theoretical values of C_L.

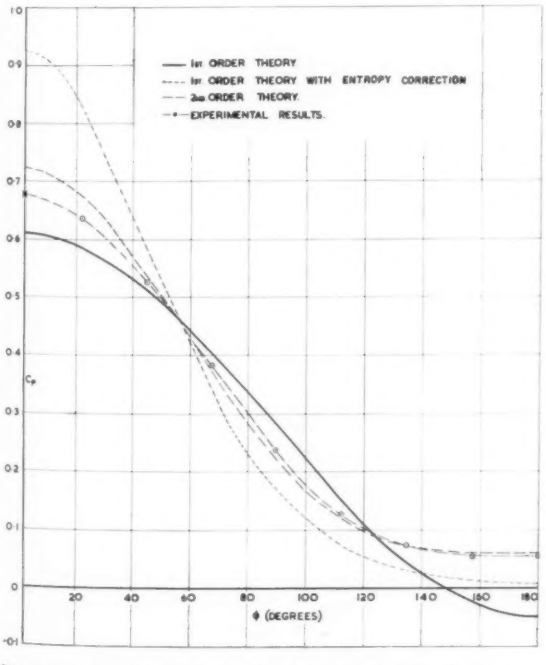

FIG. 15. Comparison of experimental and theoretical values of pressure coefficient. 20° cone, $M = 3.53$, $\epsilon = 15°$.

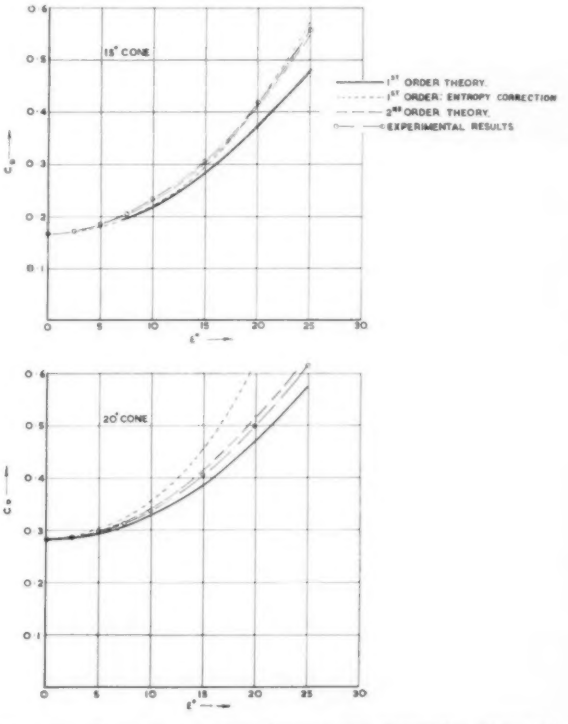

FIG. 17. Comparison of experimental and theoretical values of C_D.

windward face. At $\epsilon = 15°$ on this cone, the first-order theory in its original and modified form is a poor approximation. The second-order theory gives uniformly good results.

Figs. 16 and 17 show curves of C_L and C_D, respectively, for the two cones. On the 15° cone the corrected first-order theory gives very good agreement with the observed C_L values up to angles of yaw of 10° but not at higher angles. The other calculated curves agree well with experiment in the higher ϵ range. On the 20° cone the corrected first-order theory gives much too high a value of C_L over the whole range and the original theory is much better. The second-order curve is quite close to observed values at all values of ϵ.

The entropy correction produces a particularly good C_D curve on the 15° cone and improves the original theory considerably, but the second-order curve is the best of the three. On the 20° cone the first-order results are considerably below observed values, but the entropy correction brings them much too far above the observed values. The second-order theory is again in closest agreement with observation.

The comparison of theory with experiment shows that cross-wind and viscosity effects are not important on cones at this high Mach Number. If they were, we should expect to find marked differences between calculated and measured values of pressure on the leeward side of the cone. In fact the biggest differences between the second-order theory and observation are found on the windward side.

We conclude that the entropy correction applied here improves the first-order theory on cones of moderate angle at small angles of yaw, but does not improve matters on cones of larger angle or on those of moderate angle at large incidence, for which the uncorrected first-order theory is poor. The second-order theory is in remarkably good agreement with experiment on both cones, even at large angles of yaw. This is particularly true of the integrated lift and drag coefficients, which are, apparently, not sensitive to the actual form of entropy distribution round the cone.

When the work described here was complete, the results were shown to Professor Ferri. The final comments which follow take some account of his remarks and, also, of remarks by reviewers of the paper.

In its present form, based on the concept of a vortical singularity, the entropy correction is only responsible indirectly for the improvement in first-order values of the surface pressure. The vortical layer introduces first-order changes in the entropy and velocity distribution on the cone, but, as Ferri[4] points out, does not affect the surface pressure distribution. The changes in pressure values obtained here, and in Ferri's paper, are due primarily to the inclusion in the pressure equation of certain first-order terms which were discarded in Stone's analysis. In the second-order analysis developed by Kopal the terms discarded by Stone are restored, so it is not surprising that second-order values of surface pressure are in closest agreement with experiment.

To effect a further improvement on present results, the authors feel that a more complete account of the entropy singularity should be taken, both in the first- and second-order theories. Consideration should be given to its influence on the whole flow pattern behind the conical shock and not merely on the region adjacent to the cone surface. In this connection the analysis of the singularity made by one of the present authors (Holt[7]) may be of value.

References

[1] Ferrari, C., *Determination of the Pressure Exerted on Solid Bodies of Revolution with Pointed Noses Placed Obliquely in a Stream of Compressible Fluid at Supersonic Velocity*, R.T.P. Trans. No. 1105, British Ministry of Aircraft Production. (From Atti R. Accad. Sci. Torino, Vol. 72, pp. 140–163, November-December, 1936.)

[2] Sauer, R., *Supersonic Flow about Projectile Heads of Arbitrary Shape at Small Incidence*, R.T.P. Translation 1573, British Ministry of Aircraft Production. (From Luftfahrtforschung, Vol. 19, No. 4, pp. 148–152, May, 1942.)

[3] Stone, A. H., *On Supersonic Flow Past a Slightly Yawing Cone*, Jour. Math. and Phys., Vol. 27, No. 1, pp. 67–81, April, 1948.

[4] Ferri, Antonio, *Supersonic Flow Around Circular Cones at Angles of Attack*, NACA TR 1045, 1951.

[5] Staff of the Computing Section, Centre of Analysis (under direction of Zdenek Kopal) *Tables of Supersonic Flow Around Cones of Large Yaw*, Tech. Rep. No. 5, Massachusetts Institute of Technology, 1949.

[6] Roberts, Richard C., and Riley, James D., *A Guide to the Use of the M.I.T. Cone Tables*, Journal of the Aeronautical Sciences, Vol. 21, No. 5, pp. 336–342, 1954.

[7] Holt, M., *A Vortical Singularity in Conical Flow*, Quart. J. Mech. & Appl. Math., Vol. 7, No. 4, pp. 438–445, 1954.

On Heat Transfer in Laminar Boundary Layers at High Prandtl Number*

GEORGE W. MORGAN† AND W. H. WARNER‡
Brown University

SUMMARY

A study of the asymptotic behavior of the heat transfer in laminary boundary layers for large Prandtl Number is presented. The analysis is based on the observation that, for large Prandtl Number, the conduction term in the energy equation must be important only in a region that is very narrow compared with the velocity boundary layer, but that, in that region, both convection and conduction are essential. A transformation (based on the Prandtl Number) of the coordinate normal to the body surface leads to a form of the energy equation in which the appropriate convection and conduction terms can be balanced with respect to their asymptotic dependence on the Prandtl Number, and the behavior of the local heat-transfer coefficient can be deduced immediately.

The general method is applied to the well-known problems of forced convection over a body and of the plate thermometer, where it confirms results previously obtained by other methods. The problems of natural convection over a vertical body, of the flow above a rotating disc, and of the Hamel converging channel flow are then treated; new theoretical results are obtained for these cases.

(1) INTRODUCTION

THE PROBLEM OF COMPUTING the heat transfer through laminar boundary layers by analytical methods is generally a difficult one due to the complicated nature of the governing differential equations. The situation is considerably simplified if we restrict our attention to fluids (especially those with constant properties) with large Prandtl Number. In this case the thermal boundary layer is much thinner than the velocity boundary layer, so that the velocity distributions in the thermal layer can be approximated by the first terms in their power series expansions. Lighthill[1] has used this type of consideration to find an approximate solution of the energy equation for plane boundary-layer flows in forced convection with given arbitrary distributions of free-stream velocity and body surface temperature. Levy[2] has calculated numerical solutions to the energy equation for forced convection over a plate for various values of Prandtl Number up to 20 with the simple Hartree power law distributions for the free-stream velocity and the body temperature. Schuh,[3] in the process of considering the energy equation for the flat plate using the Hartree power law distribution cx^n for the temperature, has introduced transformations of the independent variable based on the power n and on the Prandtl Number σ in order to study the asymptotic behavior of the solutions for large values of these parameters. The σ transformation is of the same nature as one which will be of primary importance in the following work, but its general significance does not seem to be recognized. Schuh uses it to write the energy equation in a nicer form but does not utilize its physical and mathematical implications which enable one to determine the heat-transfer coefficient, as will be shown here. His resulting equation has been solved in closed form by Punnis;[4] similar equations and their solutions arise in the present work in the sections on the rotating disc and on the Hamel flow. Herbeck[5] has considered the same basic problem as Lighthill and Schuh but allows a somewhat more general stream function and hence permits a somewhat different velocity distribution in the thermal layer. Tifford and Chu[6] have treated the flat plate problem also, using a power series development $\Sigma c_n x^n$ for the surface temperature distribution, and have considered the behavior of solutions to the energy equation corresponding to the large values of n in the power series. This type of temperature distribution is intermediate between the arbitrary one of Lighthill and the simple power law of Schuh and Levy.

In this paper, we propose to exploit the assumption that the Prandtl Number is large more fully by developing an analysis for the thermal boundary layer in which, as a result of the large Prandtl Number, the thermal boundary layer appears as a narrow region within the relatively thick velocity boundary layer, much as the latter is itself a narrow region within the entire flow whenever the Reynolds Number is much larger than one. It will be shown that this method allows one to arrive very rapidly at partial analytical results at least—e.g., the asymptotic dependence of the temperature gradient at the wall on Prandtl Number—in cases where the differential equations are still too difficult to solve exactly. In other cases, it is possible to give a complete analytical solution of the equations that are satisfied by the asymptotic expressions of the desired temperature functions.

The method will be illustrated by means of the relatively simple cases of the forced convection over a body and of the thermometer problem, where it confirms quickly results already known. It will then be

Received August 16, 1955.

* The results in this paper were obtained in the course of research sponsored by the Office of Naval Research under Contracts Nonr 562(10) and Nonr 562(07).

† Associate Professor of Applied Mathematics, Brown University.

‡ Formerly, Research Associate in Applied Mathematics, Brown University. Now, Assistant Professor, Department of Mechanics and Materials, University of Minnesota.

applied to the more difficult problems of free convection over a nearly vertical slender body and to the flows above a rotating disc and in a converging channel, for which new results are obtained in all cases.

(2) Preliminary Discussion: The Thermal Boundary-Layer Equation

Consider the two-dimensional steady flow of a viscous fluid of constant properties about a body. We distinguish between two types of flow: forced convection flows, where the body forces per unit mass are unimportant, and natural or free convection flows, where the body forces are important. We wish to determine the behavior of the local heat-transfer coefficient for flows at high Prandtl Number, or, in terms of the standard nondimensional quantities, the dependence of the Nusselt Number on the Prandtl Number and the Reynolds or Grashof Number for large values of the Prandtl Number.

Before discussing the method developed and applied in this paper, we wish to consider briefly the derivation of the thermal boundary-layer equation in order that the terminology used in the rest of the paper may be standardized. We shall reduce the equations to nondimensional form for the purposes of the discussion.

Let x_1 and y_1 be coordinates along and normal to the body surface, u_1 and v_1 the velocity components in these directions, p_1 the pressure, q_1 and r_1 the body forces per unit mass in the x_1 and y_1 directions, and t_1 the temperature; let ρ, μ, ν, c_p, and k have their usual meanings of density, absolute viscosity, kinematic viscosity, specific heat at constant pressure, and thermal conductivity, respectively.

The boundary conditions on velocity and temperature which will be considered fall into the following classes:

$$u_1(x_1, 0) = 0, \quad v_1(x_1, 0) = 0, \quad t_1(x_1, \infty) = t_\infty \tag{2.1}$$

$$u_1(x_1, \infty) = U_1(x_1) \tag{2.2}$$

$$u_1(x_1, \infty) = 0 \tag{2.3}$$

$$t_1(x_1, 0) = t_0(x_1) \tag{2.4}$$

$$\partial t_1/\partial y_1|_{y_1=0} = 0 \tag{2.5}$$

The conditions (2.1) apply in all problems; conditions (2.2) and either (2.4) or (2.5) will be used in forced convection problems; and conditions (2.3) and (2.4) apply in free convection.

Consider the equations of motion and the energy equation. In forced convection we shall choose $q_1 = r_1 = 0$; in free convection, $q_1 = g\beta(t_1 - t_\infty)\cos\alpha$, $r_1 = g\beta(t_1 - t_\infty)\sin\alpha$, where g is the acceleration due to gravity, β is taken as the coefficient of expansion for liquids and as t_∞^{-1} for gases, and α is the angle from the x-axis to the vertical direction (direction of the body force vector in the fluid). Introduce the nondimensional quantities x, y, u, v, p, t, q, and r into the equations of motion and the energy equation by the relations

$$x_1 = Lx, \quad y_1 = Ly, \quad t_1 = (t_0^* - t_\infty)t(x, y) + t_\infty \tag{2.6}$$

$$u_1 = U_0 u(x, y), \quad v_1 = U_0 v(x, y), \quad p_1 = \rho U_0^2 p(x, y) \tag{2.7}$$

$$\left.\begin{aligned} u_1 &= \nu L^{-1}u(x, y), \quad v_1 = \nu L^{-1}v(x, y), \quad p_1 = \rho(\nu L^{-1})^2 p(x, y) \\ q_1 &= \nu^2 L^{-3} q(x, y), \quad r_1 = \nu^2 L^{-3} r(x, y) \end{aligned}\right\} \tag{2.8}$$

where Eqs. (2.6) and (2.7) hold for forced convection and Eqs. (2.6) and (2.8) hold for free convection. Here L is a characteristic body length, U_0 is a characteristic velocity far from the body in forced convection [for example, $U_0 = \max U_1(x_1)$], and t_0^* is a characteristic temperature [for example, $t_0^*(\not\equiv t_\infty) = \max t_0(x_1)$ if condition (2.4) applies and $t_0^* = 2t_\infty$ if condition (2.5) applies].

Finally, introduce the nondimensional stream function $\psi(x, y)$ such that $u = \partial\psi/\partial y$, $v = -\partial\psi/\partial x$. The equations and boundary conditions become:†

(a) Forced convection:

$$\left.\begin{aligned} &\frac{\partial\psi}{\partial y}\frac{\partial^2\psi}{\partial x\partial y} - \frac{\partial\psi}{\partial x}\frac{\partial^2\psi}{\partial y^2} = R^{-1}\left(\frac{\partial^3\psi}{\partial x^2\partial y} + \frac{\partial^3\psi}{\partial y^3}\right) - \frac{\partial p}{\partial x} \\ &-\frac{\partial\psi}{\partial y}\frac{\partial^2\psi}{\partial x^2} + \frac{\partial\psi}{\partial x}\frac{\partial^2\psi}{\partial y\partial x} = -R^{-1}\left(\frac{\partial^3\psi}{\partial x^3} + \frac{\partial^3\psi}{\partial x\partial y^2}\right) - \frac{\partial p}{\partial y} \\ &\frac{\partial\psi}{\partial y}\frac{\partial t}{\partial x} - \frac{\partial\psi}{\partial x}\frac{\partial t}{\partial y} = (R\sigma)^{-1}\left(\frac{\partial^2 t}{\partial x^2} + \frac{\partial^2 t}{\partial y^2}\right) + K_1 R^{-1}\left[4\left(\frac{\partial^2\psi}{\partial x\partial y}\right)^2 + \left(\frac{\partial^2\psi}{\partial y^2} - \frac{\partial^2\psi}{\partial x^2}\right)^2\right] \\ &\psi(x, 0) = (\partial\psi(x, 0)/\partial y) = 0; \quad (\partial\psi(x, \infty)/\partial y) = U(x); \quad t(x, \infty) = 0 \end{aligned}\right\} \tag{2.9}$$

and either

$$t(x, 0) = \theta(x)$$

or

$$\partial t(x, 0)/\partial y = 0$$

(b) Free convection:

$$\left.\begin{aligned} &\frac{\partial\psi}{\partial y}\frac{\partial^2\psi}{\partial x\partial y} - \frac{\partial\psi}{\partial x}\frac{\partial^2\psi}{\partial y^2} = \frac{\partial^3\psi}{\partial x^2\partial y} + \frac{\partial^3\psi}{\partial y^3} - \frac{\partial p}{\partial x} + q \\ &-\frac{\partial\psi}{\partial y}\frac{\partial^2\psi}{\partial x^2} + \frac{\partial\psi}{\partial x}\frac{\partial^2\psi}{\partial y\partial x} = -\left(\frac{\partial^3\psi}{\partial x^3} + \frac{\partial^3\psi}{\partial x\partial y^2}\right) - \frac{\partial p}{\partial y} + r \\ &\frac{\partial\psi}{\partial y}\frac{\partial t}{\partial x} - \frac{\partial\psi}{\partial x}\frac{\partial t}{\partial y} = \sigma^{-1}\left(\frac{\partial^2 t}{\partial x^2} + \frac{\partial^2 t}{\partial y^2}\right) + K_2 G^{-1}\left[4\left(\frac{\partial^2\psi}{\partial x\partial y}\right)^2 + \left(\frac{\partial^2\psi}{\partial y^2} - \frac{\partial^2\psi}{\partial x^2}\right)^2\right] \\ &\psi(x, 0) = \partial\psi(x, 0)/\partial y = \partial\psi(x, \infty)/\partial y = 0; \quad t(x, \infty) = 0; \quad t(x, 0) = \theta(x) \end{aligned}\right\} \tag{2.10}$$

† To conserve space, we have omitted all terms involving the curvature of the boundary in anticipation of the well-known fact that these are negligible in the boundary-layer formulation of the equations.

Here R is the Reynolds Number, σ is the Prandtl Number, G is the Grashof Number, K_1 and K_2 are two other nondimensional numbers, and $U(x)$ and $\theta(x)$ are nondimensional velocity and temperature ratios given by

$$\left.\begin{aligned} R &= U_0 L/\nu \\ \sigma &= c_p\mu/k \\ G &= \frac{g\beta(t_0^* - t_\infty)L^3}{\nu^2} \\ K_1 &= \frac{U_0^2}{c_p(t_0^* - t_\infty)} \\ K_2 &= Lg\beta/c_p \\ U(x) &= U_1(x_1)/U_0 \\ \theta(x) &= [t_0(x_1) - t_\infty]/(t_0^* - t_\infty) \end{aligned}\right\} \quad (2.11)$$

If we consider the body forces in Eqs. (2.10) more carefully, we find:

$$q_1 = (\nu^2/L^3)q = g\beta\cos\alpha(t_1 - t_\infty) = g\beta\cos\alpha(t_0^* - t_\infty)t(x, y)$$

$$r_1 = (\nu^2/L^3)r = g\beta\sin\alpha(t_1 - t_\infty) = g\beta\sin\alpha(t_0^* - t_\infty)t(x, y)$$

so that

$$q = Gt(x, y)\cos\alpha, \quad r = Gt(x, y)\sin\alpha \quad (2.12)$$

where G is the Grashof Number.

From Eqs. (2.9) or (2.10) we wish to determine the behavior of the Nusselt Number as a function of the Prandtl Number and Reynolds Number or Grashof Number for large values of the Prandtl Number. (In the case of no heat transfer at the body surface, $\partial t/\partial y_{y=0} = 0$, we are interested in the dependence of $t(x, 0)$ itself on σ.) The Nusselt Number is defined by

$$N = Q_1/[kb(t_0^* - t_\infty)] \quad (2.13)$$

where Q_1 is the heat flow per unit time through an element of surface, say of length L and breadth b:

$$Q_1 = -kb\int_0^L \left.\frac{\partial t_1}{\partial y_1}\right|_{y_1=0} dx_1 \quad (2.14)$$

Thus

$$N = -\int_0^1 \left.\frac{\partial t}{\partial y}\right|_{y=0} dx \quad (2.15)$$

in terms of the nondimensional coordinates and temperature.

To determine N, we first transform the equations into the boundary-layer equations. The normal coordinate y is changed by so-called boundary-layer stretching. In the case of forced convection, introduce $\xi = R^{1/2}y$; in the case of free convection, $\xi = G^{1/4}y$. Then, either by the usual qualitative boundary-layer considerations or by the search for solutions in the form of asymptotic series in $R^{1/2}$ in the one case, and in $G^{1/4}$ in the other, the hydrodynamic equations are reduced to the usual boundary-layer equations. The energy equation is also transformed; it is with the latter that we are concerned here.

In forced convection, let $\xi = R^{1/2}y$, $\psi(x, y) = R^{-1/2}w(x, \xi)$, $t(x, y) = T(x, \xi)$. Then the energy equation from Eqs. (2.9) becomes:

$$\frac{\partial w}{\partial \xi}\frac{\partial T}{\partial x} - \frac{\partial w}{\partial x}\frac{\partial T}{\partial \xi} = \sigma^{-1}\frac{\partial^2 T}{\partial \xi^2} + (R\sigma)^{-1}\frac{\partial^2 T}{\partial x^2} + K_1\left(\frac{\partial^2 w}{\partial \xi^2}\right)^2 + K_1R^{-1}\left[4\left(\frac{\partial^2 w}{\partial x\partial \xi}\right)^2 - 2\frac{\partial^2 w}{\partial x^2}\frac{\partial^2 w}{\partial \xi^2}\right] + K_1R^{-2}\left(\frac{\partial^2 w}{\partial x^2}\right)^2$$

Considering only the convection and conduction terms, we see that, if σ is of order one, for large Reynolds Number the second conduction term can be neglected with respect to the first. For σ large, however, it would seem that both conduction terms are small. But we know that a conduction term is necessary near the body surface, for otherwise we could not satisfy the temperature boundary condition there. Thus, for σ large, the temperature gradient $\partial T/\partial \xi$ and its derivative $\partial^2 T/\partial \xi^2$ in the normal direction must be large compared to one and the ratio of the first conduction term to the second is even greater than for σ about one. This leads to the conclusion that the thermal boundary layer is much thinner than the velocity boundary layer for σ large.

From the argument given above, the thermal boundary-layer equation is

$$[(\partial w/\partial \xi)(\partial T/\partial x)] - [(\partial w/\partial x)(\partial T/\partial \xi)] = \sigma^{-1}(\partial^2 T/\partial \xi^2) + K_1(\partial^2 w/\partial \xi^2)^2 \quad (2.16)$$

and the Nusselt Number can be written as

$$N = -R^{1/2}\int_0^1 \left.\frac{\partial T}{\partial \xi}\right|_{\xi=0} dx \quad (2.17)$$

For free convection, let $\xi = G^{1/4}y$, $\psi = G^{1/4}w$, $t = T$; then, upon substitution of these quantities into the energy equation of Eqs. (2.10), we obtain the thermal boundary-layer equation by an argument, based on large values of the Grashof Number, which is exactly analogous to that based on the Reynolds Number.

Thus, the thermal boundary-layer equation in free convection is

$$[(\partial w/\partial \xi)(\partial T/\partial x)] - [(\partial w/\partial x)(\partial T/\partial \xi)] = \sigma^{-1}(\partial^2 T/\partial \xi^2) + K_2(\partial^2 w/\partial \xi^2)^2 \quad (2.18)$$

and the Nusselt Number is given by

$$N = -G^{1/4}\int_0^1 \left.\frac{\partial T}{\partial \xi}\right|_{\xi=0} dx \quad (2.19)$$

(3) Dependence of the Nusselt Number on the Prandtl Number; Description of the Method

By the derivation given above, for large Prandtl Number the thermal boundary-layer equation has the same basic form in all cases. In each particular problem, a decision must be made as to the magnitude

of the effect of the dissipation term $K(\partial^2 w/\partial\xi^2)^2$ on the temperature distribution; sometimes it is kept, and sometimes it is dropped. In any case, we have for large σ a singular perturbation problem in the parameter σ^{-1}, since the highest derivative of the temperature is multiplied by σ^{-1}.

Consider now a further transformation of the normal coordinate of the form $\eta = \sigma^m \xi$, $m > 0$. This amounts to a further stretching of the thermal boundary layer based on the Prandtl Number, much as the velocity and thermal boundary layers were effectively expanded or stretched by the transformation from y to ξ based on the Reynolds or Grashof Numbers. Assume further that any function $f(x, \xi)$ appearing in the boundary-layer equation which is dependent on σ can be transformed by $f(x, \xi) = \sigma^n F(x, \eta)$ in such a way that F and its first few derivatives with respect to η are independent of σ to a first approximation in the thermal boundary layer.

If these substitutions are made in the energy equation and if the terms in the equation which must be of equal importance near the boundary are balanced with respect to their σ dependence, then the exponents m, n, etc., appearing in the transformation can be determined. This enables us to calculate the dependence of the Nusselt Number on σ and also the dependence on σ of other quantities of interest in particular cases.

So far, nothing has been said about the treatment of the stream function $w(x, \xi)$ in the energy equation. In the thermal layer, we can replace w by the first term in its ξ power series development for σ large, since the thermal layer is much thinner than the velocity layer. The details of this treatment will be considered in each example. The important thing to note is that in no case can the initial prescribed temperature distribution or the prescribed free-stream velocity, when these are present in a problem, affect the Prandtl Number dependence to the first order; they only affect the coefficients appearing in the formulas. This presupposes, of course, that these prescribed conditions are of such a nature that they do not violate the boundary-layer theory assumptions.

(4) Example I: Forced Convection over a Body

In the forced convective flow over a body with arbitrary free-stream velocity distribution and arbitrary body surface temperature, the dissipation terms in the energy equation can be neglected in comparison with the conductive and convective terms. The nondimensional energy equation and Nusselt Number, after the Reynolds Number transformation, are thus of the form of Eqs. (2.16) and (2.17) with $K_1 \cong 0$:

$$\left.\begin{aligned} \frac{\partial w}{\partial \xi}\frac{\partial T}{\partial x} - \frac{\partial w}{\partial x}\frac{\partial T}{\partial \xi} &= \sigma^{-1}\frac{\partial^2 T}{\partial \xi^2} \\ N &= -R^{1/2}\int_0^1 \left.\frac{\partial T}{\partial \xi}\right|_{\xi=0} dx \end{aligned}\right\} \tag{4.1}$$

For Prandtl Number large, the stream function can be approximated by the first term in its ξ power series:

$$w(x, \xi) \cong A(x)\xi^2 \tag{4.2}$$

Note that the free-stream velocity distribution affects the form of $A(x)$ but not the ξ dependence of w; the latter is determined by the surface velocity boundary conditions.

We now apply the method of the Prandtl Number expansion of the thermal layer. Let

$$\eta = \sigma^m \xi, \; T(x, \xi) = \sigma^n S(x, \eta) \tag{4.3}$$

Since the temperature of the body surface is prescribed, $T(x, 0) = \sigma^n S(x, 0) = \theta(x)$, and cannot depend on σ; hence we have $n = 0$ immediately. Under the transformations (4.3) and the assumption (4.2), the relations (4.1) become

$$\left.\begin{aligned} 2A(x)\sigma^{-m}\eta(\partial S/\partial x) - A'(x)\sigma^{-m}\eta^2(\partial S/\partial \eta) &= \\ \sigma^{-1+2m}(\partial^2 S/\partial \eta^2) & \\ N = -R^{1/2}\sigma^m \int_0^1 \left.\frac{\partial S}{\partial \eta}\right|_{\eta=0} dx & \end{aligned}\right\} \tag{4.4}$$

Assume that S and its first two derivatives with respect to the variable η are independent of the Prandtl Number to the first approximation. Then, in order that the convective and conductive terms may have the same dependence on σ for large σ, $-m = -1 + 2m$, or $m = 1/3$. Thus,

$$\left.\begin{aligned} 2A(x)\eta(\partial S/\partial x) - A'(x)\eta^2(\partial S/\partial \eta) &= \partial^2 S/\partial \eta^2 \\ N = -R^{1/2}\sigma^{1/3}\int_0^1 \left.\frac{\partial S}{\partial \eta}\right|_{\eta=0} dx & \end{aligned}\right\} \tag{4.5}$$

If the integral in Eqs. (4.5) can be estimated or calculated from the equation for S, then a specific numerical coefficient can be given for the Nusselt Number formula. The important thing to note is that the $\sigma^{1/3}$ behavior can be derived from the energy equation without attempting to solve it at all.

The $\sigma^{1/3}$ dependence is well known, of course. In particular, the case of forced convection over a flat plate with constant free-stream velocity and constant plate temperature was treated by Pohlhausen;[7] Pohlhausen finds the $\sigma^{1/3}$ behavior after solving the equations by use of a similarity hypothesis and by use of numerical calculations for various values of σ. Lighthill's[1] detailed analysis for arbitrary free-stream velocity and arbitrary body temperature again leads to the $\sigma^{1/3}$ behavior.

(5) Example II: The Thermometer Problem

Consider now the forced convection flow over a body, where now the temperature boundary condition at the body is that of no heat transfer instead of that of a prescribed temperature distribution. The dissipative term is now important, and the full relation (2.16) is used as the nondimensional thermal boundary-layer equation:

$$[(\partial w/\partial \xi)(\partial T/\partial x)] - [(\partial w/\partial x)(\partial T/\partial \xi)] = \sigma^{-1}(\partial^2 T/\partial \xi^2) + K_1(\partial^2 w/\partial \xi^2)^2 \quad (5.1)$$

Again, $w(x, \xi) \cong A(x)\xi^2$. Let

$$\eta = \sigma^m \xi, \; T(x, \xi) = \sigma^n S(x, \eta) \quad (5.2)$$

Since the boundary condition is $\partial T/\partial \xi|_{\xi=0} = 0$, we cannot determine n immediately in this case. Substituting these relations in Eq. (5.1), we find

$$2A\sigma^{n-m}\eta(\partial S/\partial x) - A'\sigma^{n-m}\eta^2(\partial S/\partial \eta) = \sigma^{-1+n+2m}(\partial^2 S/\partial \eta^2) + 4K_1A^2$$

If all terms are to be equally important in their σ dependence (with S, $\partial S/\partial \eta$, $\partial^2 S/\partial \eta^2$ independent of σ),

$$n - m = -1 + n + 2m = 0 \quad \text{or} \quad m = n = 1/3$$

Hence,

$$\left.\begin{aligned} 2A(x)\eta(\partial S/\partial x) - A'\eta^2(\partial S/\partial \eta) &= (\partial^2 S/\partial \eta^2) + 4K_1A^2 \\ T(x, 0) &= \sigma^{1/3}S(x, 0) \end{aligned}\right\} \quad (5.3)$$

In this case, the quantity of interest is the nondimensional temperature variation from the free-stream temperature due to the dissipative effects

$$t(x, 0) = T(x, 0) = \sigma^{1/3}S(x, 0) \quad (5.4)$$

Again, if Eqs. (5.3) can be solved approximately for $S(x, 0)$, a coefficient that is a function of x only can be obtained. Note the $\sigma^{1/3}$ behavior is again obtained without actual solution of the problem.

Comparison of this result can be made with the well-known treatments of other authors. The first investigation for the flat plate thermometer (as well as the simple forced flow over a plate at constant temperature) is due to Pohlhausen.[7] His results for constant velocity in the main stream give $t(x, 0) \sim \sigma^{1/2}$ for σ near one. For larger σ, the $\sigma^{1/2}$ relation breaks down. Crocco[8] obtained the $\sigma^{1/3}$ relation for σ greater than 200 or 300 by the use of the asymptotic forms of the integrals appearing in the solution of the energy equation (written in his form with the stream function replacing the normal coordinate y as an independent variable and for the compressible case $\rho\mu$ = constant). Lighthill,[1] in his general discussion of the heat-transfer problem in forced convection flows, also treats the plate thermometer problem for arbitrarily prescribed main-stream velocity and free-stream temperature. Again, the basic result that the deviation from the free-stream temperature near the plate varies as $\sigma^{1/3}$ appears. Thus, by simple consideration of the boundary-layer energy equation, a result can be obtained which otherwise depends on the process of solution or approximate solution of the equation.

(6) Example III: Free Convection over a Slender Body; The Vertical Plate

In natural or free convection problems the effect of the buoyancy forces in the fluid adds a further complication to heat-transfer considerations in that the temperature effect on the hydrodynamic part of the problem must be considered; indeed, the latter is essential in producing such a flow. The appropriate nondimensional flow equations are Eqs. (2.10), with the body forces q and r given by relations (2.12). If the Grashof Number transformation, similar to the Reynolds Number transformation for forced convection flows, is applied, the appropriate boundary-layer equations result. If we assume that the body surface deviates little from the direction of the buoyancy force, so that the angle α is small, the pressure gradient can be neglected as can the effect of the body force r. Thus we shall consider primarily slender bodies oriented in the direction of the body force q.

The application of the transformation $\xi = G^{1/4}y$, $\psi(x, y) = G^{1/4}w(x, \xi)$, $t(x, y) = T(x, \xi)$ leads to the boundary-layer equations in x and ξ:

$$\left.\begin{aligned} \frac{\partial w}{\partial \xi}\frac{\partial^2 w}{\partial x \partial \xi} - \frac{\partial w}{\partial x}\frac{\partial^2 w}{\partial \xi^2} &= \frac{\partial^3 w}{\partial \xi^3} + T\cos\alpha \\ \frac{\partial w}{\partial \xi}\frac{\partial T}{\partial x} - \frac{\partial w}{\partial x}\frac{\partial T}{\partial \xi} &= \sigma^{-1}\frac{\partial^2 T}{\partial \xi^2} + K_2\left(\frac{\partial^2 w}{\partial \xi^2}\right)^2 \\ w(x, 0) = \frac{\partial w\,(x, 0)}{\partial \xi} &= \frac{\partial w\,(x, \infty)}{\partial \xi} = 0; \\ T(x, 0) &= \theta(x), \; T(x, \infty) = 0 \end{aligned}\right\} \quad (6.1)$$

Here $\cos\alpha$ is one, or almost one, since $\alpha \cong 0$.

If we now apply the Prandtl Number transformation for large Prandtl Number, then the behavior of the Nusselt Number and of the viscous shear stress can be determined. Let

$$\eta = \sigma^m \xi, \; w(x, \xi) = \sigma^n \Omega(x, \eta), \; T(x, \xi) = S(x, \eta) \quad (6.2)$$

Then Eqs. (6.1) are transformed into

$$\sigma^{2n+2m}\left(\frac{\partial \Omega}{\partial \eta}\frac{\partial^2 \Omega}{\partial x \partial \eta} - \frac{\partial \Omega}{\partial x}\frac{\partial^2 \Omega}{\partial \eta^2}\right) = \sigma^{n+3m}\frac{\partial^3 \Omega}{\partial \eta^3} + S\cos\alpha$$

$$\sigma^{n+m}\left(\frac{\partial \Omega}{\partial \eta}\frac{\partial S}{\partial x} - \frac{\partial \Omega}{\partial x}\frac{\partial S}{\partial \eta}\right) = \sigma^{-1+2m}\frac{\partial^2 S}{\partial \eta^2} + K_2\sigma^{2n+4m}\left(\frac{\partial^2 \Omega}{\partial \eta^2}\right)^2$$

$$\Omega(x, 0) = \frac{\partial \Omega\,(x, 0)}{\partial \eta} = \frac{\partial \Omega\,(x, \infty)}{\partial \eta} = 0; \quad S(x, 0) = \theta(x), \; S(x, \infty) = 0$$

In the first of these equations, we must have the buoyancy term $S\cos\alpha$ and the viscous term $\sigma^{n+3m}(\partial^3\Omega/\partial\eta^3)$ of the same order of magnitude near the boundary; since we have assumed that S and Ω and their first few derivatives are independent of σ, we have that $n + 3m = 0$. In the second equation, the convective and conductive terms must balance; hence $n + m = -1 + 2m$. Thus $m = 1/4$, $n = -3/4$, and

$$\left.\begin{aligned} \sigma^{-1}\left(\frac{\partial\Omega}{\partial\eta}\frac{\partial^2\Omega}{\partial x\partial\eta}-\frac{\partial\Omega}{\partial x}\frac{\partial^2\Omega}{\partial\eta^2}\right) &= \frac{\partial^3\Omega}{\partial\eta^3}+S\cos\alpha \\ \sigma^{-1/2}\left(\frac{\partial\Omega}{\partial\eta}\frac{\partial S}{\partial x}-\frac{\partial\Omega}{\partial x}\frac{\partial S}{\partial\eta}\right) &= \\ \sigma^{-1/2}\frac{\partial^2 S}{\partial\eta^2} &+ K_2\sigma^{-1/2}\left(\frac{\partial^2\Omega}{\partial\eta^2}\right)^2 \end{aligned}\right\} \quad (6.3)$$

We see that the inertial terms on the left of the first equation appear small compared to the viscous and buoyant terms for large σ and that the dissipative term in the energy equation is not larger than the rest on the basis of its σ dependence.†

From this result and relation (2.19) for the Nusselt Number, we have

$$N = -G^{1/4}\sigma^{1/4}\int_0^1 \left.\frac{\partial S}{\partial\eta}\right|_{\eta=0} dx \quad (6.4)$$

and noting that the viscous shear stress is proportional to $\partial^2 w/\partial\xi^2$ at $\xi = 0$,

$$\partial^2 w/\partial\xi^2 = \sigma^{-1/4}(\partial^2\Omega/\partial\eta^2) \quad (6.5)$$

or the shearing stress $\tau(x_1)$ is given by

$$\tau(x_1) = \mu\left.\frac{\partial u_1}{\partial y_1}\right|_{y_1=0} = \frac{\mu^2}{\rho L^2}G^{3/4}\sigma^{-1/4}\left.\frac{\partial^2\Omega}{\partial\eta^2}\right|_{\eta=0} \quad (6.6)$$

Thus the heat-transfer coefficient in free convection behaves as $\sigma^{1/4}$ and the shearing stress as $\sigma^{-1/4}$. There does not seem to be any statement of the latter result in the literature.

In order to compare results obtainable by this method with those obtained by other authors, we select a particular example. Consider a vertical flat plate of length L kept at a constant temperature $t_1(x_1, 0) = t_0{}^*$. The angle α appearing in the body force expressions is exactly equal to zero in this case. Assume that the dissipative terms in the energy equation can be neglected. The usual method found in the literature for treating this problem (whether the plate be considered as finite or semi-infinite in extent) is to search for solutions in terms of a similarity variable. For comparison with those results, we use the similarity transformation before applying the Prandtl Number method.

Let

$$\zeta = \xi x^{-1/4}, \quad w(x,\xi) = 4x^{3/4}f(\zeta), \quad T(x,\xi) = h(\zeta) \quad (6.7)$$

Then Eqs. (6.1) in this case reduce to the following ordinary differential equations in the variable ζ:

$$\left.\begin{aligned} f''' + 3ff'' - 2f'^2 + h &= 0 \\ h'' + 3\sigma fh' &= 0 \\ f(0) = f'(0) = f'(\infty) = h(\infty) &= 0 \\ h(0) &= 1 \end{aligned}\right\} \quad (6.8)$$

† It must be noted that the form of Eqs. (6.3) and the conclusions drawn from them about the relative size of terms are valid only in the thermal boundary layer; the inertial terms in the momentum equation are not negligible outside this region.

TABLE 1
The Heat-Transfer Coefficient $N/(G\sigma)^{1/4}$ as a Function of Prandtl Number

σ	0.733	10	100	1,000
Schuh	0.731	0.865	0.922	0.923
Ostrach	0.732	0.877	0.924	0.940
Eqs. (6.14)		0.924	0.924	0.924

where the prime indicates differentiation with respect to ζ.

The Nusselt Number becomes, from Eq. (2.19),

$$N = -(4/3)G^{1/4}h'(0) \quad (6.9)$$

and the viscous shear stress can be written as

$$\tau(x_1) = 4\rho\nu^2(x_1G^3L^{-9})^{1/4}f''(0) \quad (6.10)$$

If we now apply the thermal boundary-layer expansion method based on the Prandtl Number to Eqs. (6.8) and use the same type of balancing arguments described in connection with Eqs. (6.3), we determine as before the dependence to the first order on σ of $h'(0)$ and $f''(0)$. In particular, the transformations

$$\eta = \sigma^{1/4}\zeta, \quad f(\zeta) = \sigma^{-3/4}F(\eta), \quad h(\zeta) = H(\eta) \quad (6.11)$$

lead to the results

$$\left.\begin{aligned} N/(G\sigma)^{1/4} &\cong -(4/3)H'(0) \\ [(\sigma L^9)/(x_1G^3)]^{1/4}[\tau(x_1)/(\rho\nu^2)] &\cong 4F''(0) \end{aligned}\right\} \quad (6.12)$$

where $H'(0)$ and $F''(0)$ are independent of σ to the first order.

Let us now consider the known numerical solutions of Eqs. (6.8) and some other approximate theoretical treatments.

Schuh[9] and Ostrach[10] have calculated numerical solutions of Eqs. (6.8) for various values of σ. If Ostrach's values for $\sigma = 100$ are accepted and if it is assumed that our asymptotic analysis holds for $\sigma = 100$, then we can calculate that

$$\left.\begin{aligned} -h'(0) &= 0.693\sigma^{1/4} \\ f''(0) &= 0.796\sigma^{-1/4} \end{aligned}\right\} \quad (6.13)$$

$$\left.\begin{aligned} &\text{Hence,} \quad N/(G\sigma)^{1/4} \cong (4/3)(0.693) = 0.924 \\ &[(\sigma L^9)/(x_1G^3)]^{1/4}[\tau(x_1)/(\rho\nu^2)] \cong \\ &\qquad 4(0.796) = 3.184 \end{aligned}\right\} \quad (6.14)$$

We first compare these results with those of Schuh[9] and Ostrach.[10] Since Schuh's results in the original reference are not readily available, we have compared them with the values given by Squire,[11] p. 806, Table 8, and by Schlichting,[12] p. 259, Table 14.4. The numbers given in these tables for the basic heat-transfer quantity $[K_N/(Ra)^{1/4}$ in reference 11 and $Nu_m/(GrPr)^{1/4}$ in reference 12] must be multiplied by $\sqrt{2}$ to be comparable with Eqs. (6.14). Ostrach's numbers must be multiplied by 4/3 to be comparable.‡ Table 1 lists the results of the comparison.

‡ If ζ_1, $f_1(\zeta_1)$, and $h_1(\zeta_1)$ represent the similarity variable and functions used by Ostrach, then the relation with the present variables is $\zeta = \sqrt{2}\,\zeta_1$, $\sqrt{2}f(\zeta) = f_1(\zeta_1)$, $h(\zeta) = h_1(\zeta_1)$.

TABLE 2
The Viscous Shear Stress
as a Function of Prandtl Number

σ	1	10	100	1,000
Ostrach: $4\sigma^{1/4} f''(0)$	2.568	2.980	3.184	3.260
Eqs. (6.14)		3.184	3.184	3.184

The asymptotic relation (6.14) agrees with Schuh's results of $\sigma = 100$ and 1,000 almost exactly, while it gives a result about 6.8 per cent too high for σ as low as ten.

For the sake of completeness, we give in Table 2 a comparison of Ostrach's figures for the viscous shear stress quantity with the asymptotic relation given by the second relation of Eq. (6.14). In Ostrach's terms, this must equal $4\sigma^{1/4} f_1''(0)$*.

The result given by Eqs. (6.14) is about 6.9 per cent too large at $\sigma = 10$; since Ostrach's results for $\sigma = 1{,}000$ vary from those of Schuh in the heat-transfer case (see Table 1), there is some doubt as to the validity of the comparison for $\sigma = 1{,}000$, but the agreement appears to be fairly good.

Eckert[13] has used momentum integral methods to obtain an approximate relation for the heat-transfer coefficient; expressed in terms of the quantities used here, it can be written as

$$N/(G\sigma)^{1/4} = 0.957\sigma^{1/4}/(\sigma + 0.952)^{1/4} \cong 0.957, \quad \sigma \text{ large} \qquad (6.15)$$

The coefficient 0.957 is seen to be high compared to that given by Schuh or by Ostrach.

An empirical relation obtained by fitting a curve to experimental results is given by McAdams;[14] again adjusting to the present notation, we have

$$N/(G\sigma)^{1/4} = 0.775 \qquad (6.16)$$

Since this is a fit primarily to the data for air—that is, for low σ—the results of Lorenz[15] for oils are of more interest for high Prandtl Number studies. He obtains, as a best fit to his experimental results, the empirical relation

$$N/(G\sigma)^{1/4} = 0.784 \qquad (6.17)$$

The discrepancy between this result and the result [Eq. (6.14)] is probably due, as Schlichting[12] says, to the fact that the viscosity of the oil—or of any other liquid—varies with the temperature so rapidly that, for a given temperature range $t_0 - t_\infty$, the assumption that the fluid has constant physical properties used in the theoretical analysis may not be good enough.

The above analysis has been carried out for a plate of finite length. For the semi-infinite plate, where no characteristic length exists, the results obtained still apply. Instead of the Grashof Number based on the length L, a Grashof Number based on the distance x along the plate or on some average length L of a region $x_2 - x_1$ away from the leading edge where the laminar flow hypothesis holds can be used. Also, the Grashof Number as defined here occurs together with the length L in such a way that the combination can be reduced to the similarity parameter $C = [g\beta(t_0 - t_\infty)/4\nu^2]^{1/4}$ used by Squire[11] and others in their treatment of the semi-infinite plate.† For instance, the combination $(L^9/G^3)^{+1/4}$ appearing in Eqs. (6.14) for the shear stress reduces to $(4C^4)^{-3/4}$.

(7) EXAMPLE IV: THE ROTATING DISC

An example of an axially symmetric flow using the full Navier-Stokes equations to which the asymptotic expansion technique developed here is applicable is that of the infinite plane disc rotating about an axis perpendicular to it with a constant angular velocity ω. Let (r, θ, z) be cylindrical coordinates, with $z = 0$ the plane of the disc, and (u, v, w) the velocity components in these directions. Von Kármán[17] has shown that the hydrodynamic equations can be reduced to ordinary differential equations in the variable z. He has noted that, although the analysis is based on the full three-dimensional Navier-Stokes equations, the resulting flow near the plate is consistent with the Prandtl boundary-layer hypothesis. The ordinary differential equations of von Kármán can be made nondimensional by appropriate transformations; the solutions to these latter equations have been given in numerical form by Cochran.[18] Recently Millsaps and Pohlhausen[19] have considered the associated heat-transfer problem with the plate at constant temperature $t = t_w$* and the distant fluid at constant temperature $t = t_\infty$. They found that a reduction of the form of von Kármán's velocity transformations could be applied to the temperature t, thus changing the energy equation into two ordinary differential equations in z. These, coupled with Cochran's results, have been solved numerically by Millsaps and Pohlhausen for values of σ up to ten. In this section the problem will be considered for large σ, and variable disc temperature and asymptotic solutions will be obtained for the case when the disc temperature varies as r^λ, $\lambda \geq 0$.

The substitutions $u = rf(z)$, $v = rg(z)$, $w = h(z)$, $p = p(z)$ reduce the hydrodynamic equations to ordinary differential equations for f, g, h, p. The energy equation becomes

$$c_p\left(rf\frac{\partial t}{\partial r} + h\frac{\partial t}{\partial z}\right) = \frac{k}{\rho}\left(\frac{\partial^2 t}{\partial r^2} + \frac{1}{r}\frac{\partial t}{\partial r} + \frac{\partial^2 t}{\partial z^2}\right) + \nu(12f^2 + r^2 g'^2 + r^2 f'^2) \qquad (7.1)$$

We assume the solution in the form

$$t = r^2 s(z) + q(r, z) \qquad (7.2)$$

† A detailed discussion of the work of Schmidt and Beckmann, Pohlhausen, Schuh, Saunders, and others on natural convection is given by Squire.[11] The recent work of Merk and Prins[16] on the development of the similarity hypothesis and its use in connection with the Saunders polynomial method or a refined Squire-Eckert integral method for approximate solution of the equations is also of interest; Merk and Prins treat some additional natural convection problems, such as the flow near the lower stagnation point of a sphere. Again, of course, for large Prandtl Number, the $(G\sigma)^{1/4}$ behavior of the Nusselt Number appears.

This is similar to the solution assumed in reference 19, but there q is a function of z only. Substitution in Eq. (7.1) leads to the following equations for $s(z)$ and $q(r, z)$:

$$c_p(2fs + hs') = (k/\rho)s'' + \nu(g'^2 + f'^2) \quad (7.3)$$

$$c_p\left(rf\frac{\partial q}{\partial r} + h\frac{\partial q}{\partial z}\right) = \frac{k}{\rho}\left(4s + \frac{\partial^2 q}{\partial r^2} + \frac{1}{r}\frac{\partial q}{\partial r} + \frac{\partial^2 q}{\partial z^2}\right) + 12\nu f^2 \quad (7.4)$$

The boundary conditions $t(r, 0) = t_w(r)$ and $t(r, \infty) = t_\infty$, a constant, are satisfied by requiring

$$s(0) = s(\infty) = 0, \quad q(r, 0) = t_w(r), \quad q(r, \infty) = t_\infty \quad (7.5)$$

Since s satisfies a nonhomogeneous equation and homogeneous boundary conditions, its existence is entirely due to the nonhomogeneous terms representing dissipation. The function q results from the imposed temperature difference $t_w - t_\infty$ as well as from dissipation; the latter factor will be seen to be negligible, however. In rendering the equations dimensionless, it is therefore convenient to use different characteristic quantities for r^2s and q, respectively. We set

$$\left.\begin{aligned} r &= LR \\ z &= (\nu/\omega)^{1/2}\xi \\ f &= \omega F(\xi) \\ g &= \omega G(\xi) \\ h &= (\nu\omega)^{1/2}H(\xi) \\ s &= (\omega^2/c_p)S(\xi) \\ q &= (t_w^* - t_\infty)Q(R, \xi) + t_\infty \end{aligned}\right\} \quad (7.6)$$

where L denotes a characteristic length to be decided upon and t_w^* denotes a characteristic wall temperature. The beginning terms in the power series developments of F, G, H are

$$F = A\xi, \quad G = 1 - B\xi, \quad H = -A\xi^2 \quad (7.7)$$

where $A = 0.510$, $B = 0.616$ as given by Cochran.[18] The equations and boundary conditions for Q and S become

$$\left.\begin{aligned} &\frac{\nu}{\omega L^2}\left(\frac{\partial^2 Q}{\partial R^2} + \frac{1}{R}\frac{\partial Q}{\partial R}\right) + \frac{\partial^2 Q}{\partial \xi^2} - \sigma FR\frac{\partial Q}{\partial R} - \sigma H\frac{\partial Q}{\partial \xi} = -\frac{4\nu\omega}{c_p(t_w^* - t_\infty)}S - \sigma\frac{12\nu\omega}{c_p(t_w^* - t_\infty)}F^2 \\ &S'' - \sigma HS' - \sigma 2FS = -\sigma(F'^2 + G'^2) \\ &S(0) = S(\infty) = 0, \quad Q(R, 0) = (t_w - t_\infty)/(t_w^* - t_\infty), \; Q(R, \infty) = 0 \end{aligned}\right\} \quad (7.8)$$

To determine the asymptotic behavior for large σ, we set

$$\eta = \sigma^m\xi, \; Q(R, \xi) = Q^*(R, \eta), \quad S(\xi) = \sigma^n S^*(\eta) \quad (7.9)$$

noting that the boundary condition on Q at the disc precludes any explicit dependence of Q on σ. Since the thermal boundary layer is expected to be much thinner than the velocity layer, the velocity components can be approximated by the relations (7.7). Substitution of Eqs. (7.7) and (7.9) into Eqs. (7.8) yields

$$\left.\begin{aligned} &\frac{\nu}{\omega L^2}\left(\frac{\partial^2 Q^*}{\partial R^2} + \frac{1}{R}\frac{\partial Q^*}{\partial R}\right) + \sigma^{2m}\frac{\partial^2 Q^*}{\partial \eta^2} - \sigma^{1-m}A\eta R\frac{\partial Q^*}{\partial R} + \sigma^{1-m}A\eta^2\frac{\partial Q^*}{\partial \eta} = -\sigma^n\frac{4\nu\omega}{c_p(t_w^* - t_\infty)}S^* - \sigma^{1-2m}\frac{12\nu\omega A^2}{c_p(t_w^* - t_\infty)}\eta^2 \\ &\sigma^{n+2m}S^{*\prime\prime} + A\sigma^{1-m+n}(\eta^2 S^{*\prime} - 2\eta S^*) = -\sigma(A^2 + B^2) \end{aligned}\right\} \quad (7.10)$$

Since the dissipative terms must be retained in the second equation (without them S would be identically zero), we must have $n + 2m = 1$. Substitution of this relation into the first equation immediately shows that the two terms on the right side—the conductive term S^* (which is indirectly due to dissipation) as well as the dissipative term $A^2\eta^2$—are of order σ^{1-2m} and hence are dominated by the convective terms of order σ^{1-m} on the left side (since m must be greater than zero). Hence the conduction term $\partial^2 Q^*/\partial\eta^2$, which must be retained, has to be balanced by the convection terms. Thus, setting $2m = 1 - m$, we obtain $m = n = 1/3$.

In terms of the dimensionless quantities, the asymptotic expressions for temperature and for temperature gradient at the disc are

$$\left.\begin{aligned} t &= L^2R^2(\omega^2/c_p)\sigma^{1/3}S^*(\eta) + (t_w^* - t_\infty)Q^*(R, \eta) + t_\infty \\ \left.\frac{\partial t}{\partial z}\right|_{z=0} &= \left(\frac{\omega}{\nu}\right)^{1/2}(t_w^* - t_\infty)\sigma^{1/3} \times \left[\frac{L^2\omega^2}{c_p(t_w^* - t_\infty)}\sigma^{1/3}R^2S^{*\prime}(0) + \frac{\partial Q^*(R, 0)}{\partial \eta}\right] \end{aligned}\right\} \quad (7.11)$$

We must now distinguish between two cases. If the disc temperature $t_w(r)$ is constant—i.e., $t_w = t_w^*$—then the only characteristic length in the problem is $(\nu/\omega)^{1/2}$, and L is chosen to be equal to this quantity. The coefficient multiplying $R^2S^{*\prime}(0)$ in Eq. (7.11) then becomes $\sigma^{1/3}\nu\omega/c_p(t_w^* - t_\infty)$, and its magnitude determines the relative importance of the two contributions (by S^* and Q^*) to the temperature gradient. In this case Q^* is a function of η only. From the first of Eqs. (7.10) it is seen that the two terms on the right are negligible whenever $\sigma^{-1/3}\nu\omega/c_p(t_w^* - t_\infty) << 1$. It is also seen that the contribution that these terms make to Q^* and hence to the temperature is much smaller than the contribution made to the temperature by S^* whenever σ is large. In the second case, that of variable wall temperature t_w, the temperature t_w^* together with a characteristic magnitude of the wall temperature gradient dt_w/dr define a length that is the characteristic length L for this problem. We then see from the first of Eqs. (7.10) that the conduction terms involving

derivatives of Q^* with respect to R (in brackets) are negligible provided $\sigma^{-2/3}(\nu/\omega L^2) << 1$. The convective term involving $\partial Q^*/\partial R$ is of the same order as the other convective term.

The asymptotic forms of Eqs. (7.10) and the boundary conditions when $t_w = t_w^*$ are†

$$\left.\begin{aligned} (d^2Q^*/d\eta^2) + A\eta^2(dQ^*/d\eta) &= 0 \\ S^{*\prime\prime} + A\eta^2 S^{*\prime} - 2A\eta S^* &= -(A^2 + B^2) \\ S^*(0) = S^*(\infty) = 0, \quad Q^*(0) = 1, \quad Q^*(\infty) &= 0 \end{aligned}\right\} \tag{7.12}$$

When the wall temperature is variable, the equation for S^* remains unchanged, but the equation for Q^* becomes

$$(\partial^2 Q^*/\partial\eta^2) + A\eta^2(\partial Q^*/\partial\eta) - A\eta R(\partial Q^*/\partial R) = 0 \tag{7.13}$$

and the boundary conditions are given by the relations (7.8).

The solutions of the system (7.12) in terms of the functions $Q(\xi)$, $S(\xi)$ are‡

$$\left.\begin{aligned} Q(\xi) &= \frac{1}{\Gamma(4/3)}\left(\frac{\alpha}{3}\right)^{1/3}\int_\xi^\infty e^{-(\alpha/3)\xi^3}\,d\xi \\ S(\xi) &= -\frac{\beta}{2}\xi^2 + \frac{\beta}{2}\frac{\Gamma(5/3)}{\Gamma(4/3)}\left(\frac{3}{\alpha}\right)^{1/3}\times \\ &\qquad \xi e^{-(\alpha/3)\xi^3}\Phi\left(\frac{5}{3};\frac{4}{3};\frac{\alpha}{3}\xi^3\right) \end{aligned}\right\} \tag{7.14}$$

where $\Phi(a;\ c;\ x)$ is the confluent hypergeometric function satisfying

$$\left.\begin{aligned} x(d^2\Phi/dx^2) + (c - x)(d\Phi/dx) - a\Phi &= 0 \\ \text{and} \qquad \alpha = A\sigma, \quad \beta &= (A^2 + B^2)\sigma \end{aligned}\right\} \tag{7.15}$$

The derivatives at the wall are

$$\left.\begin{aligned} \frac{dQ(0)}{d\xi} &= \sigma^{1/3}\frac{dQ^*(0)}{d\eta} = -\sigma^{1/3}\frac{(A/3)^{1/3}}{\Gamma(4/3)} \\ \frac{dS(0)}{d\xi} &= \sigma^{2/3}\frac{dS^*(0)}{d\eta} = \sigma^{2/3}\frac{A^2 + B^2}{2}\left(\frac{3}{A}\right)^{1/3} \end{aligned}\right\} \tag{7.16}$$

or (with Cochran's values for A and B)

$$\left.\begin{aligned} dQ^*(0)/d\eta &= 0.620 \\ dS^*(0)/d\eta &= 0.584 \end{aligned}\right\} \tag{7.16a}$$

To compare these results with those of Millsaps and Pohlhausen, it must be noted that the function Q used here corresponds to a sum of functions $Q_1 + Q_2 \div (T_0 - T_\infty)$ used by them. Q_2 is essentially the particular integral of the first of Eqs. (7.8) and hence corresponds to the contribution made to Q by the dissipation which is negligible in our analysis for large σ. Thus our $Q(\xi)$ corresponds to their Q_1. Table 3 shows

† Equations of the general type of that for $S(\xi)$ have been considered before in heat-transfer work; see, for example, Schuh[3] and Punnis.[4]

‡ The transformation of the S equation into the confluent hypergeometric equation and the obtaining of the appropriate solution are discussed in reference 20.

TABLE 3

$dQ(0)/d\xi$ and $dS(0)/d\xi$ for $\sigma = 10$ at Constant Wall Temperature

	$dQ(0)/d\xi$	$dS(0)/d\xi$
Eq. (7.16)	−1.34	2.71
Reference 19	−1.1	2

the results for the temperature gradient at the wall found in this analysis and by Millsaps and Pohlhausen for $\sigma = 10$, which is the largest value for which they have carried out computations.

Evidently the approximation is good only when σ is considerably larger than 10. We note that the asymptotic approximation for Q, the response to the imposed temperature difference, can be expected to be good for much lower σ than that for S, the temperature rise due to dissipation. This situation may be expected to exist in all similar problems and may be made plausible on the ground that for large σ—i.e., small conductivity (ν, c_p, fixed)—the heat diffusing from the boundary (assuming $t_w^* > t_\infty$) cannot penetrate far into the fluid before being swept away by convection, while the heat due to dissipation is created wherever the velocity is appreciable. Thus the thermal boundary layer due to dissipation must be expected to be thicker than that due to an imposed temperature difference, and therefore the asymptotic approximation, which is based on the assumption of a very thin thermal layer, is not so good. No other results for large Prandtl Number, either theoretical or experimental, appear to be available for comparison at the present time.

Turning to the problem with variable wall temperature, we note that, from Eq. (7.11), the asymptotic variation of the temperature gradient with σ is independent of the particular boundary condition. Solutions of Eq. (7.13) may be obtained readily for the particular boundary condition

$$Q^*(R, 0) = R^\lambda, \quad \lambda \geq 0 \tag{7.17}$$

If we seek solutions in the form

$$Q^*(R, \eta) = R^\lambda \chi(\eta) \tag{7.18}$$

then χ must satisfy the equation and boundary conditions

$$\left.\begin{aligned} \chi'' + A\eta^2\chi' - \lambda A\eta\chi &= 0 \\ \chi(0) = 1, \quad \chi(\infty) &= 0 \end{aligned}\right\} \tag{7.19}$$

This equation is a generalized form of the second of Eqs. (7.12), for which $\lambda = 2$. The substitutions

$$\left.\begin{aligned} \chi(\eta) &= \eta e^{-A(\eta^3/3)}\chi^*(\eta) \\ x &= \frac{A}{3}\eta^3 \\ \chi^*(\eta) &= \Phi(x) \end{aligned}\right\} \tag{7.20}$$

lead to Eq. (7.15) for Φ with $c = 4/3$, $a = 1 + (\lambda/3)$. The solution satisfying the boundary conditions of Eqs. (7.19) is

$$\chi(\eta) = \left(\frac{A}{3}\right)^{1/3} \eta e^{-(A/3)\eta^3} \left\{ \left(\frac{3}{A}\right)^{1/3} \eta^{-1} \times {}_1F_1\left(\frac{2+\lambda}{3}; \frac{2}{3}; \frac{A}{3}\eta^3\right) - \frac{\Gamma(2/3)\Gamma[1+(\lambda/3)]}{\Gamma[(2+\lambda)/3]\Gamma(4/3)} \times {}_1F_1\left(1+\frac{\lambda}{3}; \frac{4}{3}; \frac{A}{3}\eta^3\right) \right\} \quad (7.21)$$

where ${}_1F_1[1 + (\lambda/3);\ 4/3;\ x]$ and $x^{-1/3}{}_1F_1[(2 + \lambda)/3;\ 2/3;\ x]$ are two linearly independent solutions of Eq. (7.15) and are defined in Magnus and Oberhettinger.[25] The derivative at the disc is

$$\chi'(0) = -\left(\frac{A}{3}\right)^{1/3} \frac{\Gamma(2/3)\Gamma[1+(\lambda/3)]}{\Gamma[(2+\lambda)/3]\Gamma(4/3)} \quad (7.22)$$

This result is seen to agree with the one obtained previously [Eq. (7.16)] for the special case of constant disc temperature ($\lambda = 0$).

(8) Example V: The Flow in a Converging Channel

The Jeffery-Hamel flows[21,22] in converging or diverging channels are other well known examples of flows for which the exact Navier-Stokes equations can be reduced to ordinary differential equations. Recently Millsaps and Pohlhausen[23] have reduced the energy equation to an ordinary differential equation and have obtained numerical solutions for the thermal distribution when the wall temperature is constant. We shall here concern ourselves with the converging channel for large Reynolds and Prandtl Numbers and variable wall temperature.

Let the straight walls be defined by the lines $\theta = \pm\alpha$, θ denoting the angle in a plane polar coordinate system (r, θ). A steady radially inward flow is introduced with a volume flow V per unit time past any section r = constant. The wall temperature is $t_w(r)$. The velocity has a radial component u_r only which is proportional to r^{-1}. Let $u^*(r)$ denote the average velocity over a section r = constant, so that $V = 2\alpha r u^*(r)$, and let $u_r(r, 0) = \gamma u^*(r)$. Setting

$$u_r(r, \theta) = u_r(r, 0) f(\theta) = [\gamma V/(2\alpha r)] f(\theta) \quad (8.1)$$

the radial momentum equation gives, after differentiation with respect to θ to eliminate the pressure term,

$$f''' + (4 - 2Rf)f' = 0 \quad (8.2)$$

where $R = -\gamma V/2\alpha\nu = -r u_r(r, 0)/\nu$ denotes the Reynolds Number, the negative sign being introduced to make R positive (V being negative). The boundary conditions are

$$\left.\begin{aligned} f(-\alpha) &= 0 \\ f(0) &= 1 \\ f(\alpha) &= 0 \text{ [or } f'(0) = 0\text{]} \end{aligned}\right\} \quad (8.3)$$

The energy equation becomes

$$c_p u_r \frac{\partial t}{\partial r} = \frac{k}{\rho}\left(\frac{\partial^2 t}{\partial r^2} + \frac{1}{r}\frac{\partial t}{\partial r} + \frac{1}{r^2}\frac{\partial^2 t}{\partial \theta^2}\right) + \nu\left(\frac{\gamma V}{2\alpha}\right)^2 \frac{1}{r^4}(4f^2 + f'^2) \quad (8.4)$$

Assume the solution in the form

$$t = [s(\theta)/r^2] + q(r, \theta) \quad (8.5)$$

This is similar to the form assumed in reference 23, but there q is a constant equal to the uniform wall temperature. Substitution in Eq. (8.4) leads to the following equations for s and q.

$$\left.\begin{aligned} s'' + (4 - 2\sigma R f)s &= -\sigma(1/c_p)[\gamma V/(2\alpha)]^2 \times (4f^2 + f'^2) \\ \frac{\partial^2 q}{\partial r^2} + \frac{1}{r}\frac{\partial q}{\partial r} + \frac{1}{r^2}\frac{\partial^2 q}{\partial \theta^2} + \sigma R \frac{f}{r}\frac{\partial q}{\partial r} &= 0 \end{aligned}\right\} \quad (8.6)$$

The boundary conditions $t(r, \pm\alpha) = t_w(r)$ are satisfied by requiring

$$\left.\begin{aligned} s(-\alpha) = 0, \quad s(\alpha) = 0 \quad [\text{or } s'(0) = 0] \\ q(r, -\alpha) = t_w(r), \quad q(r, \alpha) = t_w(r) \\ \left[\text{or } \left.\frac{\partial q}{\partial \theta}\right|_{\theta=0} = 0\right] \end{aligned}\right\} \quad (8.7)$$

Since s satisfies a nonhomogeneous equation and homogeneous boundary conditions, its existence is entirely due to the nonhomogeneous terms representing dissipation. The function q is the response to the imposed wall temperature. If the latter is a constant, t_w^*, then the obvious solution of the equation and boundary conditions for q is $q(r, \theta) = t_w^*$.

We are concerned with solutions for large σ when the thermal layer is thin, so that $f(\theta)$ can be replaced by its first term in a power series expansion about $\theta = \pm\alpha$. Since this term (essentially the shear force) depends on R, we shall here simplify the problem by confining our attention to large R. In this case a simple dependence on R is readily given by boundary-layer theory.[24] We set

$$\left.\begin{aligned} s &= (1/c_p)[\gamma V/(2\alpha)]^2 S(\varphi) \\ q(r, \theta) &= t_w^*[1 + Q(r, \varphi)] \\ f(\theta) &= \tau(\varphi) \\ \varphi &= R^{1/2}(\theta + \alpha) \end{aligned}\right\} \quad (8.8)$$

where we consider the flow in the range $-\alpha \le \theta \le 0$, and t_w^* is a characteristic wall temperature, say, the temperature at infinity. Eqs. (8.2) and (8.6) become

$$\left.\begin{aligned} \tau''' + (4R^{-1} - 2\tau)\tau' &= 0 \\ S'' + (4R^{-1} - 2\sigma\tau)S &= -\sigma(4R^{-1}\tau^2 + \tau'^2) \\ R^{-1}\frac{\partial^2 Q}{\partial r^2} + R^{-1}\frac{1}{r}\frac{\partial Q}{\partial r} + \frac{1}{r^2}\frac{\partial^2 Q}{\partial \varphi^2} + \sigma\frac{\tau}{r}\frac{\partial Q}{\partial r} &= 0 \end{aligned}\right\} \quad (8.9)$$

For large Reynolds Number the terms containing R^{-1}

in the first two equations are immediately seen to be negligible. The leading term of the solution for τ subject to the appropriate boundary conditions $\tau(0) = 0, \tau(\infty) = 1$ is[24] $\tau(\varphi) \approx (4/3)^{1/2}\varphi$. As usual, the energy equations present a singular perturbation problem when σ is large. Replacing τ by the first term in its power series and setting

$$\eta = \sigma^m \varphi, \quad S(\varphi) = \sigma^n S^*(\eta), \quad Q(r, \varphi) = Q^*(r, \eta) \tag{8.10}$$

we obtain

$$\left.\begin{aligned} &\sigma^{2m+n} S^{*\prime\prime} - 2(4/3)^{1/2}\sigma^{1-m+n}\eta S^* = \\ &\qquad -(4/3)\sigma \\ &R^{-1}\frac{\partial^2 Q^*}{\partial r^2} + R^{-1}\frac{1}{r}\frac{\partial Q^*}{\partial r} + \sigma^{2m}\frac{1}{r^2}\frac{\partial^2 Q^*}{\partial \eta^2} + \\ &\qquad \sigma^{1-m}\left(\frac{4}{3}\right)^{1/2}\frac{\eta}{r}\frac{\partial Q^*}{\partial r} = 0 \end{aligned}\right\} \tag{8.11}$$

Since conduction, convection, and dissipation must balance in the first equation, $2m + n = 1 - m + n = 1$ and $m = n = 1/3$. In the second equation the convection balances the conduction normal to the wall, and the conduction parallel to the wall is negligible provided $R^{-1}\sigma^{-2/3} << 1$. Thus the asymptotic solutions for large σ must satisfy the equations

$$\left.\begin{aligned} S^{*\prime\prime} - 2(4/3)^{1/2}\eta S^* &= -4/3 \\ (\partial^2 Q^*/\partial\eta^2) + (4/3)^{1/2}\eta r(\partial Q^*/\partial r) &= 0 \end{aligned}\right\} \tag{8.12}$$

The boundary conditions are

$$\left.\begin{aligned} &S^*(0) = 0, && \lim_{\eta\to\infty} S^*(\eta) \to \text{finite} \\ &Q^*(r,0) = t_w'(r)/t_w^* - 1, && \lim_{\eta\to\infty} Q^*(r,\eta) \to \text{finite} \end{aligned}\right\} \tag{8.13}$$

where the limiting boundary conditions on the asymptotic solutions replace the original exact symmetry conditions at $\theta = 0$.

In terms of the dimensionless quantities, the asymptotic expressions for the temperature and for the temperature gradient at the wall are

$$\left.\begin{aligned} t &= (\nu^2/c_p)\sigma^{1/3}R^2[S^*(\eta)/r^2] + t_w^*[1 + Q^*(r,\eta)] \\ \frac{\partial t}{\partial\theta}_{\theta=-\alpha} &= \frac{\nu^2}{c_p}\sigma^{2/3}R^{5/2}\frac{S^{*\prime}(0)}{r^2} + \\ &\qquad t_w^*\sigma^{1/3}R^{1/2}\frac{\partial Q^*(r,0)}{\partial\eta} \end{aligned}\right\} \tag{8.14}$$

The solution for S^* may be obtained in terms of Bessel functions of imaginary argument. It is

$$\left.\begin{aligned} S^*(\eta) &= bz^{1/3}g(z), \quad \text{where } z = a\eta^{3/2} \\ a &= (4/3)(1/3)^{1/4} \\ b &= (2/9)(12)^{1/6}\pi \\ g(z) &= I_{1/3}(z) + I_{-1/3}(z)\int_0^z I_{1/3}(\xi)d\xi - \\ &\qquad I_{1/3}(z)\int_0^z I_{-1/3}(\xi)d\xi \end{aligned}\right\} \tag{8.15}$$

and

$$\left.\begin{aligned} S^{*\prime}(0) &= (3/2)a^{2/3}\, b \lim_{z\to 0}[z^{2/3}g'(z) + \\ &\qquad (1/3)z^{-1/3}g(z)] \\ &= \frac{2^{7/3}}{3^{5/3}}\frac{\pi}{\Gamma(1/3)} \end{aligned}\right\} \tag{8.16}$$

A comparison of this result with those of Millsaps and Pohlhausen[23] (given in graphical form for three values of the Reynolds Number and various σ) cannot properly be made because their calculations are restricted to a maximum value of σ equal to ten and because the value of the temperature gradient at the wall cannot be read accurately enough from the graph for present purposes.

Turning to the function Q^*, it has already been noted that the solution for constant wall temperature t_w^* is $Q^*(r, \eta) = 0$. The asymptotic variation with σ of the temperature and temperature gradient at the wall is seen by Eqs. (8.14) to be independent of the particular boundary conditions. Solutions for Q^* may be obtained readily for the particular boundary condition $Q^*(r, 0)$ proportional to $r^{-\lambda}$, $\lambda > 0$. To make r dimensionless, we note that $(V^2/c_p t_w^*)^{1/2}$ defines an appropriate length, so that we may set

$$\left.\begin{aligned} r &= [V^2/(c_p t_w^*)]^{1/2}\xi, \quad Q^*(r,\eta) = \chi(\xi,\eta) \\ \text{and} \qquad \chi(\xi, 0) &= \xi^{-\lambda}, \quad \lambda > 0 \end{aligned}\right\} \tag{8.17}$$

Seeking solutions in the form

$$\chi(\xi, \eta) = \xi^{-\lambda}\chi^*(\eta) \tag{8.18}$$

one is led to the equation and boundary conditions

$$\left.\begin{aligned} \chi^{*\prime\prime} - (4/3)^{1/2}\lambda\chi^* &= 0 \\ \chi^*(0) = 1, \quad \lim_{\eta\to\infty}\chi^*(\eta) &\to \text{finite} \end{aligned}\right\} \tag{8.19}$$

The solution may be written in terms of modified Bessel functions. It is

$$\chi^*(\eta) = \frac{3^{1/2}\Gamma(2/3)}{2^{1/3}\pi}(\alpha\eta^{3/2})^{1/3}K_{1/3}(\alpha\eta^{3/2}) \tag{8.20}$$

where $\alpha = (2/3)\beta^{1/2}$, $\beta = (4/3)^{1/2}\lambda$

and $$\chi^{*\prime}(0) = -2^{1/3}3^{1/6}\Gamma(2/3)\lambda^{1/3}/\Gamma(1/3) \tag{8.21}$$

(9) Other Examples

The method illustrated in the foregoing sections has been applied successfully to other well-known problems. Among these is the problem of the thermal entry length in a pipe with fully developed Poiseuille flow.[11] The problem of the heat transfer associated with the flow along a surface of revolution near the forward stagnation point is completely analogous to that of the rotating disc treated in Section (7). Considering that portion of the solution which gives the temperature distribution due to a temperature difference between the wall and the fluid far away [denoted by q in Section (7)], we note that the solutions obtained for the disc apply to the present problem, provided we replace ω by β_1 and A by $f''(0)$, where $u_1 = \beta_1 r$ denotes the radial velocity component away from the surface and $u =$

$\beta_1 rf'(\xi)$ with $\xi = (\beta_1/\nu)^{1/2}z$ gives the radial velocity in the boundary layer.[24]

(10) Conclusions

The method of asymptotic approximation for the thermal boundary-layer problem developed here seems to give a relatively rapid way of obtaining information analytically from the differential equations governing heat transfer, even when these equations cannot be solved. It is worth noting that the method depends on the form of the equations and the type of boundary conditions only and is independent of the precise values of the physical constants of the flow or of the exact description of the conditions at the boundary of the body. Thus, the forced convection type of problem neglecting dissipation always leads to the $\sigma^{1/3}$ behavior for the heat-transfer coefficient for large values of σ. The natural convection problems will lead to the $\sigma^{1/4}$ behavior of the same quantity. To be sure, the determination of the coefficient multiplying the $\sigma^{1/3}$ or $\sigma^{1/4}$ will depend on an exact description of the particular problem, but the process of obtaining the asymptotic behavior with σ of the various quantities does not.

One cause of difficulty in the comparison of such asymptotic results with those obtained by experiment arises from the nature of fluids for which the Prandtl Number is large. As we mentioned in the section on the free convection problem, for such a fluid—oil, say—the viscosity usually varies drastically with the temperature. Thus, if the temperature range considered is sufficiently large, the viscosity may vary enough so that the assumption that the fluid possesses constant properties is no longer valid, and the boundary-layer equations as used here are not adequate as a description of the phenomena.

In summary, we have shown that the new method of "thermal boundary-layer stretching" based on the Prandtl Number is applicable in some well-known problems, and that its use has led to new results and to theoretical confirmation of previously derived empirical and numerical results in the case of free convection over a vertical plate, in the case of the Hamel flow, and in the case of the rotating disc. It is hoped that the method will be of value in further problems, where only numerical and very approximate analytical treatments for large Prandtl Number have been possible before.

References

[1] Lighthill, M. J., *Contributions to the Theory of Heat Transfer Through a Laminar Boundary Layer*, Proc. Roy. Soc. London, A, Vol. 202, p. 369, 1950.

[2] Levy, S., *Heat Transfer to Constant-Property Laminar Boundary-Layer Flows with Power-Function Free-Stream Velocity and Wall-Temperature Variation*, Journal of the Aeronautical Sciences, Vol. 19, No. 5, p. 341, May, 1952.

[3] Schuh, H., *On Asymptotic Solutions for the Heat Transfer at Varying Wall Temperatures in a Laminar Boundary Layer with Hartree's Velocity Profiles*, Journal of the Aeronautical Sciences, Vol. 20, No. 2, Readers' Forum, p. 146, February, 1953.

[4] Punnis, B., *A Remark on "On Asymptotic Solutions for the Heat Transfer at Varying Wall Temperatures in a Laminar Boundary Layer with Hartree's Velocity Profiles,"* Journal of the Aeronautical Sciences, Vol. 20, No. 7, Readers' Forum, p. 505, July, 1953.

[5] Herbeck, M., *Approximate Solutions for Heat Transfer with Convection Flows*, Journal of the Aeronautical Sciences, Vol. 21, No. 2, Readers' Forum, p. 142, February, 1954.

[6] Tifford, A. N., and Chu, S. T., *On Asymptotic Solutions for the Heat Transfer at Varying Wall Temperatures in a Laminar Boundary Layer with Hartree's Velocity Profiles*, Journal of the Aeronautical Sciences, Vol. 20, No. 9, Readers' Forum, p. 643, September, 1953.

[7] Pohlhausen, E., *Der Wärmeaustausch zwischen festen Körpern und Flüssigkeiten mit kleiner Reibung und kleiner Wärmeleitung*, Z.A.M.M., Vol. 1, p. 115, 1921.

[8] Crocco, L., *The Laminar Boundary Layer in Gases* (Italian) Monografie Scientifiche di Aeronautica No. 3, December, 1946; English Translation, North American Aviation, Inc., Report CF-1038, p. 50–54, July, 1948.

[9] Schuh, H., *Einige Probleme bei freier Strömung zäher Flüssigkeiten*, unpublished, 1946; see Göttingen Monographien, 1946, Vol. B, Grenzschichten; *Boundary Layers of Temperature*, Repts. and Trans. 1007, AVA Monographs, British M.A.P., April 15, 1948.

[10] Ostrach, S., *An Analysis of Laminar Free-Convection Flow and Heat Transfer About a Flat Plate Parallel to the Direction of the Generating Body Force*, NACA Report 1111, 1953.

[11] Squire, H. B., *Heat Transfer*, Chap. XIV, Vol. II of *Modern Developments in Fluid Mechanics: High Speed Flows*, Howarth, L., Ed., Oxford University Press, 1953.

[12] Schlichting, H., *Grenzschicht-Theorie*, pp. 257–262; G. Braun, Karlsruhe, 1951.

[13] Eckert, E., *Einführung in den Wärme-und Stoffaustausch*, p. 116; Springer-Verlag, Berlin, 1949.

[14] McAdams, W. H., *Heat Transmission*, 2nd Ed., p. 241; McGraw-Hill Book Company, Inc., New York, 1942.

[15] Lorenz, H. H., *Die Wärmeübertragung an einer ebenen senkrechten Platte an Oel bei natürlicher Konvektion*, Zeit. Techn. Physik, Vol. 15, No. 9, p. 362, 1934.

[16] Merk, H. J., and Prins, J. A., *Thermal Convection in Laminar Boundary Layers I, II, III*, Applied Sci. Res., A, Vol. 4, Nos. 1, 3; p. 11, 1953, p. 195, 207, 1954.

[17] von Kármán, T., *Über laminare und turbulente Reibung*, Z.A.M.M., Vol. 1, p. 233, 1921, especially pp. 244–247.

[18] Cochran, W. G., *The Flow Due to a Rotating Disc*, Proc. Camb. Phil. Soc., Vol. 30, p. 365, 1934.

[19] Millsaps, K., and Pohlhausen, K., *Heat Transfer by Laminar Flow from a Rotating Plate*, Journal of the Aeronautical Sciences, Vol. 19, No. 2, p. 120, February, 1952.

[20] Erdelyi, A., et al., Eds., *Higher Transcendental Functions*, Vol. 1, Chap. VI, pp. 248–253, 264–278; Bateman Manuscript Project, McGraw-Hill Book Company, Inc., 1953.

[21] Jeffrey, G. B., *Steady Motion of a Viscous Fluid*, Phil. Mag., Ser. 6, Vol. 29, p. 455, 1915.

[22] Hamel, G., *Spiralförmige Bewegungen zäher Flüssigkeiten*, Jahresbericht der Deutschen Math. Vereinigung, Vol. 25, p. 34, 1916.

[23] Millsaps, K., and Pohlhausen, K., *Thermal Distributions in Jeffery-Hamel Flows Between Nonparallel Plane Walls*, Journal of the Aeronautical Sciences, Vol. 20, No. 3, p. 187, 1953.

[24] Goldstein, S., *Modern Developments in Fluid Dynamics*, Vol. I; Clarendon Press.

[25] Magnus, W., and Oberhettinger, F., *Formulas and Theorems for the Special Functions of Mathematical Physics;* Chelsea Publishing Company.

The Behavior of Transverse Cylindrical and Forward Facing Total Pressure Probes in Transverse Total Pressure Gradients

J. L. LIVESEY*

University of Manchester, England

SUMMARY

When a total pressure probe is used for measuring flows with transverse total pressure gradients, a displacement of the effective center of the probe toward the higher total pressure is sometimes observed. This paper gives the results of an investigation of the effect for certain transverse cylindrical and forward facing (or pitot type) total pressure probes. An estimate of the error is given for the transverse cylindrical type of probe, and the errors due to position of hole, depth of hole, and wall proximity with this type of probe are considered incidentally.

A design of a probe of the forward facing type possessing negligible displacement error is suggested.

(1.0) SYMBOLS

D = outside or maximum diameter of either cylindrical or pitot type probe
d = hole diameter for cylindrical type probe or internal diameter for pitot type probe
a = distance of hole center from tip of cylindrical probe
y = distance of geometric center of hole from wall, in.
E = displacement of effective center of probe from its geometric center
P = total pressure
p = static pressure
Q = tunnel dynamic pressure
q = dynamic pressure obtained from total pressure indicated by probe and wall static reading
q_t = true dynamic pressure

(2.0) INTRODUCTION

TRANSVERSE CYLINDRICAL total pressure probes are extensively used in gas turbine aerodynamic work; for ease of insertion and removal in traversing they are preferable to forward facing or pitot type probes, especially in confined spaces such as duct boundary layers, combustion chambers, and in interstage traversing. In Fig. 1, (a) shows the forward facing type of total pressure probe and (b) the transverse cylindrical type.

The errors of cylindrical total pressure probes have been investigated previously, and references 1 and 2 deal with the errors due to size of hole, angle of inclination of the tube, and position of hole. The recommendations of these reports are discussed later. Previous work by Young and Maas (see reference 3) on pitot type total pressure probes in transverse total pressure gradients indicated an error, and, in consequence, a similar error was expected from the cylindrical type of probe under similar circumstances. This paper deals primarily with the errors of cylindrical total pressure probes in transverse total pressure gradients; the errors due to position and depth of hole are treated incidentally.

Measurements of a boundary layer used as standard were made, using pitot type total pressure probes, in order to establish a true boundary layer with which the errors of the cylindrical type probes could be investigated by comparison. During this work it was observed that the results for pitot type probes were in disagreement with the work of Young and Maas.[3] It is probable that this work which has been taken as generally applicable by other workers, notably Fage and Ower,[4-6] is only applicable to pitot type probes with square-cut faces. The latter part of this report deals with the errors of pitot type probes in transverse total pressure gradients and with a method of reducing the error by correct design of the pitot probe nose.

(3.0) APPARATUS AND TESTS

The tests were carried out in the 7- by 5-ft. wind tunnel at Rolls-Royce, Ltd., Hucknall, England. A grid was used to produce an artificially enlarged boundary layer downstream of the working section of the tunnel. The general arrangement of the tunnel working section as used in these tests is shown in Fig. 2. The boundary layer produced was traversed using two geometrically similar pitot type probes of 0.056 and 1 in. diameter in order to establish the boundary layer accurately; incidentally, these tests could be used to check the work of Young and Maas for the application of their corrections to boundary-layer traverses. The boundary layer thus established was then traversed using four geometrically similar cylindrical type probes of 1/8-, 1-, 2-, and 3-in. outside diameter, and the effect of the position of the hole was investigated using the 2-in. diameter probe. Further tests were carried out using pitot type probes of different inside to outside diameter ratios d/D and with different nose shapes.

The details of the cylindrical type probes used in the tests are shown in Fig. 3.

The 3-in. diameter cylindrical probe was made of wood and the tapping from the stagnation hole was

Received September 1, 1955.

* Lecturer in Mechanical Engineering.

The author wishes to acknowledge his indebtedness to Rolls-Royce, Ltd., England, for permission to publish the major portion of the work of this paper.

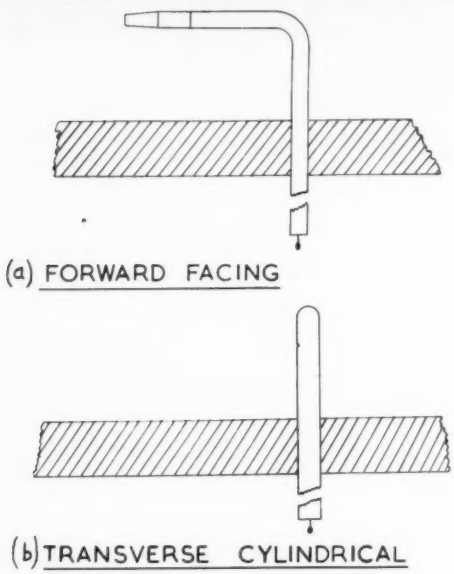

FIG. 1. The two types of probe considered.

brought along the downstream side of the cylinder. The 2-in. and 1-in. diameter cylindrical probes were made from 18-gage mild steel tube fitted with wooden plugs to form the hemispherical ends. Initially the stagnation holes were simply drilled; after the first tests wooden plugs were inserted behind the stagnation holes to give the deep hole found necessary to eliminate the error due to a shallow hole. The 1/8-in. diameter cylindrical probe was made from thick walled tube, the end being filled with solder and then drilled to produce a hole 4 d in depth.

The pitot type probes were of the main proportions shown in Fig. 4, several different nose shapes being used. The two pitot type probes used to establish the standard boundary layer were geometrically similar with $d/D = 0.7$ and had conical noses of included angle $8^1/_2°$. The outside diameters (D) were, respectively, 0.056 in. and 1 in. The 1-in. probe is shown in Fig. 4(a). The effect of diameter ratio d/D in the conical nosed probes was investigated by traversing with a 1-in. diameter probe having $d/D = 0.5$ with the same cone angle of $8^1/_2°$ [see Fig. 4(b)]. The effect of nose shape was investigated, using a hemispherically nosed probe with $d/D = 0.5$ [see Fig. 4(c)] and a flat nosed probe, not shown in Fig. 4, having $d/D = 0.6$—i.e., the type used by Young and Maas.

(4.0) TEST RESULTS—CYLINDRICAL TYPE PROBES WITH $d/D = 0.12$

(4.1) *Effect of Depth of Hole*

When the first tests were made with the cylindrical type probes, it was discovered that the four probes were not giving the same type of error—the 3-in. and 1/8-in. probes gave the same type of error but the 1-in. and 2-in. probes gave another type, the two pairs of probes differing considerably in their respective indications of the level of velocity at any particular point in the traverse. This was found to be due to the type of stagnation hole used in the side of the cylinder; the 1-in. and 2-in. probes were manufactured from 18-gage mild steel tube giving a comparatively shallow hole (depth/diameter 0.4 and 0.2, respectively) whereas the 3-in. tube was of wood, giving a deep hole, and the 1/8-in. tube was of thick-walled brass tube, giving a comparatively deep hole (depth/diameter 2.41). See Fig. 3.

Fig. 5 shows the type of error due to this effect for the 2-in. probe. The full line shows the boundary-layer profile obtained using a hole depth of four times the hole diameter (formed by a wooden plug—see Fig. 3) and the broken line indicates the profile obtained using the shallow hole (0.048-in. deep).

This error is considered to be due to secondary flows, which occur inside the cylinder, preventing the actual stagnation pressure being registered. A deep hole will prevent these flows, and the pressure measured will be effectively the stagnation pressure. For the remainder of these tests a hole depth of 4 d was used in all the probes this being the greatest depth which could be obtained practically in the 1/8-in. probe.

Since the error is a certain percentage of q (not the gradient) it would naturally be corrected for in a regular pipe calibration of the tube.

(4.2) *Effect of Position of Hole*

The flow round the hemispherical end of the cylindrical type probe will cause a local displacement of the main flow outwards from the wall, and the effective center of the stagnation hole will, therefore, be moved toward the wall by an amount depending on the distance of the hole from the end of the probe. It is possible to remove this error by placing the hole sufficiently far away from the end of the probe. On the other hand, it is convenient to have the hole near to the end of the probe in order to traverse as far across a duct as possible for a given total insertion of probe—e.g., to get as near as possible to the level of the inner

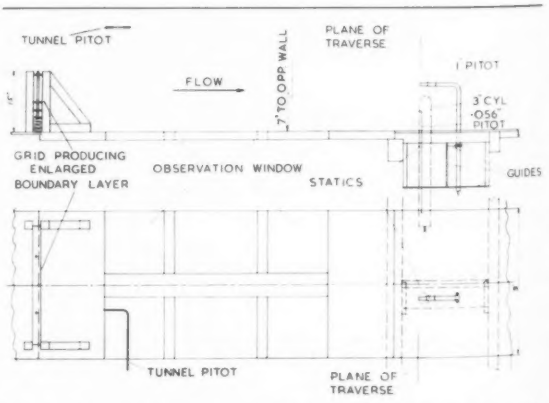

FIG. 2. General arrangement of test in 7- by 5-ft. wind tunnel.

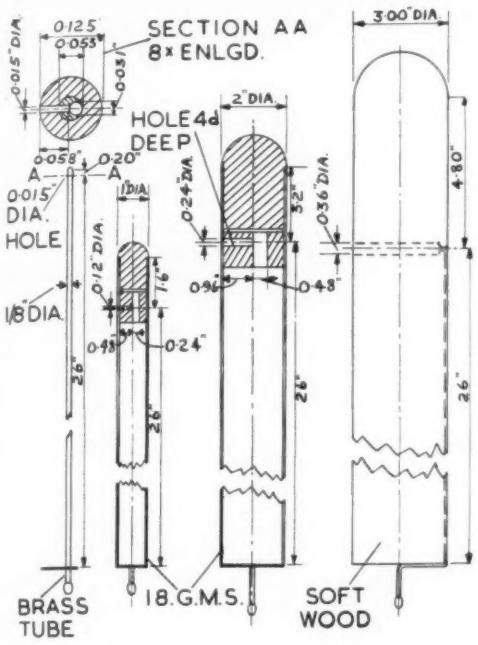

FIG. 3. Details of cylindrical type probes.

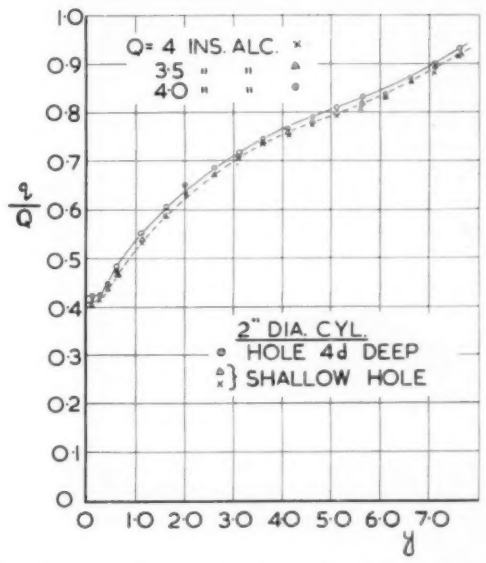

FIG. 5. Effect of depth of hole in cylindrical type probes.

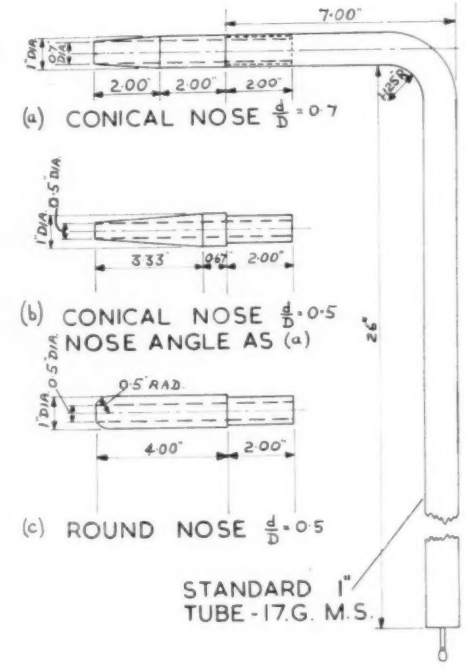

FIG. 4. Three of the nose shapes for pitot type probes.

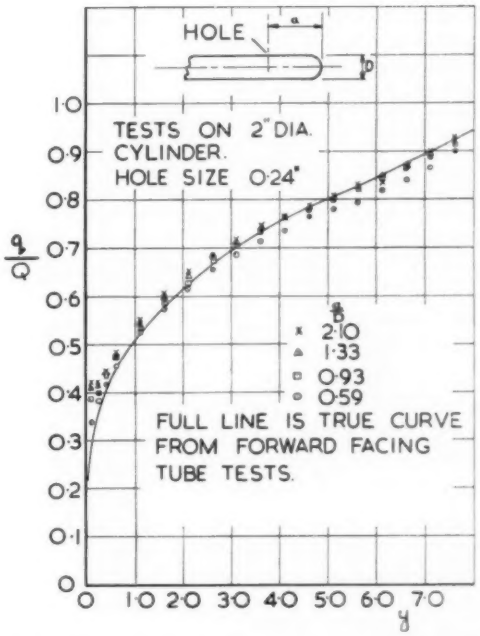

FIG. 6. Traverses of standard boundary layer using cylindrical type probes of varying a/D.

diameter in interstage traversing. Tests were carried out to determine a suitable distance from the end of the probe which would make this error negligible. Fig. 6 shows the results of traverses of the boundary layer using the 2-in. diameter probe for values of a/D equal to 0.59, 0.93, 1.33, and 2.10. It can be seen that the displacement of the effective center of the probe, as the hole is moved toward the tip of the probe is toward the wall. Fig. 7 shows values of q/Q plotted against a/D for several values of y, and it can be seen that for values of a/D greater than 2.0 there is little further change in q/Q. These results show that, for values of a/D greater than 2.0, the error due to the position of the hole will be negligible. The standard value of a/D used in subsequent tests was 2.1.

The results obtained here are in agreement with references 1 and 8, which also recommend that a/D should be greater than 2.

(4.3) *Effect of Transverse Total Pressure Gradient*

Previous work (see reference 3) has indicated that when a total pressure probe is used to measure flows with total pressure gradients or vorticity—e.g., boundary layers or wakes—a displacement of the effective center of the probe toward the higher total pressure is observed. The mechanism of this displacement is that of induced secondary flows caused by the presence of a body of finite thickness in a flow possessing vorticity—e.g., a boundary layer or a wake—and has received much attention by other investigators (see reference 7). The vortex lines which are straight in the undisturbed flow become curved due to the distortion of the flow near the body, and secondary components of vorticity are introduced which have the effect of displacing the streamlines toward the lower total pressure regions—i.e., toward the wall in a boundary layer. Referring to Fig. 8, if P_b is the total pressure of the streamline which lies at the same distance from the wall as the centerline of the probe, then this streamline will be deflected toward the wall by the presence of the body (the probe tip in Fig. 8) and the streamlines actually stagnating in the probe will be those corresponding to higher total pressures such as P_a, which were originally further from the wall than the centerline of the probe. Thus the probe will measure a total pressure at a distance farther from the wall than its centerline and its effective center may be said to have been displaced toward the higher total pressure.

In order to investigate this effect for cylindrical type probes the standard boundary layer was traversed using four geometrically similar probes of 1/8-, 1-, 2-, and 3-in. diameter. Details of the probes have been given previously in Section (3.0). Fig. 9 shows the profiles obtained from the four probes. It can be seen that the effective center of the probe is in fact displaced away from the wall toward the higher total pressure, and that this displacement increases with the diameter of the probe. At the wall there is an unusual effect, the tube apparently reading the same total pressure for a short distance from the wall. This effect is considered in detail in the next paragraph.

The results for the four probes tested have been analyzed, taking as standard a boundary layer obtained from the pitot type probe traverses [see Section (5.0)]. For any particular value of y, the error was expressed as $(q - q_t)/q_t$, and this was plotted against the nondimensional parameter $(D/q_t)\cdot(dq_t/dy)$. This parameter is a convenient dimensionless group giving a measure of the shear or vorticity of the flow and includes the effect of probe size. The results of this analysis are shown in Fig. 10, where a large number of points at the lower values of $(D/q_t)\cdot(dq_t/dy)$ have been omitted for clarity. It can be seen from Fig. 10 that the points lie closely about a straight line. This method of analysis demonstrates that, when expressed in this form, the error is a simple function of one nondimensional parameter which includes the effect of vorticity in the flow (or total pressure gradient) and probe diameter; unfortunately, it is extremely difficult to apply this function in the correction of any particular traverse, as it involves a knowledge of the value of $(D/q_t)\cdot(dq_t/dy)$, and the correction of any particular traverse would involve a tedious successive approximation. These considerations made it necessary to try another approach, and it was decided to follow reference 3, which treats the error as a displacement, E, of the effective center of the hole and considers E/D as a function of $(D/q_t)\cdot(dq_t/dy)$. Fig. 11 shows the results of this analysis applied to the results. For values of $(D/q_t)\cdot(dq_t/dy)$ from 0.2 to 1.2 the value of E/D does not differ much from 0.09, but below $(D/q_t)\cdot(dq_t/dy) = 0.2$ the variation of the points becomes so large that nothing can be said about the value of E/D. For these low values of $(D/q_t)\cdot(dq_t/dy)$, the error is of the order of the accuracy of the determination of the boundary-layer profile. The effect of other nondimensional parameters, y/D and Reynolds Number, was investigated, but no systematic effect could be detected, and, although it cannot be stated definitely, it is probable that the behavior of E/D for the small values of $(D/q_t)\cdot(dq_t/dy)$ is due purely to experimental error. Points for higher values of $(D/q_t)\cdot(dq_t/dy)$ are not included in Fig. 11 since, if included, the interesting range of $(D/q_t)\cdot(dq_t/dy)$ from 0.2 to 1.2, which includes most practical cases, would have become very cramped. For these large values of $(D/q_t)\cdot(dq_t/dy)$ with the conditions of these tests, the curve in Fig. 11 will rise because of the large error at the wall.

The fact that E/D remains sensibly constant over a wide range of $(D/q_t)\cdot(dq_t/dy)$, which includes most practical cases, makes the method very suitable for the correction of any particular traverse.

(4.4) *Wall Proximity Error*

The results of the traverses shown in Fig. 9 indicate an unusual effect when the stagnation hole of the

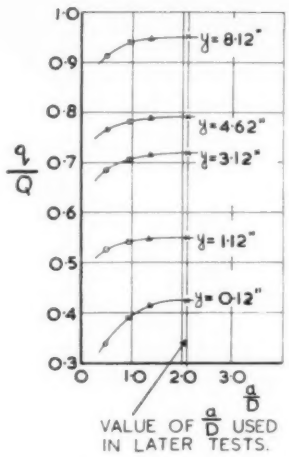

FIG. 7. Cross plot of Fig. 6 to show optimum value of a/D.

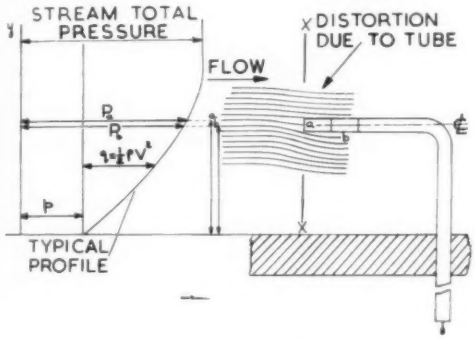

FIG. 8. Diagrammatic illustration of displacement error.

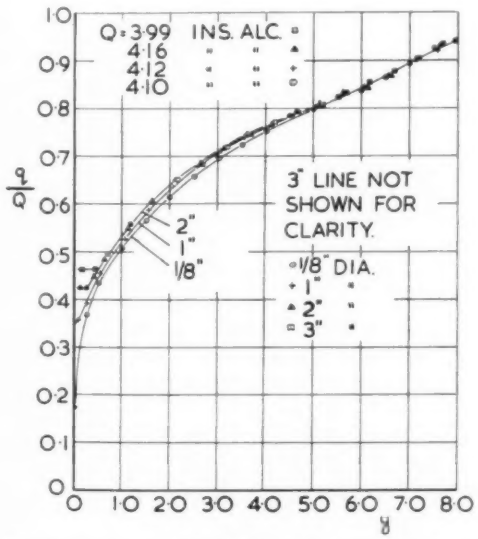

FIG. 9. Traverses of standard boundary layer with four geometrically similar cylindrical probes.

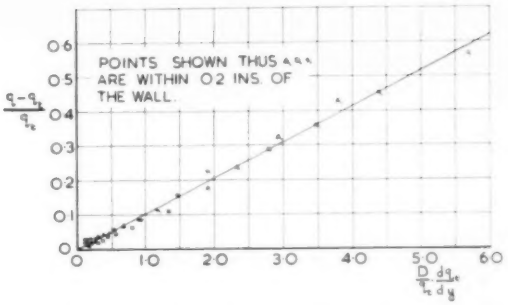

FIG. 10. Correlation of error in terms of dynamic head and shear parameter.

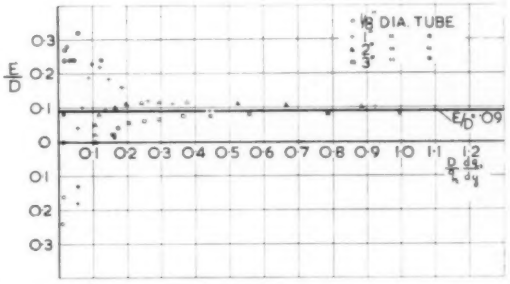

FIG. 11. Dimensionless displacement error versus shear parameter following reference 3.

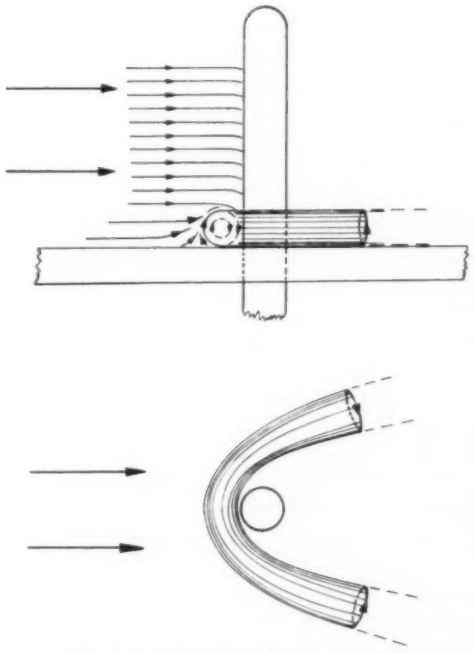

FIG. 12. Vortex at the wall drawn from flow visualization tests.

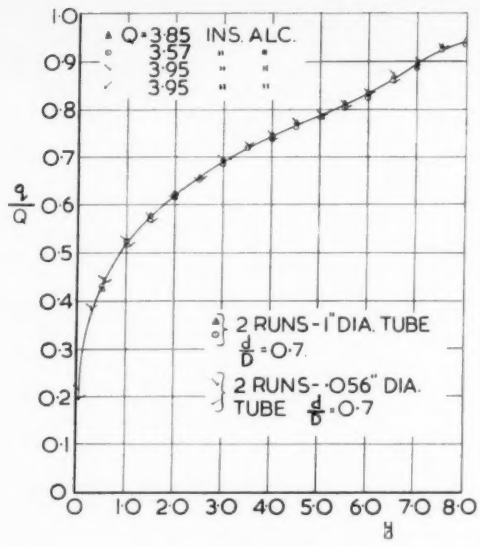

FIG. 13. Showing absence of displacement error for conical nosed pitot type probes.

probe is close to the wall. This was assumed at first to be due to leakage inward into the tunnel along the guides for the probe. A compressed air supply at 100 lbs. per sq.in. was applied to the guides at the outside of the tunnel, and the traverses were successfully repeated, indicating that the guides were an effective seal against such inward leakage.

Flow visualization tests have since shown that the large error at the wall is due to the presence of a discrete vortex as shown diagrammatically in Fig. 12. The secondary vortices mentioned in Section (4.3) roll up at the wall into a discrete vortex which is powerful enough to induce a reversed flow at the wall. The form of this vortex when viewed along the probe axis (see the lower part of Fig. 12) illustrates very well the distortion of the vortex lines of the approach flow due to the presence of the cylinder.

(4.5) *General Remarks and Recommendations*

From the previous work (see references 1 and 2), and the work in this paper the following main recommendations can be made in connection with the use of the transverse cylindrical total pressure probe.

(1) The ratio of the stagnation hole diameter to the diameter of the probe should be less than 1/8th (see reference 2).

(2) The angle of inclination of the probe to the direction of flow should not be greater than 5° from the normal (see reference 1).

(3) The distance of the stagnation hole from the end of the probe should be greater than two probe diameters.

(4) The stagnation hole itself should not be shallow but preferably several hole diameters in depth.

(5) In traversing flows with transverse total pressure gradients the correction to be applied to the traverse because of the displacement of the effective center of the hole is given by $E/D = 0.09$, the displacement of the effective center being towards the higher total pressure.

(6) This type of probe should not be used for boundary-layer work where $y < 0.2\ D$ because of the wall proximity error described in the last paragraph.

(5.0) PITOT TYPE PROBES

The standard boundary layer was traversed using pitot type probes of varying diameter in order to establish the profile accurately so that a standard profile would exist for the estimation of the errors of the cylindrical type probes. Incidentally, these tests could be used to check the applicability of the work of Young and Maas[3]—on the displacement of the effective center of pitot type probes in transverse total pressure gradients—to the correction of boundary-layer traverses.

The two pitots used initially in the establishment of the standard boundary layer were geometrically similar probes of 1-in. and 0.056-in. external diameter having $d/D = 0.7$ together with conical noses of included angle $8^1/_2°$. See Fig. 4.

With the experimental error of the tests both these probes gave precisely the same profile (see Fig. 13), whereas the work of Young and Maas[3] indicates that there should be a displacement of the order of 0.17 in. between the profiles obtained from these two probes.

The standard boundary layer utilized in the previous tests was considered established by these two probes—i.e., either probe gave the correct or standard boundary layer.

(5.1) *The Effect of d/D and Nose Shape on Pitot Type Probes*

Traverses were carried out with a pitot having the same cone angle of $8^1/_2°$ but with $d/D = 0.5$ and a 1-in. outside diameter [see Fig. 4(b)]. The profile was once again repeated (see Fig. 14), although the work of reference 3 indicates that there should have been a displacement between the two traverses of 0.016 in.

Traverses were now carried out to investigate the effect of nose shape; one pitot used had a hemispherical nose with $d/D = 0.5$ [see Fig. 4(c)], and the other a flat or square cut nose with $d/D = 0.6$ (this being the type used in reference 3). Both of these probes showed a displacement of the profile toward the wall—i.e., a displacement of the effective center toward the higher total pressure—the flat faced probe producing a displacement of the order of 0.16 in. as indicated by Young and Maas,[3] and the hemispherically nosed probe producing a displacement somewhat less than this (of the order of 0.1 in.). See Fig. 14.

(5.2) *General Remarks and Discussion*

Young and Maas measured the displacement effect of pitot type probes in a transverse total pressure gradient by traversing the wake of a symmetrical

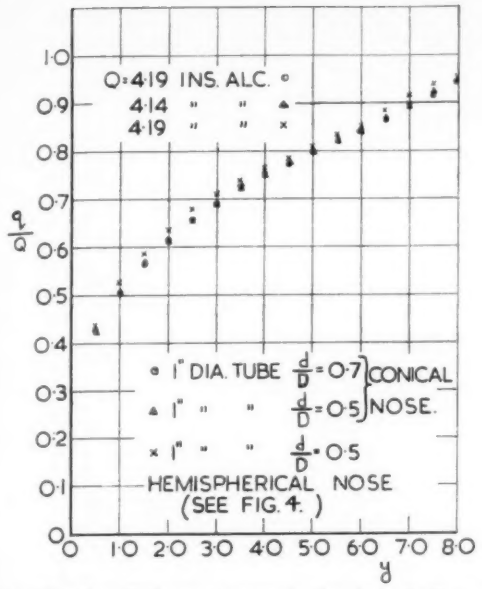

FIG. 14. Showing displacement error for hemispherically nosed pitot type probe and effect of d/D in conical nosed probes.

wing section.[3] This work appears to have been taken as generally applicable by many workers, notably Fage and Ower.[4–6] The pitots used by Young and Maas had square cut or flat noses. The displacement effect might be expected to be accentuated by pitots with square cut noses and to depend to some extent on the value of d/D. The results described above indicate that the displacement effect can for practical purposes be eliminated by using conical nosed pitots with sharp lips. To the accuracy of these tests the displacement error E/D is less than 0.02. The hemispherically ended pitot probably shows a displacement effect because it approaches, in shape, the square cut form.

The work of Fage and Ower[4–6] is concerned with general corrections to mass flow and velocity, measured by pitot probes in pipes with fully developed one-seventh power boundary layers, and assumes the corrections given by Young and Maas. The work of this paper shows that these corrections are not generally applicable—e.g., they do not apply to conical nosed forward facing pitot probes with sharp lips.

The main application of the correction for displacement effect is in the measurement of profile drag by means of wake traverses. This was the reason for the work carried out by Young and Maas. In measurements of this kind errors introduced by the displacement effect are serious, and it would be advantageous to use a probe which reduces the error to negligible proportions; this would appear to be possible by the use of conical noses as suggested here.

(6.0) Further Work

The writer is at present engaged in a further series of tests to confirm the applicability of the results of this paper to wake flows and to investigate in more detail the effect of nose shape on the displacement error for forward facing probes. It is hoped the effect of the aspect ratio of the transverse nose cross section will also be investigated.

References

[1] *The Accuracy of Total Head Measurement with Cylindrical Transverse Type Total Head Tubes*, LOV/FG/H.J.M. 6/J.F. 9.4.45, Rolls-Royce, Ltd., Unpublished Report.

[2] *The Accuracy of Total Head Measurements by Use of the Forward Stagnation Point on a Cylinder*, R.A.E. Tech. Note, Eng 326, November, 1944.

[3] Young, A. D., and Maas, J. N., *The Behaviour of a Pitot Tube in a Transverse Total Pressure Gradient*, British R&M 1770, September, 1936.

[4] Ower, E., *The Measurement of Airflow*, 3rd Ed. rev.; Chapman & Hall, Ltd., 1949.

[5] Fage, A., *Estimation of Pipe Delivery from Pitot-Tube Measurements*, Engineering, Vol. 145, p. 616, 1938.

[6] Ower, E., Trans. Inst. Chem. Engineers, Vol. 18, p. 87, 1940.

[7] Hawthorne, W. R., *The Secondary Flow about Struts and Aerofoils*, Journal of the Aeronautical Sciences, Vol. 21, No. 9, pp. 588–608, 648, September, 1954.

[8] Winternitz, F. A. L., *Cantilevered Pitot Cylinder*, The Engineer, Vol. 200, p. 729, May, 1955.

Notice to Contributors

Manuscripts submitted for publication *must* be double- or triple-spaced originals. There should be wide margins on both sides of the sheets and triple spacing around formulas to allow for the marking of directions for the printer.

Original drawings (jet black India ink on white paper or tracing cloth) should accompany the manuscript. *(Blueprints are not acceptable.)* Photographs *must* be on glossy white paper. The smallest lettering on 8- by 10-in. figures should be no less than 1/4 in. high.

Only the simplest formulas should be typewritten; all others should be carefully written in pen and ink. The difference between capital and lower-case letters and Greek symbols should be clearly distinguished.

See Inside Back Cover of this issue for further details

Nonlinear Minimum-Weight Design of Planar Structures*

LOUIS G. VARGO†

The Ramo-Wooldridge Corporation

SUMMARY

A direct method has been developed for determining the minimum-weight fully plastic moments of a planar structure subject to a set of concentrated loads. A general nonlinear relationship between the fully plastic moments and areas of the series of sections available to the designer is included in the method. The mathematical formulation of the problem has been shown to be isomorphic to problems in other fields in which computational procedures are well developed.

Solutions for the two-span beam and rectangular bent under concentrated loads are obtained, and a comparison with the results of a linearity assumption is made. When geometrically similar sections are used, the linearity assumption results in up to a 15 per cent weight penalty.

Consideration is given to a possible extension of the nonlinear theory to planar structures under distributed loads and space frames.

(1) INTRODUCTION

(1.1) *Limit Design and the Greenberg-Prager Principle*

A LIMIT DESIGN[1] or analysis of a structure considers the formation of a sufficient number of plastic hinges to transform the structure from a statically stable condition to one of kinematic instability—that is, the structure becomes a mechanism under the action of a given set of loads. In the most generalized case of analysis, one must consider the bending moments, torques, shears, and axial forces which contribute to hinge formation for all points on the structure and determine where hinges will actually occur. If these locations are such that the deflections of some points increase without limit, then collapse is said to obtain.

The analysis for planar structures is greatly facilitated by the use of a principle formulated and proved by Greenberg and Prager.[2] For this class of problems no torques are present, and the effects of shear and axial forces are ignored. A knowledge of the fully plastic moments of all sections is assumed. The fully plastic moment is a property of the section shape, size, and material, and it is defined as the maximum bending moment that the section will sustain in pure bending. The principle is best stated in terms of a load factor, a number by which all of the design loads may be multiplied. Use of the principle allows the load factor at collapse to be bounded from above and below and ascertained if the bounds are equal. Its magnitude relative to unity then either establishes a factor of safety or implies collapse.

The problem of designing for minimum total structural weight could be approached with the Greenberg-Prager principle. Several basic difficulties are present, however. The relative weight of each member must be assumed before a determination of the load factor at collapse is made. From this assignment the relative magnitudes of the fully plastic moments can be obtained. In structures containing many members, the number of possible choices is large, and the best choice is not always readily apparent from an inspection of the loading and geometry of the structure. Further, the analysis of a proposed design often becomes quite laborious because bending moment distributions and hinge locations must be assumed in determining the bounds, and the convergence of the bounds may be slow.

(1.2) *Previous Work*

Heyman[3, 4] and Foulkes[5] have investigated the minimum-weight design problem and have obtained solutions for certain classes of structures. Their methods differ somewhat, but each is based on a linear relationship existing between the section fully plastic moment and the section area. This we will call the linear theory. In practice, it would be difficult for the designer to select a series of cross sections such that the fully plastic moment increases linearly with weight (or, equivalently, with section area for a structure of one material). Generally, such plastic relationships are nonlinear. For example, Heyman refers to a series of English structural shapes for which the area is proportional to the three-fifths power of the fully plastic moment.

It is the purpose of this paper to develop a nonlinear theory leading to a minimum-weight design method for planar structures and to compare this with the results of the linear theory.

(2) THE NONLINEAR THEORY FOR CONCENTRATED LOADS

(2.1) *Virtual Work Inequalities and Fundamental Sets of Collapse Modes*

Consider a planar structure composed of n straight members of lengths, $L_j (j = 1, 2, \ldots, n)$, and designed to resist a set of m concentrated loads, $P_i (i = 1, 2, \ldots, m)$, acting in the plane of the structure. We assume that

Received August 4, 1955.

* This paper is based on the author's M.S. thesis presented to Southern Methodist University, Dallas, Tex.

† Member, Technical Staff, Guided Missile Research Division.

these loads have incorporated a factor of safety and that the formation of a plastic hinge at any point is due entirely to the bending moment M at that point. Possible hinge locations will then be at points of local maximum moment. For concentrated loads, these may occur only at the loads or at the reaction points of the members. Let each member be uniform in cross section throughout its length so that, for a given series of sections, the structure is characterized by the section area, $A_j (j = 1, 2, \ldots, n)$.

We define a collapse mode to be a set of hinge locations sufficient to transform the structure into a mechanism either locally or totally. Since the collapse mode for the minimum weight design is not known *a priori*, there will exist r equations giving the internal work done by the structure,

$$(V_{int})_k = \sum_{j=1}^{s} M_j \theta_{jk}, \qquad k = 1, 2, \ldots, r \tag{1}$$

where $(V_{int})_k$ is the internal work of the kth mode, M_j is the fully plastic moment of the jth member, and θ_{jk} is the sum of the hinge rotations in the jth member in the kth mode. Here $s \leq n$ since not all members are necessarily involved in any one collapse mode. The external work done on the structure is given by

$$(V_{ext})_k = \sum_{i=1}^{t} P_i \delta_{ik}, \qquad k = 1, 2, \ldots, r \tag{2}$$

where δ_{ik} is the deflection of the ith load in the kth mode. Here $t \leq m$ since not all loads necessarily experience a finite deflection in any one collapse mode.

If the structure is not to fail in the kth mode, $(V_{int})_k \geq (V_{ext})_k$, and using Eqs. (1) and (2),

$$\sum_{j=1}^{s} M_j \theta_{jk} \geq \sum_{i=1}^{t} P_i \delta_{ik}, \qquad k = 1, 2, \ldots, r \tag{3}$$

The set of inequalities, Eq. (3), may be considered as imposing conditions on the magnitudes of the fully plastic moments. Any design which satisfies these conditions will not fail provided the set, Eq. (3), represents collapse modes which preclude failure in *any* mode. We define a fundamental set of collapse modes to be a set such that the preceding statement holds true. A theorem which allows us to test the existence of a fundamental set is given in the Appendix. Its utility lies in the fact that we need not consider every possible collapse mode once such a fundamental set is established.

(2.2) *Mathematical Statement of the Problem*

The weight of a member may be written as $W_j = C_1 L_j D_j A_j$, where C_1 is a constant of proportionality and D_j is the material density. Since the structure is composed of the same series of sections, the total weight,

$$W = C_1 \sum_{j=1}^{n} L_j D_j A_j \tag{4}$$

Now A is a specific function of M for each series of sections. Further, this function must possess certain properties—namely, $A(0) = 0$ and $(dA/dM) > 0$. A good approximation to functions possessing these properties is

$$A = C_2 M^a, \qquad a \geq 0 \tag{5}$$

In fact, if the sections are geometrically similar, Eq. (5) with a equal to $2/3$ is the exact expression. The expression for the total weight of the structure may now be written in terms of the M_j:

$$W = C_3 \sum_{j=1}^{n} L_j D_j M_j^a \tag{6}$$

The problem is then reduced to minimizing Eq. (6) subject to the restrictions of the set of inequalities, Eq. (3).

Mathematically, the weight expression is a nonlinear functional defined on an n-dimensional vector space composed of column vectors of the form $||M_j||$. We may also consider it as a transformation which takes the points of the positive region of an n-dimensional space into the positive real line. Each of the inequalities of Eq. (3) represents a half space, and their intersection given by the set, Eq. (3), defines a region which we will call the permissible region. Any point in this region corresponds to a set of fully plastic moments for which the structure will not collapse. The permissible region is bounded by the hyperplanes denoted by the set Eq. (3), with the inequality signs deleted. The hyperplanes intersect in at most $r!/n!(r - n)!$ points, which include the extreme points of the permissible region. It may be shown that W is minimized only at extreme points when suitable restrictions are placed on a. Since $(\partial W/\partial M_j) \geq 0$ and $(\partial^2 W/\partial M_j^2) \leq 0$ when $0 \leq a \leq 1$, W is a monotonic increasing concave function of $||M_j||$, so that we may use a theorem from convex set theory which states that a concave functional takes on its minimum value on a convex set (permissible region) only at an extreme point.[6] This is geometrically evident in the solution of problems where $n \leq 3$ and may be formally applied in cases involving more members.

From the preceding, the possible solutions (extreme points) are the same for the linear theory when $a = 1$ and for the nonlinear theory when $0 \leq a \leq 1$. This is not to say that the solutions will be the same but only that each is obtained from the same set of points. A possible exception to this is the case when a bounding hyperplane coincides with the minimum weight functional. This will occur only if W is linear in the M_j—that is, only if $a = 1$. Then points on a hyperplane between some extreme points will make up a range of solutions together with the extreme points. Since the extreme points are included in the nonlinear theory, no essential difference results from this exceptional condition.

The case $a > 1$ is of little practical importance. A series of sections for which A increases more rapidly than M represents an inefficient selection initially. Foulkes states that a lies between $1/2$ and 1 "for most structural sections." The lower limit for a does not affect the method of the nonlinear theory, so that a will be taken as non-negative and not greater than one.

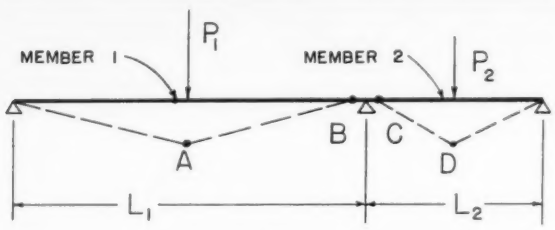

FIG. 1. Two-span beam with central concentrated loads.

(3) TWO-SPAN CONTINUOUS BEAM

(3.1) *Nonlinear Solution*

For the two-span centrally loaded beam shown in Fig. 1, the smallest fundamental set of collapse modes is as follows:

mode	1	2	3	4
hinge locations	AB	CD	AC	BD

That this set is fundamental may be verified by noting that every conceivable mode includes at least one of the four given above. The virtual work inequalities, Eq. (3), now may be written for this particular problem.

mode 1: $$6M_1 \geq P_1L_1 \tag{7}$$

mode 2: $$6M_2 \geq P_2L_2 \tag{8}$$

mode 3: $$4M_1 + 2M_2 \geq P_1L_1 \tag{9}$$

mode 4: $$2M_1 + 4M_2 \geq P_2L_2 \tag{10}$$

We may take $P_1L_1 \geq P_2L_2$ without loss of generality. Using this inequality and Eqs. (7) and (8), it can be shown that Eq. (10) is redundant and may be neglected. The region of permissible values of M_1 and M_2 is shown in Fig. 2. There are three extreme points denoted by π_1, π_2 and π_3. The coordinates of these points are $M_1 = (3P_1L_1 - P_2L_2)/12$, $M_2 = P_2L_2/6$; $M_1 = M_2 = P_1L_1/6$; and $M_1 = P_1L_1/6$, $M_2 = P_2L_2/6$, respectively.

In any set of extreme points which are obtained by formally solving, for example in this problem, three equations taken two at a time, some points may dominate others. $(M_1)_i, (M_2)_i, \ldots (M_n)_i$ is said to dominate $(M_1)_j, (M_2)_j, \ldots (M_n)_j$, if, and only if, $(M_k)_i \geq (M_k)_j$, $k = 1, 2, \ldots n$. Since no coordinate of the ith point is less than the corresponding coordinate of the jth, the jth point can never be an actual extreme point of the permissible region and thus may be ignored.

Both π_1 and π_2 dominate π_3 in the present example, for $(M_1)_1 \geq (M_1)_2 = (M_1)_3$ and $(M_2)_2 \geq (M_2)_1 = (M_2)_3$. Hence, only two possible solutions exist, π_1 and π_2. We now inquire as to when either π_1 or π_2 will be a solution for a particular beam. The weight of the beam from Eq. (6) is

$$W = C_3(L_1D_1M_1^a + L_2D_2M_2^a) \tag{11}$$

If W is considered as a parameter, this equation represents a family of curves which are concave outward from the origin. As W increases, the curves approach the permissible region until contact is made at π_1 or π_2 or at both π_1 and π_2. We may obtain conditions for which these cases occur by considering the minimum weight curve through both π_1 and π_2. Equating the weight expression, Eq. (11), evaluated at these two points and letting $L_2D_2/L_1D_1 = \rho$ and $P_2L_2/P_1L_1 = \sigma$,

$$\rho = \frac{[(3 - \sigma)/2]^a - 1}{1 - \sigma^a} = F(\sigma, a) \tag{12}$$

Since ρ determines the slope of the weight curve at any point, the minimum weight curve touches the permissible region at π_1 or π_2 or at both π_1 and π_2 depending on whether $\rho \lessgtr F$. When $\rho > F$, it can be shown that the intersection of the curve through π_1 with the line $M_2 = (M_2)_2 = P_1L_1/6$ lies below the ordinate of π_2. Therefore, π_1 gives the minimum-weight fully plastic moments when $\rho > F$, and, by elimination, π_2 gives the minimum values when $\rho < F$. By referring back to the equations from which these points were obtained, the hinge locations can be ascertained for each solution. These results are summarized in Table 1.

TABLE 1
Minimum-Weight Fully Plastic Moments for Two-Span Beam

Cases	Fully Plastic Moments		Hinge Locations
$P_1L_1 \geq P_2L_2$	M_1	M_2	
$L_2D_2/L_1D_1 \leq F$	$P_1L_1/6$	$P_1L_1/6$	ABC
$L_2D_2/L_1D_1 \geq F$	$(3P_1L_1 - P_2L_2)/12$	$P_2L_2/6$	ACD

(3.2) *Comparison with the Linear Theory*

It has already been shown that the two theories produce solutions from the same set of extreme points of the permissible region. For $a = 1$, the weight curves are straight lines of slope $-\rho$. The slope of the line connecting π_1 and π_2 is $-1/2$. Thus, the linear theory implies that π_1 or π_2 or all points on the closed line segment $(\pi_1\pi_2)$ minimize W in the permissible region depending on whether $\rho \lessgtr 1/2$. From Fig. 2, π_1 becomes the solution as the slope of the straight lines decreases algebraically. Hence, when $\rho > 1/2$, π_1 is the solution, and, similarly, $(\pi_1\pi_2)$ for $\rho = 1/2$ and π_2 for $\rho < 1/2$.

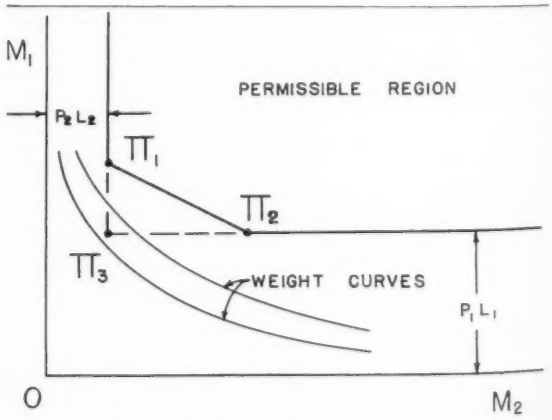

FIG. 2. M_1M_2 plane for two-span beam.

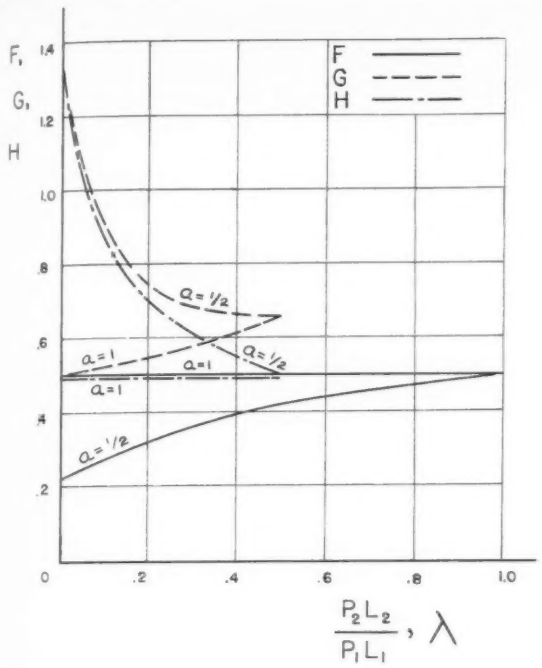

FIG. 3. $F(P_2L_2/P_1L_1)$, $G(\lambda)$, and $H(\lambda)$ for $a = 1$ and $a = 1/2$.

To compare these results with those of the nonlinear theory, we observe from Fig. 3 that $F(\sigma, 1) = 1/2$. Since F is never greater than $1/2$, $\rho < F$ implies $\rho < 1/2$. The linear theory then always exactly agrees with the nonlinear theory if the latter gives π_2 as the only solution. If $\rho > 1/2$, it must be greater than F, and the two theories give π_1 as the only solution. Differences appear when $F \leq \rho \leq 1/2$. Each combination of the equality and inequality signs may be considered in turn and the solutions compared. Doing this, one obtains:

Cases	Linear	Nonlinear
$F = \rho = 1/2$	$(\pi_1\pi_2)$	π_1 and π_2
$F = \rho < 1/2$	π_2	π_1 and π_2
$F < \rho = 1/2$	$(\pi_1\pi_2)$	π_1
$F < \rho < 1/2$	π_2	π_1

The relative weight difference between the two theories is given by the expression,

$$\Delta W = \frac{W_{\pi_2}}{W_{\pi_1}} - 1 = \frac{(1+\rho)}{[(3-\sigma)/2]^a + \rho\sigma^a} - 1 \quad (13)$$

Since the denominator of the first term never exceeds the numerator, use of the linear theory represents a weight penalty to the designer when $F < \rho < 1/2$. It can be shown that ΔW increases with ρ and decreases with σ. The value of ΔW at $\rho = 1/2$, $\sigma = 0$ is $(3/2)^{1-a} - 1$, so that, for small a, the maximum weight penalty approaches 50 per cent of the actual minimum weight given by the nonlinear solutions. A more realistic case is when $a = 2/3$ for which $(\Delta W)_{max} \cong 15$ per cent.

(4) Rectangular Bent with a Concentrated Side Load

As an example of the nonlinear theory applied to a structure consisting of three members, consider the rectangular bent shown in Fig. 4. The smallest fundamental set of collapse modes is as follows:

mode	1	2	3	4	5	6
hinge locations	ABC	ABD	ACEG	ACFG	ADEG	ADFG

The virtual work inequalities for each of these in order are

$$2M_1 \geq \lambda(1-\lambda)PL_4 \quad (14)$$

$$(2-\lambda)M_1 + \lambda M_2 \geq \lambda(1-\lambda)PL_4 \quad (15)$$

$$2M_1 + M_2 + M_3 \geq \lambda PL_4 \quad (16)$$

$$2M_1 + 2M_3 \geq \lambda PL_4 \quad (17)$$

$$M_1 + 2M_2 + M_3 \geq \lambda PL_4 \quad (18)$$

$$M_1 + M_2 + 2M_3 \geq \lambda PL_4 \quad (19)$$

We may take $M_1 \geq M_3$, and, using Eqs. (17), (18), and (19), Eqs. (14), (15), and (16) are redundant when $\lambda \geq 1/2$. The three remaining bounding planes intersect in only one point, π_4. The coordinates are $M_1 = M_2 = M_3 = \lambda PL_4/4$. Thus, when $\lambda \geq 1/2$, a unique solution results irrespective of the relative lengths of the columns and cross members.

For the case, $\lambda \leq 1/2$, only Eqs. (16) and (17) are redundant, so that possible solutions are given by the points of intersection of the four remaining planes. Denoting these points by π_5, π_6, π_7, and π_8, the coordinates are $M_1 = M_2 = \lambda(1-\lambda)PL_4/2$, $M_3 = \lambda(3\lambda-1)PL_4/2$; $M_1 = M_2 = \lambda(1-\lambda)PL_4/2$, $M_3 = \lambda^2 PL_4/2$; $M_1 = \lambda(1-\lambda)PL_4/2$, $M_2 = M_3 = \lambda(1+\lambda)PL_4/6$; and $M_1 = \lambda(3-4\lambda)PL_4/2(3-2\lambda)$, $M_2 = M_3 = \lambda PL_4/2(3-2\lambda)$, respectively. Since $(M_1)_5 = (M_2)_5 = (M_1)_6 = (M_2)_6$ and $(M_3)_6 \geq (M_3)_5$, π_6 dominates π_5. It can further be shown that the three remaining points do not dominate each

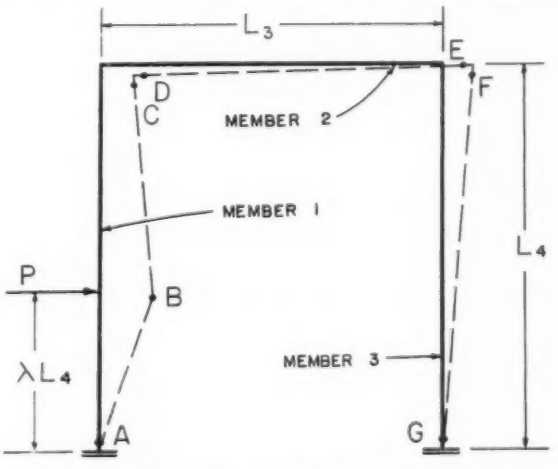

FIG. 4. Rectangular bent with concentrated side load.

TABLE 2
Minimum-Weight Fully Plastic Moments for Rectangular Bent

Cases	Fully Plastic Moments M_1	M_2	M_3	Hinge Locations
$\lambda \geq 1/2$	$\frac{\lambda PL_4}{4}$	$\frac{\lambda PL_4}{4}$	$\frac{\lambda PL_4}{4}$	ACDEFG
$\lambda \leq 1/2$, $L_2/L_4 \leq H$	$\frac{\lambda(1-\lambda)PL_4}{2}$	$\frac{\lambda(1-\lambda)PL_4}{2}$	$\frac{\lambda^2 PL_4}{2}$	ABCDFG
$\lambda \leq 1/2$, $H \leq L_2/L_4 \leq G$	$\frac{\lambda(1-\lambda)PL_4}{2}$	$\frac{\lambda(1+\lambda)PL_4}{6}$	$\frac{\lambda(1+\lambda)PL_4}{6}$	ABCDEFG
$\lambda < 1/2$, $L_2/L_4 \geq G$	$\frac{\lambda(3-4\lambda)PL_4}{2(3-2\lambda)}$	$\frac{\lambda PL_4}{2(3-2\lambda)}$	$\frac{\lambda PL_4}{2(3-2\lambda)}$	ABDEFG

other, for $(M_1)_8 \geq (M_1)_7 = (M_1)_6$, $(M_2)_6 \geq (M_2)_7 \geq (M_2)_8$, and $(M_3)_7 \geq (M_3)_8 \geq (M_3)_6$.

$$W = C_4[L_4(M_1^a + M_3^a) + L_3 M_2^a] \qquad (20)$$

if the material is the same throughout the structure. If $W_{\pi_6} < W_{\pi_8}$, and letting $L_3/L_4 = \tau$,

$$\tau < \frac{(3-4\lambda)^a + 1 - (3-2\lambda)^a[\lambda^a + (1-\lambda)^a]}{(1-\lambda)^a(3-2\lambda)^a - 1} = G(\lambda, a) \qquad (21)$$

If $W_{\pi_6} < W_{\pi_7}$,

$$\tau < \frac{(1+\lambda)^a - (3\lambda)^a}{[3(1-\lambda)]^a - (1+\lambda)^a} = H(\lambda, a) \qquad (22)$$

The functions G and H are plotted in Fig. 3 for $a = 1/2$ and $a = 1$. Since $H < G$, cases, for which only a single point is the solution, correspond to the inequalities $\tau < H$, $H < \tau < G$, and $\tau > G$, and corresponding solutions, π_6, π_7, and π_8. Table 2 summarizes these results.

A comparison with the results of the linear theory could be made similarly to that for the two-span beam problem. No detailed investigation will be made in this paper; however, one interesting point is worth noting. Since the solution, π_4 when $\lambda \geq 1/2$, was obtained independently of the weight expression, a linear design consideration would produce the same result.

(5) Discussion

Use of the nonlinear theory offers a direct rather than an iterative method for optimum structural design on the basis of minimum weight. The number of concentrated loads or members does not affect the validity of the method so that approximations to distributed loading and curved frames may be checked to determine how closely the obtained solutions approximate the actual solution. When the number of loads or members becomes large, however, the establishment of design tables is impracticable without employing machine methods of computation. In this regard, the similarity between the minimum weight structural problem, optimum programing in the field of economics,[7] and optimum strategy in the theory of games should be pointed out. Each requires the determination of points in a region defined by linear inequalities for which a functional is extremized. Hence, computational procedures developed in the latter two fields are applicable to the problem considered in this paper.

For space structures, the effect of torques on hinge formation requires knowledge of the breakdown criterion relating the applied torques and bending moments to the fully plastic moments.[8] One difficulty here is that the form of this relationship depends upon the geometry of the cross section, so that the resulting solution would strictly hold only for a series of geometrically similar sections. Hill and Siebel[9] have shown this relationship to be quite insensitive to changes in geometry, however. Therefore, the use of one breakdown criterion for a series of sections of practical importance should produce errors of small magitude.

Appendix

Let p_k, $k = 1, 2, \ldots, r$, denote the proposition, *the structure will collapse in the kth mode*, and q the proposition, *the structure will collapse in some mode*. If q implies (p_1 or p_2 or . . . or p_r), then not (p_1 or p_2 or . . . or p_r) implies not q. But, by DeMorgan's rule, not (p_1 or p_2 or . . . or p_r) is equivalent to (not p_1 and not p_2 and . . . and not p_r), so that a set of r collapse modes is fundamental if every possible mode includes at least one of the r modes.

References

[1] Van den Broek, J. A., *Theory of Limit Design*, 1st Ed.; John Wiley & Sons, Inc., New York, 1948.

[2] Greenberg, H. J., and Prager, W., *Limit Design of Beams and Frames*, Proc. ASCE, Vol. 77, Separate No. 59, February, 1951.

[3] Heyman, J., *Minimum Weight Design of Plane Frames*, TR 45, Grad. Div. of Appl. Mech., Brown University, 1950.

[4] Heyman, J., *Limit Design of Continuous Beams for Minimum Weight*, TR 47, Grad. Div. of Appl. Mech., Brown University, 1950.

[5] Foulkes, J., *The Minimum-Weight Design of Structural Frames*, Proc. of the Royal Society, Vol. 223, No. 1155, pp. 482–494, May 20, 1954.

[6] Bonnesen, T., and Fenchel, W., *Theorie der Konvexen Körper*, 1st Ed., pp. 18–19; Chelsea Publishing Co., New York, 1948.

[7] Charnes, A., Cooper, W. W., and Henderson, A., *An Introduction to Linear Programming*, 1st Ed., Part II; John Wiley & Sons, Inc., New York, 1953.

[8] Heyman, J., *The Limit Design of Space Frames*, J. Appl. Mech., Vol. 18, No. 2, pp. 157–162, June, 1951.

[9] Hill, R., and Siebel, M. P. L., *On the Plastic Distortion of Solid Bars by Combined Bending and Twisting*, J. Mech. & Phys. of Solids, Vol. 1, No. 3, pp. 189–206, April, 1953.

On Transonic Airfoil Theory

GOTTFRIED GUDERLEY*
Wright Air Development Center

SUMMARY

The paper is concerned with the development of the flow over an airfoil with respect to the reciprocal of the aspect ratio. For an infinite aspect ratio, the flow at each airfoil section is essentially plane. The hodograph transformation, applied to the velocity components normal to the span, brings the flow equation into a form in which the terms pertaining to plane flow patterns occur linearly, while the spatial terms give a nonlinear contribution. For sufficiently large aspect ratio and close to the profile, the linear terms in this equation will prevail, but, no matter how large the aspect ratio is chosen, it is never possible to disregard the nonlinear terms throughout the field—thus, the effect of the flow field at a distance from the profile on the flow field close to the profile must be taken into account. This is done in the form of a boundary condition which the flow at a distance imposes to the flow close to the airfoil. This condition is formulated by means of the transonic similarity law. Hereafter, the flow close to the airfoil can be treated similarly to plane flows with a free-stream Mach Number close to one.

In the lowest order approximation, the deviation of the pressure distribution from the pressure distribution in a plane flow has the same form as the deviations that would be caused in a plane flow by a suitable change of the free-stream Mach Number of the angle of attack, and by a lowering of the pressure level. All of these effects are proportional to the $-6/5$ power of the aspect ratio. Subsequent terms of the development are proportional to the $-8/5$ power. In contrast to subsonic flow patterns, the effect of the angle of attack is not independent of the displacement of the airfoil.

(1) Introduction

For the flow over an airfoil with a finite aspect ratio, there exist two strictly separated approaches—one for small and the other for large aspect ratios. The theory for small aspect ratios is the same for all subsonic and transonic Mach Numbers; its range of validity even increases as the free-stream Mach Number approaches one. A theory for large aspect ratios is the subject of the present paper. There one expects the flow over the airfoil to be essentially plane and treats the spatial influence as a correction.

A complete solution can hardly be expected; transonic flow patterns, especially those close to plane flows, are characterized by the occurrence of a nonlinear term in the simplified flow differential equation, which makes the solution of the flow problem extremely cumbersome, if not impossible. But the main trend of the spatial influence can at least be established; we shall, for example, see that the deviation from the pressure distribution in a plane flow at Mach Number one is proportional to the $-6/5$ power of the aspect ratio. A detailed description of the results is found at the end of the paper.

Received August 8, 1955.

* Chief, Applied Mathematics Branch, Aeronautical Research Laboratory, Directorate of Research, ARDC.

(2) Formulation of the Problem

Under the assumption that the deviation of the flow field from a sonic parallel flow is small, the velocity potential Φa^* which describes this deviation fulfills the following simplified differential equation:

$$-(\gamma + 1)\Phi_x \cdot \Phi_{xx} + \Phi_{yy} + \Phi_{zz} = 0 \qquad (2.1)$$

Here x is the coordinate in the streamwise direction, y is the coordinate in the direction of the span, and z is the coordinate perpendicular to x and y; γ is the ratio of the specific heats and a^* is the sonic velocity. Let us now consider a family of affine airfoils which originate from each other by a change of the scale in the x and z directions. The surface of these airfoils may be given by $g(x/t, y, z/t) = 0$, where t is a parameter that has a fixed value for a given airfoil. For fixed arguments of the function g—e.g., for points that correspond to the leading edge—x and z are proportional to t while y is fixed. Thus, the aspect ratio is inversely proportional to t. For $t = 0$, the airfoil contracts into a straight line, which might be referred to as lifting line. This paper tries to represent the flow problem in the form of a development with respect to t.

(3) Hodograph Transformation

A hodograph transformation in the conventional sense would use as independent variables the velocity components in space. But then the dependence of the flow field upon y would be rather hard to recognize. It is more practical to use as independent variables the velocity components Φ_x and Φ_z and the coordinate y. The transition to these variables is made by means of Legendre's transformation

$$\Phi(x, y, z) = -\varphi(u, w, y) + u \cdot \varphi_u(u, w, y) + w\varphi_w(u, w, y) \qquad (3.1)$$

with

$$\Phi_x = u \qquad (3.2a)$$

$$\Phi_z = w \qquad (3.2b)$$

As long as one forms derivatives with respect to x, z, u, or w only, the dependence of these expressions upon y is unessential. Therefore, one has immediately the well known results

$$x = \varphi_u \qquad (3.3a)$$

$$z = \varphi_w \qquad (3.3b)$$

$$\left.\begin{aligned} \Phi_{xx} &= \varphi_{ww}/(\varphi_{uu}\varphi_{ww} - \varphi_{uw}^2) \\ \Phi_{zz} &= \varphi_{uu}/(\varphi_{uu}\varphi_{ww} - \varphi_{uw}^2) \\ \Phi_{xz} &= -\varphi_{uw}/(\varphi_{uu} \cdot \varphi_{ww} - \varphi_{uw}^2) \end{aligned}\right\} \qquad (3.4)$$

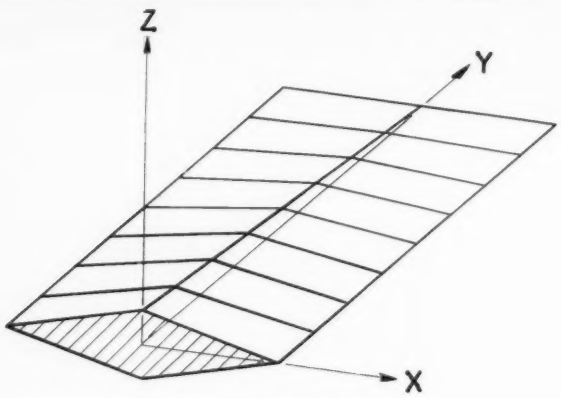

FIG. 1. Airfoil in x, y, z-space.

In forming the partial derivative of $\Phi\ (x, y, z)$ with respect to y, one must express the condition that $x = \varphi_u$ and $z = \varphi_w$ are to be kept constant. One finds from Eq. (3.1)

$$\Phi_y = -\varphi_y - \varphi_u \cdot \frac{du}{dy} - \varphi_w \cdot \frac{dw}{dy} + x \cdot \frac{du}{dy} + z \cdot \frac{dw}{dy}$$

Hence, $$\Phi_y = -\varphi_y$$

Furthermore,

$$\Phi_{yy} = -\varphi_{yy} - \varphi_{uy} \cdot (du/dy) - \varphi_{wy} \cdot (d_w/dy)$$

Here du/dy and dw/dy must be computed from the condition that x and z are constant. Eqs. (3.3) yield

$$\varphi_{uu} \cdot (du/dy) + \varphi_{uw} \cdot (dw/dy) = -\varphi_{uy}$$
$$\varphi_{uw} \cdot (du/dy) + \varphi_{ww} \cdot (dw/dy) = -\varphi_{wy}$$

hence,

$$\frac{du}{dy} = \frac{-\varphi_{uy}\varphi_{ww} + \varphi_{wy}\varphi_{uw}}{\varphi_{uu} \cdot \varphi_{ww} - \varphi_{uw}^2}$$

$$\frac{dw}{dy} = \frac{-\varphi_{wy} \cdot \varphi_{uu} + \varphi_{uy}\varphi_{uw}}{\varphi_{uu} \cdot \varphi_{ww} - \varphi_{uw}^2}$$

Thus,

$$\Phi_{yy} = -\varphi_{yy} + \frac{\varphi_{uy}^2\varphi_{ww} - 2\varphi_{uy} \cdot \varphi_{wy}\varphi_{uw} + \varphi_{wy}^2\varphi_{uu}}{\varphi_{uu} \cdot \varphi_{ww} - \varphi_{uw}^2} \quad (3.5)$$

Inserting Eqs. (3.4) and (3.5) into Eq. (2.1), one obtains the following hodograph equation:

$$-(\gamma + 1)u \cdot \varphi_{ww} + \varphi_{uu} - \varphi_{yy}(\varphi_{uu} \cdot \varphi_{ww} - \varphi_{uw})^2 + \varphi_{uy}^2\varphi_{ww} + \varphi_{wy}^2\varphi_{uu} - 2\varphi_{uy}\varphi_{wy}\varphi_{uw} = 0 \quad (3.6)$$

This equation is linear in all terms which do not contain y. To obtain a closer agreement with the notations used in other papers on plane transonic flow patterns, we introduce

$$(\gamma + 1)^{1/3}u = \eta \quad (3.7)$$

$$w = \theta \quad (3.8)$$

One then obtains the differential equation

$$\varphi_{\eta\eta} - \eta\varphi_{\theta\theta} = \varphi_{yy}(\varphi_{\eta\eta}\varphi_{\theta\theta} - \varphi_{\eta\theta}^2) - \varphi_{\eta y}^2 \cdot \varphi_{\theta\theta} - \varphi_{\theta y}^2 \cdot \varphi_{\eta\eta} + 2\varphi_{\eta\theta}\varphi_{\eta y}\varphi_{\theta y} \quad (3.9)$$

Let us assume, that, for each airfoil section, $y =$ const., the plane flow at Mach Number one is known. Then the hodograph map of these airfoil sections is known, too. These maps form a surface in the η, θ, y-space which is the map of the surface of the airfoil for $t = 0$. This surface will be denoted as S_1. Fig. 1 shows the right half of a wing to which the present theory can be applied. The plane $y = 0$ is the plane of symmetry of the wing. For ease of representation a wedge profile with a constant chord has been chosen. In order to avoid too abrupt a change of the cross section at the tips of the airfoil, it has been assumed that the thickness of the wing changes linearly and assumes the value zero at the wing tip. Fig. 2 shows the map of the wing in the η, θ, y-space. The sides of the individual sections $y =$ const. map into lines $\theta =$ const. As one moves towards the wing tips the values of θ decrease linearly. These lines $\theta =$ const. extend naturally to $\eta = -\infty$—i.e., to a stagnation point for each individual wing section—in Fig. 2 they are terminated at a finite value of $-\eta$. In each section $y =$ const., the Meyer expansion that occurs at the shoulder of the wedge is mapped into a characteristic running through the point where the map of the side of the wedge intersects the surface plane $\eta = 0$. These maps give the curved part of the surface S_1 in Fig. 2. For the determination of the subsonic part of the flow pattern, only the part of the supersonic region bounded by the so-called limiting characteristic needs to be known. Thus, a boundary of the surface S_1 arises in the region $\eta > 0$. The surface S_2 which occurs also in Fig. 2 will be introduced later.

At large distances from the airfoil, the velocity components Φ_x and Φ_y and with them η and θ are small; so infinity in the physical space will map into the y axis of the hodograph space.

(4) Some Properties of Plane Flow Patterns

For the subsequent investigations some properties of plane transonic flow patterns are needed. The results presented in this paragraph are compiled from references 1, 2, and 3.

Plane flows are described by the differential equation

$$\varphi_{\eta\eta} - \eta\varphi_{\theta\theta} = 0 \quad (4.1)$$

which arises from Eq. (3.9) by omitting all derivatives with respect to y. Tricomi has given a uniqueness and existence proof for a certain class of boundary value problems governed by this differential equation; therefore, it is usually called Tricomi's equation. One of the important conditions imposed in this proof requires that φ is bounded and that along the line $\eta = 0$ the expression $\varphi_\eta \cdot \theta^{5/6}$ is bounded. This condition will be referred to as Tricomi's condition.

Using Eqs. (3.3) and (3.7) one finds the following expressions for the coordinates in the physical plane:

$$x = (\gamma + 1)^{1/3}\varphi_\eta \tag{4.2a}$$

where

$$z = \varphi_\theta \tag{4.2b}$$

In the lowest order approximation the streamlines are lines z = const.—i.e., they are represented by the streamlines of the undisturbed flow. This is the form in which streamlines are characterized in the η, θ-plane. Naturally, in the physical plane this formulation is practically meaningless. There one must determine a higher approximation by integrating the streamline slope along a line z = const. with respect to x. In this manner, the form of a profile belonging to a certain hodograph solution can be found.

A class of particular solutions of Eq. (4.1) can be written in the form

$$\varphi = |\eta|^n f(\zeta, n) \tag{4.3}$$

where

$$\zeta = [(9/4)\theta^2]/\eta^3 \tag{4.3a}$$

and n is a constant. Other forms of this hypothesis are found in reference 2.

symmetric	antisymmetric
$\varphi_{-1-3h} = \lvert\eta\rvert^{-1-3h} f^s(\zeta, -1-3h)$	$\varphi_{-2.5-3h} = \lvert\eta\rvert^{-2.5-3h} f^a(\zeta, -2.5-3h)$
$\varphi_0 = 1$	
$\varphi_{1+h} = \lvert\eta\rvert^{1+h} f^s(\zeta, 1+h)$	$\varphi_{0.5+h} = \lvert\eta\rvert^{0.5+h} f^a(\zeta, 0.5+h)$

(4.4)

here h is a non-negative integral number. All of these expressions can be written in a closed form. The solution $\varphi_0 = 1$ will play a somewhat exceptional role. If the symmetric and antisymmetric particular solutions are considered simultaneously, then the positive exponents n are evenly spaced with an interval of 1/2 and the negative exponents are evenly spaced with an interval of 3/2.

It has been shown in reference 3 that, in the vicinity of the origin, any solution of Eq. (4.1) which is bounded along the characteristics $\zeta = 1$ and whose derivatives are bounded, too, can be represented by a superposition of Eqs. (4.4), but, in general, the region of convergence will not extend to the profile. If this function φ further fulfills Tricomi's condition, then the representation will contain only functions with a non-negative subscript. In a plane flow with the free-stream Mach Number one, all streamlines originate from a point of the sonic line; in our present considerations this point is the origin of the η, θ-system. The prevalent solution in the vicinity of this point is given by $c \cdot \varphi_{-1}$. The constant c is determined by the size of the body. The entire solution for the flow with a free-stream Mach Number one over a given profile may be denoted as $\varphi_{-1}{}^*$ and can be written as

$$\varphi_{-1}{}^* = c \cdot \varphi_{-1} + \omega_{-1} \tag{4.5}$$

Here ω_{-1} is a solution of Tricomi's equation which fulfills Tricomi's condition at point 0. It is chosen in such a manner that along the hodograph map of the profile (usually not known in advance) the condition

$$\varphi_{-1;\,\theta}{}^* = 0$$

is fulfilled [cf. Eq. (4.2b) and the subsequent remark].

In the vicinity of the origin, the solution ω_{-1} can be developed in terms of the particular solutions (4.4), and one finds

$$\omega_{-1} = a^{0.5} \cdot \varphi_{0.5} + a^1 \cdot \varphi_1 + a^{1.5}\varphi_{1.5} + \ldots \tag{4.6}$$

the coefficients $a^{0.5+0.5h}$ are determined by the form of the profile. The superscripts occurring with the a's are the same as the subscripts of the functions ω to which they belong. An unsymmetry of the profile—including an angle of attack—is expressed by the presence of antisymmetric particular solutions $\varphi_{0.5}$, $\varphi_{1.5}$, etc.

Furthermore, solutions φ can be found, which, if superimposed to the expression (4.5), leave the profile unchanged. In general this will require a linearization of the boundary conditions in the hodograph. Let the map of the profile in the original flow Eq. (4.5) be given by

$$\eta = \eta_0(\theta) \tag{4.7}$$

Then one obtains as boundary conditions for the superimposed solutions (see reference 2)

$$\varphi_\eta(\eta_0, \theta) + \eta_0 \varphi_\theta(\eta_0, \theta) \cdot (d\eta_0/d\theta) = 0 \tag{4.8}$$

A solution of Tricomi's equation fulfilling Eq. (4.8) can be written in the form

$$\varphi_{-2.5-1.5h}{}^{*} = \varphi_{-2.5-1.5h} + \omega_{-2.5-1.5h}\, h = 0, 1, 2, \ldots \tag{4.9}$$

for $\omega_{-2.5-1.5h}$, one has the boundary condition

$$\omega_{-2.5-1.5h;\,\eta} + \eta_0 \omega_{-2.5-1.5h;\,\theta}\,(d\eta_0/d\theta) = -\varphi_{-2.5-1.5h;\,\eta} - \eta_0 \varphi_{-2.5-1.5h;\,\theta}\cdot(d\eta_0/d\theta) \tag{4.10}$$

to be fulfilled along the map of the profile in the original flow. The subscripts after the semicolon indicate partial differentiations.

The function on the right-hand side of the last equation is known. A boundary value problem of this type has been denoted in reference 2 as boundary value problem of the second kind, because of its similarity with such boundary value problems in potential theory. In general, such a boundary value problem does not have a physically admissible solution which fulfills Tricomi's condition. This can be seen from the following physical reasoning: Assume that the boundary value problem of the second kind could always be solved. Then one could construct a solution in the form of Eq. (4.9) in which the first term is given by φ_{-1}. By superimposing this solution on the original flow at a free-stream Mach Number one, one would obtain a new flow field with a free-stream Mach Number one for the same body—i.e., the flow over a body at a free-stream Mach Number one would not be unique. Thus it appears likely that an additional condition must be imposed to the boundary values. In analogy to the boundary value problems of potential theory, one will expect it to have the form

$$\int K(s)\cdot k(s)\, ds = 0 \tag{4.11}$$

where s is a parameter defined along the map of the profile, $k(s)$ is the right-hand side of Eq. (4.10), and $K(s)$ is a function determined by the form of the boundary. Because of the physical reasons given above, the function φ_{-1} will not fulfill this condition; therefore $\omega_{-2.5-(3/2)h}$ can be represented in the form

$$\omega_{-2.5-(3/2)h} = b_{-2.5-(3/2)h}{}^{-1}\varphi_{-1} + \bar{\omega}_{-2.5-(3/2)h} \tag{4.12}$$

where $\bar{\omega}$ fulfills Tricomi's condition and $b_{-2.5-1.5h}{}^{-1}$ is a constant. Naturally, if the right-hand side of Eq. (4.10) is given arbitrarily, the solution will also have the form of Eq. (4.12).

Thus, Eq. (4.9) assumes finally the form

$$\varphi_{-2.5-1.5h}{}^{*} = \varphi_{-2.5-1.5h} + \omega_{-2.5-1.5h} = \varphi_{-2.5-1.5h} + b_{-2.5-1.5h}{}^{-1}\varphi_{-1} + \bar{\omega}_{-2.5-1.5h} \tag{4.13}$$

The last expression can be developed in terms of the particular solutions of Eqs. (4.4)

$$\varphi_{-2.5-1.5h}{}^{*} = \varphi_{-2.5-1.5h} + b_{-2.5-1.5h}{}^{-1}\varphi_{-1} + \sum_{k=0}^{\infty} b_{-2.5-1.5h}{}^{0.5+0.5k}\varphi_{0.5+0.5k} \tag{4.14}$$

Here the b's are constants, their subscripts correspond to the subscript of the function φ^{*} in whose representation they occur, their superscripts correspond to the subscript of the functions φ_{α} whose coefficients they are. An example in which one can see somewhat more directly how Eq. (4.14) comes about is the flow over a wedge profile.[4, 5] These investigations lead to solutions of the form of Eqs. (4.14) if one takes into account that, because of the symmetry properties of the profile, the coefficients of some of the terms will be zero.

Any solution that fulfills the boundary conditions at the surface of the profile can be represented by a superposition of Eqs. (4.5) and (4.13)

$$\varphi = \varphi_{-1}{}^{*} + \sum_{h=0}^{\infty} d^{-2.5-1.5h}\varphi_{-2.5-1.5h}{}^{*} \tag{4.15}$$

The coefficients $d^{-2.5-1.5h}$ are arbitrary constants, unknown at the present. By inserting Eqs. (4.5) and (4.14) into Eq. (4.15), one obtains

$$\varphi = (c + e^{-1})\varphi_{-1} + \sum_{h=0}^{\infty} d^{-2.5-1.5h}\varphi_{-2.5-1.5h} + \sum_{h=0}^{\infty} e^{0.5+0.5k}\varphi_{0.5+0.5k} \tag{4.16}$$

where the coefficients "e" are given by the equations

$$e^{-1} = \sum_{h=0}^{\infty} d^{-2.5-1.5h}\, b_{-2.5-1.5h}{}^{-1} \tag{4.17a}$$

$$e^{0.5+0.5k} = a^{0.5+0.5k} + \sum_{h=0}^{\infty} d^{-2.5-1.5h} b_{-2.5-1.5h}{}^{0.5+0.5k} \tag{4.17b}$$

The unknown constants are ultimately determined by the boundary conditions prescribed in the physical plane at a large distance from the profile. In the hodograph plane, these conditions are prescribed in the vicinity of point 0. They can be expressed in the following form:

$$d^{-2.5-1.5h} = F^{-2.5-1.5h}(c + e^{-1}, e^{0.5}, e^{1} \ldots) \qquad h = 0, 1, \ldots \tag{4.18}$$

The functions F occurring here are determined by these boundary conditions—at least in principle. (For examples see reference 5.) This formulation is independent of the form and size of the profile. As is shown by Eqs. (4.17), the arguments of this function F depend upon the unknown quantities $d^{-2.5-1.5h}$ and, besides, on constants "b" and "a," which express the properties of the profile. Thus the Eq. (4.18) actually represents an infinite system of equation. That these boundary conditions are sufficient to determine the constants $d^{-2.5-1.5h}$ can be shown by means of an iteration procedure. As a first approximation of the solution, one chooses the flow for the Mach Number one. Then one has

$$d^{-2.5-1.5h} = 0$$

Hence, from Eqs. (4.17), (4.5), and (4.6),

$$e^{-1} = 0, \qquad e^{0.5+0.5k} = a^{0.5+0.5k}$$

Then Eq. (4.18) gives the improved approximation for the d's

$$d^{-2.5-1.5h} = F^{-2.5-1.5h}(c, 0\ 0 \ldots)$$

Using these values one finds improved approximation for the c's.

(5) The Spatial Problem

We try now to find a representation of the spatial flow pattern in the form of a development with respect to t. For small values of t, the flow in the vicinity of the profile is expected to be plane. Along the profile x and z are proportional to t. This requires, according to Eq. (3.3), that φ is proportional to t also. Thus, in the vicinity of the profile, the transformed potential can be expected to have the form

$$\varphi = t \cdot \varphi_{-1}^*(\eta, \theta, y) \tag{5.1}$$

where the function φ_{-1}^* is defined in Eqs. (4.5) and (4.6). All coefficients "c" and "a" occurring there are functions of y. In an attempt to use this expression as a first approximation in a series of iteration steps, one might write φ in the form

$$\varphi = t \cdot \varphi_{-1}^* + \Delta\varphi \tag{5.2}$$

where $\Delta\varphi$ is considered as small in comparison with the first term. Furthermore, t may be small. The expression φ_{-1}^* fulfills the left-hand side of Eq. (3.9). Thus, one obtains the following equation for $\Delta\varphi$:

$$\Delta\varphi_{\eta\eta} - \eta\Delta\varphi_{\theta\theta} = t^3(\varphi_{-1;\,\eta\eta}^* \cdot \varphi_{-1;\,\theta\theta}^* \cdot \varphi_{-1;\,yy}^* + \text{similar terms}) \tag{5.3}$$

The form of this equation suggests a development of the solution in powers of t. The function φ_{-1}^* behaves for small values of η as η^{-1}; a differentiation with respect to θ can be expressed as a differentiation with respect to ζ; and, in this process, a factor $\eta^{-3/2}$ occurs for each derivative with respect to θ. Thus, for small values of η, the term on the right-hand side of the last equation is proportional to η^{-8}. This shows that, no matter how small t is chosen, there is always a region in the flow field in which the term on the right-hand side cannot be considered as small; the hypothesis of Eq. (5.2) cannot be applied for the entire flow field.

Therefore, a surface S_2 is introduced which lies between the map of the profile S_1 and the y-axis (see Fig. 2). The regions between S_1 and S_2 and between S_2 and the y-axis are called R_1 and R_2, respectively. In the region R_1, a development carried out in the manner just mentioned is feasible—i.e., one can first disregard the right-hand terms in Eq. (3.9), and take the influence of the right-hand terms into account later. Along S_2 certain boundary conditions are imposed on the region R_1 which depend upon the solution in the region R_2. These boundary conditions will be seen to have an important influence upon the pressure distribution over the airfoil.

On the other hand, the flow in the region R_2 is determined by the boundary conditions which are imposed to it because of the flow R_1. For $t = 0$, the flow in the region R_1 is given by Eq. (5.1). If S_2 is sufficiently remote from the profile, the prevalent term in this expression is

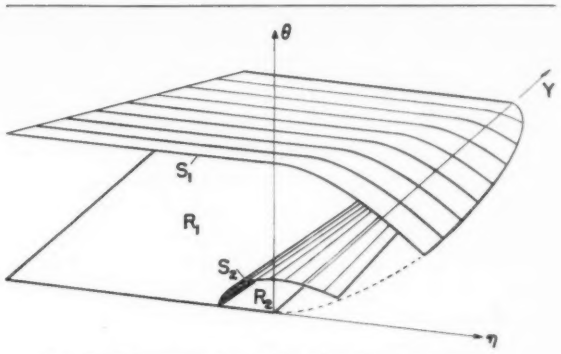

Fig. 2. Representation of the wing in the η, θ, y-space.

$$\varphi = t \cdot c(y) \cdot \varphi_{-1} \tag{5.4}$$

Let us discuss the flow in the region R_2 under the assumption that along S_2 the solution will assume the form of Eq. (5.4). Later we shall show in which sense the expression so obtained can be considered as the solution for $t = 0$.

In Eq. (5.4) the occurrence of the factor t is inconvenient. It can be eliminated from the boundary conditions without being introduced into the differential equation by the following transformation:

$$\varphi(\eta, \theta, y) = t^{3/5}\bar{\varphi}(\bar{\eta}, \bar{\theta}, y) \tag{5.5}$$

with

$$\bar{\eta} = t^{-0.4} \cdot \eta \tag{5.6a}$$

$$\bar{\theta} = t^{-0.6}\theta \tag{5.6b}$$

Then one must consider a solution of the differential equation

$$\bar{\varphi}_{\bar{\eta}\bar{\eta}} - \bar{\eta}\bar{\varphi}_{\bar{\theta}\bar{\theta}} = \bar{\varphi}_{yy}(\bar{\varphi}_{\bar{\eta}\bar{\eta}} \cdot \bar{\varphi}_{\bar{\theta}\bar{\theta}} - \bar{\varphi}_{\bar{\eta}\bar{y}}^2) - \bar{\varphi}_{\bar{\eta}y}^2 \cdot \bar{\varphi}_{\bar{\theta}\bar{\theta}} - \bar{\varphi}_{\bar{\theta}y} \cdot \bar{\varphi}_{\bar{\eta}\bar{\eta}} + 2\bar{\varphi}_{\bar{\eta}\bar{y}} \cdot \bar{\varphi}_{\bar{\eta}y} \cdot \bar{\varphi}_{\bar{\theta}y} \tag{5.7}$$

The transformation moves the surface S_2 to infinity, if $t \to 0$. Therefore, (Eq. 5.4) yields the condition

$$\bar{\varphi} \sim c(y)\varphi_{-1}(\bar{\eta}, \bar{\theta}) \qquad \text{for} \qquad \bar{\eta} \to \infty \tag{5.8}$$

One notices that the transformation (5.6) does not affect the values of ζ (Eq. 4.3).

Let us introduce a fixed surface $\bar{S}_3$ in the $\bar{\eta}$, $\bar{\theta}$, y-space. The region outside of this surface may be denoted by R_3, the region inside of this surface by R_4. If the behavior at a large distance is given by Eq. (5.8), the right-hand terms of Eq. (5.7) become smaller in comparison to the left-hand terms if one proceeds to larger values of $\bar{\eta}$. A first insight into the behavior of the desired solution at large values of $\bar{\eta}$ is, therefore, obtained if one neglects in the region R_3 the right-hand terms of Eq. (5.7) entirely. Then the differential equation is the same as for a plane flow and the solution can be represented by means of the particular solutions of Eqs. (4.4) with negative subscripts (if the particular solutions of Eqs. (4.4) with positive subscripts were admitted, the expression φ_{-1} would not prevail for large values of $\bar{\eta}$). The solution will then have the form

$$\bar{\varphi} = c(y) \cdot \varphi_{-1}(\bar{\eta}, \bar{\theta}) + d^0(y) + \sum_{h=0}^{\infty} d^{-4-3h} \cdot \varphi_{-4-3h}(\bar{\eta}, \bar{\theta}) \tag{5.9}$$

Here the coefficients are functions of y. The coefficient $c(y)$ is given by the condition (5.8); it represents a property of the airfoil. All other functions are determined by the flow field as a whole. Ultimately they depend upon the function $c(y)$, which expresses the only boundary condition occurring here.

We have here a strong analogy to Eq. (4.18), which expresses the boundary conditions at a far distance from a profile in plane flow. One difference is that, presently, only the function $c(y)$ occurs, while functions which would correspond to the constants "e" in Eq. (4.18) are zero. It is perhaps unnecessary to mention that the function $d(y)$ depends upon the behavior of the function $c(y)$ along the entire span, not only on the value which $c(y)$ assumes at the cross section $y = \text{const.}$ under consideration. Since the function φ_{-1} is symmetric with respect to the plane $\bar{\theta} = 0$, the entire flow field expressed by Eq. (5.9) will be symmetric. For this reason, no terms $\varphi_{-2.5-3h}$ appear in this equation. The term $d^0(y)$ does not have a counterpart in Eq. (4.18). There it would have been an unessential constant. But here, the term $d^0(y)$ gives a contribution to the velocity component in the y-direction which introduces in the flow equations a coupling between different cross sections $y = \text{const.}$

If the terms of the right-hand side of Eq. (5.7) are taken into account also in R_3, one will expect that the solution can be characterized in a similar manner as previously—i.e., that it is determined by a number of functions $d(y)$ which are given by the flow field as a whole. To show this we try to represent the flow in the form of a development with respect to η.

We start with an expression which is suggested by the solution for a plane flow

$$\bar{\varphi} = c(y)\cdot\varphi_{-1}(\bar{\eta}, \bar{\theta}) + d^0(y) + d^{-4}(y)\cdot\varphi_{-4}(\bar{\eta}, \bar{\theta}) \quad (5.10)$$

The terms in this equation satisfy the left-hand side of Eq. (5.7). They are products of powers of η, of functions of y, and of functions of ζ. If they are inserted into the right-hand side of Eq. (5.7), terms of the same form will arise, and, thus, it is possible—at least formally—to find correction terms for the expression on the right-hand side.

Let us consider the term of the right-hand side which appears with the highest power of η. Using Eq. (5.10) one finds

$$\frac{d^2[d^0(y)]}{dy^2}\,(\varphi_{-1,\bar{\eta}\bar{\eta}}\cdot\varphi_{-1,\bar{\theta}\bar{\theta}} - \varphi^2_{-1,\bar{\eta}\theta}) \sim \frac{d^2[d^0(y)]}{dy^2}\cdot\eta^{-7}\cdot\text{function of }\zeta$$

Hence, it follows that the expression which corrects for this term will have the form

$$\frac{d^2[d^0(y)]}{dy^2}\cdot\eta^{-5}m(\zeta) \quad (5.11)$$

The function $m(\zeta)$ is found as solution of an inhomogeneous linear differential equation of the second order; the power of η which appears in Eq. (5.11) appears as a parameter on the left-hand side of this equation. The boundary conditions imposed on m are the same as those imposed previously on the function f—i.e., we require that $m(\zeta)$ and all its derivatives are bounded for $\zeta = 1$. The procedure described is typical for the determination of subsequent terms in the development of the solution in powers of η. The only expressions fulfilling the corresponding *homogeneous* equation and the boundary conditions prescribed are the functions f listed in Eq. (4.4). Their coefficients $d(y)$ are the only expressions which are not directly determined by the differential equation, but they are determined by the flow field as a whole, which is dependent upon $c(y)$. The similarity between this result and the one obtained when the right-hand terms of Eq. (5.7) were neglected in the region R_3 is evident.

The first terms of the solution $\bar{\varphi}$ are, thus, given by

$$\bar{\varphi} = c(y)\varphi_{-1}(\bar{\eta}, \bar{\theta}) + d^0(y) + d^{-4}(y)\varphi_{-4}(\bar{\eta}, \bar{\theta}) + [d^2(d^0)/dy^2]\eta^{-5}m(\zeta) \quad (5.12)$$

The derivation of the last equation seems to be quite similar to the development attempted at the beginning of this section. But the present representation is constructed for a limited region only; thus, the convergence difficulties, which were the cause of the failure of the first procedure, do not occur. In the present result the functions $d(y)$ appear, and their determination requires the solution of the boundary value problem for the region R_2. Naturally, this is an extremely difficult problem. For the discussion of the essential trends of our problem, it is sufficient to know that the solution can be written in the form of Eq. (5.12), and that the coefficients $d(y)$ are, in principle, determined by the function $c(y)$.

Now it can be shown in which sense Eq. (5.12) can be considered as a solution of the flow problem for $t \to 0$. Actually we have two representations which are supposed to be valid for $t \to 0$—i.e., Eq. (5.1) and Eq. (5.12). The first is supposedly valid close to the profile, the second at a large distance from the profile. It will now be shown that, after one introduces a slight correction into Eq. (5.1), there is a region in-between in which these expressions agree in the limiting case $t \to 0$. A region suitable for this purpose may be bounded by the surfaces $\eta = t^{0.24}f_1(y, \zeta)$ and $\eta = t^{0.24}f_2(y, \zeta)$.

Now Eq. (5.1) is rewritten, using Eqs. (4.5) and (4.6) in such a manner that η occurs always in the combination $\eta\cdot t^{-0.24}$

$$\varphi = c(y)\cdot t^{0.76}(\eta\cdot t^{-0.24})^{-1}f^s(\zeta, -1) + a^1(y)\cdot t^{1.24}(\eta\cdot t^{-0.24})f^s(\zeta, 1) + \ldots \quad (5.13)$$

Using Eqs. (5.5) and (5.6), one obtains similarly for Eq. (5.12)

$$\varphi = c(y)t^{0.76}(\eta\cdot t^{-0.24})^{-1}f^s(\zeta, -1) + t^{0.6}d^0(y) + d^{-4}t^{1.24}(\eta\cdot t^{-0.24})^{-4}f^s(\zeta, -4) \quad (5.14)$$

The two expressions agree for sufficiently small values of t if one adds in Eq. (5.13) the term $t^{0.6}\,d_0(y)$, which, for small values of t, is without influence in the fulfill-

ment of the boundary conditions at the airfoil. The region in which this transition from one solution to the other one can be made moves with decreasing values of t to smaller and smaller values of η. Thus, the surface S_2 which is fixed in the η, θ, y-space is not suitable to make the transition from one solution to the other. This is obvious from Eq. (5.1) together with Eq. (4.5); the relative magnitude of the solution ω_{-1} in comparison with φ_{-1} does not change in dependence upon t at a fixed point of the η, θ, y-space.

Naturally, if $t \neq 0$, additional terms will occur in the solution. In the region R_1, these additional terms are given by the solutions (4.9), which leave the surface of the body unchanged, and by correction terms which take into account the spatial terms in the flow differential equation.

For the region R_2, correction terms are obtained by a linearization of the flow dffierential Eq. (5.7) in the vicinity of the solution for $t = 0$. Again it is possible to express particular solutions obtained for the linearized equation in the form of a development with respect to η^{-1}.

To obtain the form of such a development, we write down the linearized differential Eq. (5.7) but retain in it only those terms of the right-hand side which are predominant for large values of η. Denoting the deviation from the solution for $t = 0$ by χ, one finds

$$\chi_{\bar\eta\bar\eta} - \bar\eta\chi_{\bar\theta\bar\theta} = [d^2(d^0)/dy^2]\cdot c(y)[\varphi_{-1;\bar\eta\bar\eta}\,\chi_{\bar\theta\bar\theta} + \varphi_{-1;\bar\theta\bar\theta}\cdot\chi_{\bar\eta\bar\eta} - 2\varphi_{-1;\bar\eta\bar\theta}\cdot\chi_{\bar\eta\bar\theta}]$$

Solutions of this equation have, in principle, the form

$$\chi_{-1} = e^{-1}(y)\varphi_{-1}(\bar\eta, \bar\theta) + d_{-1}{}^0(y) + d_{-1}{}^{-4}(y)\varphi_{-4}(\bar\eta, \bar\theta) + [d^2(d^0)/dy^2]\cdot c(y)\bar\eta^{-5}m_{-1}(\zeta) \quad (5.15)$$

$$\chi_{1+h} = e^{1+h}(y)\varphi_{1+h}(\bar\eta, \bar\theta) + d_{1+h}{}^0(y) + d_{1+h}{}^{-4}(y)\varphi_{-4}(\bar\eta, \bar\theta) + [d^2(d^0)/dy^2]\cdot c(y)\bar\eta^{-h-3}m_{1+h}(\zeta) \quad (5.16)$$

$$\chi_{0.5+h} = e^{0.5+h}(y)\,\varphi_{0.5+h}(\bar\eta, \bar\theta) + d_{0.5+h}{}^{-2.5}\varphi_{-2.5}(\bar\eta, \bar\theta) + [d^2(d^0)/dy^2]\cdot c(y)\cdot\bar\eta^{h-3.5}m_{0.5+h}(\zeta) \quad (5.17)$$

Here the coefficients $e(y)$ are arbitrary; they correspond to the constants e in Eq. (4.18), which express properties of the profile. The coefficients d would occur in this solution, even if, in a certain region R_3, the spatial terms of the differential equation were neglected; they are not directly determined by the differential equation but by the solution of the linearized boundary value problem as a whole. This boundary value problem must fulfill the boundary condition that for large values of $\bar\eta$ the function χ is represented by the first term in the Eqs. (5.15), (5.16), or (5.17). Thus the $d(y)$ depend in principle upon the $e(y)$. The functions m arise from the differential equation by a systematic development with respect to $\bar\eta$. Their subscripts correspond to the subscript of χ in whose representation the m's occur. Since the flow for $t = 0$ is symmetric with respect to $\theta = 0$, certain symmetry conditions will be found in these particular solutions—i.e., if the first function in the above expressions is symmetric, the entire expression is symmetric; if the first function is antisymmetric, the entire expression is antisymmetric.

The boundary conditions at a far distance from the body are fulfilled if the flow field is represented by a superposition of the particular solutions of Eqs. (5.15), (5.16), and (5.17) to the basic flow Eq. (5.9). This system of particular solutions can be expected to be complete because of its close relation to similar solutions in the plane flow. One will remember that the functions $e(y)$ are arbitrary.

(6) The Airfoil with a Finite Aspect Ratio

Up to now we obtained two expressions for $t = 0$, one valid in the vicinity of the profile, the other at a large distance from it. There is a region in which the prevalent terms of these expressions agree. For a finite aspect ratio, one must superimpose on each of these expressions further terms such that a smooth transition from one representation to the other is achieved also for higher powers of t.

The comparison of the two solutions will be carried out along the surface S_2. Along this surface, which is fixed in the η, θ, y-space, the solution for the vicinity of the airfoil will not reduce for $t = 0$ to its first terms; thus, by carrying out the matching along this surface, we are likely to take into account terms which are unnecessary for an approximation of a low order in t. But S_2 is practical for the estimation of the spatial terms in the differential Eq. (3.9).

The difference between the solutions found for $t = 0$ in the regions R_1 and R_2 occurs because of the function ω_{-1} in R_1, because of the spatial terms in R_1, and because of the function φ_{-4} and all subsequent terms which occur in the representation for the region R_2 given in Eq. (5.12).

In correcting for this difference, the spatial terms will first be disregarded entirely—i.e., we shall try to construct a solution with a smooth transition through S_2 using only those particular solutions which would occur in a plane flow. Afterwards the influence of the spatial terms will be taken into account.

Omitting the spatial terms, one has, as basic flow in R_1,

$$\varphi = t\cdot\varphi_{-1}{}^* + t^{0.6}d^0(y) = tc(y)\varphi_{-1}(\eta, \theta) + t\omega_{-1}(\eta, \theta) + t^{0.6}d^0(y) \quad (6.1)$$

and, as basic flow in R_2 [as found from Eq. (5.9) in conjunction with Eq. (5.5) and Eq. (5.6)],

$$\varphi = t\cdot c(y)\varphi_{-1}(\eta, \theta) + t^{0.6}\,d^0\,(y) + \sum_{h=0}^{\infty} d^{-4-3h}t^{2.2+1.2h}\varphi_{-4-3h}(\eta, \theta) \quad (6.2)$$

The function ω_{-1} can be developed according to Eq. (4.6); then one has, in the region R_1,

$$\varphi = t\cdot c(y)\varphi_{-1}(\eta, \theta) + t^{0.6}d^0(y) + \sum_{h=0}^{\infty} a^{0.5+0.5h}(y)\,\varphi_{0.5+0.5h}(\eta, \theta) \quad (6.3)$$

Here the a's are considered as functions of y since the profile will in general change in the y direction. To

correct for the infinite sum in Eq. (6.2), particular solutions are added in the region R_2. For this purpose, functions $\chi_{0.5+0.5h}$ [Eqs. (5.16) and (5.17)] are computed, in which the functions $e^{0.5+0.5h}$ are given by $a(y)^{0.5+0.5h}$ This computation determines the functions d occurring in Eqs. (5.16) and (5.17); they may now be denoted by δ with the same indices as previously. Written in terms of the coordinates η and θ, these particular solutions are given by

$$\chi_{1+h} = t^{-0.4-0.4h} a^{1+h}(y)\varphi_{1+h}(\eta, \theta) + \delta_{1+h}{}^{0}(y) + \sum_k \delta_{1+h}{}^{-4-3k} t^{1.6+1.2k} \varphi_{-4-3k}$$

$$\chi_{0.5+h} = t^{-0.2-0.4h} a^{0.5+h}(y)\varphi_{0.5+h}(\eta, \theta) + \sum_k \delta_{0.5+h}{}^{-2.5-3k} t^{1+1.2k} \varphi_{-2.5-3k}$$

In the region R_2, the following expression is added to Eq. (6.2):

$$t\left[\sum_{h=0}^{\infty} t^{0.2+0.4h}\chi_{0.5+h} + \sum_{h=0}^{\infty} t^{0.4+0.4h}\chi_{1+h}\right] = t\sum_{h=0}^{\infty} a^{0.5+0.5h}\varphi_{0.5+0.5h} + \sum_{h=0}^{\infty} t^{1.4+0.4h}\delta_{1+h}{}^{0}(y) + \sum_{h=0}^{\infty}\sum_{k=0}^{\infty} t^{3+1.2k+0.4h}\delta_{1+h}{}^{-4-3k}(y)\varphi_{-4-3k} + \sum_{h=0}^{\infty}\sum_{k=0}^{\infty} t^{2.2+1.2k+0.4h}\delta_{(1/2)+h}{}^{-2.5-3k}\varphi_{-2.5-3k}$$

The first terms in this expression are obviously equal to the sum in Eq. (6.3). The difference which now exists between the representations in the regions R_1 and R_2 is given by

$$\sum_{h=0}^{\infty} d^{-4-3h} t^{2.2+1.2h}\varphi_{-4-3h}(\eta, \theta) + \sum_{h=0}^{\infty} t^{1.4+0.4h}\delta_{1+h}{}^{0}(y) + \sum_{h=0}^{\infty}\sum_{k=0}^{\infty} t^{3+1.2k+0.4h} \times \delta_{1+h}{}^{-4-3k}(y)\varphi_{-4-3k} + \sum_{h=0}^{\infty}\sum_{k=0}^{\infty} t^{2.2+1.2k+0.4h} \times \delta_{0.5+h}{}^{-2.5-3k}\varphi_{-2.5-3k}$$

In this expression the terms of the lowest orders in t are

$$t^{1.4}\delta_1{}^{0}(y) + t^{2.2}d^{-4}(y)\varphi_{-4} + t^{2.2}\delta_{0.5}{}^{-2.5}\varphi_{-2.5}$$

As a compensation, we add in the region R_1 the expression

$$t^{1.4}\delta_1{}^{0}(y) + t^{2.2}d^{-4}(y)\varphi_{-4}{}^{*} + t^{2.2}\delta_{0.5}{}^{-2.5}\varphi_{-2.5}{}^{*}$$

This addition would, in turn, require a compensation in the region R_2, which would, however, be of a higher power in t. This procedure could be continued. The representation obtained so far is sufficient for the present purpose.

Now the spatial terms must be taken into account. For the determination of the particular Eqs. (5.15), (5.16), and (5.17), a linearization in the vicinity of the expression which gives the basic flow in the region R_2 was carried out; therefore, it is important that the deviation of the actual solution from the basic flow is small in the region considered. As mentioned before, the relative deviation of the two representations for the flow at $t = 0$ is finite along S_2. But it can be made arbitrarily small by choosing S_2 sufficiently close to the y-axis. Thus, the linearization is justified.

The prevalent spatial terms in the region R_2 are those of the basic flow. According to Eq. (5.12), they are of the order $t^{2.6}$ for fixed values of η and θ. The spatial influence in the region R_1 is found as a correction to the plane basic flow given by Eq. (6.1). This correction may be denoted by $\Delta\varphi$. It is determined (in the lowest order in t) by the following differential equation:

$$\Delta\varphi_{\eta\eta} - \eta\Delta\varphi_{\theta\theta} = [d^2(d^0)/dy^2]\cdot t^{2.6}(\varphi_{-1;\,\eta\eta}{}^{*}\varphi_{-1;\,\theta\theta}{}^{*} - \varphi_{-1;\,\eta\theta}{}^{*2})$$

The solution is subject to a homogeneous boundary condition at the surface S_1 which expresses that the surface of the airfoil is not changed by the superposition of the expression $\Delta\varphi$ and another linear homogeneous boundary condition along S_2 whose exact form is unessential. The factor $t^{2.6}$ on the right-hand side of the last equation indicates the order of magnitude of the correction thus obtained.

In general, there will be no smooth transition between the spatial correction terms in the regions R_1 and R_2; the difference along the surface S_2 is of the order $t^{2.6}$. This will account for an additional correction in the region R_1 of this order of magnitude.

According to these considerations, the flow in the vicinity of the profile will have the following form:

$$\varphi = t^{0.6}d_0(y) + t[\varphi_{-1}{}^{*}(\eta, \theta, y) + t^{1.2}d^{-4}(y)\varphi_{-4}{}^{*}(\eta, \theta, y) + t^{1.2}\delta_{0.5}{}^{-2.5}\varphi_{-2.5}{}^{*}(\eta, \theta, y) + t^{1.6}\Delta\bar{\varphi}(\eta, \theta, y) + \ldots] \quad (6.4)$$

In this expression $\Delta\bar{\varphi}$ denotes the influence of the spatial terms in the differential equation.

(7) Discussion

From the last equation the velocity which one obtains in the physical plane can be computed. The first term gives a velocity in the y-directions—it is independent from x and z. The first term in the bracket gives the plane flow over the airfoil sections at the free-stream Mach Number one. All subsequent terms can be considered as a perturbation of this flow. The next two terms are also known from investigations of plane flow patterns. If the body is symmetric, the term $\varphi_{-4}{}^{*}$ gives the change of the velocity distribution which is due to a deviation of the free-stream Mach Number from 1. If the body is unsymmetric, a change of the free-stream Mach Number would express itself by a linear combination of the two terms $\varphi_{-4}{}^{*}$ and $\varphi_{-2.5}{}^{*}$; a change of the angle of attack would express itself by another linear combination of these expressions. Therefore, the influence of the terms $\varphi_{-4}{}^{*}$ and $\varphi_{-2.5}{}^{*}$ in Eq. (6.4) would correspond in a plane flow to a combined change of the free-stream Mach Number and of the angle of attack; they are of the same order of magnitude.

If one computes the pressures along the profile from Bernoulli's equation, the velocity component Φ_x, which

is proportional to η, enters the computation in the first power—the velocity components Φ_y and Φ_4 in the second power. The terms φ_{-4}^* and $\varphi_{-2.5}^*$ give additional velocities at the profile (in comparison with the plane flow at a Mach Number one), which are proportional to $t^{1.2}$; the y-component of the velocity obtained from the term d^0 is proportional to $t^{0.6}$. Thus, their contributions to the pressure changes are of the same order of magnitude; the deviation from a plane flow at a Mach Number can be interpreted in the lowest order of t as a combination of a change of the free-stream Mach Number and a change of the angle and of the pressure level. These changes are proportional to $t^{1.2}$. The spatial terms in the differential equation give an effect proportional to $t^{1.6}$.

The coefficients d^0 and d^{-4} are found from the solution for the basic flow. In this boundary value problem the only given function is $c(y)$. Thus, different airfoils for which the function $c(y)$ is the same will have the same correction coefficients d^0 and d^{-4}. The determination of the coefficient $\delta_{0.5}{}^{-2.5}$ requires the solution of a linearized boundary value problem. In the linearized differential equation the coefficients are given by the basic flow—i.e., ultimately by $c(y)$. The boundary condition imposed to this linearized flow is given by $a^{0.5}(y)$. This function expresses the unsymmetry of the profile. Thus, for two profiles for which $c(y)$ and $a^{0.5}(y)$ are the same, the lowest order correction terms for the pressure distribution are related to each other. It is quite doubtful that one could perform the necessary analytical computations even in the simplest cases, but one might try to verify these effects experimentally.

In the computations the basic flow is determined by the displacement of the model; the unsymmetries of the airfoil appear as a correction. This is in marked contrast to the subsonic flow where the trailing vortices caused by the lift have the predominant effect on the pressure distribution. Incidentally, this effect is proportional to t. In the transonic flow, the determination of the lift corrections without prior knowledge of the displacement of the airfoil is impossible. The trailing vortices do not play a role here, since the flow behind the airfoil is supersonic and is unable to send signals to the airfoil.

(8) The Flat Plate of a Finite Length with an Angle of Attack

A somewhat extreme case is the flat plate at an angle of attack. Although the flat plate does not have a thickness, it gives a displacement in the flow which depends naturally upon the angle of attack. If the angle of attack is fixed, then the changes of the pressure distribution are proportional according to our previous results to t.[1, 2]

By the transonic similarity law, such a flow pattern can be connected to the flow over an airfoil with a different angle of attack. The relative deviation from the plane flow remains the same; if the angle of attack is multiplied with a factor τ and the span is multiplied with a factor τ^{-3}. Choosing τ proportional $t^{-1/3}$ such that the aspect ratio is unchanged while t changes, the deviation from the plane flow becomes proportional to $\theta^{-3.6}$. Accordingly, if the angle of attack tends to zero for a given aspect ratio, the present approach is not applicable—i.e., one comes into the realm of linearized theory.

(9) Conclusions

The present paper does not give the full solution for the problem of an airfoil of a finite aspect ratio at a free-stream Mach Number one. But it establishes the trends for the influence of the aspect ratio. In order to determine the deviation from a plane flow, one must solve two boundary value problems in space—one for which a displacement parameter is given along the span and a second for which the angle of attack (or, more generally speaking, the unsymmetry of the airfoil) is given along the span. For airfoils for which these two quantities are the same, the coefficients which characterize the deviation from the pressure distribution for a plane flow over the airfoils will be the same. The differences in the pressure distribution are the same as those caused in a plane flow by a change of the free-stream Mach Number, a change of the angle of attack, and a lowering of the overall pressure. This last effect is due to the wind component in the direction of the span of the airfoil.

It is quite typical for transonic flow problems that the effect of an angle of attack upon the pressure distribution depends upon the displacement of the model—i.e., a thicker body will have a smaller angle of attack correction for the pressure distribution. But one will remember that for the present investigations even the flat plate at an angle of attack possesses a displacement effect.

The effects of a higher order appear with a power $t^{1.6}$. Their dependence upon the original data is more complex. Since this power of the aspect ratio differs only slightly from the power$^{1.2}$, which gives the corrections of the lowest order, it may be difficult to separate them by experimental means.

References

[1] Guderley, Gottfried, *Singularities at the Sonic Velocity*, Technical Report F-TR-1171-ND, Hq. Air Materiel Command, Wright-Patterson Air Force Base, Dayton, Ohio.

[2] Guderley, Gottfried, *Two Dimensional Flow Patterns with a Free Stream Mach Number Close to One*, AF Technical Report 6343 United States Air Force, Wright Air Development Center, Wright-Patterson Air Force Base, Dayton, Ohio, May, 1951.

[3] Guderley, Gottfried, *On the Development of Solutions of Tricomi's Differential Equation in the Vicinity of the Origin*, (to be published in the Journal of Rational Mechanics and Analysis).

[4] Marschner, Bernard W., *The Flow over a Body in a Choked Wind Tunnel and in a Sonic Free Jet*, Journal of the Aeronautical Sciences, Vol. 23, No. 4, pp. 368–376, April, 1956.

[5] Guderley, Gottfried, *The Flat Plate with an Angle of Attack in a Choked Wind Tunnel*, Journal of the Aeronautical Sciences, Vol. 22, No. 12, pp. 844–866, December, 1955.

Readers' Forum

BRIEF REPORTS of investigations in the aeronautical sciences and discussions of papers published in the JOURNAL are presented in this special department. Entries must be restricted to a maximum of 1,300 words or the equivalent of one JOURNAL page including formulas and illustrations. Publication is completed as soon as possible after receipt of the material. The Editorial Committee does not hold itself responsible for the opinions expressed by the correspondents.

Contents

The Correction of Hot-Wire Readings in a Boundary Layer for Proximity to the Solid Boundary...E. G. RICHARDSON 970

A Principle of Maximum Power for Real Fluids in Steady Motion.....CARLO RIPARBELLI 971

Buckling Loads of Pin-Ended Fluid Columns.M. J. FORRAY 972

On the Nonlinear Buckling of Shallow Spherical Domes.....EDWARD L. REISS 973

On the Evaluation of the Schwarz Function.....YUDELL L. LUKE AND HENRY E. FETTIS 975

A Note on the Effects of Gas Dissociation on Boundary-Layer Heat Transfer.....ROBERT BROMBERG 976

Viscous Flow Along a Flat Plate Moving at High Supersonic Speeds.....Y. H. KUO 977

Comments on Viscous Heating.....H. M. DEGROFF 978

Further Comments on the Decay of a Nonuniform Velocity Distribution.....WILLIAM J. GUMAN 979

A Least Squares Matrix Interpolation of Flexibility Influence Coefficients.....ALFRED F. SCHMITT 980

The Correction of Hot-Wire Readings in a Boundary Layer for Proximity to the Solid Boundary

E. G. Richardson

Physics Department, University of Durham, King's College, Newcastle-on-Tyne, England

April 30, 1956

FREQUENTLY, the investigator in aerodynamics wishes to use the hot-wire anemometer in close proximity to an extensive solid surface in order to explore the flow in the boundary layer of a model. The wire being heated to a temperature above that of the fluid and solid loses heat by convection not only to the stream but also to the cold surface, so that the theory of King[1] is not directly applicable. In a paper by Piercy, Winny, and the writer,[2] King's theory is developed for the case of a hot wire moving through a fluid in a direction perpendicular to its axis and parallel to an infinite plate at the same temperature as the fluid. Experiments are also described in which the wire of radius a was carried round a large brass cylinder at a fixed distance b therefrom while data on heat loss from the wire at different velocities U were obtained. The heat loss H was actually derived from measurements of the increase of electrical power supplied to the wire to maintain its temperature (θ) constant.

Results from this work are presented in the form of Nusselt Number $H/2\pi k\theta$ (k = thermal conductivity) for values of the parameter Uan (n = reciprocal of thermal diffusivity) against b/a on Fig. 1, which shows satisfactory agreement between experiment and theory. The parameter Uan can be expressed, of course, in terms of the product of Reynolds Number for the wire and reciprocal Prandtl Number for the fluid, the latter being 1.35 in air; thus $Uan = (Ua\nu)(c\nu/k)^{-1}$, c being the specific heat per unit volume and ν the kinematic viscosity.

The horizontal lines of Fig. 1 which the curves attain at large values of b/a correspond to the calibration of the hot wire in the free stream. The amount of heat loss which must be subtracted

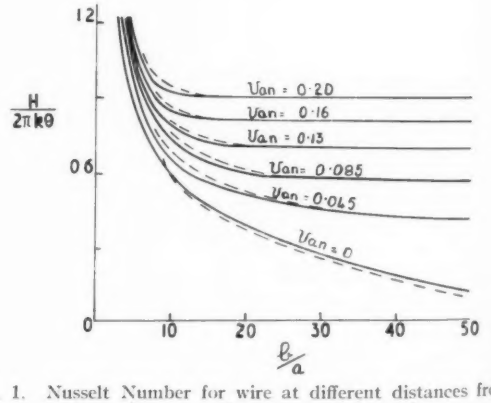

FIG. 1. Nusselt Number for wire at different distances from plate. (—— experiment, – – – – theory.)

from a reading at a given b/a to bring it down to this level is the correction, which must be read off from the curves.

The case for $U = 0$ (the lowest curve of Fig. 1) is a problem in pure conduction, since we neglect "natural" convection, and can readily be solved by the method of images, the solution being formally equivalent to that for the capacitance of a charged cylinder near a flat plate. It is evident that to use *this* curve at all velocities to correct hot-wire measurements in boundary layers, as some previous experimenters have done, can lead to quite erroneous results. Alternatively, the calibration in the *free stream* may be applied to the whole of the results of Fig. 1 to give new curves of "apparent velocity" against distance from the boundary for a wire of given diameter. This has been done, for example, for a wire of diameter 0.001 in. on Fig. 2. The horizontal portions of these curves represent "true velocity"; the broken line delimits the region in which a correction is necessary. A test of the application of these results can be made by traversing a hot wire along the normal to the boundary layer of a flat plate, set edge-on to the wind, and correcting the apparent velocities with the aid of Fig. 2. Such a profile trace is shown in Fig. 3. It will be noted how the convection to the plate sets in quite suddenly, making the apparent velocity rise as the plate is approached but that, on applying the correction, the true velocity falls smoothly and steadily toward zero at the plate itself.

Nowadays, most people using hot wires are interested in the intensity of turbulence in a boundary layer. The indications of the hot wire so used will also be affected by proximity to the solid as can be seen from Fig. 2 where two vertical arrows have been inserted to correspond to a given velocity fluctuation. These arrows represent, in terms of the parameter Uan, the apparent velocity fluctuation which would result—one at a considerable distance from and the other close to the plate. It is clear that the latter is longer and would require correction down to the length of the former. Thus, proximity to the surface exaggerates the indication of a hot wire in respect of turbulence to the same degree that, when it is used for steady flow, it exaggerates the apparent velocity. This has been confirmed by experiments in which the response of a wire oscillating in a *laminar* boundary layer close to a plate has been measured. At a given amplitude, the oscillatory heat loss goes up as the wire approaches the plate.

These results are equally applicable in hydrodynamics; in fact the writer is using them at the present time to correct the readings of hot-wire indicators mounted under ship model hulls towed in the tanks of the British Admiralty Experiment Works. It is to be noted that the thermal diffusivity of water is 0.0014 as against 0.22 for air at laboratory temperature; consequently, the heat loss coefficient for a given wire at a given speed is 150 times greater in water than in air and consequently, even when operating at low speeds in water, one is concerned with high values of Uan to which the correction is not obligatory except very close to the solid surface.

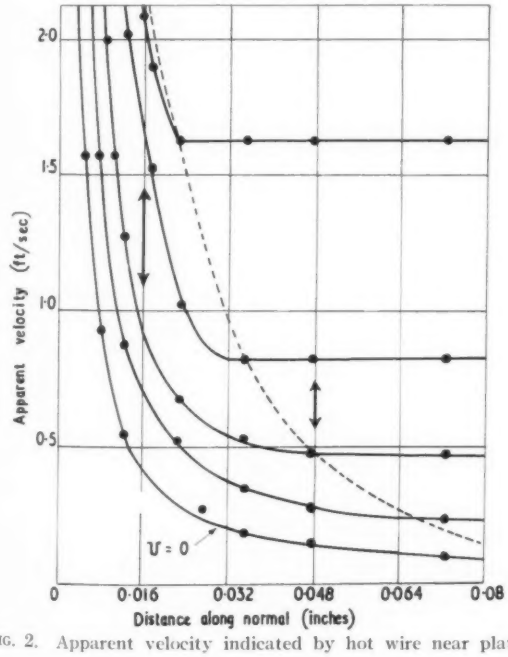

FIG. 2. Apparent velocity indicated by hot wire near plate.

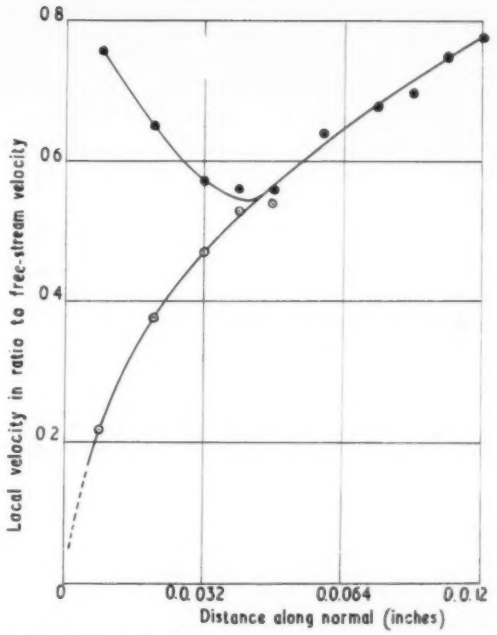

FIG. 3. Correction to indications of hot wire in a boundary layer. (● as measured, ○ as corrected.)

REFERENCES

[1] King, L. V., Phil. Trans. Roy. Soc., Series A, Vol. 124, p. 373, 1914.

[2] Piercy, N. A. V., Richardson, E. G., and Winny, H. F., Proc. Phys. Soc., Vol. 69, p. 731, 1956.

A Principle of Maximum Power for Real Fluids in Steady Motion

Carlo Riparbelli

Convair, San Diego, A Division of General Dynamics Corporation

May 7, 1956

REAL INCOMPRESSIBLE FLUIDS in steady subsonic flow are considered. An example would be a river, for which the hydraulic engineer is able to draw a map of the velocity distribution at any section. The indicated velocity is an average over a time interval (sudden small deviations are not considered) and, at any station, is independent of time. Such a flow presents empirical stability because, if disturbed, it returns to its steady configuration when the disturbance is removed. Because of such empirical stability, the velocity distribution must be determined by some maximum or minimum condition of the energy connected with the flow. This can be defined by means of the following analogy.

The relation between the shear stress τ and the velocity gradient dV/dn,

$$\tau = f(dV/dn) \qquad (1)$$

is assumed to be known from the physical properties of the fluid

and the local conditions. It can be different at different points of the fluid body.

An analogy is established between the velocity distribution in the fluid and the displacement distribution in an ideal elastic material deformable in shear but having constant volume. The relation between the shear stress τ and the distortion γ in such an ideal elastic material is assumed as

$$\tau = f(\gamma) \tag{2}$$

in which the function f is the same as in Eq. (1). We will indicate such a material as gelatin, since gelatin offers an example of a material deformable in shear and with constant volume. The boundary conditions are assumed to be the same for the fluid and for the gelatin.

Continuity and equilibrium being satisfied, all the deductions of linear and nonlinear elasticity obtained for such a material find their correspondents in the flow, provided

displacement	is replaced by	*velocity*
distortion	is replaced by	*velocity gradient*
deformation energy	is replaced by	*dissipated power*

Assuming the head pressure distribution in the fluid (and therefore the external load distribution on the gelatin) as given, the principle of minimum potential energy is applied to the gelatin. Virtual displacements compatible with the boundary conditions in the gelatin correspond to virtual velocities in the fluid. Therefore, in the latter, the sum of the dissipated power (positive, corresponding to deformation energy) and of the power input (negative, corresponding to the potential increment of the applied forces) is a minimum for the true distribution of velocities among those compatible with the boundary conditions.

Reversing the signs—the velocity distribution is such that *the power available* (power input minus power dissipated) *is a maximum.*

Conversely—if the velocity distribution at the end sections is imposed, the power available is a minimum.

In the particular case of viscous flow, Eq. (1) is linear, and the analogy with gelatin presenting a linear shear-distortion relation allows the conclusions of linear elasticity to be extended to the flow. For instance, if a propeller at position and direction A causes a velocity V at position and direction B, the same propeller at position and direction B will cause a velocity V at position and direction A (Maxwell's reciprocity theorem).

In the case of turbulent flow, the boundary layer will be represented by a sort of elastic cement having different properties from those of the main body.

The analogy can be extended to composite systems in which an elastic structure at contact with the fluid is deformed by the flow. The fluid is replaced by gelatin while the elastic structure is kept as given. The principle of minimum potential energy is applied to the resulting elastic system. The deformation energy is the sum of the deformation energies of the two parts—structure and gelatin. Coming back to the given fluid-structure system, the previous conclusions are valid provided the deformation energy of the structure is added to the dissipated power *at every time unit.*

The same rule can be generalized to include any form of stored transformable energy, such as elastic or kinetic. The outlined principle of maximum power, written as

$$\delta\left[\frac{\text{power introduced}}{\text{time}} - \frac{\text{power dissipated}}{\text{time}} - \frac{\text{transformable}}{\text{energy}}\right] = 0$$

takes the form of Lagrange's equations applied to the fluid in motion (not to the gelatin). At this point, the restriction of the principle to incompressible fluids can be removed.

The application of this principle to bodies exhibiting viscous plasticity gives reason for Hill's principle and for the Huber-Hencky-Mises plasticity condition.[5,6] In hydraulics, it confirms Belanger's principle of maximum flow.[4]

References

[1] Prandtl, L., *Essentials of Fluid Dynamics*, Chapter III, Hafner Publishing Company, New York.

[2] Minelli, C., *Teoria delle trauri cave diaframmate*, Parte I, Editoriale Aeronautico, Roma, Italy, 1946.

[3] Hill, R., *A Variational Principle of Maximum Plastic Work in Classical Plasticity*, Quart. J. Mech. & Appl. Math., Vol. 1, Pt. 1, pp. 18–28, 1948.

[4] Masoni, U., *Idraulica*, p. 296; Pellerano, Napoli, Italy, 1921.

[5] Mises, R. S., Nachrichten Ges. d. Wiss., Goettingen, p. 582, 1913.

[6] Hencky, H., *New Theory of Plasticity, Strain Hardening, and Creep, and Testing of Inelastic Behavior of Metals*, Trans. ASME, Vol. 1, No. 4, pp. 151–155, APM-55-18, 1933.

Buckling Loads of Pin-Ended Fluid Columns

M. J. Forray

Principal Structures Engineer, *Republic Aviation Corporation, Farmingdale, N.Y.*

May 11, 1956

THE PURPOSE of this report is to present design curves for the determination of the buckling load of fluid columns.

A typical fluid column (Fig. 1) is composed of an actuating cylinder, piston, and piston rod. The fluid column differs from the simple Euler column in three respects: (1) Fluid pressure transmits the axial load over part of the length of the column. (2) The column is stepped—that is, its length is divided into two parts of different moments of inertia. (3) These two parts are not joined together rigidly but are joined in effect by a flexible coupling, consisting of the bearings and oil seals on one side and

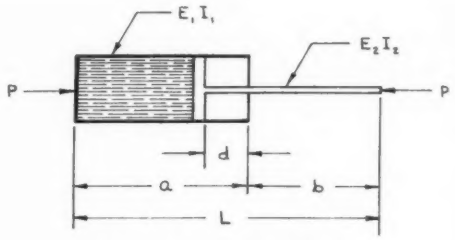

FIG. 1. Hydraulic cylinder.

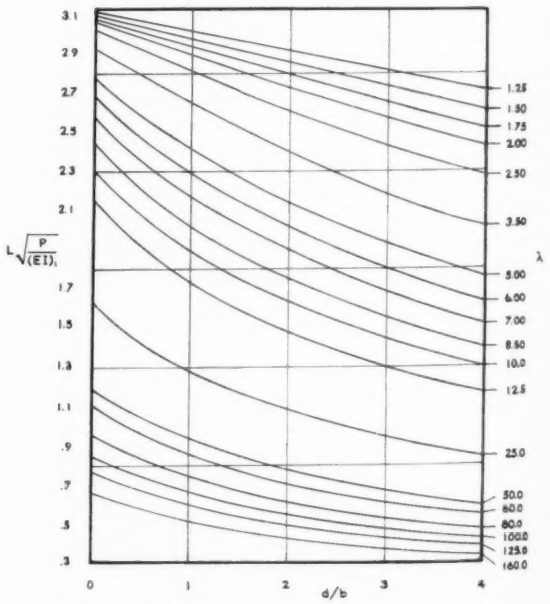

FIG. 2. Buckling load vs. geometry for $a/L = 4/5$.

the piston and oil seals on the other side. The small portion of the rod within the cylinder can deflect between the supporting bearings and piston head independently of the cylinder.

The buckling load for a fluid column may be determined from the expression*

$$P_{CR} = \frac{3LK_1K_2/ab}{K_1\beta_2 + K_2\beta_1 + (K_1K_2/K_3)} \tag{1}$$

where

$$K_1 = E_1I_1/a, \qquad K_2 = E_2I_2/b, \qquad K_3 = E_2I_2/d \tag{2}$$

* Hoblit, F., *Critical Buckling Loads for Hydraulic Cylinders*, Product Engineering, July, 1950.

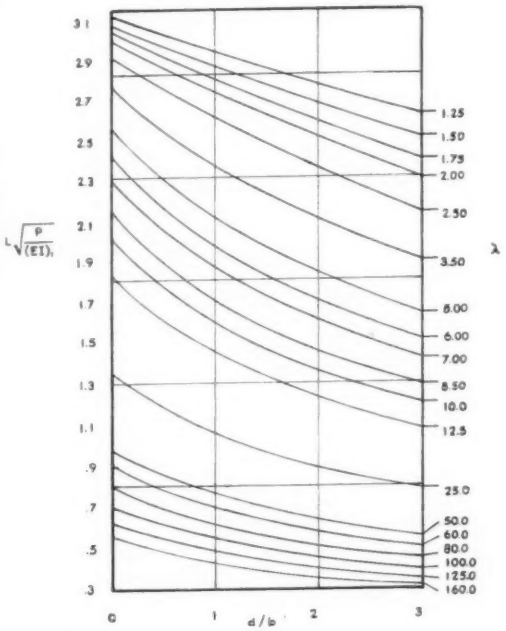

FIG. 3. Buckling load vs. geometry for $a/L = 3/4$.

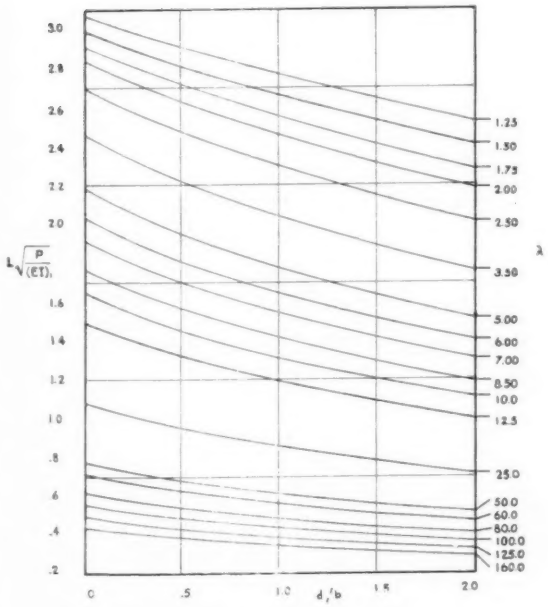

FIG. 4. Buckling load vs. geometry for $a/L = 2/3$.

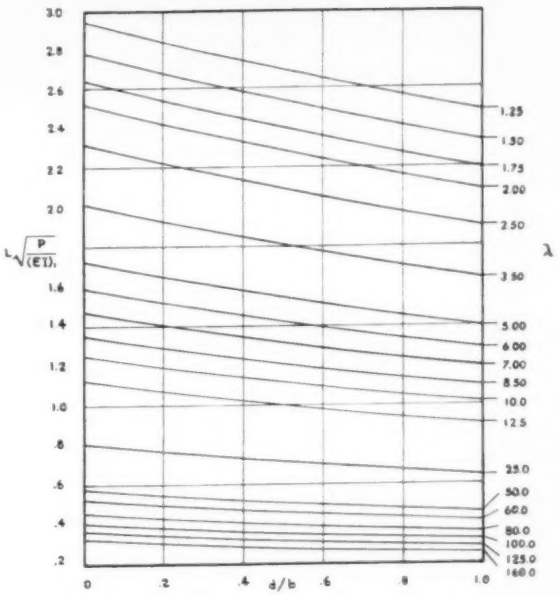

FIG. 5. Buckling load vs. geometry for $a/L = 1/2$.

$$\beta_1 = 3[1 - (a/J_1)\cot(a/J_1)]/(a/J_1)^2 \tag{3a}$$

$$\beta_2 = 3[1 - (b/J_2)\cot(b/J_2)]/(b/J_2)^2 \tag{3b}$$

$$J_1^2 = E_1I_1/P, \qquad J_2^2 = E_2I_2/P \tag{4}$$

Eq. (1) may be solved explicitly for d/b, and the expression is

$$d/b = (3J_2/b)[(1/\sqrt{\lambda})\cot(a/J_2\sqrt{\lambda}) + \cot(b/J_2)] \tag{5}$$

where

$$\lambda = E_1I_1/E_2I_2 \tag{6}$$

Eq. (5) is found to be more convenient than Eq. (1) for calculating the buckling load.

The dimensions a, b, d, L and the curves showing $L\sqrt{P/E_1I_1}$ vs. d/b for given a/L, with $\lambda = E_1I_1/E_2I_2$ as a parameter, are shown in Figs. 2–5.

The analysis leading to Eqs. (1)–(4) is based on the following assumptions: (1) The axis of the applied axial load is coincident with the centroidal axis of the fluid column. (2) The pins at the ends are frictionless. The pins are parallel and remain parallel as the load is applied. (3) The proportional limit is not exceeded—i.e., Hooke's law holds.

On the Nonlinear Buckling of Shallow Spherical Domes*

Edward L. Reiss
Institute of Mathematical Sciences, New York University, New York
May 28, 1956

THE NONLINEAR BUCKLING of thin spherical shells and domes under uniform pressure has received attention in the literature. The original investigations[1, 2, 3] were based upon energy criteria for computing the buckling loads. There have been questions concerning the completeness and validity of some of the theoretical aspects of these investigations.

Recently, Kaplan and Fung[4] presented a careful theoretical and experimental report concerning this topic. They confined their attention to shallow spherical domes. The theoretical determination of the buckling load was based upon a study of the

* This research was done under the auspices of the AEC.

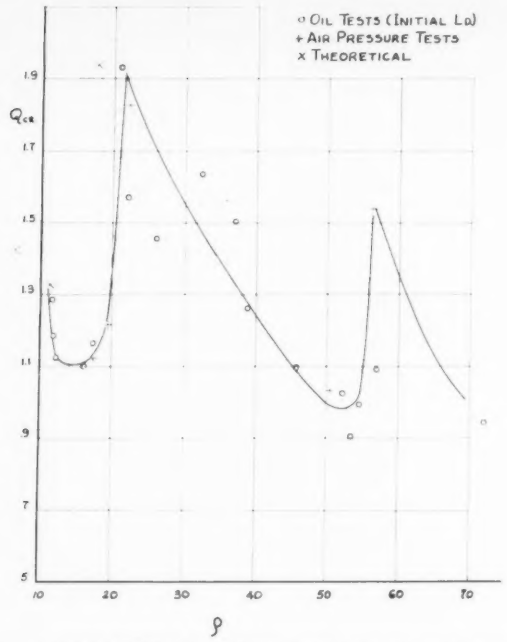

FIG. 1. Initial buckling loads for shallow spherical domes under uniform pressure, from reference 4.

load vs. deflection characteristics of the shell, or, as it is called in reference 4, the "classical criterion." In terms of the parameters employed in reference 4, there appears to be a considerable scatter in the results. Klein[5] attempted to explain this scatter on the basis of initial irregularities.

In an attempt to extend the range of calculations of Kaplan and Fung by solving their equations (or, equivalently, those obtained by Chien[6]) by power-series expansions, slightly different parameters were employed. It is the purpose of this note to present a reinterpretation of the theoretical and experimental results of reference 4 in terms of these new parameters. There then appears to be a very definite and unusual trend in the buckling loads as well as an interesting correlation between the other experimental and the theoretical results.

The new parameters are

$$\rho = C(\beta^2 R/h) \qquad \text{(the geometric parameter)}$$

$$Q = (1/2)\ (CqR^2/Eh^2) \qquad \text{(the loading parameter)}$$

where

$$C = [3(1 - \nu^2)/2]^{1/2}$$

ν is Poisson's ratio, R is the radius of the shell, β is the semi-included angle of the shell, h is half the thickness, E is Young's modulus, and q is the uniform pressure on the surface of the shell taken positive inwards.

These parameters are related to λ, P, and K of reference 4 by

$$\rho = (2)^{-1/2}\ \lambda^2$$

$$Q = 12C(P/\rho^2) = 4CK$$

The theoretical and experimental results for initial buckling loads at $\nu = 0.32$ are shown in Fig. 1. The curves drawn through the experimental points are not calculated from a curve-fitting method. They are included to indicate the apparent trend of the data. The final buckling loads exhibit a similar behavior.

It could be stated that other less drastic curves may be drawn through the experimental points. Based on the following evidence, it is believed that the indicated curves reveal the actual Q_{cr} vs. ρ characteristics. The theoretical calculations of Kaplan and Fung have the same general trend, and the peak points of the curves occur in the region where both experimental measurements and theoretical calculations reveal a change in the mode of deformation (see Figs. 12 and 16 of reference 4). That is, in the region from ρ equals 6 to approximately 20, the shell deforms with a single maximum deflection point located at the center [see Fig. 2(a)]. In the region from ρ equals approximately 20 to approximately 55, the shell deforms with a local minimum deflection point at the center and a local maximum deflection point between the center and the edge [see Fig. 2(b)]. For ρ greater than 55, the shell deforms with two local maximum deflection points, one at the center and the other between the center and edge [see Fig. 2(c)].

Hence, there appears to be an oscillatory behavior between the loading parameter Q_{cr} and the geometric parameter ρ. This behavior changes abruptly with a change in the mode of deflection, the violent peaks occurring at a transition point from one mode of deflection to another. Thus, in terms of these new parameters, there is a greater correlation between the theoretical and experimental results of Kaplan and Fung.

In Fig. 3, the experimental and theoretical results of reference 3 as well as those of reference 4 are presented and interpreted in the light of the previous discussion. It thus appears that Tsien's experimental results may also indicate the peaking behavior of the buckling loads.

These curves are reminiscent of the buckling coefficient vs. aspect-ratio plots encountered in the buckling of elastic plates.[7] ρ may then be considered as a type of aspect ratio, with the various branches of the curve representing modes of buckling.

From the preceding presentation of the results, it could be suspected that the asymptotic behavior as $\rho \to \infty$—i.e., the thickness ratio going to zero or the shell rising into a high arch—may be a complicated phenomenon. Furthermore, in treatments where the form of the deflection is assumed, care must be taken for the range of ρ in which the calculations are applicable.

Further experimental results, particularly for $70 < \rho < 150$, $\rho > 400$, and for ρ in the transition regions would be valuable in deciding on the validity of the interpretation presented in this note.

REFERENCES

[1] von Kármán, T., and Tsien, H. S., *The Buckling of Spherical Shells by External Pressure*, Journal of the Aeronautical Sciences, Vol. 7, No. 2, pp. 43–50, December, 1939.

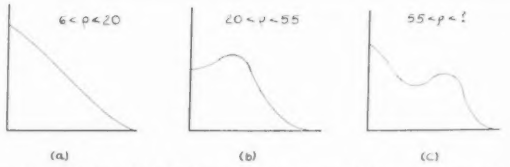

FIG. 2. Modes of deflection vs. horizontal distance from axis of symmetry for various ranges of ρ.

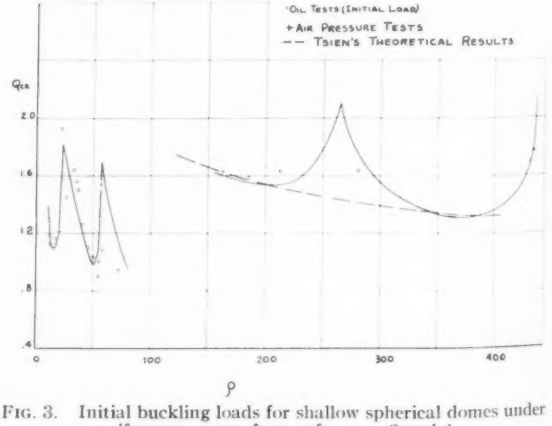

FIG. 3. Initial buckling loads for shallow spherical domes under uniform pressure, from references 3 and 4.

[2] Friedrichs, K. O., *On the Minimum Buckling Load for Spherical Shells*, von Kármán Anniversary Volume, pp. 258–272, Pasadena, Calif., 1941.
[3] Tsien, H. S., *A Theory for the Buckling of Thin Shells*, Journal of the Aeronautical Sciences, Vol. 9, No. 10, pp. 373–384, August, 1942.
[4] Kaplan, A., and Fung, Y. C., *A Nonlinear Theory of Bending and Buckling of Thin Elastic Shallow Spherical Shells*, NACA TN 3212, August, 1954.
[5] Klein, B., *Parameters Predicting the Initial and Final Collapse Pressures of Uniformly Loaded Spherical Shells*, Journal of the Aeronautical Sciences, Vol. 22, No. 1, pp. 69, 70, January, 1955.
[6] Chien, W. Z., *The Intrinsic Theory of Thin Shells and Plates*, Quart. Appl. Math., Vol. 2, pp. 120–135, 1944.
[7] Timoshenko, S., *Theory of Elastic Stability*; McGraw-Hill Book Co., Inc., New York, 1937.

On the Evaluation of the Schwarz Function

Yudell L. Luke* and Henry E. Fettis†
Midwest Research Institute, Kansas City, Mo., and WADC, Wright-Patterson Air Force Base, Ohio, Respectively

June 4, 1956

One of the most important transcendents appearing in both subsonic and supersonic unsteady aerodynamics is the well-known Schwarz function

$$f_m(\lambda, z) = \int_0^z e^{-iu} J_0(\lambda u) u^m \, du; \qquad i = \sqrt{-1} \tag{1}$$

where J_0 is the Bessel function of the first kind. In a previous note, Zartarian and Voss[1] presented a method for computation using power series. In this paper we develop a solution based on the representation of the Bessel function by circular functions. The discussion concludes with an application of the circular function representation to a problem in supersonic panel flutter.

Recently, Fettis[2] showed that the trapezoidal rule could be employed to compute a certain class of transcendents with high accuracy. Later, Luke[3] further explored the problem and found that equally good results could be achieved employing what he calls the modified trapezoidal rule. The latter procedure carries the advantage since for virtually the same accuracy the number of terms required is one less than that for the trapezoidal rule. Both techniques are useful to compute many important functions, and the reader is referred to the original papers for the details. For the problem at hand, using the modified trapezoidal rule, it can be shown that

$$J_0(\lambda u) = (1/q) \sum_{r=1}^{q} \cos(\lambda_r u) + H_q$$
$$\lambda_r = \lambda \cos\left[(2r - 1)/4q\right]\pi \tag{2}$$

where the remainder is given by

$$H_q = -2 \sum_{r=1}^{q} (-)^r J_{4qr}(\lambda u) \tag{3}$$

If x is fixed, the Bessel function $J_n(x)$ quickly approaches zero as n is increased. Indeed, the convergence of Eq. (3) is so rapid that use of the first term only is often sufficient to estimate the remainder. We can evaluate the error either by employing well-known tables or by using the inequality

$$|J_n(x)| \leq \frac{|(x/2)^n|}{n!} e^v \tag{4}$$

where $v \geq 0$ is the imaginary part of x.

Place Eq. (2) in Eq. (1). It can then be deduced that

$$_n(\lambda, z) = \frac{z^{m-1}}{2q} \sum_{r=1}^{q} \left[(A_{mr} + C_{mr}) - i(B_{mr} + D_{mr})\right] + R_q \tag{5}$$

where

$$\left.\begin{aligned} A_{mr} &= z^{1-m} \int_0^z u^m \cos(a_r u)\, du \\ C_{mr} &= z^{1-m} \int_0^z u^m \cos(b_r u)\, du \\ B_{mr} &= z^{1-m} \int_0^z u^m \sin(a_r u)\, du \\ D_{mr} &= z^{1-m} \int_0^z u^m \sin(b_r u)\, du \\ a_r &= 1 + \lambda_r, \qquad b_r = 1 - \lambda_r \end{aligned}\right\} \tag{6}$$

Here R_q is the remainder. Using Eq. (4) and the first term of Eq. (3), a convenient bound is given by

$$|R_q| \leq \frac{|\lambda z|^{4q} |z|^{m+1} e^{\theta}}{2^{4q-1}(4q)!(m + 4q + 1)} \tag{7}$$

where $\theta \geq 0$ is the imaginary part of λz.

In the applications m is an integer. If m is small, Eq. (6) is easily evaluated and the computation of Eq. (5) readily follows. However, m may be as large as 6, and it is pertinent to show how the integrals in Eq. (6) can be found by recursions without serious loss of significant figures. For this purpose it is sufficient to omit the r subscript and to deal with the integrals A_m and B_m. Let $ax = y$ and $D^k = d^k/dy^k$. Then the following relations are easily established:

$$\left.\begin{aligned} A_0 &= \sin y/y \qquad B_0 = (1 - \cos y)/y \\ A_{2k} &= (-)^k D^{2k} A_0 \qquad A_{2k+1} = (-)^k D^{2k+1} B_0 \\ B_{2k} &= (-)^k D^{2k} B_0 \qquad B_{2k+1} = -(-)^k D^{2k+1} A_0 \end{aligned}\right\} \tag{8}$$

$$\left.\begin{aligned} yD^k A_0 + kD^{k-1} A_0 &= D^k \sin y \\ yD^k B_0 + kD^{k-1} B_0 &= -D^k \cos y \qquad k > 0 \end{aligned}\right\} \tag{9}$$

From Eq. (8) and Eq. (9) we find that

$$yA_k = \sin y - kB_{k-1} \qquad yB_k = kA_{k-1} - \cos y \tag{10}$$

If y is large, say $y \geq 1$, once A_0 and B_0 are evaluated this recursive scheme is convenient for the determination of the integrals A_k and B_k. If $y << 1$, it is troublesome to avoid loss of significant figures using Eq. (10). In this event, we proceed as follows. For the largest value of k required, first compute $D^k A_0$ and $D^k B_0$ from their respective power series representations. In this instance the convergence is quite rapid since y is small. Thus A_k and B_k are known. Then use Eq. (10) in the backward form

$$kB_{k-1} = \sin y - yA_k \qquad kA_{k-1} = \cos y + yB_k \tag{11}$$

Knowledge of B_0 and A_0 serves as a check on the backward recurrence, just as prior computation of A_k and B_k can serve as a check when employing the forward recurrence systems, Eq. (10). The above procedure is easily adapted to automatic computation, and should prove useful in a wide variety of aerodynamic problems.

It may be remarked that in Eq. (1) we can replace $J_0(x)$ by $J_m(x)$ and proceed in a similar manner since $J_m(x)$ can also be represented by means of circular functions. The trapezoidal rules are applicable to any of three types of integral representations of $J_n(x)$, and all are important for applications. We omit further details, but see references 2 and 3, and the references given there.

An important virtue of the circular representations for $J_n(x)$ is that it facilitates the solution of many applied problems. For example, in supersonic panel flutter, there arises the integro-differential equation,[4]

$$B(x) \equiv \frac{d^4 z}{dx^4} - W_1 \frac{d^2 z}{dx^2} + W_2 \frac{dz}{dx} + z[ick - W_3 k^2 +$$
$$ikW_3(M^2 - 2)/\beta^2] + W_3 \int_0^x e^{-ik\theta} \frac{d^2 Q}{d\theta^2} z(x - \theta)\, d\theta = 0 \tag{12}$$

where

$$\left.\begin{aligned} Q &= e^{-i(KM-k)\theta} J_0(K\theta) \\ z &= MK/\beta^2 \qquad \beta^2 = M^2 - 1 \end{aligned}\right\} \tag{13}$$

* Head, Mathematical Analysis Section.
† Mathematician, Aeronautical Research Laboratory.

Here M is the Mach number, k is the reduced frequency, and c and the W_r are parameters defined in the reference cited. In the flutter problem, we seek the combination of parameters M, k, etc. so that the solution of Eq. (12) satisfies, for example, the boundary conditions

$$\left.\begin{array}{ll} x = 0 & z = d^2z/dx^2 = 0 \\ x = 2 & z = d^2z/dx^2 = 0 \end{array}\right\} \tag{14}$$

To obtain a solution, assume

$$z = \sum_{k=1}^{N} \mu_k \sin \frac{k\pi x}{2} \tag{15}$$

Put Eq. (15) in Eq. (12). Then use of the appropriate circular representations for the Bessel functions permits ready evaluation of the integral in Eq. (12). If we require

$$\int_0^2 B(x) \sin \frac{m\pi x}{2}\, dx = 0 \qquad m = 1, 2, \ldots, N \tag{16}$$

the problem is reduced to the determination of the eigenvalues of a matrix.

References

[1] Zartarian, G., and Voss, H. M., *On the Evaluation of the Functions $f\lambda(M, \omega)$*, Journal of the Aeronautical Sciences, Vol. 20, No. 11, pp. 781–782, November, 1953.

[2] Fettis, H. E., *Numerical Calculation of Certain Definite Integrals by Poisson's Summation Formula*, MTAC, 9, pp. 85–92, 1953.

[3] Luke, Y. L., *Simple Formulas for the Evaluation of Some Higher Transcendental Functions*, Jour. Math. Phys., Vol. 34, pp. 298–307, 1956.

[4] Luke, Y. L., St. John, A., and Goland, M., *An Exact Solution for Two-Dimensional Panel Flutter at Supersonic Speeds*, Midwest Research Institute Report, March 1956. (This work was done under Contract No. AF 33 (616)-2897, Wright Air Development Center.)

A Note on the Effects of Gas Dissociation on Boundary-Layer Heat Transfer

Robert Bromberg
The Ramo-Wooldridge Corporation, Los Angeles, Calif.

June 5, 1956

Introduction

Under conditions of very high velocity gas flow over a body the gas in the boundary layer may be at least partially dissociated. Questions then arise as to how the details of dissociation and recombination in the boundary layer affect the heat transfer at the wall.

Starting with what is believed to be a correct picture of the energy diffusion process, it is shown that all effects of dissociation can be characterized by a suitable Prandtl modulus and use of the ordinary viscosity of the actual gas together with a modified energy potential. It then follows that the usual method of predicting heat transfer in high velocity flow gives, in general, an upper limit on the heat transfer to the wall.

The results presented here are equivalent to those obtained by Lester Lees.[5] Emphasis here is on presenting a simple picture of the limiting situation for heat transfer.

The Energy Equation in an Imperfect Gas

The energy equation for the boundary layer may be written as

$$(\partial/\partial y)\{(\partial U/\partial y) + \mu[\partial(u^2/2)/\partial y]\} = \rho u(\partial/\partial x)[h + (u^2/2)] + \rho v(\partial/\partial y)[h + (u^2/2)] \tag{1}$$

where ρ is the density, h is the enthalpy per unit mass, U is an energy-transfer potential, and $\partial U/\partial y$ is the energy transferred per unit area and unit time by diffusional processes.

Eq. (1) has been derived in a completely general manner, subject to no restrictions regarding the behavior of the gas—except, of course, that the process is stationary.

Energy Diffusion in an Imperfect Gas

According to kinetic theory, the energy transfer by diffusion (excluding viscous dissipation) is

$$\frac{\partial U}{\partial y} = \frac{5}{2} K\mu \frac{\partial \bar{\epsilon}_t}{\partial y} + \sum_j \rho_j D_j \frac{\partial \bar{\epsilon}_j}{\partial y} \tag{2}$$

where K is a constant, usually near 1; $\bar{\epsilon}_t$ is the average internal energy of translation per unit mass of gas; $\bar{\epsilon}_j$ is the average internal energy per unit mass of gas of a given quantum state, or type of molecule, exclusive of the translational energy; and D_j is a diffusion constant for the particular quantum state, or type of molecule. This expression is a generalization to energy transfer (as contrasted with heat transfer) of the formulation of Meixner.[1,2] Keeping in mind that we are concerned with energy flow across a constant pressure region, Eq. (2) can be written

$$\frac{\partial U}{\partial y} = \frac{5}{2} K \left.\frac{\partial \bar{\epsilon}_t}{\partial T}\right|_P \left.\frac{\partial T}{\partial h}\right|_P \left.\frac{\partial h}{\partial y}\right|_P \mu + \left[\frac{\sum_j \rho_j D_j (\partial \bar{\epsilon}_j/\partial y)}{\overline{\rho D}(\partial \bar{\epsilon}_t/\partial y)}\right] \frac{\overline{\rho D}}{\mu} \left.\frac{\partial \bar{\epsilon}_i}{\partial T}\right|_P \left.\frac{\partial T}{\partial h}\right|_P \left.\frac{\partial h}{\partial y}\right|_P \mu$$

where $\overline{\rho D}$ is an average coefficient (over all quantum states and types of molecules at a point in space) and $\bar{\epsilon}_i$ the average corresponding internal energy (exclusive of translational energy), both so defined that the quantity in brackets is unity. T is the temperature.

Defining $\mu/\overline{\rho D}$ as the Schmidt Number, N_{SC}, we may write

$$\frac{\partial U}{\partial y} = \frac{\left[\frac{5}{2} K N_{SC} \left.\frac{\partial \bar{\epsilon}_t}{\partial T}\right|_P + \left.\frac{\partial \bar{\epsilon}_i}{\partial T}\right|_P\right]}{\left.\frac{\partial h}{\partial T}\right|_P} \frac{\mu}{N_{SC}} \left.\frac{\partial h}{\partial y}\right|_P$$

From the fact that

$$\bar{\epsilon}_i + \bar{\epsilon}_t + PV = h$$

$$\partial \bar{\epsilon}_i/\partial T = (\partial h/\partial T) - (\partial \bar{\epsilon}_t/\partial T) - [\partial(PV)/\partial T]$$

we have

$$\frac{\partial U}{\partial y} = \left[\frac{\left(\frac{5}{2} K N_{SC} - 1\right) \left.\frac{\partial \bar{\epsilon}_t}{\partial T}\right|_P - \left.\frac{\partial (PV)}{\partial T}\right|_P}{\left.\frac{\partial h}{\partial T}\right|_P} + 1\right] \frac{\mu}{N_{SC}} \frac{\partial h}{\partial y} \tag{3}$$

Eq. (3) is completely general. Under almost all conditions, and certainly most cases of practical interest, an excellent approximation to the gas law is

$$PV = ZRT$$

where Z is the number of particles per original particle in the undissociated state. This law postulates no compressibility effects. Then

$$\bar{\epsilon}_t = (3/2)ZRT$$

$$\left.\frac{\partial \bar{\epsilon}_t}{\partial T}\right|_P = \frac{3}{2} \frac{\partial}{\partial T}(ZRT)_P$$

Also

$$\left.\frac{\partial (PV)}{\partial T}\right|_P = \frac{\partial}{\partial T}(ZRT)_P$$

Further, for simplicity, let

$$\left.\frac{\partial h}{\partial T}\right|_P = \bar{\beta} \frac{\partial}{\partial T}(ZRT)_P$$

Substituting in Eq. (3), we obtain

$$\frac{\partial U}{\partial y} = \left[\frac{\left(\frac{5}{2} K N_{SC} - 1\right) \frac{3}{2} - 1}{\bar{\beta}} + 1\right] \frac{\mu}{N_{SC}} \frac{\partial h}{\partial y} = \frac{1}{N_{Pr}} \mu \frac{\partial h}{\partial y}$$

where N_{Pr} is an effective Prandtl modulus.

The variations of K, N_{Sc}, and $\bar{\beta}$ are of interest; let us consider these in turn.

K If the translational energy is transferred by a collisional process which is the same as that transferring momentum, K would be unity. K is probably very close to unity.

N_{Sc} The mechanism of diffusional mass transfer (and thus energy transfer) is similar to, but not exactly the same as, diffusional momentum transfer. Thus, although N_{Sc} is close to one, it is not in general precisely one. For air, N_{Sc} does not, however, deviate greatly from one, probably even with dissociation. See, for example, reference 3. The special case of both $K = 1$ and $N_{Sc} = 1$ corresponds to the "Euken approximation" for the thermal conductivity.[4]

$\bar{\beta}$ For a simple dumbbell molecule at low temperatures, $\bar{\beta}$ is 7/2. At high temperatures $\bar{\beta}$ increases (even neglecting the dissociation interactions) due to the effects of vibrational modes. At very high temperatures the gas becomes monatomic, and if one could completely neglect dissociation interactions (an unlikely situation), would drop to 5/2. It seems reasonable to suppose that $\bar{\beta}$ will generally be greater than 7/2, and if approximate dissociation equilibrium exists, very much greater.

It is clear that we have transferred most of our difficulty to that of determining the viscosity and the Schmidt Number. Also, in this analysis the effects of deviation from equilibrium will appear in N_{Sc} and $\bar{\beta}$.

Effect on Heat Transfer

The heat transfer at the wall, in addition to its dependence in the usual way on Prandtl modulus and viscosity, will be governed by the total enthalpy at the edge of the boundary layer less the gas enthalpy at the wall. This enthalpy difference will range from a maximum, at complete local equilibrium in the boundary layer, to a minimum corresponding to frozen equilibrium (at edge of boundary-layer gas composition). For this minimum case there would be no recombination, even at the wall, and the enthalpy difference would be given by

$$\Delta H = \frac{u_1^2}{2} + \int_{wall}^{1} c_P dT$$

where 1 refers to edge of boundary layer and c_P is the heat capacity of the frozen composition.

We may expect actual heat-transfer rates between these limits. Note that it does not matter where recombination occurs—in the boundary layer or at the wall—the heat transfer is the same (except for the effects of modified transport properties.)

Conclusion

Based on rather general arguments as to the nature of the energy diffusion process in a gas it has been shown that the heat transfer from a dissociated gas is a function primarily of the enthalpy difference across the boundary layer. The maximum heat transfer occurs when dissociation equilibrium is attained at the wall, independently of whether it exists throughout the boundary layer.

An effective Prandtl modulus will exist in such cases, probably ranging from the ordinary room temperature value to about unity, and the viscosity of the gas would be dependent on the point values of the gas composition and its temperature.

References

[1] von Meixner, J., *Zur Theorie der Wärmeleitfähgkeit von Gasen*, Zeitschrift für Naturforschung, Vol. 8a, pp. 69–73, 1953.

[2] Green, M. S., Private Communication, Thermodynamics Section, National Bureau of Standards.

[3] Kennard, E. H., *Kinetic Theory of Gases*, McGraw-Hill Book Company, Inc., New York, 1938.

[4] Euken, A., *Uber das Wärmeleitvermägen, die stezifische Wärme und die innere Reibung der Gase*, Physikalische Zeitschrift, Vol. 14, No. 8, pp. 324–332, April 15, 1913.

[5] Lees, Lester, *Laminar Heat Transfer Over Blunt-Nosed Bodies at Hypersonic Flight Speeds*, Jet Propulsion, Vol. 26, No. 4, pp. 259–268, 274, April, 1956.

Viscous Flow Along a Flat Plate Moving at High Supersonic Speeds*

Y. H. Kuo

Graduate School of Aeronautical Engineering, Cornell University, Ithaca, New York

June 7, 1956

At the Annual Meeting of the Institute of the Aeronautical Sciences, January, 1956, James M. Kendall, Jr., presented a set of highly interesting data on the characteristics of the flow over a flat plate at Mach Number 5.8, obtained from the GALCIT 5- by 5-in. hypersonic wind tunnel.[1] By measuring the impact-pressure profiles and the static pressure along the plate, as previously reported by H. T. Nagamatsu,[2] he was able to deduce the detailed structural features of the flow field. These results reveal definitely that the flow field between the shock and the plate has two distinct regions—the one which is close to the plate is of the boundary-layer type, and the other which is far from the plate is nearly inviscid and of the simple-wave type. This picture is in complete accord with the model that has been used in a theoretical calculation.[3] To substantiate this point of view, it is proposed to make further quantitative comparisons.

Of the results reported by Kendall, the surface pressure was measured with the greatest degree of certainty. As the leading edge of the plate was thin (0.0002 in.), the thickness effects must have been very much reduced, if not entirely eliminated. The surface pressure affords, for this reason, the best chance of a check of the theoretical result. This comparison is made in Fig. 1. The experimental points for three different Reynolds numbers fall very close to the theoretical curve for the parameter $\bar{\chi}$ less than 2 and lie below it beyond that value of $\bar{\chi}$, i.e., very close to the leading edge.

Previously, D. Coles has made a similar measurement at Mach 3.7, which, when compared with theoretical values, was found consistently high.[3] The good agreement now achieved by Kendall's results shows definitely that the leading-edge geometry of Cole's plate caused an additional deflection of the flow, as in the case of a wedge and, therefore, gave rise to a slightly higher pressure.

The divergence of the measurements and calculations beyond $\bar{\chi}$ equal to 2 may well be attributed to the inaccuracies of either the pressures measured or those calculated in the neighborhood of the leading edge (less than 0.08 in. from the leading edge, say). Without further careful measurements nothing definite can be said at this moment.

Based on the impact-pressure profiles, Kendall deduces approximately the flow properties behind the shock, such as ve-

* This study was carried out at the suggestion of Dr. W. R. Sears, Director of the Graduate School of Aeronautical Engineering, with the financial support of the Mechanics Branch, Office of Naval Research. Reproduction in whole or in part is permitted for any purpose of the United States Government.

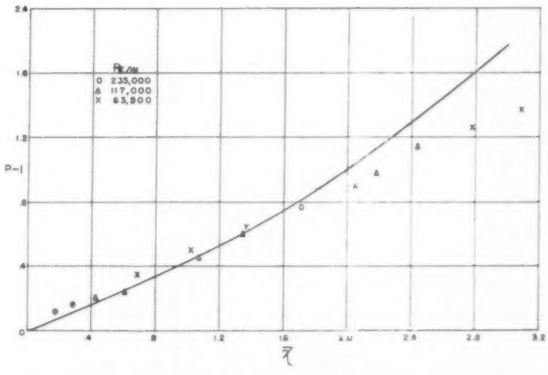

Fig. 1. Pressure distribution along the plate at $M = 5.8$.

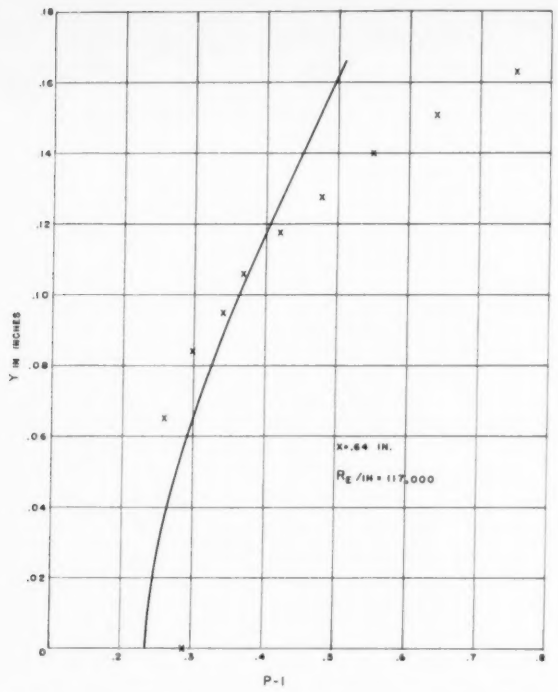

FIG. 2. Pressure distribution in layer between plate and shock.

locity, mass flow, static pressure, etc. Of these quantities, the static-pressure profile is the most interesting. It shows not only the behavior of the pressure inside the boundary layer and in the inviscid field but also the outer edge of the flow field—namely, the shock curve. The comparison with the estimated values at $x = 0.64$ in. is given in Fig. 2. That the measured surface pressure at $x = 0.64$ in. is too high—an anomaly pointed out by Kendall—seems to be borne out by the calculations. On the whole, the agreement in this case is qualitative only.

From the impact-pressure profiles, Kendall also defines the shock curve and the edge of the boundary layer. These are compared with the corresponding calculated ones in Fig. 3. The shock curve has been calculated not by means of the accurate formula but by its asymptotic form and is fitted to the measured value at $x = 0.25$ in. As a result, the agreement for large x is not so good as expected. On the other hand, the calculated boundary-layer edge lies consistently below the estimated curve. This discrepancy can possibly be explained by the fact that the calculation was based on the choice of the similarity parameter to be 7 instead of 8. In any case, the agreement in the boundary-layer curve is quite close.

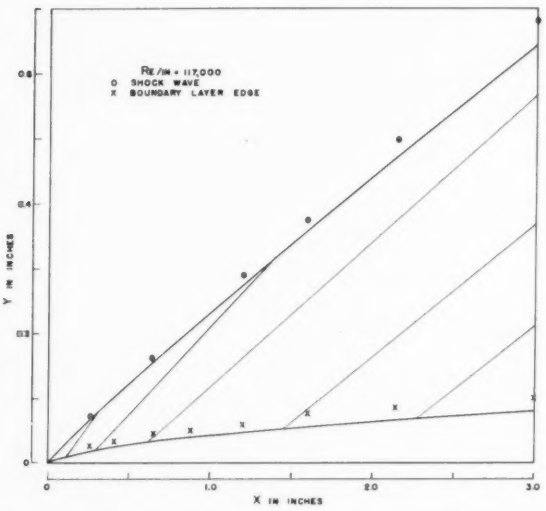

FIG. 3. Shock curve and edge of boundary layer at $M = 5.8$.

REFERENCES

[1] Kendall, Jr., James M., *Experimental investigation of leading edge shock wave-boundary layer interaction at hypersonic speeds*, Hypersonic Project Mem. No. 30, January, 1956.

[2] Nagamatsu, Henry T., *Summary of Recent GALCIT Hypersonic Experimental Investigations*, Journal of the Aeronautical Sciences, Vol. 22, No. 3, pp. 165–172, March, 1955.

[3] Kuo, Y. H., *Viscous Flow Along a Flat Plate Moving at High Supersonic Speeds*, Journal of the Aeronautical Sciences, Vol. 23, No. 2, pp. 125–136, February, 1956.

Comments on Viscous Heating

H. M. DeGroff
Head, School of Aeronautical Engineering, Purdue University, Lafayette, Indiana
June 6, 1956

DR. SYDNEY GOLDSTEIN has communicated with the present author regarding reference 1. The purpose of this note is to provide a short summary of Dr. Goldstein's analysis and to compare his results with those of reference 1.

Dr. Goldstein poses the same problem as given in reference 1. That is, consider the steady laminar flow of a viscous heat conducting perfect gas between two infinite horizontal planes. Let the lower plane at $\eta = 0$ be at rest and let the upper plane at $\eta = 1$ move parallel to itself at unit velocity. Further, assume that both planes are maintained at unit temperature. The equations governing the nondimensional temperature and horizontal velocity variations in the vertical coordinate, η, are then

$$(d/d\eta)[\mu(du/d\eta)] = 0 \tag{1}$$

$$(d/d\eta)[k(dT/d\eta)] + 2\sigma^2\mu(du/d\eta)^2 = 0 \tag{2}$$

where μ is the nondimensional viscosity, k is the nondimensional heat conductivity, $2\sigma^2 = P_r(\gamma - 1)M_0^2$, P_r is the Prandtl Number (assumed constant), γ is the ratio of specific heats (assumed constant), and M_0 is the Mach Number corresponding to velocity and temperature conditions at the moving plane. The boundary conditions are

$$u(0) = 0 \qquad u(1) = 1 \qquad T(0) = T(1) = 1$$

Since P_r is taken as constant,

$$\mu = k$$

Eq. (1) integrates to

$$\mu(du/d\eta) = C_1 \tag{3}$$

where C_1 is a constant, and substitution into Eq. (2) yields

$$(d/d\eta)[\mu(dT/d\eta)] = -2\sigma^2 C_1(d\mu/d\eta) \tag{4}$$

By integration

$$\mu(dT/d\eta) = C_2 - 2\sigma^2 C_1 u \tag{5}$$

where C_2 is a constant. Divide Eq. (5) by Eq. (3).

$$dT/du = C_3 - 2\sigma^2 u \tag{6}$$

where $C_3 = C_2/C_1$.

Upon integration of Eq. (6) and use of the conditions

$$T(u = 0) = 1 \qquad T(u = 1) = 1$$

one obtains the following relation between the temperature and velocity:

$$T = 1 + \sigma^2 u(1 - u) \tag{7}$$

Eq. (7) is independent of the relation between viscosity and temperature.

If we now assume that the viscosity is proportional to the temperature, then $\mu = T$. We make this substitution in Eq. (3), and divide Eq. (3) by Eq. (8) to obtain

$$du/d\eta = C_1/[1 + \sigma^2 u(1 - u)] \tag{8}$$

Then upon integration and substitution of the boundary conditions $u(0) = 0$, $u(1) = 1$, we find that

$$C_1 = 1 + (\sigma^2/6) \tag{9}$$

and the velocity distribution is given by

$$u + (\sigma^2/2)u^2 - (\sigma^2/3)u^3 = [1 + (\sigma^2/6)]\eta \tag{10}$$

Eqs. (7) and (10) serve to completely determine the temperature and velocity profiles. It should be noted that when $M_0 = 0$, $\sigma^2 = 0$, Eq. (10) reduces to the classical Couette result, $u = \eta$. Furthermore, it is clearly evident that an inflection in the velocity profile occurs at $\eta = 1/2$, $u = 1/2$.

Unless the (dimensional) distance, h, between the planes is so large that gh/a_0^2 is not small, where a_0 is the velocity of sound at the temperature of the planes, the pressure between the planes is almost constant. If p_0 and ρ_0 are the pressure and density at the lower plane, and $p_0 p$, $\rho_0 \rho$ the pressure and density at any point between the planes,

$$dp/d\eta = (-gh\rho_0\rho)/p_0$$

Divide by Eq. (3) with $\mu = T$. Also divide by p, use $p/\rho T = 1$, $a_0^2 = \gamma p_0/\rho_0$, and the value of C_1 in Eq. (9). The resulting equation is

$$(1/p)(dp/du) = -cu$$

with the integral

$$p = e^{-cu}$$

since

$$p = 1 \quad \text{at} \quad u = 0$$

where

$$C = \gamma gh/a_0^2[1 + (\sigma^2/6)]$$

The method used is an application of Illingsworth's method[2] to a particular case, and the results may be obtained from his general equations. The results for this particular case were mentioned by Dr. Goldstein in a lecture at the International Congress of Mathematicians, Amsterdam, 1954.

That the results of reference 1 agree with Dr. Goldstein's analysis can be seen as follows. The reference gave the mid-channel temperature, T_m, as

$$(T_m - 1)^{2/2} + (3/2)(T_m - 1)^{1/2} - (3\sigma C_1/4) = 0 \tag{11}$$

Now since $u(\eta = 1/2) = 1/2$, Eq. (7) gives $T_m - 1 = \sigma^2/4$. Substituting this result into Eq. (11) one finds that $C_1 = 1 + (\sigma^2/6)$ which agrees with Dr. Goldstein's findings. Furthermore, if these results are introduced into the analysis of reference 1, the temperature profile can be expressed by

$$\{1 - [4(T - 1)/\sigma^2]\}^{1/2}\{1 + [(1/3)(T - 1)]/[1 + (\sigma^2/6)]\} = |1 - 2\eta| \tag{12}$$

Hence, Eqs. (10) and (12) give the velocity and temperature profiles in explicit form.

It should also be noted that the above results show that the conclusion drawn in reference 1 that variable viscosity and heat conductivity increase the skin friction to a lesser extent than the heat transfer is erroneous. This can be seen as follows. In the case of constant viscosity and heat conductivity, the skin friction and heat transfer at the fixed plane are given by

$$\mu(du/d\eta) = 1 \qquad k(dT/d\eta) = \sigma^2 \tag{13}$$

If, on the other hand, the viscosity and heat conductivity are both linearly dependent upon the temperature,

$$\left.\begin{aligned} \mu(du/d\eta) &= 1 + (\sigma^2/6) \\ k(dT/d\eta) &= \sigma^2[1 + (\sigma^2/6)] \end{aligned}\right\} \tag{14}$$

Hence, the ratio of skin friction to heat transfer, evaluated at the fixed plane, is the same in both cases.

The author wishes to express his deep appreciation to Dr. Goldstein for the privilege of communicating the above analysis. Acknowledgment is also due to Dr. Stephen Malsen, Lewis Flight Propulsion Laboratory, NACA, for some very informative comments on the problem of viscous heating.

References

[1] DeGroff, H. M., *On Viscous Heating*, Journal of the Aeronautical Sciences, Vol. 23, No. 4, p. 395, April, 1956.

[2] Illingsworth, C. R., *Some Solutions of the Equations of Flow of a Viscous, Compressible Fluid*, Cambridge Philosophical Society Proceedings, Vol. 46, p. 469, 1950.

Further Comments on the Decay of a Nonuniform Velocity Distribution

William J. Guman
Assistant Professor, Department of Aeronautical Engineering, Rensselaer Polytechnic Institute, Troy, N.Y.
June 21, 1956

In an earlier note[1] the decay of a nonuniform velocity distribution in a constant area duct was treated by making use of a parameter η defined as $(\bar{u})^2/\overline{u^2}$. An examination of the same problem, but including area changes, external energy transfer and body forces, friction forces, etc., shows that from a qualitative point of view it is more convenient to use the kinetic energy carried by the velocity nonuniformity as a measure of the nonuniformity. Using the technique of influence coefficients introduced by Shapiro and Hawthorne,[2] one can obtain following relations:

$$\frac{d\bar{u}}{\bar{u}} = \frac{1}{M^2-1}\left[\frac{dA}{A} + \frac{dE}{2gC_pT} - \frac{dQ}{C_pT} + \frac{dF}{pA}\right]$$

$$\frac{dM^2}{M^2} = \frac{2\left[1 + \dfrac{\gamma-1}{2}M^2\right]}{M^2-1}\left[\frac{dA}{A} + \frac{dF}{pA}\right] + \frac{\gamma M^2+1}{M^2-1}\left[\frac{dE}{2gC_pT} - \frac{dQ}{C_pT}\right]$$

$$\frac{dT}{T} = -\frac{(\gamma-1)M^2}{M^2-1}\left[\frac{dA}{A} + \frac{dF}{pA}\right] - \frac{\gamma M^2-1}{M^2-1}\left[\frac{dE}{2gC_pT} - \frac{dQ}{C_pT}\right]$$

$$\frac{dp}{p} = \frac{-\gamma M^2}{M^2-1}\left[\frac{dA}{A} + \frac{dE}{2gC_pT} - \frac{dQ}{C_pT}\right] - \frac{1+(\gamma-1)M^2}{M^2-1}\frac{dF}{pA}$$

$$\frac{d\rho}{\rho} = -\frac{M^2}{M^2-1}\frac{dA}{A} - \frac{1}{M^2-1}\left[\frac{dE}{2gC_pT} - \frac{dQ}{C_pT} + \frac{dF}{pA}\right]$$

$$\frac{ds}{C_p} = -\frac{dE}{2gC_pT} + \frac{dQ}{C_pT} - \frac{\gamma-1}{\gamma}\frac{dF}{pA}$$

In these $\bar{u}$ denotes the velocity, p, ρ, and T the pressure, density, and temperature, respectively (the latter three are assumed to be uniform at each section of the flow). The Mach Number M is defined as $M = (\bar{u})/\sqrt{\gamma gRT}$. The term F represents the component of all body forces, etc., assumed positive in the direction of flow. The energy carried by the velocity nonuniformity is proportional to E where E is defined as $E = \overline{u^2} - (\bar{u})^2$, and where

$$\overline{u^2} = \frac{1}{m}\int_m u^2\,dm \qquad \bar{u} = \frac{1}{m}\int_m u\,dm$$

In these u is the local instantaneous velocity, m the mass flow rate with $dm = \rho u dA$. External energy transfer is denoted by Q. The entropy is represented by s.

From the relations presented it can be seen that in the presence of a velocity nonuniformity, body forces, external energy exchange, and area changes affect all flow parameters in the same manner as they affect a perfectly uniform flow. Since the coefficient of the nonuniformity term is the negative of the coefficient

of the external energy transfer term, the effect of a change in the nonuniformity affects the flow parameters in a manner analogous to external energy addition, but differing in the sign. This is because the decay of a velocity nonuniformity implies a decrease in the energy associated with the nonuniformity, and, thus, this is analogous to an increase in the external energy transferred to the flow.

It is also of interest to note that $E/\gamma gRT$ is equivalent to a Mach Number. This Mach Number, being equal to zero for a perfectly uniform flow, may be defined as the Mach Number of the nonuniformity.

References

[1] Guman, W. J., *On the Decay of a Flow Nonuniformity*, Journal of the Aeronautical Sciences, Readers' Forum, Vol. 22, No. 12, p. 869, December, 1955.

[2] Shapiro, A. H., and Hawthorne, W. R., *The Mechanics and Thermodynamics of Steady One-Dimensional Gas Flow*, Journal of Applied Mechanics, Vol. 14, pp. A-317–A-336, December, 1947.

A Least Squares Matrix Interpolation of Flexibility Influence Coefficients

Alfred F. Schmitt
Ryan Aeronautical Company, San Diego, Calif.
June 12, 1956

Introduction

In aeroelastic investigations of thin low aspect ratio wings, it is frequently desired to employ structural influence coefficients relating loads and deflections over large nets of points. Since structural information is not often directly available in such detail, it is necessary to formulate a scheme which will permit interpolation from a structural net of points (of modest size) to a larger aerodynamic net, at which aerodynamic forces are to act, and very often to still another net of control points, at which deflections and flow directions are to be matched. Application of the station function method,[1] while leading to such an interpolation, leaves much to be desired in terms of routine machine adaptation.

It is the purpose of this note to present a matrix interpolation formula, based upon a weighted least squares curve fitting procedure,[2] which is readily programmed for automatic machine computation and which is both accurate and flexible enough to handle interpolations between widely varying net sizes.

Analysis

Assume the flexibility influence coefficients are available over a net of points (p, q) here called the *structural net:* let these be C_{pq}. It is desired to relate forces on the (p, q) net to deflections on another net (k, l), called the *aerodynamic net.*

Consider one column of C_{pq}. This column describes the deformed shape of the wing resulting from application of a unit load to point q. Since an elastic curve varies continuously, we can approximate this deflection mode by a linear combination of preselected functions $E_i\,(x, y)$. Thus,

$$E_{pi}a_i \cong C_p \tag{1}$$

Here, E_{pi} is function $E_i\,(x, y)$ evaluated for the coordinate locations of point p. The a_i are undetermined coefficients. By the method of weighted least squares[2] the error $v_p = E_{pi}a_i - C_p$ is a minimum when*

$$E_{jq}W_{qp}v_p = 0$$

where W_{qp} is a diagonal matrix of weighting factors. Hence, we have

$$E_{jq}W_{qp}v_p = E_{jq}W_{qp}E_{pi}a_i - E_{jq}W_{qp}C_p = 0$$

Solving, $$a_i = T_{ij}E_{jq}W_{qp}C_p \tag{2}$$

where $$T_{ij} = (E_{jq}W_{qp}E_{pi})^{-1} \tag{3}$$

Now using the coefficients a_i from Eq. (2), the deflections at points k in this deformation mode are written as [cf. Eq. (1)]

$$C_k = E_{ki}a_i = E_{ki}T_{ij}E_{jq}W_{qp}C_p$$

Since these are deflections at points k due to a load at point q, the desired interpolation equation becomes

$$C_{kq} = E_{ki}T_{ij}E_{jq}W_{qp}C_{pq} \tag{4}$$

In the same manner, if there exists a third net of points (m, n), such as the control points of an aeroelastic problem, one has

$$C_{mq} = E_{mi}T_{ij}E_{jq}W_{qp}C_{pq} \tag{5}$$

Since, from physical reasoning, we can write

$$C_{mk} = C_{mq}C_{pq}^{-1}C_{pk}$$

then, substituting from Eqs. (4) and (5), we get

$$C_{mk} = E_{mi}T_{ij}E_{jq}W_{qp}C_{pq}W_{qp}E_{pj}T_{ji}E_{ik} \tag{6}$$

Eq. (6) is the desired end result—it relates the deflections at control points (m, n) to loads at the *aerodynamic net* (k, l) when initially structural data were available for only the structural net (p, q). It will be noted that the matrix triple products immediately to either side of C_{pq} are the transpose of each other.

In the application of the method it is necessary to use care in selecting the functions $E_i(x, y)$ and the factors W_{qp}, since Eq. (3) calls for an inversion of the triple product $E_{jq}W_{qp}E_{pi}$. It is desirable that this matrix be well conditioned if the inverse is to be formed accurately. By observing that the triple product $E_{jq}W_{qp}E_{pi}$ is essentially a numerical evaluation of the integral $\int E_jE_i\,dW$, it is seen that use of functions $E_i(x, y)$, having weighted orthogonality, would lead to a very well conditioned matrix. Use of the normal free vibration modes of the wing would be ideal for this purpose. Unfortunately, simple analytic expressions are not readily available for such modes on most low aspect ratio wings.

It has been the writer's experience that product combinations of the normal modes of a uniform cantilever beam[3] provide very satisfactory functions for plate-like wing surfaces. Thus, for example, if the first three normal modes of such a beam are φ_1, φ_2, and φ_3, then for a delta wing, with origin of coordinates at the apex, one might use

$$\begin{aligned} E_1(x, y) &= \varphi_1(x)\cdot\varphi_1(y) \\ E_2(x, y) &= \varphi_1(x)\cdot\varphi_2(y) \\ E_3(x, y) &= \varphi_1(x)\cdot\varphi_3(y) \\ E_4(x, y) &= \varphi_2(x)\cdot\varphi_1(y) \end{aligned}$$

. . .

etc.

For the weighting factors W_{qp}, the areas surrounding each point (p, q) may be used, the sum of the W_{qp} being the total wing area.

With such choices for the $E_i(x, y)$ and W_{qp}, the lion's share of the work of solving Eq. (6) may be preprogrammed for a digital computer such that the solution for a specific wing problem is quickly accomplished.

References

[1] Rauscher, M., *Station Functions and Air Density Variations in Flutter Analysis*, Journal of the Aeronautical Sciences, Vol. 16, pp. 345–353, June, 1949.

[2] Scarborough, J. B., *Numerical Mathematical Analysis*, Second Ed., pp. 451–463; The Johns Hopkins Press, Baltimore, Md., 1950.

[3] Young, Dana, and Felger, R. P., Jr., *Tables of Characteristic Functions Representing Normal Modes of Vibration of a Beam*, Univ. of Texas Publication No. 4913, 1949.
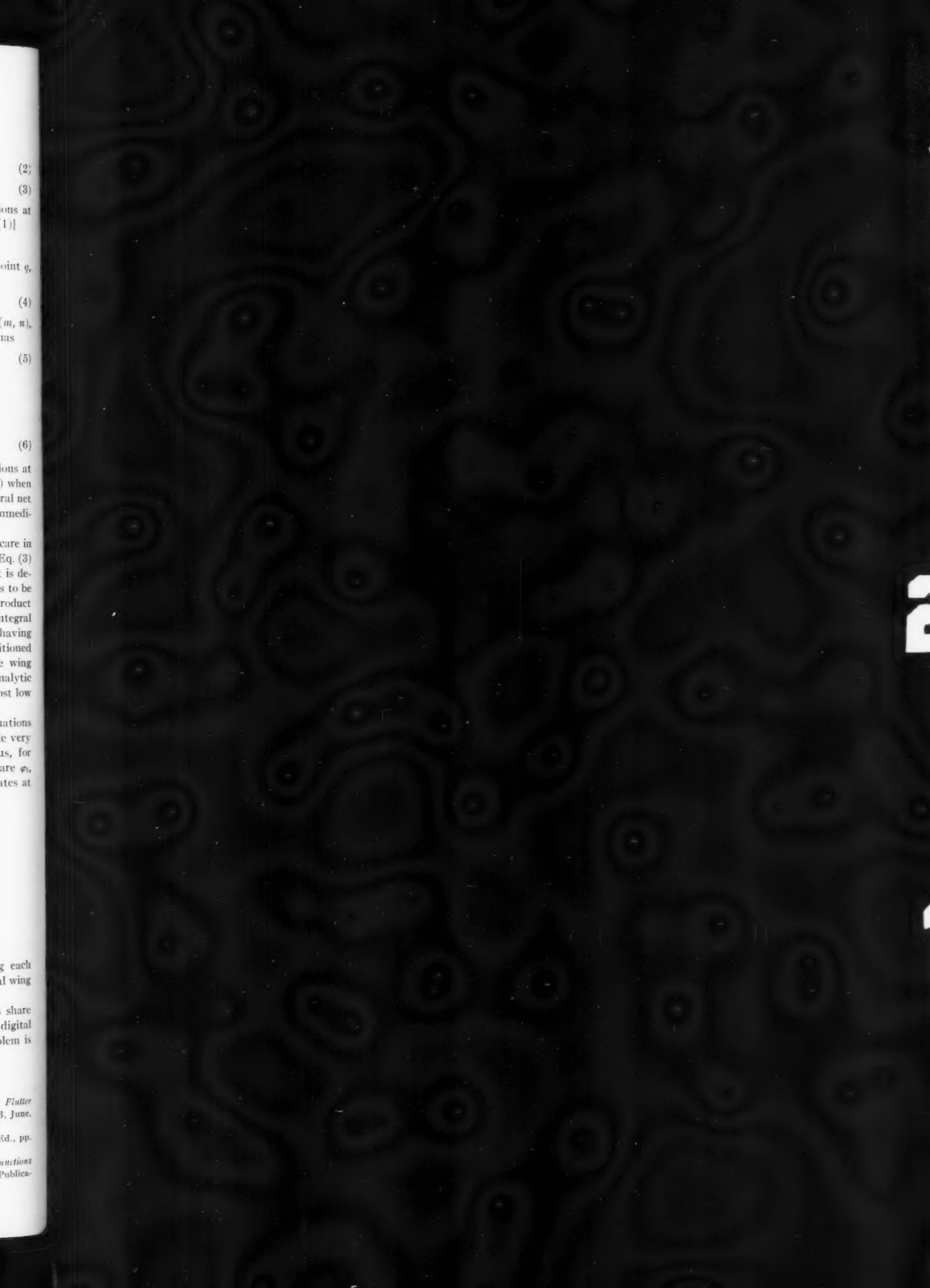
* Within each subscript pair (ij), (k, l), (m, n), and (p, q), the subscripts are used interchangeably. Thus, the matrix E_{qj} is identical with E_{pi} and E_{jq} is its transpose.